APPROPRIATE DESIGN OF LONGWALL COAL MINING SYSTEM UNDER WEAK GEOLOGICAL CONDITIONS IN INDONESIA

パントゥデッ, ポンパンニャ

https://doi.org/10.15017/1931894

出版情報：九州大学, 2017, 博士（工学）, 課程博士
バージョン：
権利関係：

APPROPRIATE DESIGN OF LONGWALL COAL MINING SYSTEM UNDER WEAK GEOLOGICAL CONDITIONS IN INDONESIA

A DOCTORAL DISSERTATION

Submitted to the Department of Earth Resources Engineering
Graduate School of Engineering
Kyushu University

As a partial fulfillment of the requirement for the degree of

Doctor of Engineering

By
Phanthoudeth PONGPANYA

Supervised by
Assoc. Prof. Dr. Takashi SASAOKA

Department of Earth Resources Engineering
Graduate School of Engineering
Kyushu University
Fukuoka, Japan
March 2018

ABSTRACT

Indonesia is one of the largest coal producers and exporters in the world. The coal production of Indonesia has increased significantly in recent years. Indonesia exports 70%-80% of the total coal production abroad and the remaining is consumed in domestic markets. In Indonesia, the coal is mainly produced from the surface mines. Recently, the conditions of surface mines have worsened each year because stripping ratio has increased due to the increase in mining depth. The resource of high quality coal located in accessible areas has decreased due to the rapid expansion of coal production. Moreover, the development of new surface mines is constrained due to its environmental impacts and protection law. Therefore, in order to meet the increased demands of the coal, underground coal mines have to be developed in Indonesia. According to the experiences of underground coal mining in Indonesia, due to the coal measure rocks becoming very weak and the design guidelines of underground mining under weak geological conditions not being developed, ground control issues have occurred frequently. As a result, some underground coal mines have been abandoned. From these backgrounds, the purpose of this research is to develop an appropriate design guideline of underground mining system under weak geological conditions. To accomplish the purpose of this research, The PT Gerbang Daya Mandiri (GDM) underground coal mine in Indonesia, where the rocks are weak and the coal is planned to be mined by the longwall mining method, is chosen as the representative mine site. This dissertation consists of six chapters and the main contents in each chapter are listed as follows:

Chapter 1: This chapter introduces the background of this research, geotechnical issues and technology related to the longwall mining method, and objectives and outlines of the dissertation.

Chapter 2: This chapter describes the conditions of the PT Gerbang Daya Mandiri (GDM) mine site. Based on the results of laboratory tests, the rocks of this underground coal mine are classified into very weak and low strength rock masses. Furthermore, this chapter also discusses the current situation of the main roadway stability at the shallow depth. According to the field measurement data, a small roof

displacement occurs when the roadway is excavated in the undeteriorated claystone, and when the coal layer is present in the roof. The current support system using the steel arch SS400 with 1.0 m spacing is effective to control the main roadway stability, although, a very large roof displacement occurs when the roadway is excavated in the deteriorated claystone. Under this situation, the use of stronger steel arch SS540 with 0.5 m spacing should be adopted.

Chapter 3: This chapter focuses on the stability analysis and support design of the main roadway prior to longwall mining at the deeper depth. The stability of the main roadway at the GDM coal mine under various depths and stress ratios is studied by means of numerical simulations. According to the results of a series of numerical simulations, the stability of the main roadway decreases by increasing the depth and stress ratio. Ground control problems such as falling roof, sidewall collapse, and floor heave can be expected unless an appropriate support system is provided. Three support systems, i.e. friction rockbolt, steel arch (SS540), and shotcrete, are discussed as methods to stabilize the roof and sidewalls of the main roadway. The steel arch is considered to be the most effective support system comparing with other systems. The steel arch meets the qualifications of stability control. The steel arch with closer space and larger size of cross section provides a better stability condition to the roof and sidewalls of the main roadway. Although the stability of roof and sidewalls of the main roadway can be controlled by steel arch support, the occurrence of floor heave can be expected according to the increase of mining depth. Therefore, three techniques using cablebolt, invert-arch floor, and grooving method are selected and discussed in order to control the floor heave. Heaving of the floor is controlled effectively after the cablebolt, invert-arch floor, and grooving methods are employed. However, controlling the floor heave by cablebolt support may be the most appropriate technique in GDM coal mine compared with other methods in terms of installation process, providing a flat and safe working condition of floor, and economy. In addition, the cablebolt with closer row space and longer length works more effectively to control the floor heave.

Chapter 4: This chapter studies the effect of longwall mining on the stability of main and gate roadways at GDM coal mine. According to the results of a series of numerical simulations, the extraction of longwall panel significantly affects the

main and gate roadway stabilities. The stability of main or gate roadways decreases by decreasing the barrier or chain pillar width, especially when a wide panel width of 130 m is applied. Here, the barrier pillar is the coal pillar left between the longwall panel and main roadway and the chain pillar is the one left between the adjacent longwall panels. Ground control issues are to be expected under the event that an appropriate width of barrier/chain pillar is not provided. In the case that the main and gate roadways are supported by 0.5 m spaced steel arches (SS540), a 20 m barrier pillar width and a 30 m chain pillar width can be used sufficiently at 50 m, 100 m, and 150 m depth, while a wider barrier pillar width of 34 m and a wider chain pillar width of 50 m should be applied at 200 m depth in order to keep the main and gate roadways stable during the extraction of longwall panel, respectively. The simulation results also reveal that the effect of a longwall panel extraction on the stability of main and gate roadways can be minimized by decreasing the width of a longwall panel. By applying a narrower longwall panel, not only the main/gate roadway stability can be improved, but also a smaller barrier/chain pillar width can be adopted. At a 200 m depth, the stability of the main roadway can be controlled effectively by a smaller barrier pillar width of 20 m and 23 m, while the stability of gate roadway can be maintained efficiently by a smaller chain pillar width of 32 m and 40 m, when a narrower panel width of 70 m and 100 m is applied, respectively. Therefore, as the mining depth is increased, the coal recovery can be increased under the better mining conditions by applying narrower panel width.

Chapter 5: This chapter discusses the surface subsidence induced by extracting longwall panel at GDM coal mine. The characteristics of surface subsidence induced by single-panel and multi-panel mining under various depths are discussed. Based on the results of a series of numerical analyses, a large surface subsidence can be expected at all mining depths (50 m, 100 m, 150 m, and 200 m) when a wider panel width of 130 m is applied. When a single panel is extracted, a larger surface subsidence occurs at the shallow depth; therefore, a narrower panel width should be applied, especially in case the depth is less than 100 m. After several panels have been mined in a series, the surface subsidence increases with increasing mining depth. This indicates that a wider chain pillar is needed at the deeper depth. In order to control the surface subsidence, three countermeasures, i.e. applying a wider chain

pillar, a narrower panel width, and a backfilling system, are investigated. As a wide panel width of 130 m is applied, a large surface subsidence still occurs at all depths, even though the chain pillar width is increased from 30 m to 60 m. From these results, it can be considered that the width of longwall panel should be decrease and/or a backfill system should be applied in order to control the surface subsidence. The surface subsidence decreases significantly by decreasing the panel width. A small chain pillar width of 30 m can be used sufficiently at all depths when a 100 m or 70 m panel width is applied. Although the surface subsidence can be controlled effectively by decreasing the panel width, a decrease in coal recovery can be expected when a narrower panel width is used. On the other hand, the surface subsidence can also be controlled effectively by using a backfilling system with cohesive material. A small surface subsidence occurs after backfilling. The simulation results also indicate that a backfilling system with cohesive material may be the most appropriate countermeasure for control surface subsidence and the coal recovery can be increased because a narrow chain pillar width of 30 m can be used with a wider panel width of 130 m. Moreover, based on the results of a series of numerical simulations, the prediction graph for the maximum subsidence due to the extraction of longwall panel in GDM coal mine is proposed.

Chapter 6: This chapter concludes the results of this research.

ACKNOWLEDGEMENTS

I would like to express my very great appreciation to Associate Prof. Dr. Takashi SASAOKA, my research supervisor, Laboratory of Rock Engineering and Mining Machinery, Kyushu University, for his patient guidance, encouragement, and kind support during doing this research. His willingness to give his time so generously has been very much appreciated.

I would like to extend my deep gratitude to Prof. Dr. Hideki SHIMADA, my co-supervisor from Laboratory of Rock Engineering and Mining Machinery, Kyushu University, for his precious and constructive suggestions during the planning and development of this research. Additionally, I would like to thank you for his professional advice and kind assistance in keeping my progress on schedule.

My sincerest thanks go to the members of my examination committee, Prof. Dr. Yasuhiro MITANI, Department of Civil Engineering, Kyushu University, and Associate Prof. Dr. Masahiro INOUE, Department of Earth Resources Engineering, Kyushu University, for raising a number of interesting points for discussion. The generous time that they gave for valuable comments toward improving my work is very much appreciated.

I wish to acknowledge the staff of the PT Gerbang Daya Mandiri (GDM) underground coal mine in Indonesia for enabling me to visit their mine site to observe their daily operations and to collect the data those are necessary for conducting this research.

I am particular grateful for the financial support given by the AUN-SEED/Net Scholarship (JICA) for sponsoring my doctoral study at Kyushu University, Japan. Thanks to your generous support. I am much honored to be the recipient of this scholarship.

A very special gratitude goes out to all my friends at the Laboratory of Rock Engineering and Mining Machinery, Kyushu University, for their helps, encouragements, and friendships. The times I spent with them were worth more than I can express on this paper.

To my dad, Hing PONGPANYA, who is always in my thoughts, your last word is still resounding in my ears. This is to tell you that I have done all the promises that I have given to you. Many thanks for everything you did for me. Your support and care mattered a lot. I am very proud to be your son. I miss you.

My special and deepest thanks go to my mom, Kaisone PONGPANYA, for her unconditional love and endless support. You were always by my side with a word of encouragement or listening ear whenever I felt down.

Finally, I would like to thank my wife, Malisone MONCHANDY, for her love, caring, patience, and encouragement. You knew my study in Japan would be a long road, but you always encouraged and supported me along the way. Thank you very much that you have made this possible. Additionally, I would not forget to thank a little boy who has recently come to my life, my son, Pattaphithack PONGPANYA, for bringing me a massive inspiration. Your coming has reminded me not to give up for any tough thing in life. I may not have everything that I want, but I am blessed enough to have you in my life.

Fukuoka, February 2018

Phanthoudeth PONGPANYA

TABLE OF CONTENTS

LIST OF FIGURES

LIST OF TABLES

CHAPTER 1

INTRODUCTION

1.1. Background

Coal is one of the world's most important sources of energy which has been widely used as fuel in many industrial sectors such as electricity generation, cement and steel production, and other manufacturing activities. The coal production in Indonesia has increased significantly in the past years (see Figure 1.1). Indonesia exports the coal mostly to China and India, accounted for 70 to 80% of the total coal production, while the remaining is consumed in domestic markets (Indonesia-Investments, 2016). The coal production in Indonesia is mainly from the surface mines. Recently, many surface mines have been stopped in their operations due to an increase in stripping ratio as the mining depth increased (Matsui, Shimada, Furukawa, Kramadibrata, & Anwar, 2003; Sasaoka et al., 2007; Sasaoka et al., 2014; Takamoto et al., 2014). In addition, there are many problems concerning the environmental impacts and protection challenges to expand the current surface mines and develop new ones, especially where the coal seams are located beneath agricultural areas, protected forests, and man-maid structures. Therefore, in order to meet the increased demands of the coal, underground coal mines have to be developed.

In general, two main methods of coal extraction by underground mining are commonly used, such as room-and-pillar and longwall mining systems. The longwall mining method is an efficient and safe coal producing technique which requires fewer workers and gives higher coal productivity than that of room-and-pillar mining (Peng, Chiang, John, Wiley, & Sons, 1984; Brady & Brown, 2004; PB, 2007; Manteghi, Shahriar, & Torabi, 2012; IESC, 2015). In most longwall mining systems, the roadway stability and surface subsidence are the major issues that must be taken into consideration in order to ensure the safety of mine workers, coal production rate, and environmental impacts. The application of longwall mining has been successful in many underground coal mines around the world, e.g., Australia, China, India, Europe, US, etc. Numerous researches have been focused

on roadway stability analyses and surface subsidence predictions in longwall coal mines. However, most researches have been carried out at the mine sites where the rock strengths are medium to strong (Yasitli & Unver, 2005; Keilich, Seedsman, & Aziz, 2006; Zhang, Mitra, Hebblewhite, & Tarrant, 2006; Sahebi, Jalalifar, & Ebrahimi, 2010; Manteghi, Shahriar, & Torabi, 2012; Shabanimashcool & Li, 2012; Xu et al., 2013; Bai et al., 2014), only few researches have been carried out at the mine sites where the rocks are weak (Takamoto et al., 2014; Sasaoka et al., 2015b). Thus, the understandings of roadway stability and surface subsidence in longwall mining under weak geological conditions have still been limited.

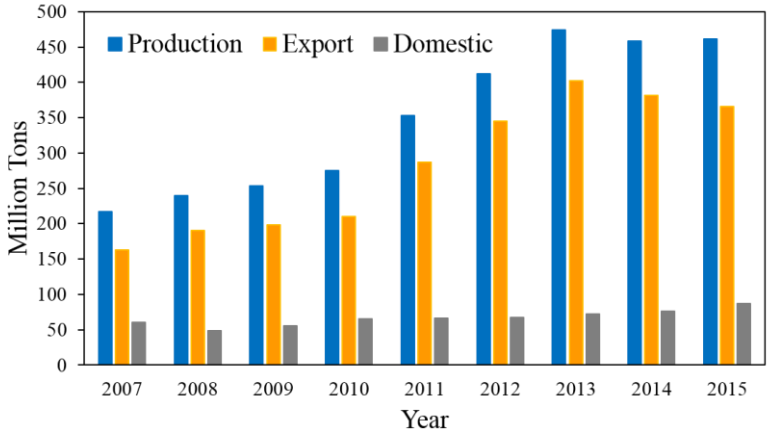

Figure 1.1 Production, export, and domestic consumption of Indonesian coal (http://www.indonesia-investments.com/business/commodities/coal/item236).

In Indonesia, the coal measure strata consists of sedimentary rocks such as sandstone, claystone, siltstone, shale, and mudstone. Their mechanical properties are generally weak and deteriorated due to water. Results of uniaxial compressive strength (UCS) tests indicated that the strengths of rocks in Indonesian coal mines are much lower than that of coal mines in other countries (see Figure 1.2). The UCS value of coal measure rock is mostly less than 25 MPa (Matsui, Shimada, Furukawa, Kramadibrata, & Anwar, 2003; Sasaoka et al., 2007; Garcia, Altounyan, Nitaramorn, & Lewis, 2010; Sasaoka et al., 2014; Sasaoka et al., 2015a; Sasaoka et al., 2015b). According to Bieniawski (1974) and Hoek & Brown (1997), the rocks of Indonesian coal mines can be classified into weak and low strength rocks. In addition, the coal measure rocks in Indonesia generally contain clay minerals (i.e. smectite). They present a considerable slaking within a short period of time when

they are contacting with water, or being exposed to the atmosphere, resulting in reduction of the strengths. Figure 1.3 demonstrates the slaking characteristics of coal measure rocks determined by means of static slaking index test (Sadisun, Shimada, Ichinose, & Matsui, 2004). The results indicated that the slaking index increased with increasing the amount of smectite. Therefore, based on the mechanical properties and characteristics of coal measure rocks, a series of ground control issues such as roof fall, sidewalls collapse, and floor heave of the roadway, and a large subsidence at the surface can be expected when a conventional longwall mining system used in other countries is applied in Indonesia.

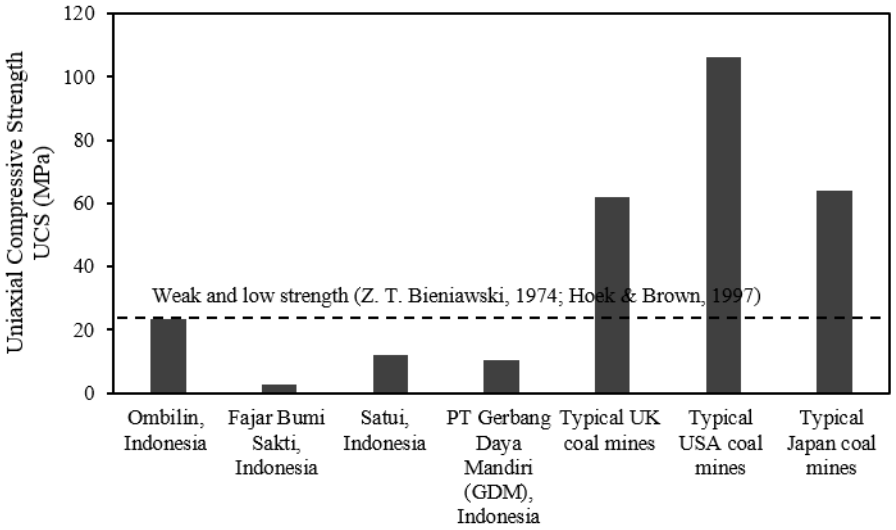

Figure 1.2 Uniaxial compressive strength of coal measure rocks in Indonesia, UK, USA, and Japan.

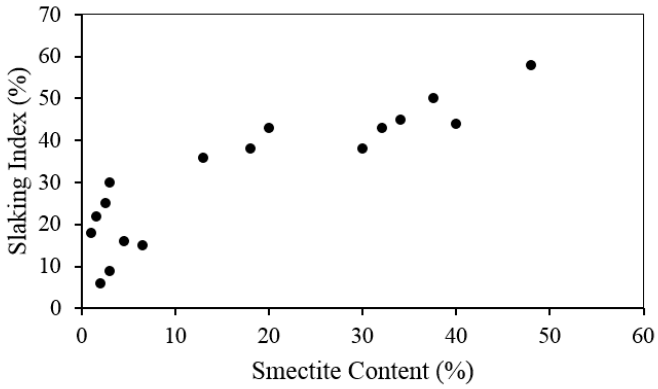

Figure 1.3 Relationship between slaking index and smectite content of Indonesian coal measure rocks (Sadisun, Shimada, Ichinose, & Matsui, 2004).

Originally, three underground coal mines were operated by longwall mining method in the past in Indonesia, such as Ombilin, Fajar Bumi Sakti, and Kitadin Embalut coal mines. These coal mines were developed in 1892, 1978, and 1983, and closed in 2005, 2006, and 2010, respectively. Although these three underground coal mines had been operated successfully, many geotechnical issues occurred during their mining operations. For example, at Ombilin coal mine, the ground control problem of serious roof falls happened in 1998 while the roadways were driving in weak rock mass, and it took a couple of months to go through the failed area (Matsui, Shimada, Furukawa, Kramadibrata, & Anwar, 2003). In recent years, furthermore, several attempts have been made to develop underground mines from the final highwall of the surface mines, such as Satui coal mine in South Kalimantan and Indominco coal mine in East Kalimantan. Satui underground mine was commenced in 2002. This coal mine adopted an Australian roof bolt support system for the development of the roadway. Unfortunately, this underground coal mine was abandoned in 2005 due to a fatal accident of a falling roof in the main roadway. Two miners were killed, and other two were injured. The accident occurred due to inadequate roof supports in weak ground conditions (Sasaoka et al., 2007). Indominco coal mine started the trial underground operation in 2009. When this underground mine was proposed, it was recognized that the ground control issue happened at Satui trial underground mine needs to be solved. Even though rock bolting is well established as support technology in Australian coal mines, but this

technique alone is not capable to maintain the roadway stability in Indonesia due to weak ground conditions coupled with the lack of local experience. Therefore, a new immediate roof classification system called Coal Mine Roof Rating (CMRR) was adopted for a roof bolting design in this trial mine. According to the monitoring result of ground behaviour, the large displacement of the roof was recognized, and it increased constantly within the elapsed time after drivage of the roadway. The phenomenon indicated that the rock bolting system would control the roof only for a short period of time, but it would not work effectively after a long period even additional roof bolts are installed (Sasaoka et al., 2014). However, although a trial underground mine at Indominco coal mine completely recovered the reserves without any fatal accident, it could not go further for full mining operations at deeper levels because too much cost is required for support installation. As a result, this underground coal mine was eventually abandoned. Figure 1.4 shows the location map of underground coal mines in Indonesia.

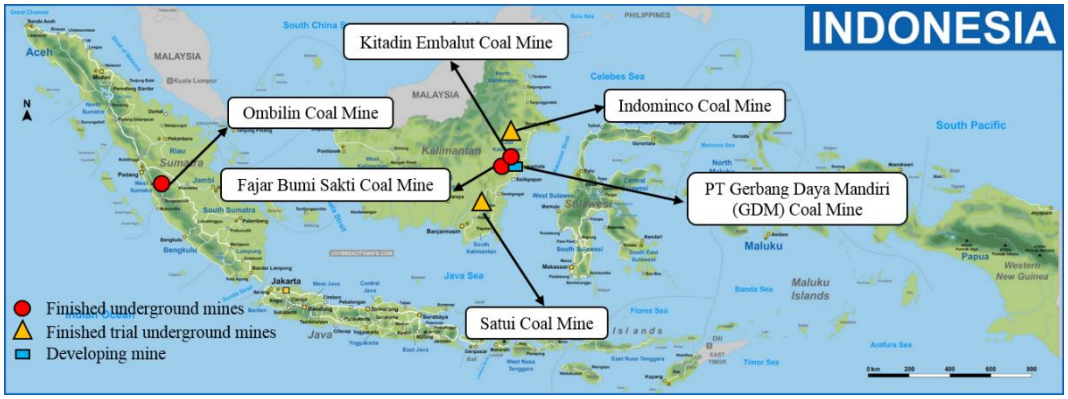

Figure 1.4 Location of underground coal mines in Indonesia.

According to the ground control problems that occurred at underground coal mines in Indonesia, it can be said that the guidelines of underground mining design used in Australia or other countries cannot be directly applied in Indonesia due to the rocks are very weak. As appropriate guidelines of underground mining are lacking, the experiences and expertise of local mining engineers concerning the underground mining are restrained. As a result, severe ground control problems have occurred regularly, and some underground operations have failed. Therefore, in order to develop the underground coal mine in Indonesia, by ensuring the roadway stability and avoiding the adverse impacts at the surface due to the

subsidence, it is very important to develop the design guidelines of underground mines, particularly longwall mining system that suit to geological conditions in Indonesia. This research would give benefits to future underground mining projects in Indonesia by adopting the design guidelines or techniques developed in this study.

1.2. Literature Review

Coal is one of the most abundant fossil fuels that has been used as an energy resource for decades, primarily burned for the production of electricity and steel. Coal can be mined either on the surface or from the underground. In underground coal mining, room-and-pillar and longwall mining systems are the two basic methods of coal extraction. In these two underground coal mining methods, the longwall mining is the most productive and popular technique of coal extraction from underground.

Longwall mining is a highly productive, efficient, and safe underground mining method, which applies to extract the coal seams of relatively large horizontal extent and uniform thickness with an orebody dip of less than 20°. Up to 80% of the coal can be recovered by this mining method (Hamrin, 1986; Whittaker & Reddish, 1989; Hartman & Muntmansky, 2002; Brady & Brown, 2004). In longwall mining, several entries are made from the surface in order to reach the coal seams. These entries are known as main roadways. After reaching the targeted coal seams, the coalbed is blocked out into panels, typically around 150-300 m in width, 1,000-3,000 m in length, and 2-5 m in thickness. Figure 1.5 shows a typical panel layout of a longwall mining system. Before the extraction of a longwall panel commences, a continuous mining equipment is used to extract the coal to form entries along the longwall panel, known as gate roadways. These gate roadways form the mine ventilation passages, accesses for miners, and coal transportation pathways (Mine Subsidence Engineering Consultants [MSEC], 2007; Energy and Minerals Field Institute [EMFI], 2011). In multi-entry gate roadways, a pillar between two adjacent entries is left called as chain pillar. Another pillar with large dimensions is also formed, and used to separate a longwall panel from the main roadways of the mine. This pillar is called as a barrier pillar. The geometries and configurations of the

chain pillar and barrier pillar considerably influence the stabilities of the main and gate roadways, as well as the productivity and safety of the longwall mining operation.

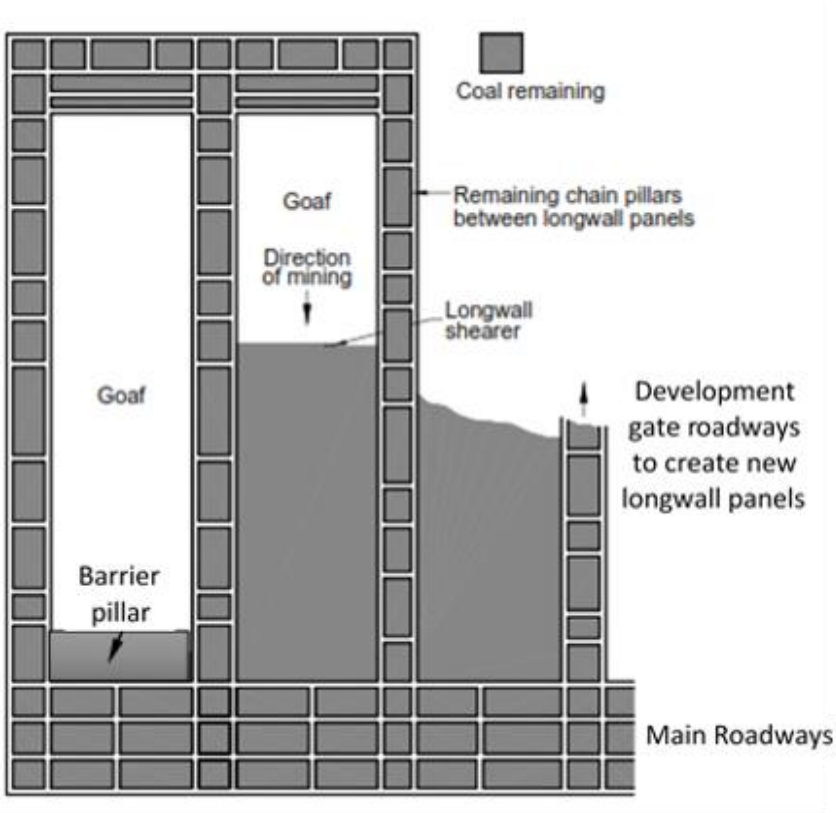

Figure 1.5 Typical panel layout of a longwall coal mine (MSEC, 2007).

Figures 1.6 & 1.7 illustrate the 3-D view of longwall mining operation and the cross-section of a typical longwall face. The mining method uses the hydraulic roof supports, a coal-shearing machine, and a face conveyor which install parallel to the coal face. The coal is extracted along the stope face by a shearing machine which travels back and forth across the coalface. The shearer cuts a slice of coal from the coalface on each pass, and the coal is spilled onto the face conveyor which runs along the full length of the coalface. The face conveyor carries the coal away from the longwall face and discharges onto a belt conveyor for transport out of the mine. In longwall mining, the area immediately in front of the coalface is supported by a series of hydraulic roof supports which temporarily hold up the roof strata and provide a working space for the shearing machinery and face conveyor. After each slice of coal is removed, the hydraulic roof supports, the face conveyor, and the

coal-shearing machinery are moved forward. When the coal is extracted using logwall mining method, the immediate roof strata above the coal seam is allowed to collapse and cave in to fill the stope void. The fully filled cave-in area is called as the goaf, gob, or cave-in zone. Miners working along the longwall face, and operating the machinery are protected from the collapsing strata by the canopies of the hydraulic roof support. As the roof collapses into the goaf behind the hydraulic roof suppots, the fracturing and settlement of the rocks progress through the overlying strata, resulting in subsiding of the immediate roof strata toward the surface. The fracturing and settlement of the roof strata behind the coalface significantly affect the stability of main and gate roadways (Hamrin, 1986; Brady & Brown, 2004; MSEC, 2007; Parsons Brinckerhoff [PB], 2007; EMFI, 2011; Independent Expert Scientific Committee [IESC], 2015).

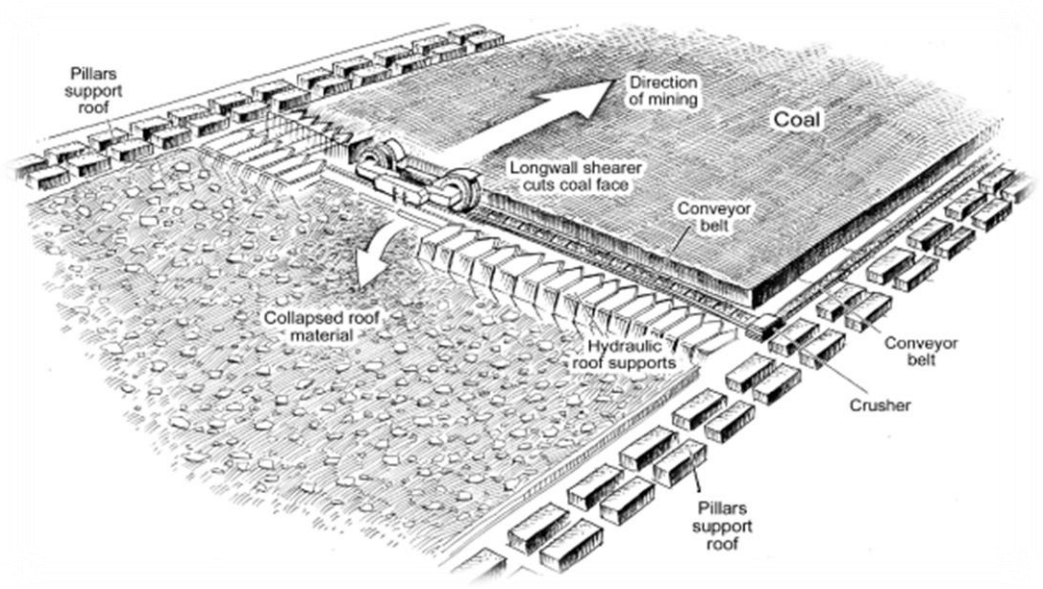

Figure 1.6 3-D view of longwall mining operation (EMFI, 2011).

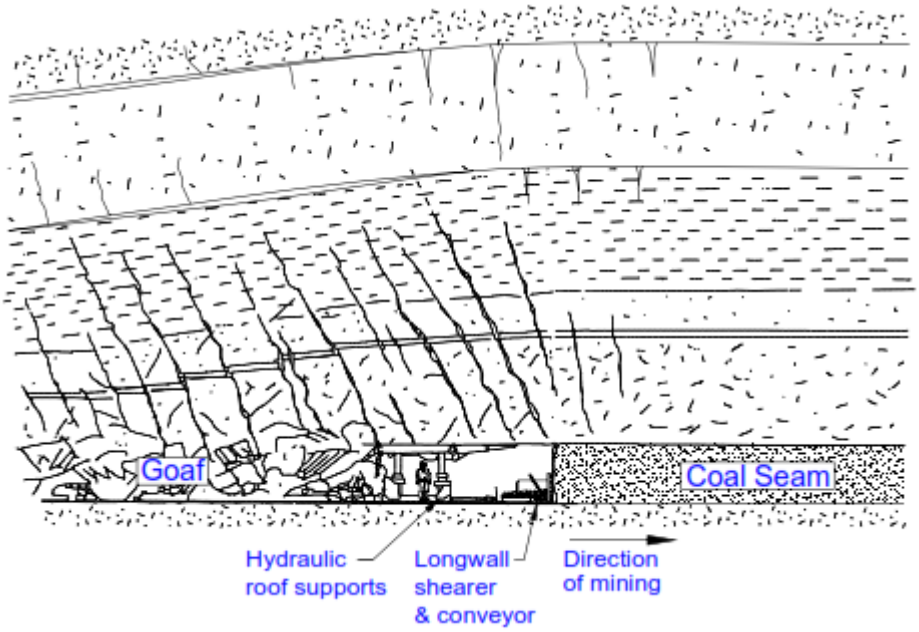

Figure 1.7 Cross-section of a typical longwall face (IESC, 2015).

The process of a roof cave-in in longwall mining is a dynamic complex process including strata fracturing, disintegration, and movement in downward (Lehmann & Konietzky, 2015). The disturbed zones above an excavation are divided into four zones (see Figure 1.8) such as caved zone, fractured zone, continuous deformation zone, and surface cracking zone (Peng & Chiang, 1984). As the longwall face advances, the immediate roof above the mining horizon caves into the void from which the coal seam was extracted, forming a caved zone. The caved zone extends upwards 2-10 times the extracted seam height. The caved zone is characterized by irregular rock fragments that may have rotated relative to their initial locations, resulting in relatively high void ratios and permeability. Immediately, above the caved zone is a zone of fractured strata. The near vertical fractures, strata sagging, and bed separations have occurred in this zone. The bed separation results in increasing the horizontal permeability of the strata. The height of fractured zone mainly depends on the brittleness of the strata above the mined-out area, and the thickness and width of an extraction. However, the fractured zone can approximately extend 30-60 times of the extraction thickness. Above the fractured zone is the continuous deformation zone. This zone is a compression zone where the apertures of pre-existing fractures have reduced. The rock strata in this zone

flexes without creating a linked vertical fracture pattern. This zone is considered as a protective barrier to prevent the hydraulic connections between the overlying water bodies and the fractured zone. This is also called as an aquiclude zone (Singh, 1986). On the surface, there is a surface cracking zone which varies in depth depending on the lithogical type and the excavation extent. In this zone, the cracks open and close as the longwall face comes and goes (Peng & Chiang, 1984).

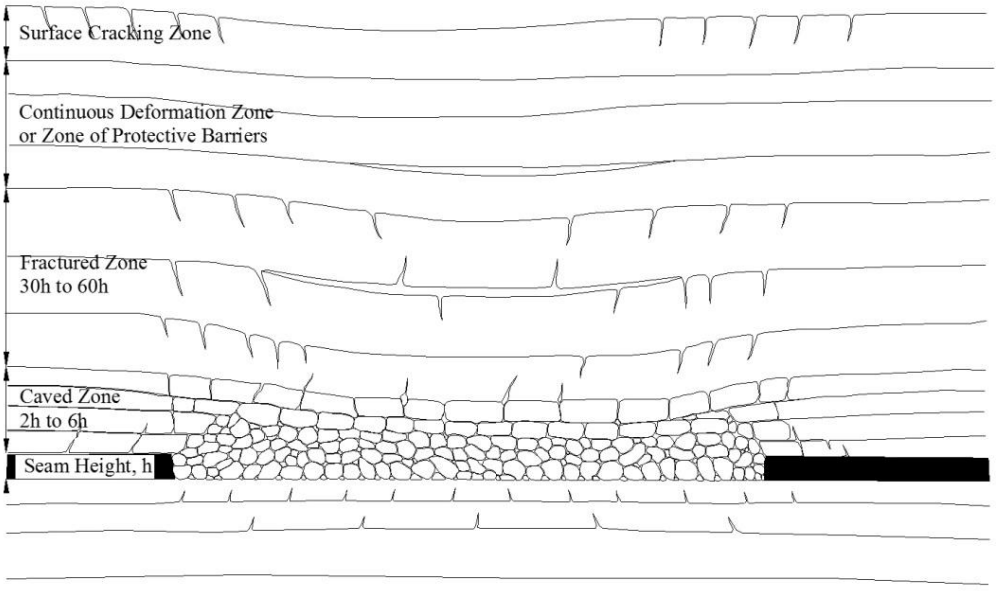

Figure 1.8 Strata deformation zones and overburden movement induced by longwall mining (after Peng & Chiang, 1984).

Cave-in of the roof strata dramatically changes the in-situ stress conditions in the rock mass surrounding the longwall panels. The redistribution of the rock stresses is mainly affected by the panel layouts and mining sequence. Generally, the vertical stress in panel walls and the horizontal stresses in roof and floor increase with an enlargement of longwall panel (Shabanimashcool & Li, 2012; Lehmann & Konietzky, 2015). Figure 1.9 shows the vertical stress distribution along a longwall panel. The vertical stress is zero both at the face and at the rib, and it increases very quickly with a few meters ahead of the face. With increasing the distance behind the face, the stress level returns to cover load (Whittaker, 1974; Hudson, 1993). These stress changes and redistributions due to the cave-in of roof strata above a mined-out panel have pronounced impacts on stability of main and gate roadways.

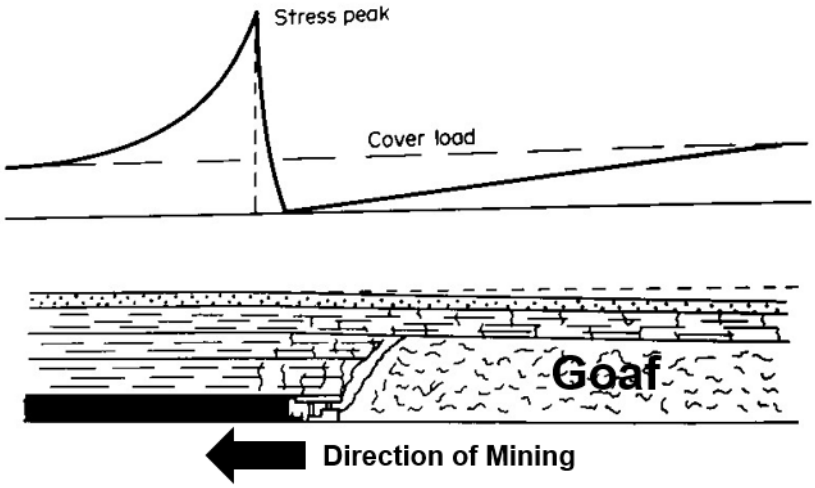

Figure 1.9 Vertical stress distribution at a longwall panel from stope to goaf (Hudson, 1993).

It is apparent that during mining of the longwall panels, the main roadways, gate roadways, and pillars protecting them will be subjected to changing loading conditions and complex stress paths throughout their operation lives. The roadway stability and support requirements are of particular interest. Obviously, the design of rock support system will depend on the longwall layout geometry, the geomechanical characteristics of the strata, and the in-situ and induced stresses (Brady & Brown, 2004). There are several types of supports that have been used to stabilize the underground roadways for decades, such as rockbolt, cablebolt, shotcrete, and steel set. Rockbolts have been used for many years as the support of the main roadways and gate roadways. They are probably the oldest form of the rock support used in underground mining, and are still the most common form of rock reinforcement used in many longwall coal mines, e.g. Canada, UK, Australia, etc. In fact, this support type is used to tighten the loose blocks and wedges of the rock near the surface of excavation. It helps the rock to support itself, and prevents the falls of loose rocks that may create unsafe working conditions (Hoek & Wood, 1987). Rockbolts generally consist of plain steel rods with a mechanical or chemical anchor at one end, and a face plate and nut at the other end. They are always tensioned after installation. For short term applications, the rockbolts are generally left ungrouted. For more permanent applications or in which corrosive groundwater is present, the space between the rockbolts and rock can be filled with cement or

resin grout (Hoek, Kaiser, & Bawden, 1993; Hoek, 2006). In some cases, rockbolts will be replaced by means of cablebolts where shorter rockbolts are inadequate and when rockbolts cannot be installed in roadway openings with very low headroom (Hoek & Wood, 1987; Brady & Brown, 2004). The main objective of using cablebolts is that the same with rockbolts. They are used in order to hold up the dead weight of the loose materials. The cablebolts can be grouted in place without tensioning, or they can be tensioned before grouting. However, the use of rockbolt and cablebolt will be effective only if the rock is hard enough to provide a good grip for the anchor. An expansion anchor which is well seated in the rock will usually allow a rockbolt or cablebolt to be tensioned in order to achieve its maximum load-carrying capacity (Hoek & Wood, 1987; Hoek, 2006).

When the use of rockbolts or cablebolts in the poor rock mass is not appropriate because of the difficulty of achieving adequate anchorage, the support consequently has to be in the form of shotcrete or concrete lining, or closely spaced steel sets. Shotcrete is widely used for the support of underground excavations in civil engineering construction for many years, and in recent years the mining industry has become a major user of shotcrete as the support in underground mining, including longwall mining. Shotcrete is the genetic name for cement and fine aggregate concretes which are applied pneumatically and compacted dynamically under high velocity. Currently, a more impermeable and durable shotcrete with stronger strength can be achieved by addition of the micro-silica and steel fiber reinforcement to the mortar/aggregate mix (Hoek, Kaiser, & Bawden, 1993; Hoek, 2006). The shotcrete is a very effective support medium, and used to prevent small pieces of rocks from unravelling from the excavation surface. It helps to retain the interlocking and self-supporting characteristics of the rock mass, and also helps to block the pathway of the water that can flow into the underground opening by sealing the joints in the rock mass (Hoek & Wood, 1987). Although the shotcrete is an effective support medium in stabilizing the underground roadways and openings, the use of this support has a limitation due to the fact that it takes time for these materials to harden, and to achieve the desired strength which require to provide an adequate support. The use of accelerators or thick linings can partially overcome these problems but may introduce another set of practical problems. The shotcrete

is normally applied as the support for the permanent and important areas in underground mines such as ramps, main roadways, and shafts where the long-term stability is necessary (Hoek, Kaiser, & Bawden, 1993; Hoek & Wood, 1987; Hoek, 2006). The use of shotcrete in controlling the rock mass deformation around the roadways and openings will be very effective if it is used in combination with rockbolts or cablebolts.

Steel sets have generally replaced timber as the one of the traditional support systems in underground mine. The steel sets do not interact with the rock mass in the same way as rockbolts or cablebolts. Generally, steel sets can only respond to loads imposed on them by inward movement of the rocks. Since they are normally placed some distance behind the advancing face, most of the short-term movement in the rock mass has already taken place before the steel sets are in place, and only the load which is the dead weight of a rock failing around the roadways is carried by the steel sets. In hard rock mining, steel sets have very limited application since the rock mass deformation can be effectively controlled by rockbolts, cablebolts, or shotcrete, or by combination of these support systems. The steel sets are normally used in underground mines, where the excavation of the roadways is made through the fault zones, or in very badly broken and soft ground. In such cases, it may be impossible to anchor the rockbolts or cablebolts in the rock mass, and steel sets may be required in order to carry the dead weight of the failed rocks surrounding the roadway openings (Hoek & Wood, 1987).

In longwall coal mines, the stability of the main and gate roadways not only can be maintained by the use of rock supports as mentioned above, but it also can be improved by leaving the appropriate size of the barrier and chain pillars. As the main and gate roadways are subjected to a change of loading conditions and complex stress paths during the mining of a coal panel, the adequate width of barrier and chain pillars can help to prevent excessive abutment stresses which induced by longwall panel extraction. These excessive abutment stresses significantly affect the stability of the main and gate roadways. The pillars are designed to separate the roadways from panel extraction areas, and to maximize the coal recovery (Hebblewhite, Galvin, & Vasundhara, 1999; Colwell, Frith, & Mark, 1999). The design of the barrier and chain pillars has been traditionally based on precedent

practices which often represented by “rules of thumb”. Modern design methods may use empirical, analytical, or computational methods combined with the performance monitoring. The width of barrier pillar and chain pillar may be varied from 20 m to more than 100 m depending on the mining depths, in-situ stresses, mining geometries, coal strengths, geological structures, and mechanical properties of underlying and overlying strata (Brady & Brown, 2004).

Although longwall mining method provides high productivity and safe working conditions in underground mining, because of a large extent of coal is removed from the seam, many underground mines have been experienced with the geotechnical problems due to surface subsidence. As a longwall face advances, the immediate roof strata above the mined-out panel collapse into the goaf, the rocks above them lose support and sag to fill the void. This can change the surface topography which can potentially damage houses, roads, dams, and other man-made structures. Subsidence induced by longwall mining can also change the flow paths of surface and groundwater in certain areas. Several mining and geological parameters affect the magnitude and extent of surface subsidence. Rock mass, geological structures, in-situ stresses, panel and pillar sizes, and mining depths are the key factors influencing surface subsidence. Several types of subsidence deformations caused by longwall mining have been discussed by Shadbolt (1978). The overlying strata experience stress redistributions as a result of the longwall mining (see Figure 1.10). Continuous of a trough subsidence forms as a gentle depression over a large area. Materials over the central part of the mined void move vertically downward at the same time as materials from the adjacent sides move toward the center and downward. Whittaker and Reddish (1989) illustrated the basic subsidence profile resulting from longwall mining of a single panel (see Figure 1.11). Two parameters are used to define the magnitude, shape, and limitation of the subsidence at the surface, such as maximum surface subsidence (S_{max}) and angle of draw (AoD).

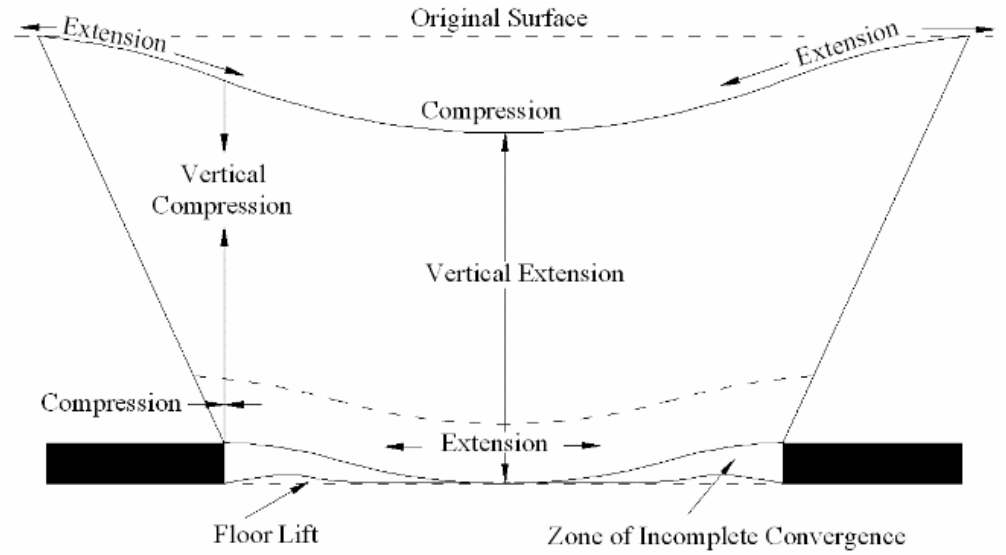

Figure 1.10 State of stress after longwall extraction (Shadbolt, 1978).

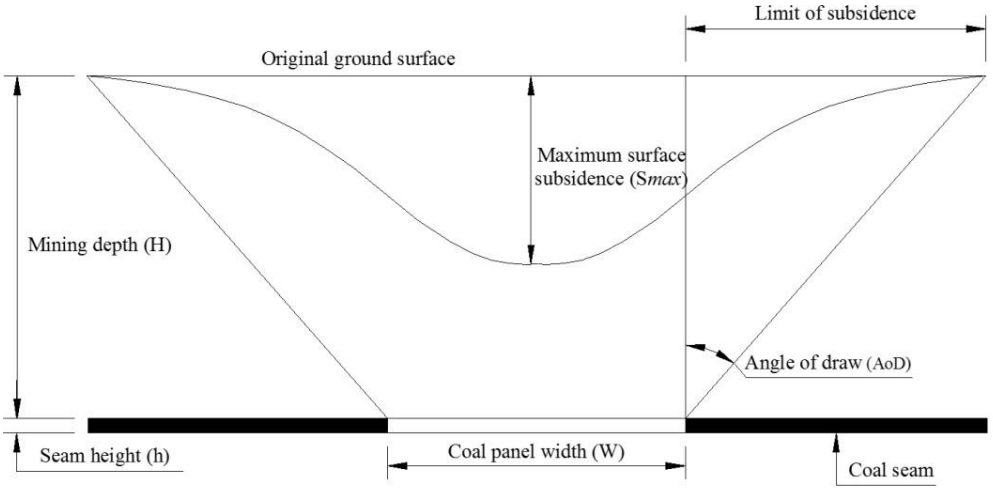

Figure 1.11 Basic subsidence profile above single longwall mining (Whittaker & Reddish, 1989).

Maximum surface subsidence (S_{max}) is defined as the maximum extent of settlement at the surface which occurred above a mined-out panel. The magnitude of surface subsidence is considerably less than the thickness of extracted coal seam due to some voids have been left within the goaf. The extent of the settlement at the surface is therefore dependent upon the strength and nature of the rocks overlying the coal seam, and it is a function of their capacity to bridge over the mined-out area. The subsidence at the surface does not occur suddenly but develops progressively as the

coal is extracted. Generally, all significant subsidence from the extraction of a longwall panel is complete within 1 to 2 years (IESC, 2015).

Angle of draw (AoD) is commonly used as a subsidence engineering term to determine the limit of subsidence trough at the surface. AoD is defined as an angle between the vertical line above an extraction edge and the inclined line joining the extraction edge with the edge of the subsidence trough (see Figure 1.11). The surface subsidence of less than 2-5 cm is generally accepted as a value that have no effect on any man-made structures and surface environments. This value is normally adopted as the cut-off point for determination of the AoD (Holla & Barclay, 2000; MSEC, 2007; IESC, 2015). AoD value depends upon the strata strength and the mining depth, typically ranges from a few degrees (near-vertical step at the panel edge) up to 60 degrees, but is most commonly in the range of 10 to 35 degrees (MSEC, 2007). The magnitude of the AoD varies widely among the coalfields. Whittaker and Reddish (1989) recorded the variation in draw-angles for different coalfields such as 32-38 degrees (Yorkshire Coalfield, U.K), 35-40 degrees (South Limburgh Coalfield, U.K), 4-21 degrees (Indian coalfields), 12-34 degrees (US coalfields), and 25-30 degrees (Czechoslovakian coalfields). Holla and Barclay (2000) also reported the draw angles of 2-56 degrees which obtained from the Southern Coalfield of New South Wales. In general, when a coal panel is mined at a shallow depth, or below strong overburden rocks, the AoD will be small. In contrast, when a coal panel is extracted beneath weak overlying strata, or at a deeper depth, the AoD will be larger (IESC, 2015).

Surface subsidence is considered as a geotechnical issue in longwall mining. The subsidence mitigation is of particular important, especially when coal panels are extracted under protected forests, agricultural areas, residential areas, and man-made structures. Partial extraction and backfilling application are common subsidence mitigation measures worldwide (IESC, 2015). The partial extraction is the most common longwall subsidence mitigation measure used in Australia, it is also known as shortwall or miniwall mining system. Narrow panels are extracted between wide pillars with the aim of keeping the panel width small to ensure little or no caving and roof fracturing occurs, and surface movement is small. Backfilling or stowing of goaf is to prevent the subsidence has been carried out at many

coalfields in Australia and China. Chinese and Australian experiences suggest that vertical movement can be reduced from 30 to 60 percent of the seam thickness with backfilling. Generally, three backfilling techniques are in use now a day which include solid backfilling, paste backfilling, and hydraulic backfilling. The favoured backfill material in China is a low moisture content paste. The material is made up of fly ash and fine coal washery reject which is extruded and compacted behind the longwall face supports in a continuous operation. The backfill primarily supports the seam roof, but it has a secondary role of proving lateral support for pillars.

Researches on longwall coal mining, particularly the analysis of the roadway stability and prediction of surface subsidence have been discussed for decades. Empirical and numerical methods are the common methods that used as the tools for a design of the roadway supports, and to predict the degree of surface subsidence. Empirical methods require a large database of case histories. Empirical methods have been developed based on numerous field measurements of the similar mine environments. The limitation of using the empirical methods is that they are very much site-dependent, and cannot be applied to the mine sites that have different geological and mining conditions (Elashiry, Gomma, & Imbaby, 2009; Xu et al., 2013). Therefore, numerical simulation methods using advanced computer softwares are widely used as alternative techniques to empirical methods. The methods are superior in analyzing the roadway stability and predicting the ground subsidence for complicated mining and geological conditions than empirical methods. The numerical methods can be used in any mining environments, at least if the reliable input data such as mechanical properties of rock mass, in-situ stresses, and stratigraphic columns of mine sites are available (Villegas, 2008; Iwanec, Carter, & Hambleton, 2016). At present, a vast number of different numerical methods are available. The continuum and discontinuum numerical methods have gained widely popularily in academic researches and in engineering practices. Discontinuum method is well suited for rock mass where high density of discontinuities (e.g. joints) exists, and plays a significant role on the geotechnical behavior of the rock mass. However, the method requires higher expertise to build up a representative model by discontinuum codes, and the computing time takes much longer than that it takes in the continuum codes. The discontinuum numerical

method includes distinct element codes such as UDEC, 3DEC, etc. Continuum method is well suited for the analyzing the rock formations that are comprised of massive, intact rock, weak rocks, and soil-like, or heavily fractured rock masses. The continuum numerical approach generally consists of finite element method (FEM), finite different method (FDM), and boundary element method (BEM) (Nay et al., 2014).

1.3. Objective of Research

Many surface mines in Indonesia are abandoned due to the uneconomic stripping ratio as the mining depth increases. The environmental impacts and protections have challenged the new development of surface mines. Therefore, in order to meet the increased demand of coal, and to ensure the continuous coal export capability of the country, underground coal mines have to be developed.

According to the experiences of underground coal mining in Indonesia, the roof fall and large deformation of the roadway frequently occur even though the Australian roof support system is adopted. Some of the major reasons are very weak mechanical properties of coal measure rocks. As a result, some underground mines have been abandoned. In addition, since no any appropriate design guidelines of underground mining, particularly longwall mining under weak ground conditions have been developed so far, therefore, the application of longwall mining in Indonesia still remains a challenge. From these backgrounds, the primary objective of this research is to develop the design guidelines of underground mining system for longwall coal mine under weak geological conditions. The results of this research would help the underground coal mines in Indonesia and other countries to extract the coal more efficient, economical, and safe, and in an environmentally friendly fashion.

To meet the research objectives, the PT Gerbang Daya Mandiri (GDM) underground coal mine in East Kalimantan, Indonesia is selected as a representative research mine site. The current situation of the main roadway stability at the shallow depth, the stability and support system of the main roadway prior to longwall mining at the deeper depth, the effect of coal panel extraction on gate and main roadway stabilities, and the surface subsidence induced by longwall mining, are

studied by means of numerical simulation using finite difference code software, FLAC3D.

1.4. Outline of Research

The following chapters are included in this dissertation:

Chapter 1 introduces the background of this research, geotechnical issues and technology related to longwall mining method, and objectives and outlines of the dissertation.

Chapter 2 describes the conditions of PT Gerbang Daya Mandiri (GDM) mine site. Furthermore, this chapter also discusses the current situation of the main roadway stability at the shallow depth.

Chapter 3 focusses on the stability analysis and support design of the main roadway prior to longwall mining at the deeper depth. The stability of the main roadway at GDM coal mine under various depths and stress ratios is studied, and the appropriate support system is discussed by means of numerical simulations.

Chapter 4 studies the effect of longwall mining on the stability of main and gate roadways. In this chapter, a series of numerical simulations of longwall mining with different barrier/chain pillar and panel widths are conducted at various depths, and the appropriate barrier and chain pillar widths are suggested to maintain the main and gate roadways for each panel width and mining depth.

Chapter 5 discusses the surface subsidence induced by longwall mining at GDM coal mine. The characteristics of surface subsidence induced by single-panel and multi-panel longwall mining are studied, and some countermeasures for controlling the subsidence are investigated by means of numerical simulations.

Chapter 6 summarizes the conclusions of each chapter.

References

Bieniawski, Z. T. (1997). Estimating the strength of rock materials. Journal of the South African Institute of Mining and Metallurgy, 312-320.

Brady, B. H. G., & Brown, E. T. (2004). Rock mechanics for underground mining (3rd Ed.). Dordrecht.

Bai, Q. S., Tu, S.H., Wang, F.T., Zhang, X.G., Tu, H.S., & Yuan, Y. (2014) Observation and numerical analysis of the scope of fractured zones around gateroads under longwall influence. International Journal of Rock Mechanics Engineering, 47, pp. 1939-1950.

Colwell, M., Frith, R., & Mark, C. (1999). Analysis of longwall tailgate serviceability (ALTS): A chain pillar design methodology for Australian conditions. Proceedings of the Second Internation Workshop on Coal Pillar Mechanics and Design.

Chen et al. (2013). Extraction system and slope stability analysis for remaining coal around end-wall slope at open pit mines in China (Doctoral dissertation). Kyushu University, Fukuoka, Japan.

Elashiry, A. A., Gomma, W. A., & Imbaby, S. S. (2009). Numerical modelling of surface subsidence induced by underground phosphate mines at Abu-Tatur area. Journal of Engineering Sciences, Assiut University, 37(3), 699-709.

EMFI (Energy and Minerals Field Institute). (2011). Coal mining method. Colorado School of Mines, Golden, Colorado, USA.

Garcia, A., Altounyan, P., Nitaramorn, A., & Lewis, A. (2010). Ground control aspects of a successful underground coal mine trial in weak strata in Indonesia. Proceeding of the 29th International Conference on Ground Control in Mining, pp. 1-9.

Hamrin, H. (1986). Underground mining methods and applications. Atlas Copco, Stockholm, Sweden.

Hoek, E., & Wood, D.F. (1987). Support in underground hard rock mines. Underground Support Systems, 35, pp. 1-6.

Hudson, J. A. (1993). Comprehensive Rock Engineering. Pergamon Press.

Hoek, E., Kaiser, P. K., & Bawden, W. F. (1993). Support of underground excavations in hard rock. West Broadway Professional Centre, Vancouver, British Columbia.

Hoek, E., & Brown, E. T. (1997). Practical estimates of rock mass strength. International Journal of Rock Mechanics and Mining Sciences, 34(8), 1165-1186.

Hebblewhite, B. K., Galvin, J.M., & Vasundhara. (1999). Barrier and chain pillar design research outcomes: Angus Place Golliery. Australian Geomechanics, the University of NSW.

Hartman, H. L., & Mutmansky, J.M. (2002). Introductory mining engineering. 2nd edition, Hoboken, New Jersey, John Wiley and Sons.

Holla, L., & Barclay, E. (2000). Mine subsidence in the Southern Coalfields. Report to the department of Mineral Resources NSW.

Hoek, E. (2006). Practice rock engineering. North Vancouver, B. C., Canada V7R 4X1.

IESC (Independent Expert Scientific Committee). (2015). Monitoring and management of subsidence induced by longwall coal mining activity. GPO Box 787 Canberra ACT 2601, Australia.

Iwanec, A. M. S., Carter, J. P., & Hambleton, J. P. (2016). Geomechanics of subsidence above single and multi-seam coal mining. Journal of Rock Mechanics and Geotechnical Engineering, 8(3), 304-313.

Indonesia-Investments. (2016). Coal in Indonesia. Retrieved from http://www.indonesia-investments.com/business/commodities/coal/item236

Keilich, W., Seedsman, R. W., & Aziz, N. (2006). Numerical modelling of mining induced subsidence. Coal Operators' Conference, University of Wollongong, Australia, 313-326.

Lehmann, C., & Konietzky, H.H. (2015). Geomechanical issues in longwall mining-an introduction. TU Bergakademie Freiberg, Geotechnical Institute.

Matsui, K., Shimada, H., Furukawa, H., Kramadibrata, S., an& Anwar, H.Z. (2003) Ground control problems and roadheader drivage at Ombilin coal mine, Indonesia. Proceeding of the 18th International Mining Congress and Exhibition of Turkey-IMCET.

MSEC (Mine Subsidence Engineering Consultants). (2007). Introduction to longwall mining and subsidence. PO Box 3047 Willoughby North NSW 2068, Australia.

Manteghi, H., Shahriar, K., & Torabi, R. (2012). Numerical modelling for estimate of first weighting distance in longwall coal mining-a case study. Coal Operators' Conference.

Nay et al. (2014). Mining system and design for development of underground coal mine from open-cut highwall for thick coal seam (Doctoral dissertation). Kyushu University, Fukuoka, Japan.

Peng, S. S., & Chiang, H. S. (1984). Longwall mining. John Wiley & Sons.

PB (Parsons Brinckerhoff). (2007). Literature Review on Longwall Mining. Sydney, Australia.

Singh, R. N. (1986). Mine Inundations. International Journal of Mine Water, 5, pp. 1-28.

Sadisun, I. A., Shimada, H., Ichinose, M., & Matsui, K. (2004). Textural and mineralogical properties of argillaceous rocks in relation to their propensity to slaking. The 4th Asian Symposium on Engineering Geology and Environment, Hong Kong.

Sasaoka, T., Shimada, H., Ichinose, M., Matsui, K., Kramadibrata, S., Sulistianto, B., & Watinena, R. (2007). Improvement of roof support system at a new underground coal developed from open-cut highwall in Indonesia. Proceeding of the 26th International Conference on Ground Control in Mining, 122-128.

Sahebi, A., Jalalifar, H., & Ebrahimi, M. (2010). Stability analysis and optimum support design of a roadway in faulted zone during longwall face retreat-case study: Tabas Coal Mine. Coal Operators' Conference.

Shabanimashcool, M., & Li, C.C. (2012). Numerical modelling of longwall mining and stability analysis of gates in a coal mine. International Journal of Rock Mechanics and Mining Sciences, 51, pp. 24-34.

Sasaoka, T., Shimada, H., Zarlin, N., Takamoto, H., Matsui, K., Kramadibrata, S., & Sulistianto, B. (2014). Geotechnical issues in the application of rock bolting

technology for the development of underground coal mines in Indonesia. International Journal of Mining, Reclamation and Environment, 28(3), 150-172.

Sasaoka, T., Shimada, H., Hamanaka, A., Sulistianto, B., Ichinose, M., & Matsui, K. (2015a). Geotechnical issues on application of highwall mining system in Indonesia. Vietrock 2015 an ISRM Specialized Conference, Hanoi, Vietnam.

Sasaoka, T., Takamoto, H., Shimada, H., Oya, J., Hamanaka, A., & Matsui, K. (2015b). Surface subsidence due to underground mining operation under weak geological in Indonesia. International Journal of Rock Mechanics and Geotechnical Engineering, 7(3), 337-344.

Takamoto, H., Sasaoka, T., H., Shimada, H., Oya, J., Hamanaka, A., & Matsui, K. (2014). Study on surface subsidence due to longwall mining operation under weak geological condition in Indonesia. Proceeding of the Chinese International Conference on Ground Control in Mining, China, 177-182.

Villegas, T. (2008). Numerical analyses of the hangingwall at the Kiirunavaara Mine (Master's thesis, Lulea University of Technology, Lulea, Sweden).

Whittaker, B. N. (1974). An appraisal of strata control practice. Mining Engineering, 134, pp. 9-24.

Whittaker, B. N., & Reddish, D. J. (1989). Subsidence: Occurrence, prediction and control. Amsterdam, The Netherlands.

Xu, N., Kulatilake, P. H. S. W., Tian, H., Wu, X., Nan, Y., & Wei, T. (2013). Surface subsidence prediction for WUTONG mine using a 3-D finite difference method. Journal of Computers and Geotechnics, 48, 134-145.

Yasitli, N. E., & Unver, B. (2005). 3D numerical modeling of longwall mining with top-coal caving. International Journal of Rock Mechanics and Mining Sciences, 42(2), 219-235.

Zhang, C., Mitra, R., & Hebblewhite, B. (2006). Numerical modeling of mining subsidence in the Southern Coalfield of New South Wales, Australia. FLAC/DEM Syposium, An Itasca International Company.

CHAPTER 2

SITE CONDITIONS OF GDM UNDERGROUND COAL MINE AND ITS CURRENT SITUATION OF MAIN ROADWAY

2.1. Site Conditions of GDM Underground Coal Mine

2.1.1. General Information of GDM Underground Coal Mine

PT Gerbang Daya Mandiri (GDM) underground coal mine is selected as a representative mine in this research, in order to develop the appropriate design guideline of underground mining system for longwall coal mine under weak ground conditions. GDM coal mine is a new underground coal mine which is still in the process of developing the main roadways. It is located in Kutai Kartanegara, about 15 km north of the Samarinda City of East Kalimantan, Indonesia. Figure 2.1 shows the location map of GDM coal mine. GDM Company has conducted the exploration for underground mining from June 2010 to May 2011. The geological and recoverable sub-bituminous coal reserves are approximately 58.3 million tons and 29.2 million tons, respectively. The annual coal production of this company has been planned for 1 million tons during its mine lifetime by a longwall mining method.

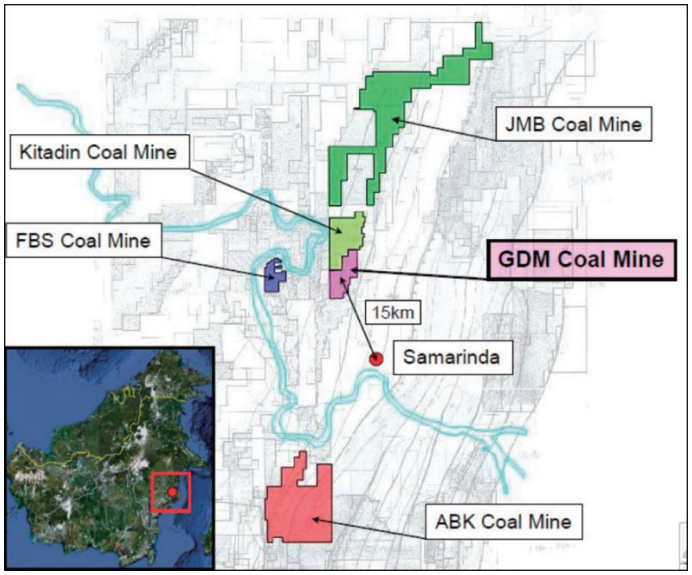

Figure 2.1 Location of GDM coal mine.

Figure 2.2 illustrates the planned layout of main roadways and longwall panels of GDM coal mine. Two main roadways namely North and South Roadway, are being excavated by using the road header machine to access the coal seams (see Figure 2.3). The main roadway excavation commenced in April 2014 from the final highwall of the surface mine. The total height of the final highwall is about 15 m from the ground surface. The main roadways are designed using semi-circular shape with 5 m in width, 3 m in height, and 6^{o} dip. The total heading length of each roadway is about 350 m where the overburden thickness above a current excavation face is 40 m approximately. The main roadways are currently stable at the shallow depth with the occurrence of some cracks and rock mass deformations along the roof and sidewalls. These rock failures are well supported by the steel arches. Additionally, the width of coal panel and chain pillar is initially designed as 130 m and 30 m, respectively in this underground coal mine.

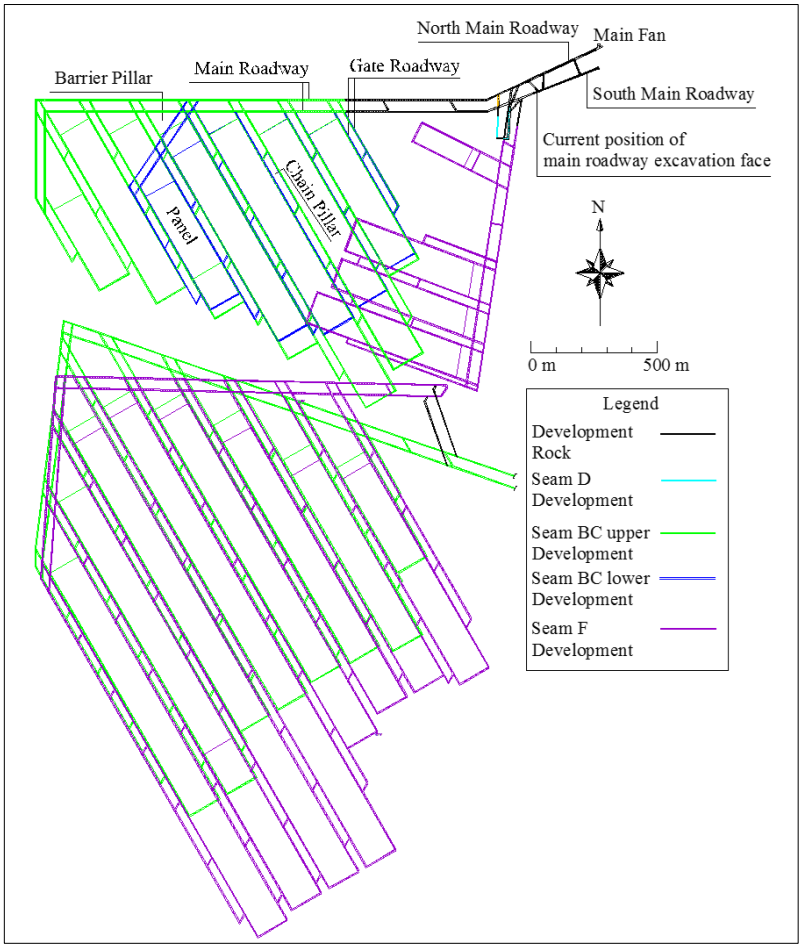

Figure 2.2 Mine layout of GDM underground coal mine.

Figure 2.3 South Main Roadway of GDM coal mine.

2.1.2. Geological Conditions of GDM Underground Coal Mine

The GDM coal mine is situated in the Kutai Tertiary Basin. Balikpapan Formation and Pulau Balang Formation are the major coal-bearing formations in this basin (see Figure 2.4). Balikpapan Formation consists of dark to light gray mudstone, dark to brownish-gray sandstone, dark to light gray siltstone and claystone, coal, and coaly shale. Pulau Balang Formation mainly composes of mudstone, sandstone, siltstone, coal, and coaly shale. In Pulau Balang Formation, mudstone is dark to light gray in color. Sandstone is dark to whitish-gray and brownish-gray, the grain size is very fine to coarse. Siltstone is dark gray to light gray. The fault was not found in GDM coal mine. Geological structure is simple monocline structure. GDM coal consists of several seams which are part of the Kutai Basin with the dip ranging from 3^{o} to 13^{o}, and the coal seam thickness varies from 0.15 m to 9.8 m. The cross-section of coal seams and the typical stratigraphy of GDM underground mine is shown in Figures 2.5 and 2.6, respectively. The major mineable seams for underground mining are found in Seam BC and Seam F. The thickness of Seam BC varies from 3.39 m to 9.80 m, whereas the thickness of Seam F varies from 0.70 m to 3.20 m. The coal seams are separated by the layers of claystone and sandstone. Claystone is a dominant rock unit in GDM coal mine.

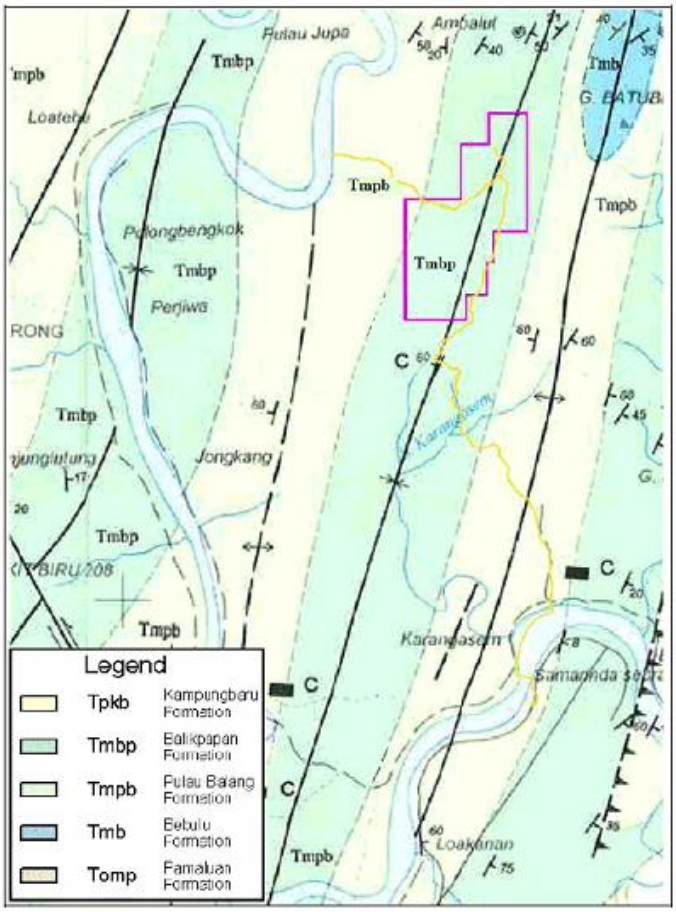

Figure 2.4 Geological map of GDM coal mine.

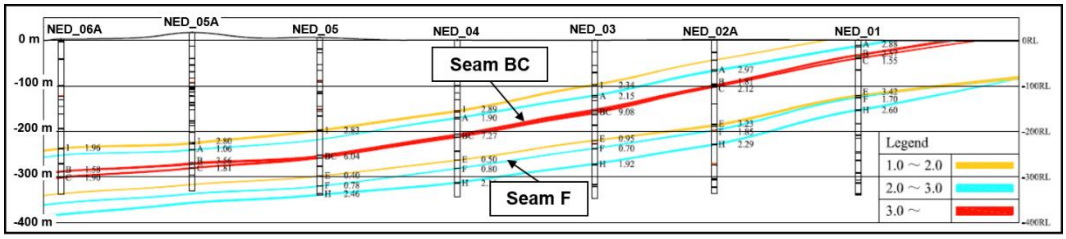

Figure 2.5 Cross-section of coal seams of GDM coal mine.

Figure 2.7 illustrates the relationship between uniaxial compressive strength (UCS) and Young's modulus of rock and coal. These results were obtained from laboratory tests of the rock and coal samples which were collected from boreholes at different depths. Based on the laboratory test results, the rock and coal in this underground mine are classified into weak and low strength rocks as the UCS values are mostly below 25 MPa (Bieniawski, 1974; Hoek & Brown, 1997).

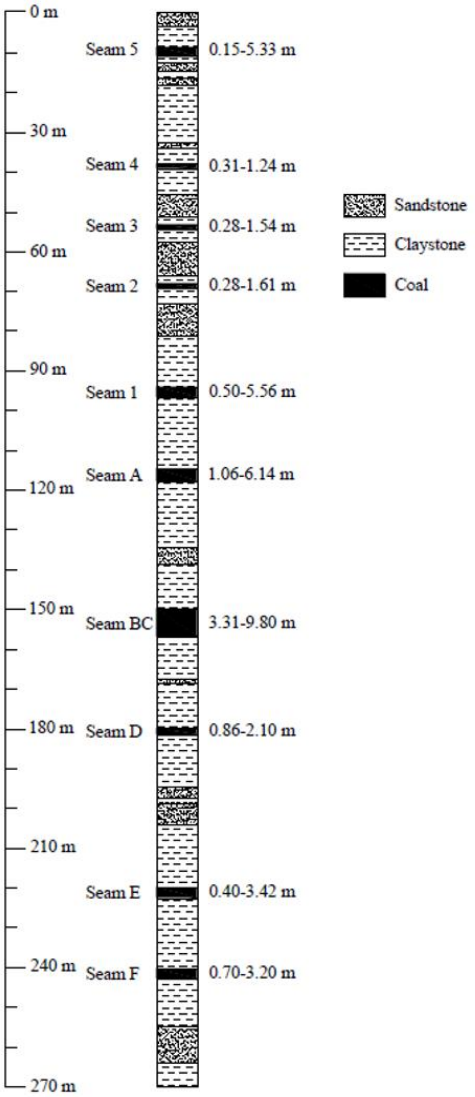

Figure 2.6 Stratigraphic column of GDM.

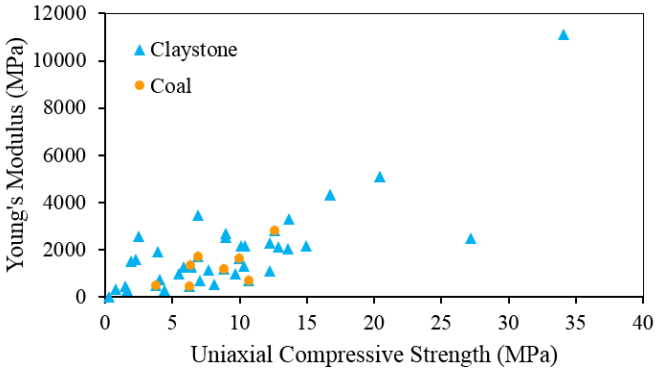

Figure 2.7 Relationship between uniaxial compressive strength and Young's modulus of claystone and coal of GDM coal mine.

In GDM coal mine, the coal quality analysis of the targeted coal seams was carried out using the core samples. Table 2.1 shows the results of the coal quality analysis (average grade) for Seam BC and Seam F. Based on the analyzed results, it can be said that the coal of GDM coal mine has a good quality. The coal contains low ash content of 3.40-5.00 %, low sulfur content of 0.18-0.75%, and high calorific value of 6,108-6,218 kcal/kg.

Table 2.1 Coal quality of GDM coal mine.

Seam	Total moisture (%)	Inherent moisture (%)	Ash content (%)	Volatile matter (%)	Fixed carbon (%)	Total sulfur (%)	Calorific value, GCV (kcal/kg)	HGI
BC	14.7	11.0	3.4	40.80	44.70	0.18	6,108	47
F	13.5	10.9	5.0	42.02	42.53	0.75	6,218	47

2.1.3. Challenges for Developing Underground Coal Mine at GDM Mine Site

As mentioned in Chapter 1, several coal mines have tried the trial operations for underground mining in Indonesia, such as Satui coal mine and Indominco coal mine. However, these trial underground coal mines were abandoned due to the ground control problems occurred, especially in the main roadway. The reasons for these trial mine failures were weak mechanical properties of rocks and inadequate supports installed in the roadway. The issues learned from the above mentioned coal mines are challenging the mining engineers of GDM coal mine on how to design a proper support system for the roadway and an appropriate mining system for subsidence control. Currently, although the roadways at GDM coal mine are stable, but they are excavated only at a shallow depth without longwall mining effect. As the rocks are very weak, when the roadway excavation moves to a greater depth, and when the longwall mining is started, a series of ground control problems such as roof fall, sidewalls collapse, and floor heave can be expected if no proper support system is anticipated. However, the appropriate support system for the roadway at the deep area is still a doubt. Furthermore, because the overburden strata is poor, a large surface subsidence can be expected when a longwall mining method is applied at

this underground coal mine. The panel width of 130 m and the chain pillar width of 30 m are only initial designs, no any analysis has been conducted to confirm these designs whether they are suitable to prevent the adverse impact of longwall mining on the roadway stability and surface subsidence or not. In addition, as some houses and rice fields exist on the surface above the underground mine, some subsidence controls and mitigation actions have to be provided. However, the methods of subsidence control and mitigation have been still unknown. According to the challenges mentioned above, the appropriate design guideline of mining system for longwall coal mine under weak geological conditions is very necessary to be developed for GDM coal mine. Future underground mining projects in Indonesia would certainly benefit by adopting the techniques which are developed at GDM underground coal mine.

2.2. Current Situation of Main Roadway Stability

Main roadway is the main and first access to the underground mine used for haulage, ventilation, or as a mainway for miners. Instability of the roadway decreases the working safety, or even results in an interruption of underground mining. At GDM underground coal mine, two main roadways namely South and North roadways are being developed from the final highwall of the surface mine using the road header machine. Figure 2.8 shows the current situation of the South roadway development and stability. The roadway is excavated in the shape of semi-circular with 5 m in width and 3 m in height, with the overburden thickness above the current excavation face is 40 m approximately. The steel arch of Japan Industrial Standard 3010 (JIS 3010) is selected as the support system for the main roadway. The steel arches SS400 with 1 m space were immediately installed in the roadway just after the excavation face had been moved forward (see Figure 2.9).

Based on the field observation inside the main roadway, it found that the roadway was excavated mostly in claystone layer, while the roadway excavation in the rock layers between claystone and coal was also observed at some locations. Generally, the roof and sidewalls of roadway are well maintained by the steel arch support, but because no support is installed in the floor, the floor heave of the main roadway was recognized. However, as the roadway is being excavated at the shallow depth,

the heaving of the floor is not a big issue at GDM coal mine, and it is still easy to overcome. Additionally, a water dripping from the roof and sidewalls of the main roadway was observed. As the claystone is very sensitive to the water, the groundwater caused the deterioration in mechanical properties of the claystone, as a result, the large roof displacement of the roadway occurred at some locations.

In GDM coal mine, two monitoring systems were applied for detecting the roof movement of the main roadway, including extensometer and telltale. The roof movements measured from these two monitoring systems show that the large roof movement was detected when the roadway excavation was conducted in the deteriorated claystone layer. Differently, the small roof movement was observed when the main roadway was excavated in the undeteriorated claystone, and the coal layer was present in the roof.

Figure 2.8 Current situation of main roadway stability at GDM coal mine.

Figure 2.10 illustrates the measurement data of main roadway displacement obtained from extensometer monitoring system. The Extensometer 31 shows the

roof displacement of the roadway excavated in the undeteriorated claystone, whereas the Extensometer 29 shows the roof displacement of the roadway excavated in the deteriorated claystone, respectively. The displacement of the roof was measured for one month. It was found from the measurement data that although the Extensometer 29 and 31 were installed at the same depth, 40 m depth approximately, but the roof displacements obtained from these two locations are obviously different. The roof displacement of about 23 mm was obtained from the Extensometer 31, while the roof displacement of about 83 mm was obtained from the Extensometer 29. The reason of this difference of roof displacement assumed to be deterioration of the claystone caused by groundwater. From the results, therefore, it can be said that the geological condition of the claystone has an obvious impact on the stability of the roadway. More attention must be paid on the support design of the main roadway when the excavation is made in deteriorated claystone layer. The roadway near the Extensometer 31 could be maintained by current support system using the steel arch SS400 (yield strength 319 MPa) with 1 m space. On the other hand, to maintain the main roadway near the Extensometer 29, the GDM has adopted the stronger steel arch SS540 (yield strength 551 MPa), and decreased the space of the steel arch from 1 m to 0.5 m.

Figure 2.9 Steel arch support installed in main roadway at GDM coal mine.

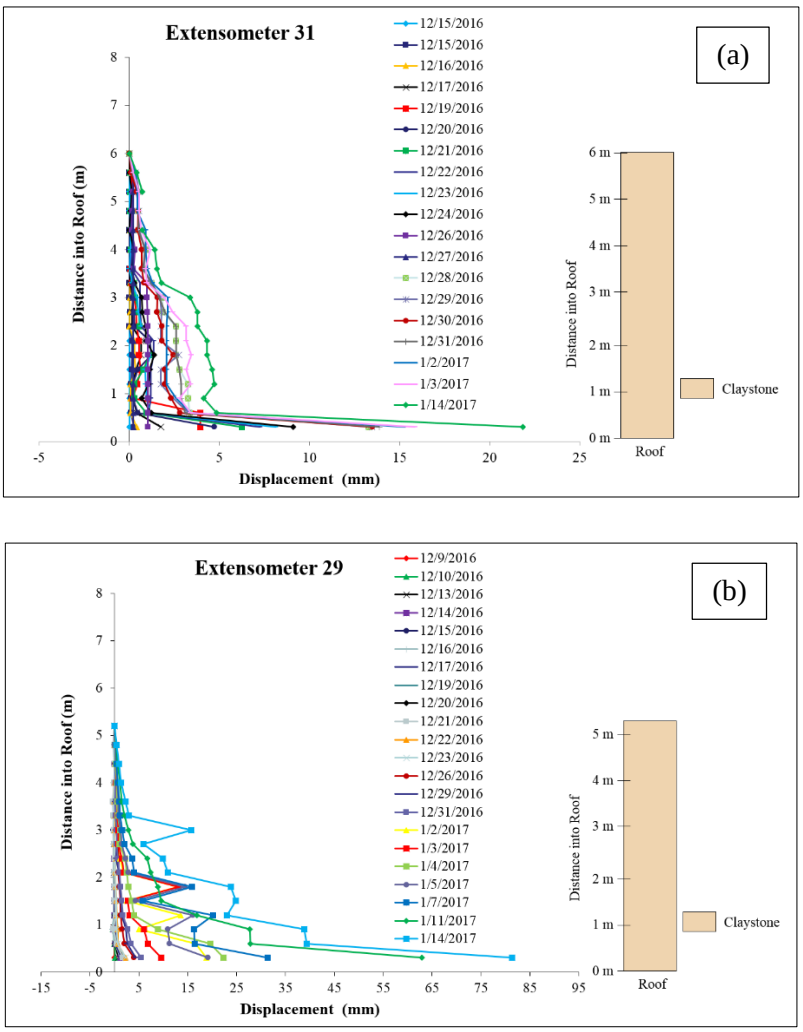

Figure 2.10 Comparison of field measurement data of roof displacement between roadway excavations in undeteriorated and deteriorated claystone (a) undeteriorated claystone (b) deteriorated claystone.

Figure 2.11 demonstrates the results of Telltale monitoring system of the roof displacement of the roadway under different roof conditions. The measurement data of Telltales 25, 29, and 28 show the roof displacement of main roadway under the conditions of no coal layer, 0.5 m thick coal layer, and 1 m thick coal layer in the roof, respectively. The displacement of the roof was measured for one month. From the measured field data, it was found that the large roof displacement occurred when the roadway was excavated in claystone layer only. Differently, the small roof displacement occurred when the coal layer was present in the roof. In addition,

smaller displacement of the roof was observed when a thicker coal layer was present in the roof. The total roof displacement obtained from Telltale 25, 29, and 28 was about 90 mm, 4.5 mm, and 1.5 mm, respectively. From these trends, it can be considered that the presence and thickness of the coal layer in the roof have an obvious impact on the stability of the main roadway. It is necessary to design the support sufficiently considering each condition.

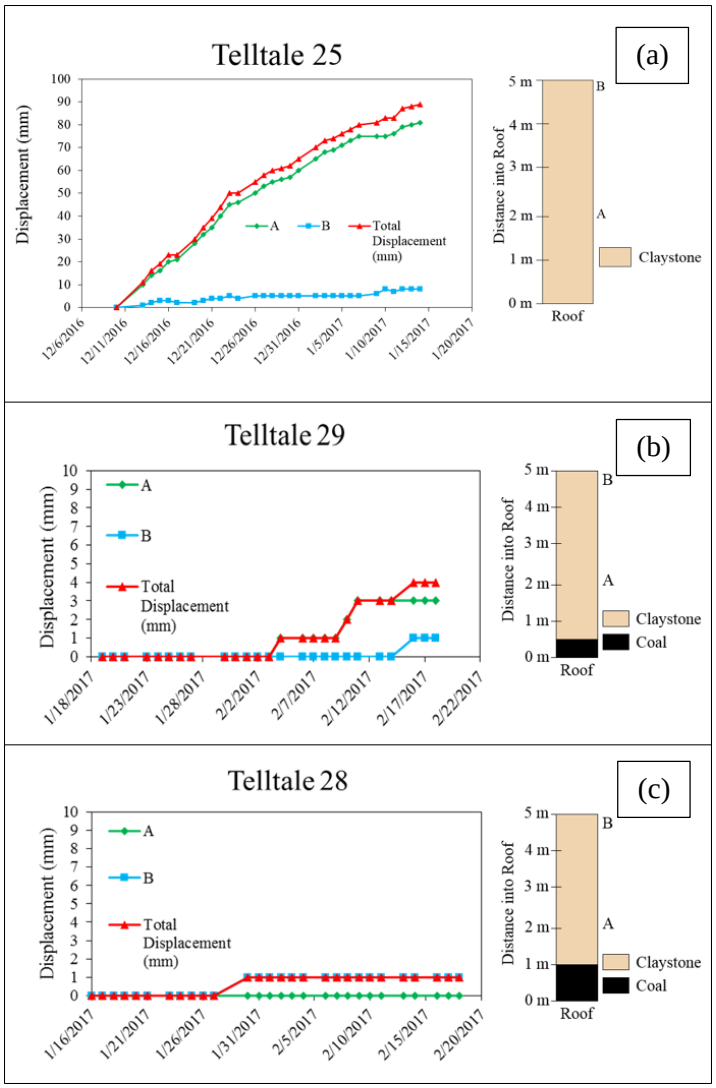

Figure 2.11 Telltale measurement data of roof displacement of main roadway under different roof conditions (a) no coal layer in roof (b) 0.5 m thick coal layer in roof (c) 1 m thick coal layer in roof.

Based on the field measurement data, it can be found that the ground behavior of the main roadway varies greatly depending on the conditions of claystone and the

presence of coal layer in the roof. It is clear that a large displacement is expected when the roadway excavation is made in a deteriorated claystone and no coal layer is present in the roof. On the contrary, a small displacement is expected when the roadway is excavated in an undeteriorated claystone and when a coal layer is present in the roof. To clarify the ground behavior of main roadway according to field measurement data, the following sections aim to investigate the ground behavior of the roadway under different conditions of claystone and roof. The numerical simulation method using the three-dimensional finite difference code software, FLAC3D was used for clarification. The results of the study provide the fundamental understanding of the main roadway stability, so that mining engineers can use as the guidelines for determining what geological and excavation conditions that they have to pay more attention on.

2.3. Numerical Analysis

In order to discuss the ground behavior of the main roadway at GDM coal mine, several numerical models were conducted in FLAC3D with different overburden depths ranging from 10 m to 40 m. Figure 2.12 demonstrates an example of a numerical model with 40 m overburden depth. The model is 150 m in width, 155 m in length, and 140 m in height. The bottom of the model was fixed in the vertical direction, the sides were fixed in the horizontal direction, and the surface was free in all directions. The roadway was modelled as semi-circular in shape with 5 m in width and 3 m in height. As the steel arch is the primary support system used in this mine, hence, the application of steel arch support for stability control of the main roadway was simulated numerically. According to the UCS values of claystone obtained from this underground coal mine, the rocks near the surface were much weaker than those at the deeper sites due to the weathering. Thus, very weak mechanical properties of claytone were used for the main roadway analysis at the shallow depth. Tables 2.2 and 2.3 show the mechanical properties of claystone and steel arch, respectively. In simulation, the vertical stress component was modeled as a function of the overburden thickness ($P_v = \gamma H$, γ is unit weight of overburden and H is overburden depth) (Hoek & Brown, 1980; Hoek, Kaiser, & Bawden, 1993; Hoek, 2006), while the horizontal stress was initialized directly through simple gravity loading. The elasto-plastic Mohr-Coulomb was used as a constitutive model

throughout the analyses. In order to obtain the most precise result of the ground behavior around the main roadway, the lateral and vertical meshes were intentionally made finer around the excavation area than remaining meshes.

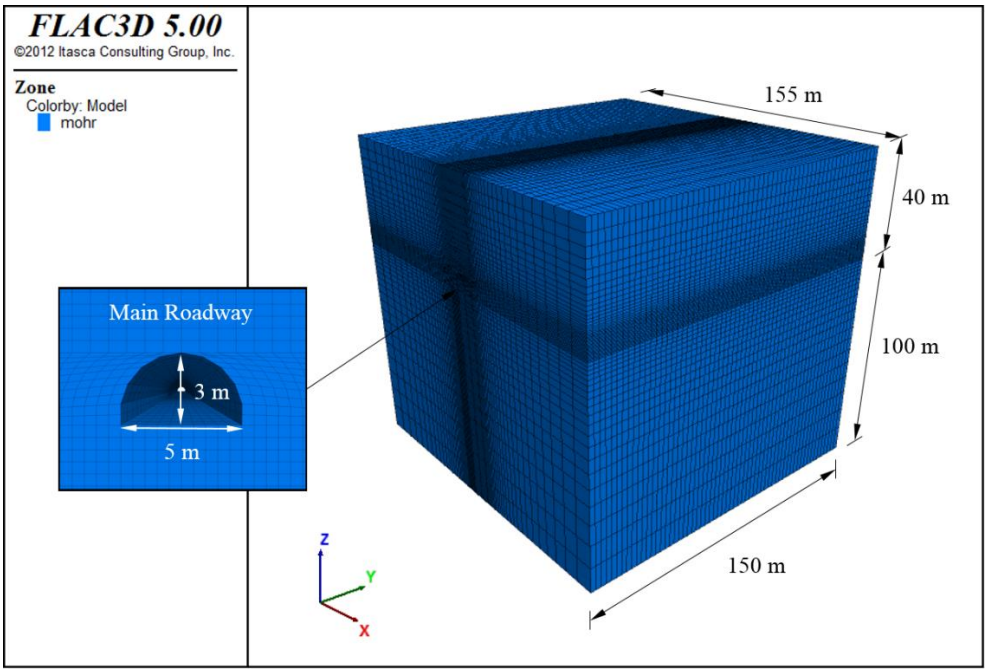

Figure 2.12 Numerical model of main roadway analysis under 40 m overburden depth.

Table 2.2 Mechanical properties of claystone used in main roadway analyses.

Parameter	Value
Uniaxial compressive strength (MPa)	1.12
Density (kg/m^3)	2,140
Young's modulus (MPa)	118.36
Poisson's ratio	0.26
Friction angle (˚)	29.9
Cohesion (MPa)	0.14

Table 2.3 Mechanical properties of steel arch (JIS 3010) used in analyses.

Parameter	Value
Dimension (mm)	95x115
Cross section area (cm^2)	36.51
Young's modulus (GPa)	200
Poisson's ratio	0.30
Yield strength, SS400 (MPa)	319
Yield strength, SS540 (MPa)	551

2.3.1. Slope Stability of Final Highwall at GDM Coal Mine

Before the development of main roadway, it is necessary to investigate the stability condition of the final highwall slope. Unstable final highwall slope will harm the safety of miners and machineries during the roadway excavation. The slope stability of the final highwall of GDM coal mine was analyzed through the factor of safety (FOS) calculation by the strength reduction method in FLAC3D. The overall slope angle and the height of the final highwall was modelled as 20 degrees and 15 m, respectively conforming the real conditions at the mine site. Figure 2.13 shows the contours of shear strain rate. The maximum value of shear strain rate was found at the toe of the final highwall slope. The surface of slope failure was observed propagating circularly from the pit floor to the crest of the slope. Based on the analyzed result, the factor of safety was found as 6.25. Therefore, it can be said that the slope of the final higwall at GDM coal mine is in a stable condition before the development of the main roadway and underground coal mine.

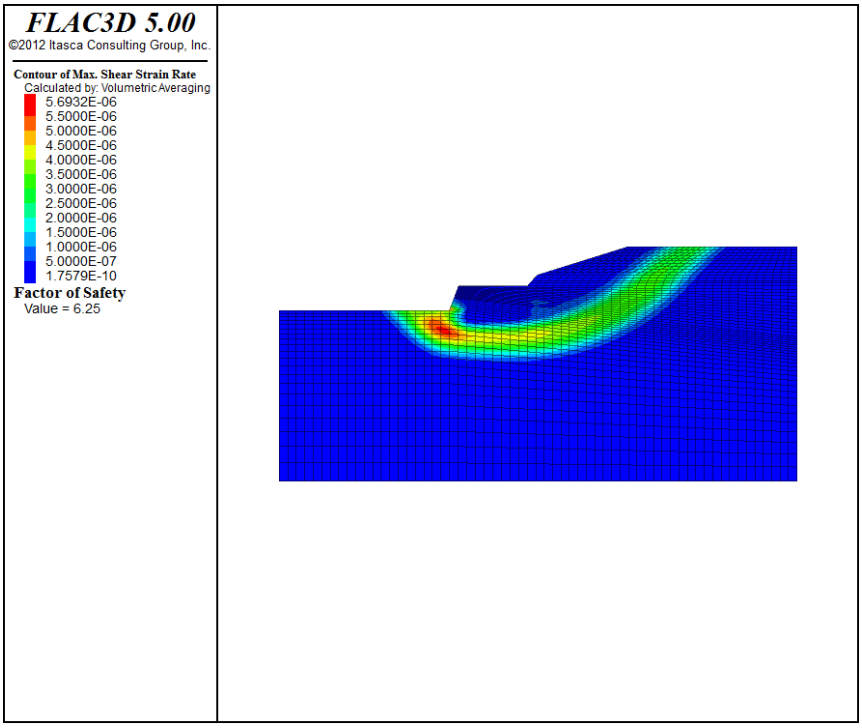

Figure 2.13 Contours of shear strain rate and factor of safety of final highwall slope at GDM coal mine.

2.3.2. Ground Behavior of Main Roadway under Undeteriorated Claystone Conditions

Figures 2.14 and 2.15 show the development of the failure zone and displacement around the main roadway excavated in the undeteriorated claystone under different depths, respectively. In here, the term of failure zone indicates the fractured/failed region induced by the main roadway excavation. This fractured/failed region can potentially fall and create unsafe working conditions for mine workers. The explanations of failure zones given in the legend in FLAC3D are as follows: “none” indicates no-failure zone, “shear-n” indicates the region failed under shear loading, and failure process is still in progress, “shear-p indicates the region failed under shear loading, and failure process is stopped due to lowered amount of shear forces, “tension-n” indicates the region failed under tensile loading, and failure process is still in progress, and the last is “tension-p indicates the region failed under tensile loading, and failure process is stopped due to lowered amount of tensile forces (Yasitli & Unver, 2005).

According to both the Figures 2.14 and 2.15, it can be seen that the overburden depth affected the development of the failure zone and displacement. Under unsupported condition, the failure zone and displacement increased with increasing the overburden depth. This happened because of the increasing of the in-situ stress as the overburden thickness increased. The roadway at a deeper depth will require higher support capacity obviously. Nonetheless, after the roadway was maintained by steel arch SS400 with 1 m space, the failure zone and displacement reduced significantly. It can be said that the current support system works well to control the failure zone and displacement of the roadway under undeteriorated conditions of claystone.

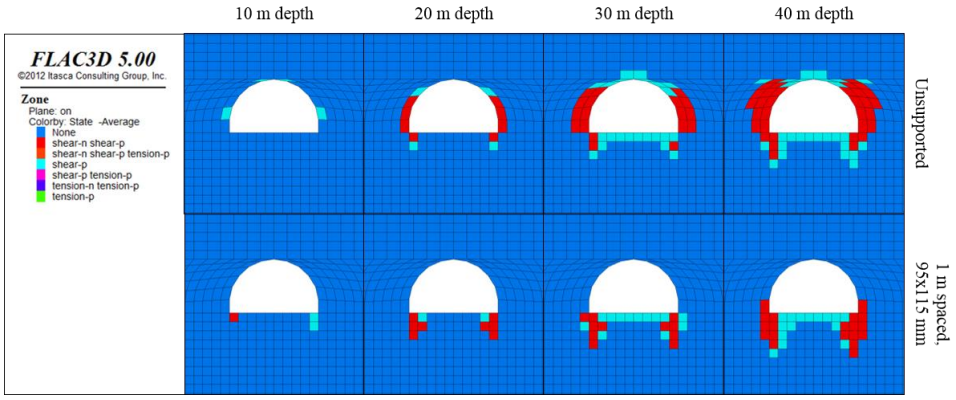

Figure 2.14 Failure zone around main roadway under different overburden depths.

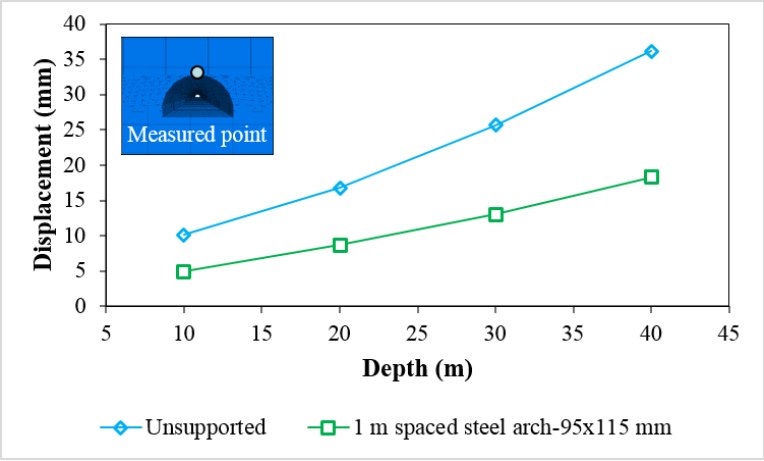

Figure 2.15 Displacement of main roadway under different overburden depths.

Figure 2.16 shows a comparison between numerical simulation results and field measurement data of the roadway displacement. The comparison was made in the

case of the roadway excavation in the undeteriorated claystone under 40 m depth, and the roadway was supported by steel arches with 1 m space. From these figures, it can be seen that the ground behavior of main roadway was well simulated. The simulated results are in good agreement with the field measurement data. The roof displacement obtained from both methods occurred largely near the roofline, and it gradually decreased with increasing the distance into the roof. Therefore, it can be said that the numerical simulation method using finite difference code FLAC3D is capable to study the ground behavior of the roadway in GDM underground coal mine.

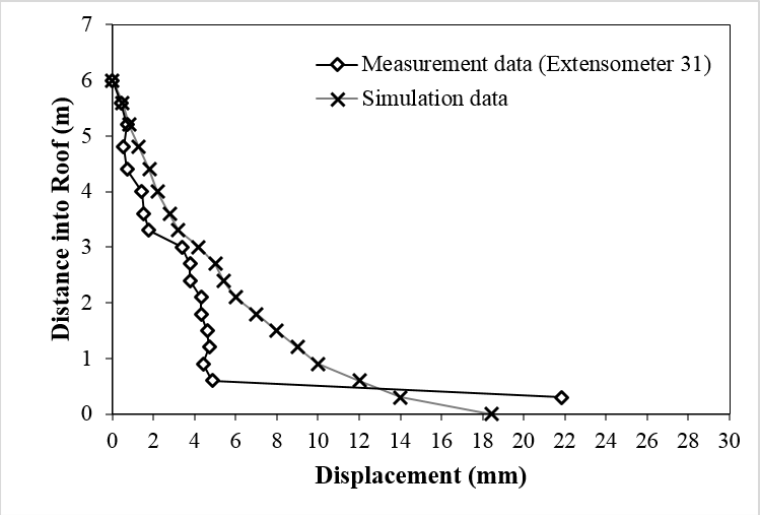

Figure 2.16 Comparison of field measurement data and simulation results of main roadway displacement.

As a steel arch is the support applied to stabilize the roadway at GDM coal mine, the stress occurring on the steel arch is apparently caused by the roadway excavation. Hence, analysis of the steel arch axial stress can be a proper method for evaluating the stability of the main roadway. The definition of the steel arch axial stress is given as the stress which is accumulated in the steel arch axially due to acted forces induced by the excavation. If it exceeds the maximum yield strength of the steel arch, the steel arch may start to deform. Figure 2.17 shows the simulated results of steel arch axial stress of the support installed in the roadway. From this figure, when the roadway was excavated in undeteriorated claystone, the steel arch SS400 support with 1 m space could only stabilize the main roadway until 35 m

depth, and it will be difficult to maintain the roadway at a deeper depth. An application of a closer spaced steel arch (0.5 m space) was investigated. It was found that the steel arch SS400 with 0.5 m space could stabilize the roadway deeper than 40 m depth. This indicates that a decrease in steel arch space significantly improves the stability of the main roadway.

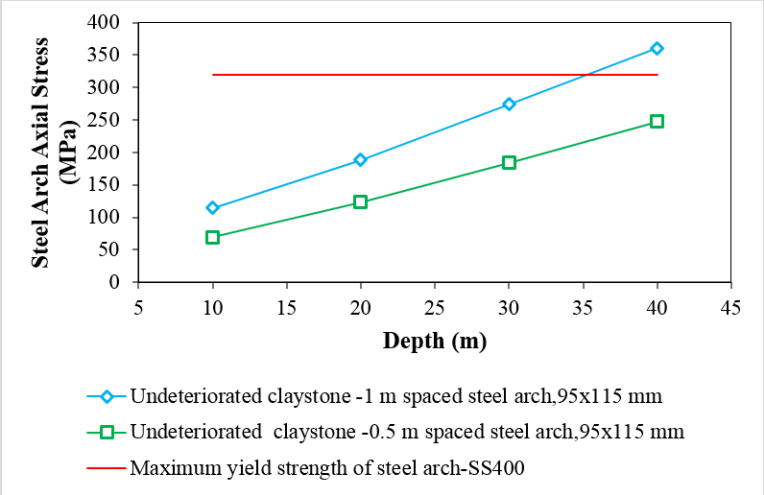

Figure 2.17 Simulated results of steel arch axial stress for main roadway excavation under undeteriorated claystone conditions.

2.3.3. Ground Behavior of Main Roadway under Deteriorated Claystone Conditions

As a great deal of the groundwater was observed inside the roadway, the mechanical properties of claystone are prone to the deterioration due to water. The failure zone and displacement may expand considerably. To investigate the ground behavior of main roadway under this condition, hence, the following equations were used in the analyses in order to understand the deterioration in the mechanical properties of claystone caused by groundwater (Ichinose, Uchino, & Matsui, 1989). The properties of deteriorated claystone are summarized in Table 2.4.

$$S_c' = 0.386 S_c \quad (2.1)$$

$$E' = 0.144 E \quad (2.2)$$

Where S_c is uniaxial compressive strength under dry condition, S_c' is uniaxial compressive strength after curing in water, E is Young's modulus under dry condition, and E' is Young's modulus after curing in water.

Figures 2.18 and 2.19 illustrate the development of failure zone and displacement of the roadway by taking the deterioration of claystone due to groundwater into account. The roadway was supported by 1 m spaced steel arches in the simulations. Compared with the roadway excavated in undeteriorated claystone layer, the failure zone and displacement expanded dramatically. Under 40 m depth, the displacement increased largely from 18.29 mm to 116.43 mm. The results indicate that the current support system may not work effectively, and the collapse of roof and sidewalls can potentially happen in this situation. According to the field measurement data of the roof displacement of the main roadway excavated under undeteriorated and deteriorated claystone conditions (see Figure 2.10), the measured field data support the numerical simulation results. The similar thing happened in the field as that resulted in the simulation. Therefore, it can be said that the mechanical conditions of claystone have a significant impact on the stability of the main roadway, more attention must be paid on the stability control of the roadway when the excavation is made in deteriorated claystone layer. The deterioration of the claystone due to water can be controlled by the introduction of an appropriate drainage system. By applying drainage system, the stability of the roadway will be maintained in a better condition. Moreover, in order to improve the stability of the roadway under deteriorated conditions of claystone, the modification of the support system must be made. The steel arch with closer space (0.5 m space) should be installed, or a stronger steel arch support (steel arch SS540, yield strength 551 MPa) should be applied. However, these improvements of support system can be very costly. On the other hand, in the case where the large roof displacement occurs continuously, it may be hard to stop the movement although the improvement of support system has been done. Under this condition, the deformed part of the roadway must be excavated and removed, and the support must be reinstalled. The activities will be repeated once the large displacement occurs. However, this method may be good for the economical point of view in term of support system, but it can disturb the production rate of the mine as it needs times to complete such those activities.

Table 2.4 Mechanical properties of deteriorated claystone used in main roadway analyses.

Parameter	Value
Uniaxial compressive strength (MPa)	0.43
Density (kg/m^3)	2,160
Young's modulus (MPa)	17.04
Poisson's ratio	0.26
Friction angle (˚)	25.9
Cohesion (MPa)	0.10

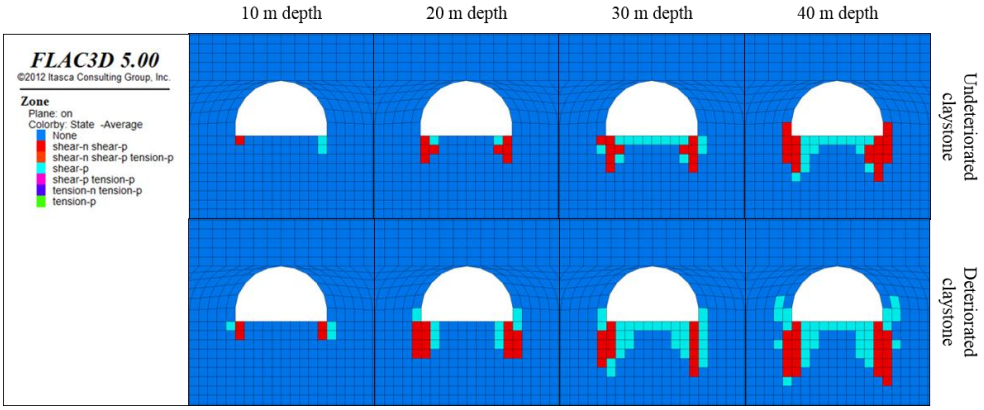

Figure 2.18 Comparison of failure zones between roadway excavations in undeteriorated and deteriorated claystone.

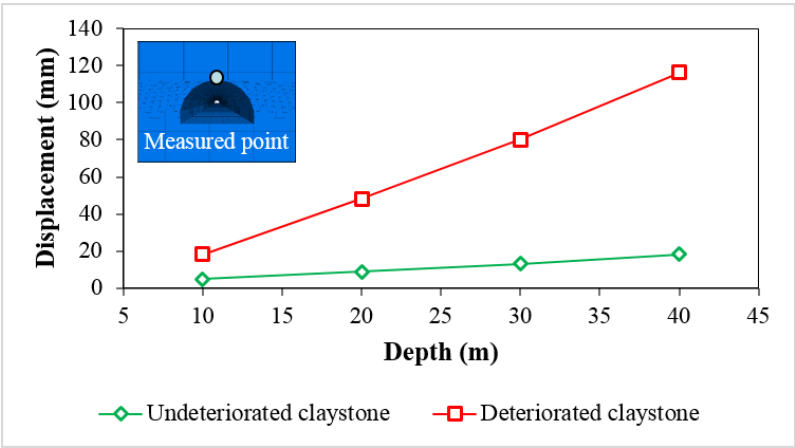

Figure 2.19 Comparison of roof displacements between roadway excavations in undeteriorated and deteriorated claystone.

Figure 2.20 shows the simulated results of steel arch axial stress of the support installed in the roadway. From this figure, when the roadway excavation was made in deteriorated claystone, it would be very hard to control the roadway stability by the steel arch SS400. The steel arch SS400 could only maintain the roadway until 28 m depth although the 0.5 m space was adopted. This indicates that a stronger steel arch must be applied in this situation. As shown in the figure below, after stronger steel arch SS540 was used, the roadway stability could be maintained until 27 m depth by 1 m space, while it was able to maintain deeper than 40 m depth by 0.5 m space. Recently, to increase the stability of the roadway, and to ensure the safety of mine workers, GDM coal mine has already adopted the steel arch SS540 for main roadway support. It works effectively at present.

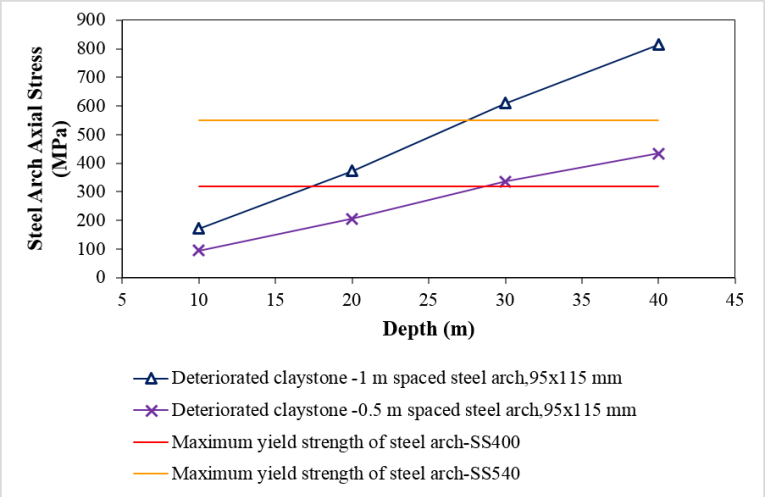

Figure 2.20 Simulated results of steel arch axial stress for main roadway excavation under deteriorated claystone conditions.

2.3.4. Ground Behavior of Main Roadway under Different Roof Conditions

As described previously according to the field observation, the roadway at GDM coal mine has been excavated not only in claystone, but also in the rock layers between claystone and coal at some locations. This indicates that the immediate roof does not only consist of the claystone, but also the coal. Under this condition, as the coal is stronger than the claystone, the ground behavior of the roadway may be different from the one which excavated in claystone only. In this section, the ground behavior of main roadway under different roof conditions was investigated

by means of numerical simulations. Three roof conditions were simulated numerically as shown in Figure 2.21. The first condition is the roadway excavation in claystone layer. The second condition is the roadway excavation in the layers of claystone and coal with presence of 1 m thick coal layer in the roof. The last case is the roadway excavation in the rock layers of claystone and coal with presence of 0.5 m thick coal layer in the roof. In the simulation, the roadway was supported by 1 m spaced steel arches. Table 2.5 describes the mechanical properties of claystone and coal used in the analyses.

Table 2.5 Mechanical properties of claystone and coal used in main roadway analyses under different roof conditions.

Parameter	Claystone (deteriorated)	Coal
Uniaxial compressive strength (MPa)	0.43	8.16
Density (kg/m^3)	2,160	1,380
Young's modulus (MPa)	17.04	1,296
Poisson's ratio	0.26	0.25
Friction angle (˚)	25.9	45.7
Cohesion (MPa)	0.10	2.63

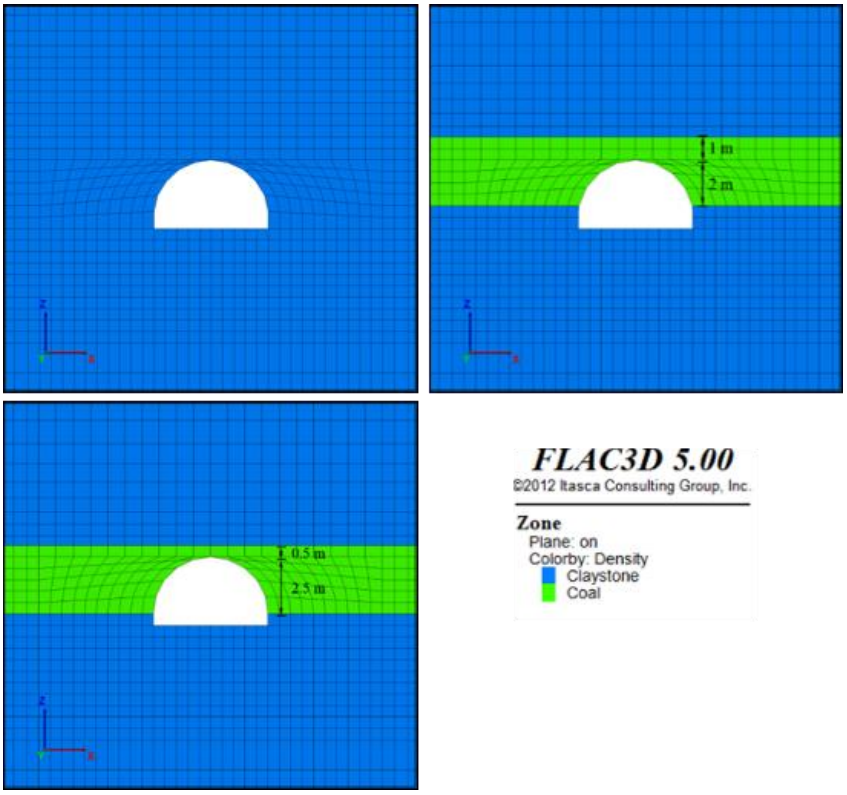

Figure 2.21 Numerical models for ground behavior analysis of main roadway under various roof conditions.

Figure 2.22 illustrates the analyzed results of roadway displacement under different roof conditions. The results show that the largest displacement occurred when the roadway excavated in claystone only. The decrement of displacement was observed with the presence of coal layer during the roadway excavation. This happened due to the strength effect of the coal. As the coal is stronger than the claystone, it was more able to bridge over the roadway opening, resulted in smaller displacement. The results also indicate that a decrease in roadway displacement was significantly associated with the thickness of coal layer in the roof. The roadway excavation with the presence of 1 m thick coal layer in the roof produced smaller displacement compared with the ones that had 0.5 m and had no coal layer in the roof, respectively. This is because of the thickness effect of coal layer left in the roof. A thicker coal layer has more ability to bridge across the roadway opening, and results in smaller displacement. According to the measurement data of the roof displacement of the roadway excavated under different roof conditions (see Figure 2.11), the measured field data of roadway displacement support the results of

numerical simulations. Very large roof displacement was obtained where the roadway excavated in claystone only. The displacement decreased apparently with the presence of coal layer in the roof, and its decrement significantly depended on the thickness of the coal in the roof. From these trends, it can be said that the presence of coal layer during the excavation considerably improves the stability of the main roadway. By leaving a thicker coal layer in the roof, a better stability condition of the roadway can be achieved. The knowledge learned from the simulation results and field measurement data in this chapter is beneficial not only to the roadway stability at the shallow depth, but also to the stability of main and gate roadways at the deep depth when the longwall mining starts. Since the main and gate roadways will be developed inside the coal seam, some parts of the coal can be left in roof and floor in order to increase the stability of the roadways.

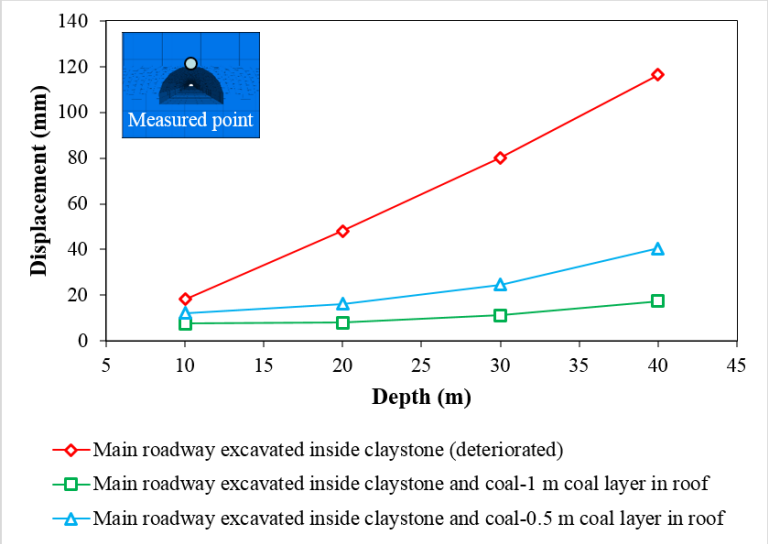

Figure 2.22 Displacement of main roadway under different roof conditions.

2.4. Conclusions

The conditions of GDM underground coal mine are described in this chapter. The GDM coal mine is a new underground coal mine and still in the process of developing the main roadways. Based on the laboratory test results, the rocks of this underground coal mine are classified into very weak and low strength rock mass. The ground behavior of the main roadway is also discussed based on field measurement data and numerical simulation results. According to the field

measurement data, it is found that the mechanical conditions of claystone and the geological conditions of the roof have an obvious impact on the stability of the main roadway. The large roof displacement of the roadway occurs when the roadway is excavated in the deteriorated claystone, whereas the small roof displacement occurs when the roadway excavation is made in the undeteriorated claystone and when the coal layer is present in the roof.

In order to clarify the ground behavior of the main roadway based on the field measurement data, the numerical simulation method using FLAC3D software is used as a tool for clarification. The simulation results are then compared with the measurement data for verification. From the comparisons, it can be found that they are in good agreement, the simulation results support the field measurement data. Under undeteriorated conditions of claystone, the small failure zone and displacement of the roadway occur. The current support system using the steel arch SS400 is effective to control the roadway stability. As the claystone has deteriorated due to groundwater, the failure zone and displacement expand considerably, and the roadway stability decreases significantly. The use of current support system (steel arch SS400) is difficult to control the stability of the roadway. Under this situation, a stronger steel arch SS540 is recommended to apply. Furthermore, presence of coal layer during the excavation considerably improves the stability of the main roadway. Compared with the roadway excavated in claystone only, the displacement decreases significantly. In addition, by leaving a thicker coal layer in the roof, a better stability condition of the roadway can be achieved.

Currently, the roadways at GDM coal mine are maintained in a stable condition at the shallow depth by steel arch support. However, the stability condition and the support system of the roadway at the deep area are still unknown, and they must be studied prior to start longwall mining operation.

References

Bieniawski, Z. T. (1997). Estimating the strength of rock materials. Journal of the South African Institute of Mining and Metallurgy, 312-320.

Hoek, E., & Brown, E. T. (1980). Underground excavations in rock. London, UK.

Hoek, E., Kaiser, P. K., & Bawden, W. F. (1993). Support of underground excavations in hard rock. West Broadway Professional Centre, Vancouver, British Columbia.

Hoek, E., & Brown, E. T. (1997). Practical estimates of rock mass strength. International Journal of Rock Mechanics and Mining Sciences, 34(8), 1165-1186.

Hoek, E. (2006). Practice rock engineering. North Vancouver, B. C., Canada V7R 4X1.

Ichinose, M., Uchino, K., & Matsui, K. (1989). Slaking properties of coal measure rocks: A study on the effect of water content on mechnical properties of coal measure rocks. MMIJ (in Japanese).

PTGDM (PT Gerbang Daya Mandiri Underground Mine Project). (2010). Geology and deposit condition (Unpublished report). The Feasibility Study of PT GDM Underground Coal Mine, Indonesia.

Yasitli, N. E., & Unver, B. (2005). 3D numerical modeling of longwall mining with top-coal caving. International Journal of Rock Mechanics and Mining Sciences, 42(2), 219-235.

CHAPTER 3

STABILITY ANALYSIS AND SUPPORT DESIGN OF MAIN ROADWAY

3.1. Background

Chapter 2 has provided the fundamental understanding of main roadway stability under different geological and excavation conditions at GDM coal mine. The results show that the roadway is currently stable. It is well maintained by the steel arch support. However, although the roadway is stable in the current situation, it is only excavated at the shallow depth. In order to reach the targeted coal seams, it has to be extended to the deeper areas. The main roadway is very important in an underground coal mine to provide an access for miners, machineries, ventilation, and coal transportation. The instability of main roadway causes the reduction of safety and productivity, or it may even lead to the failure of underground mining.

In GDM coal mine, as the main roadway has to be excavated at the deep depth and the coal measure rocks are weak, some ground control problems of roof fall, sidewall collapses, and floor heave can be expected. Excavation of the main roadway at the deep area challenges geotechnical engineers for designing the rock support system. Under-design of support system can lead to instability of the main roadway, whereas over-design will result in unnecessary high excavation costs. Therefore, the appropriate design of support system is of particular necessary for this underground coal mine. This chapter provides the design guideline of support system for main roadway by means of numerical simulations using the finite difference code FLAC3D software. The stability of main roadway prior to longwall mining is studied, and the appropriate support systems are consequently proposed in this chapter.

3.2. Description of Numerical Model

A numerical 3D finite difference code software (FLAC3D) was used in order to study the stability of main roadway in this chapter. Several numerical models were created under various overburden depths such as 50 m, 100 m, 200 m, and 300 m.

An example of the model at 200 m depth is described in Figure 3.1. The width of the model is 180 m, the length is 400 m, and the height is 303 m. The size of main roadway excavation was modeled conforming the design of the mine as 5 m in width and 3 m in height. The excavation length of 250 m was considered in the simulations. The bottom of the model was fixed in the vertical direction, the sides were fixed in the horizontal direction, while the surface was free in all directions. As the claystone is a dominant rock type in the GDM underground coal mine, the overburden and underburden were modeled as homogenous claystone layers. In order to obtain the most precise result of the simulation, the lateral and vertical meshes were intentionally made finer around the excavation area than remaining meshes. Due to the field measurement data of in-situ stresses at the mine site have been unknown, three horizontal to vertical stress ratios (k = 1.0, 1.5, and 2.0) were assumed in the simulations. The constitutive model of elasto-plastic Mohr-Coulomb was used in the analyses. The mechanical properties of claystone are given in Table 3.1. These properties are the average values obtained from labolatory test results of the claystone at the deep depths ranging from 50 m to 300 m.

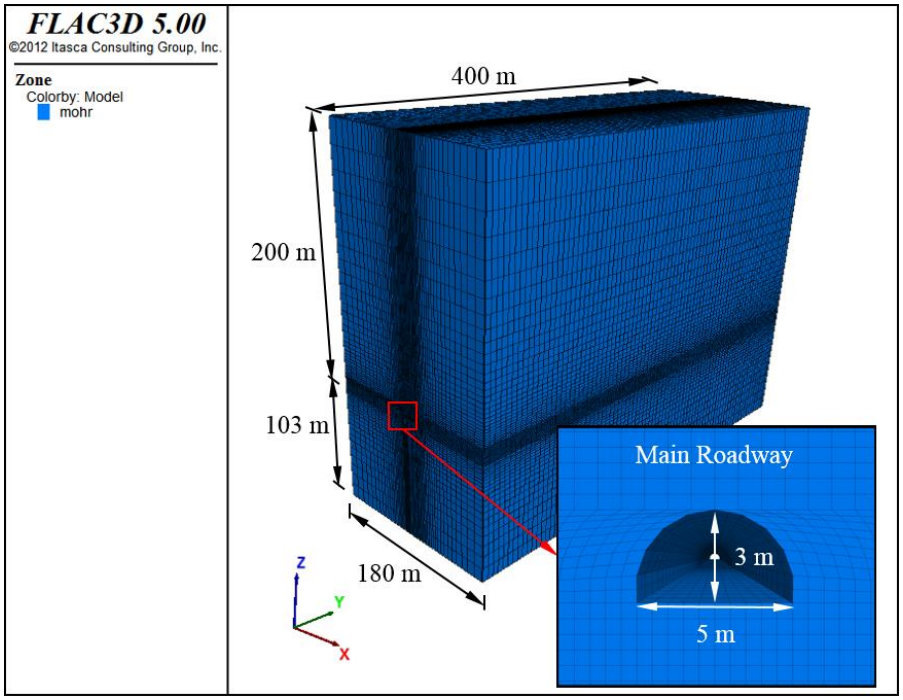

Figure 3.1 Geometries of numerical model under 200 m overburden depth.

3.3. Stability of Main Roadway under Various Overburden Depths and Stress Ratios

Failure zones of unsupported main roadway excavated at various depths under different stress ratios are presented in Figure 3.2. The results reveal that the overburden depth and high stress ratio have significant impacts on the stability of the main roadway. The failure zone considerably increased with increasing the overburden depth and stress ratio. At a deeper depth and under higher stress ratio, more severe failures occurred, especially in roof and floor. This is because of an increase of in-situ stress resulted from increasing the thickness of the overburden and stress ratio. Under this condition, serious roof fall, sidewall collapse, and floor heave of the main roadway can be expected. In order to prevent these ground control problems, there is a necessaries for GDM coal mine to select the appropriate support system for the main roadway. The support designs of the roof, sidewalls, and floor were studied and discussed in the following sections.

Table 3.1 Mechanical properties of rock mass used in simulations.

Parameter	Claystone
Uniaxial compressive strength (MPa)	10.49
Density (kg/m^3)	2,140
Young's modulus (MPa)	2,325
Poisson's ratio	0.27
Friction angle (˚)	37.5
Cohesion (MPa)	0.56

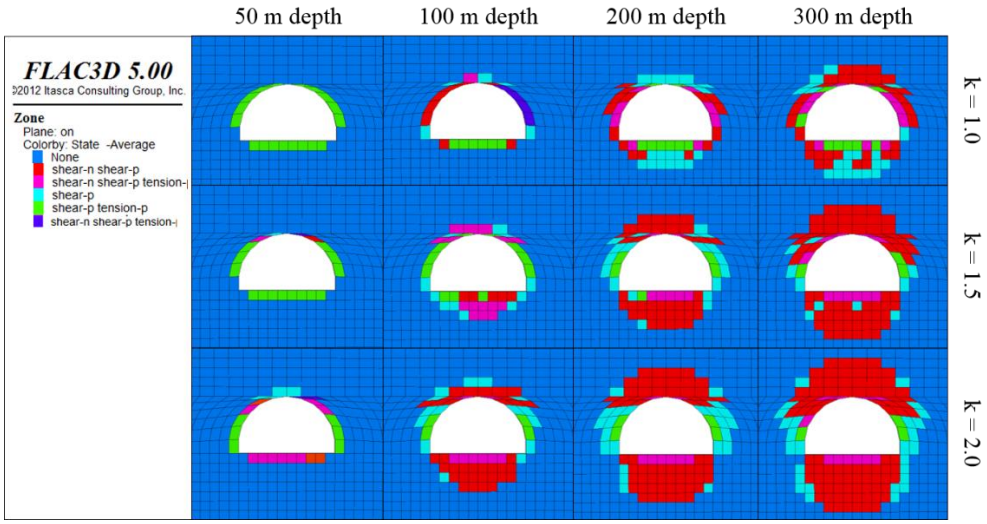

Figure 3.2 Failure zone of unsupported roadway under various overburden depths and stress ratios.

3.4. Support Design of Main Roadway in Roof and Sidewalls

Several types of supports have been used to stabilize the underground roadways for decades, such as bolting supports, steel arch, and shotcrete (Hoek & Brown, 1980; Hoek & Wood, 1987; Hoek, Kaiser, & Bawden, 1993; Hoek, 2006). In this chapter, three support systems such as friction rockbolt, steel arch, and shotcrete were simulated in order to investigate their effects for controlling the stability of the main roadway at GDM underground coal mine (see Figure 3.3). Friction rockbolt is beneficial to enhance the mechanical properties of the rock by tightening the loose blocks of the rock near the excavation surface. It helps the rock to support itself, and prevents the fall of roof and sidewalls that may create unsafe working conditions. Steel arch does not interact with the rock mass in the same way as rockbolt. Generally, this support can only respond to loads imposed on it by inward movement of the rock. The shotcrete is a very effective support medium, and used to prevent small pieces of rocks from unravelling from the excavation surface. It helps to retain the interlocking and self-supporting characteristics of the rock mass, and also helps to block the pathway of the water that can flow into the underground opening by sealing the joints in the rock mass. The mechanical properties of each support type used in the analyses are given in Tables 3.2-3.4. Ten friction rockbolts with 1 m row spacing (see Figure 3.4), steel arch of 1 m space, and shotcrete of 10

cm thickness, were considered in the simulations. Figure 3.5 illustrates a comparison of failure zones around the main roadway after three support systems were installed. From the results, the improvement of the main roadway stability was observed comparing with the roadway without support. The significant stability improvement was obtained when the steel arch and shotcrete were applied. In contrast, the least improvement was achieved as large failure zones still occurred although the friction rockbolt support was used. It was due to the difficulty of the friction rockbolt to have a sufficient anchorage in weak rock mass. It can be said that the use of friction rockbolt as the main support system is not suitable to maintain the main roadway in GDM underground coal mine. Therefore, the roadway support has to be either in the form of steel arch or shotcrete.

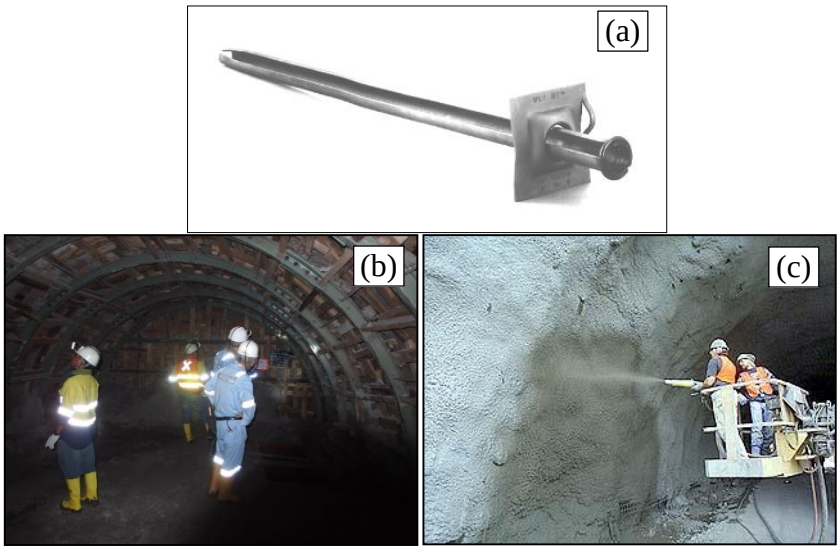

Figure 3.3 Support systems for main roadway (a) friction rockbolt (b) steel arch (c) shotcrete.

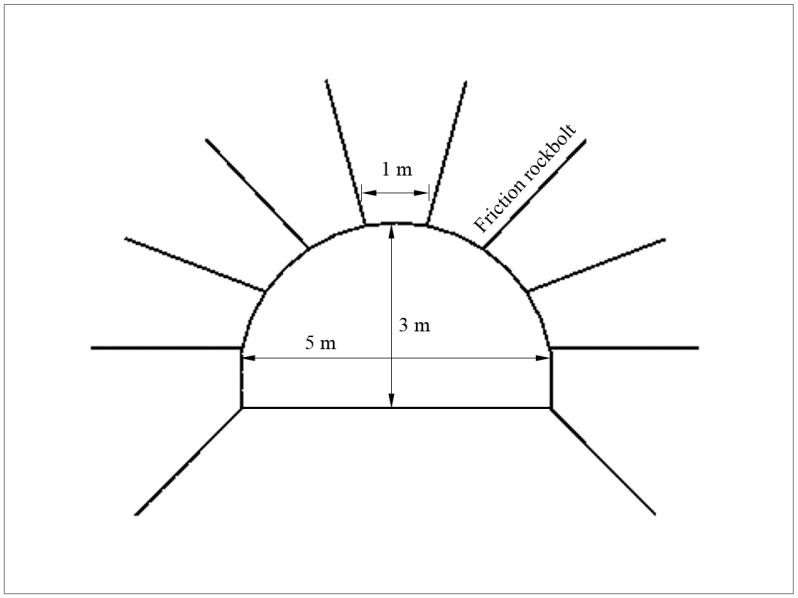

Figure 3.4 Friction rockbolt pattern of main roadway.

Table 3.2 Mechanical properties of friction rockbolt used in simulations.

Parameter	Value
Length (m)	2.5
Diameter (mm)	46
Typical tensile strength (kN)	178
Young's modulus (GPa)	200
Poisson's ratio	0.25
Yield strength (MPa)	588

Table 3.3 Mechanical properties of steel arch (JIS 3010) used in simulations.

Parameter	Value
Dimension (mm)	95x115
Cross section area (cm^2)	36.51
Young's modulus (GPa)	200
Poisson's ratio	0.30
Yield strength, SS540 (MPa)	551

Table 3.4 Mechanical properties of shotcrete used in simulations.

Parameter	Value
Uniaxial compressive strength (MPa)	35
Young's modulus (GPa)	21
Poisson's ratio	0.15
Cohesion (MPa)	10
Friction angle (˚)	30

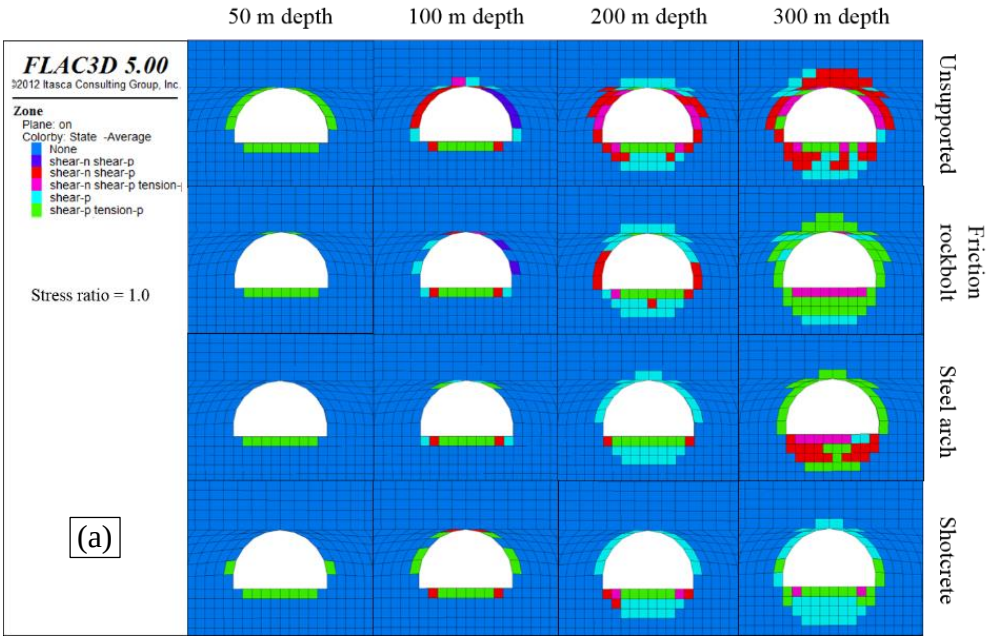

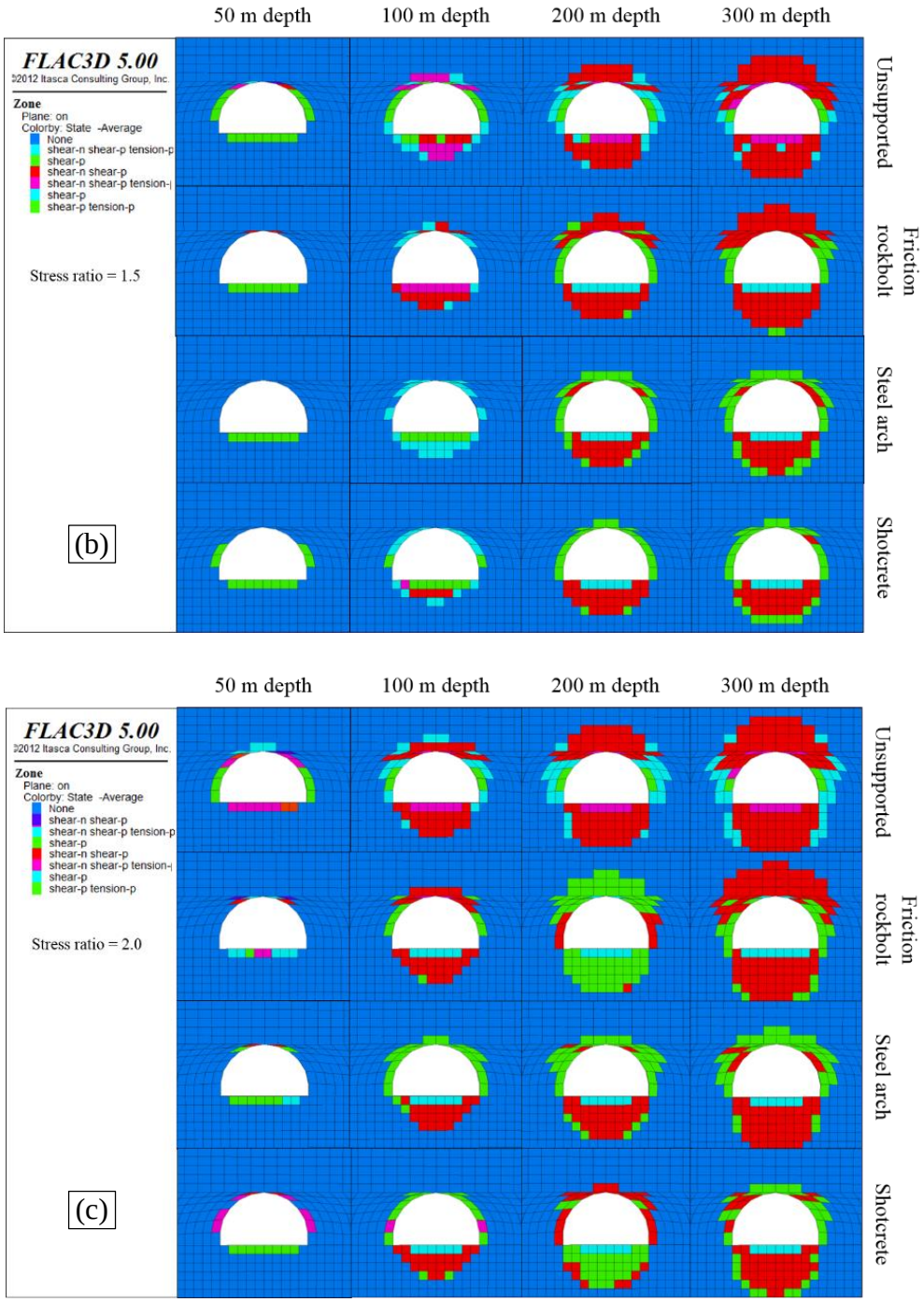

Figure 3. 5. Failure zone of roadway after installation of friction rockbolt, steel arch, and shotcrete (a) k = 1.0 (b) k = 1.5 (c) k = 2.0.

The simulated results found that no big difference of failure zone was observed between the roadways supported by steel arch and shotcrete. However, the shotcrete produced smaller failure zone than that in case of steel arch. This is due to the shotcrete possesses a higher resistance to the compressive stress than that of the

steel arch. Nonetheless, even though the shotcrete provided a better stability condition of the main roadway, since the main roadway was excavated in weak rocks, the shotcrete should be installed immediately behind the roadway advance, this makes the placement of a full shotcrete lining during the excavation is impractical due to time-consuming of the shotcrete hardening. In addition, the installation cost of the shotcrete in Indonesian underground mines is much higher than that of the steel arch as summarized in Table 3.5 (Karian, 2016). Hence, the remaining option for the support of the main roadway in GDM coal mine is using the steel arch. The steel arch is considered as the most appropriate support to be used not only because it has a good stability control and fast installation process, but it has also a justifiable cost.

Table 3.5 Price in 1 m length of support installation in Indonesian underground mine (Karian, 2016).

Support type	Price (USD)
Friction rockbolt	853
Steel arch	2,000
Shotcrete	2,368

However, although the friction rockbolt and shotcrete are inappropriate to be applied as the main support system for the main roadway, they still can be used together with the steel arch as an auxiliary support where a higher support capacity is needed. The friction rockbolt or shotcrete will be applied after the steel arch has been installed. In order to understand the effect of combined supporting system on the main roadway stability, the application of steel arch combining with friction rockbolt and shotcrete was investigated and discussed in this section. The steel arch space of 1 m, the rockbolt row space of 1 m, and the shotcrete thickness of 10 cm, were fixed in the simulations. Figure 3.6 compares the failure conditions of the roadway after the steel arch, steel arch with friction rockbolt, and steel arch with shotcrete, were applied. Compared with the roadway supported by steel arch only, the failure zones of the roadway supported by steel arch combining with rockbolt and shotcrete decreased apparently. This proves that the use of rockbolt and

shotcrete as an auxiliary support in combination with the steel arch can improves the stability of the main roadway. Nevertheless, due to the limitation of the rockbolt to have a sufficient anchorage in weak rock mass, it did not help the steel arch to maintain the roadway as much as the shotcrete did, as a result, a larger failure zone occurred. Under all depths and stress ratios, the smallest failure zone occurred when the steel arch support was used together with shotcrete. This was because of the shotcrete became part of the support system. It improved the load-bearing capacity of the steel arch as it helped to retain the interlocking and self-supporting characteristics of the rock mass. The combined supporting system of steel arch and shotcrete could respond to loads imposed on them more effectively. As a consequence, a smaller failure zone occurred. In economical point of view, to adopt this combination of the supports, it can be very costly. It should be adopted when a high support capacity is indeed needed.

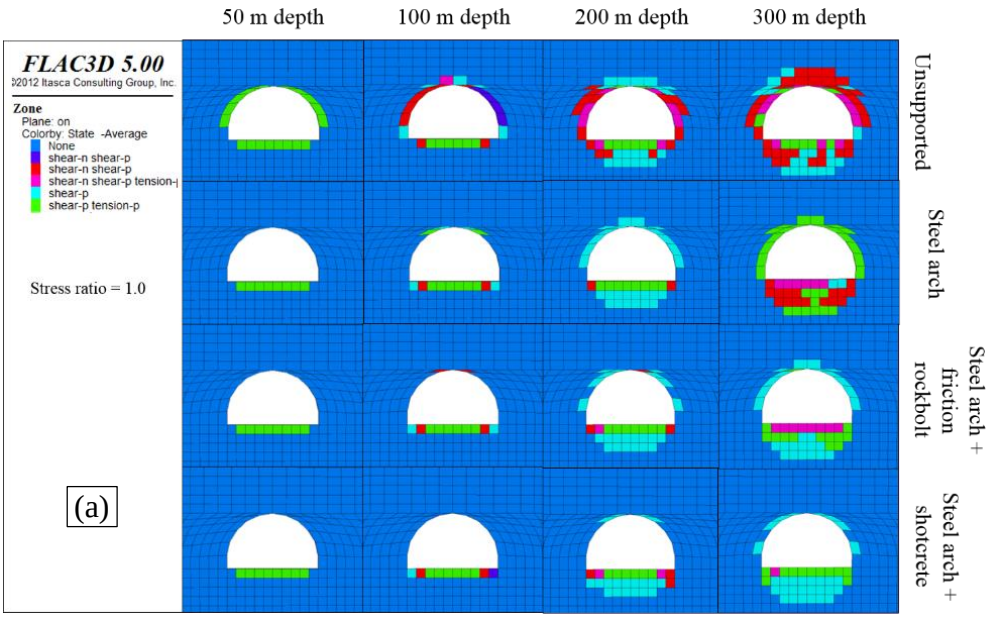

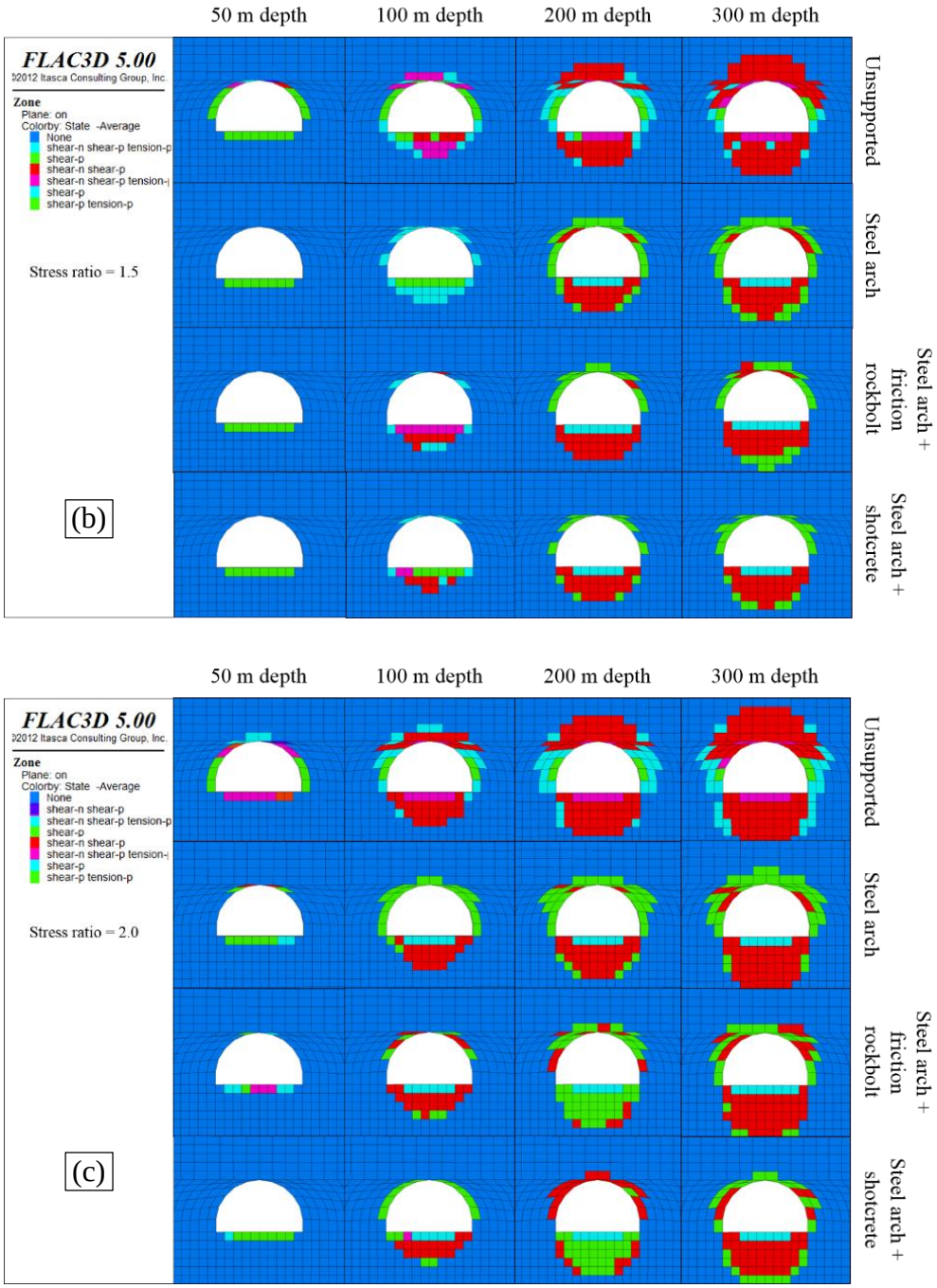

Figure 3.6 Failure zone of roadway after installation of steel arch, and steel arch in combination with friction rockbolt and shotcrete as auxiliary support (a) k = 1.0 (b) k = 1.5 (c) k = 2.0.

3.5. Effect of Space and Size of Steel Arch Support on Main Roadway Stability

As previously mentioned, the steel arch is the most appropriate support to be used in GDM underground coal mine for stabilizing the main roadway. The failure zone,

especially in roof and sidewalls dramatically decreased, and the stability condition of the roadway was improved considerably by the steel arch. In order to optimize the use of steel arch support, this section purposely studied the effect of row space and size of the steel arch on the main roadway stability. Two row spaces (0.5 m and 1 m) and two sizes of cross section (95x115 mm and 105x125 mm) of the steel arch were investigated numerically. Table 3.6 summarizes the properties of steel arch used in the simulations in this section. According to the results presenting in Figure 3.7, a smaller failure zone could be observed when a closer space and a larger size of steel arch were used. Decreasing the space from 1 m to 0.5 m, and changing the size of cross section from 95x115 mm to 105x125 mm were effective to control the development of the failure zone. Therefore, it can be said that a better stability condition of the main roadway in GDM underground coal mine can be achieved by decreasing the space and increasing the size of the steel arch.

Table 3.6 Comparison of mechanical properties of steel arch (JIS 3010) used in simulations.

Parameter	Value	Value
Dimension of cross section (mm)	95x115	105x125
Cross section area (cm^2)	36.51	44.19
Young's modulus (GPa)	200	200
Poisson's ratio	0.30	0.30
Yield strength, SS540 (MPa)	551	551

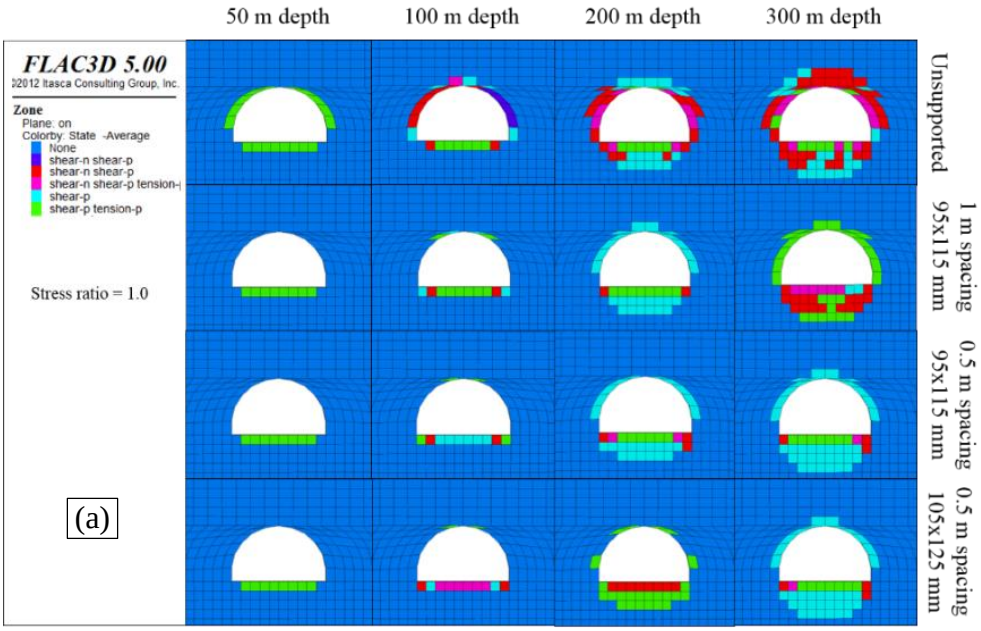
50 m depth
100 m depth
200 m depth
300 m depth
FLAC3D 5.00
2012 Itasca Consulting Group, Inc.
Zone
Plane: on
Colorby: State -Average
None
shear-n shear-p
shear-n shear-p tension-
shear-p
shear-p tension-p
Stress ratio = 1.0
(a)
Unsupported
1 m spacing 95x115 mm
0.5 m spacing 95x115 mm
0.5 m spacing 105x125 mm

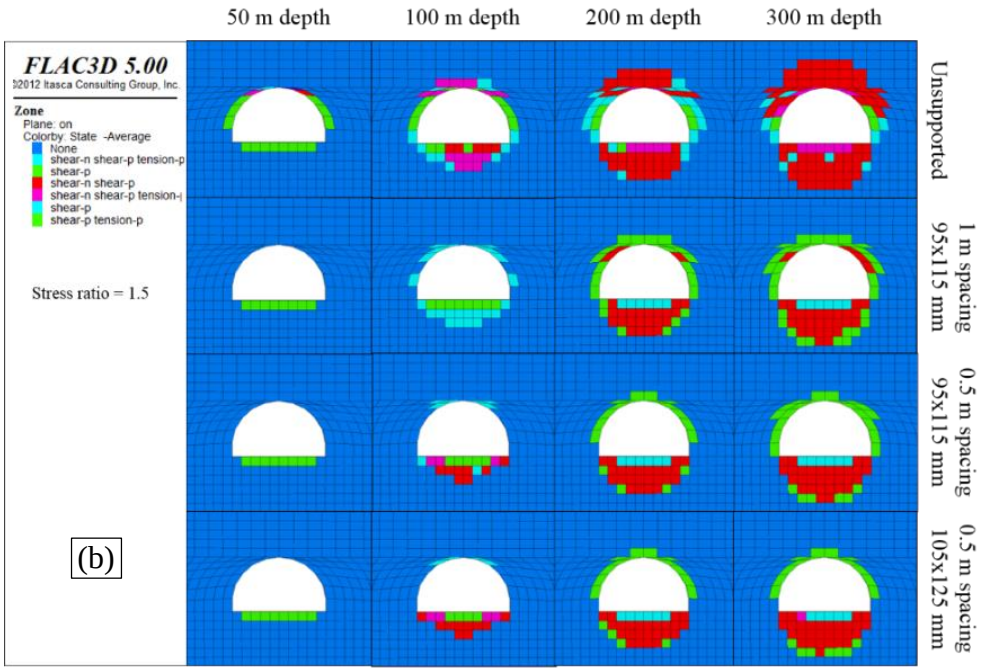
50 m depth
100 m depth
200 m depth
300 m depth
FLAC3D 5.00
2012 Itasca Consulting Group, Inc.
Zone
Plane: on
Colorby: State -Average
None
shear-n shear-p tension-p
shear-p
shear-n shear-p
shear-n shear-p tension-
shear-p
shear-p tension-p
Stress ratio = 1.5
(b)
Unsupported
1 m spacing 95x115 mm
0.5 m spacing 95x115 mm
0.5 m spacing 105x125 mm

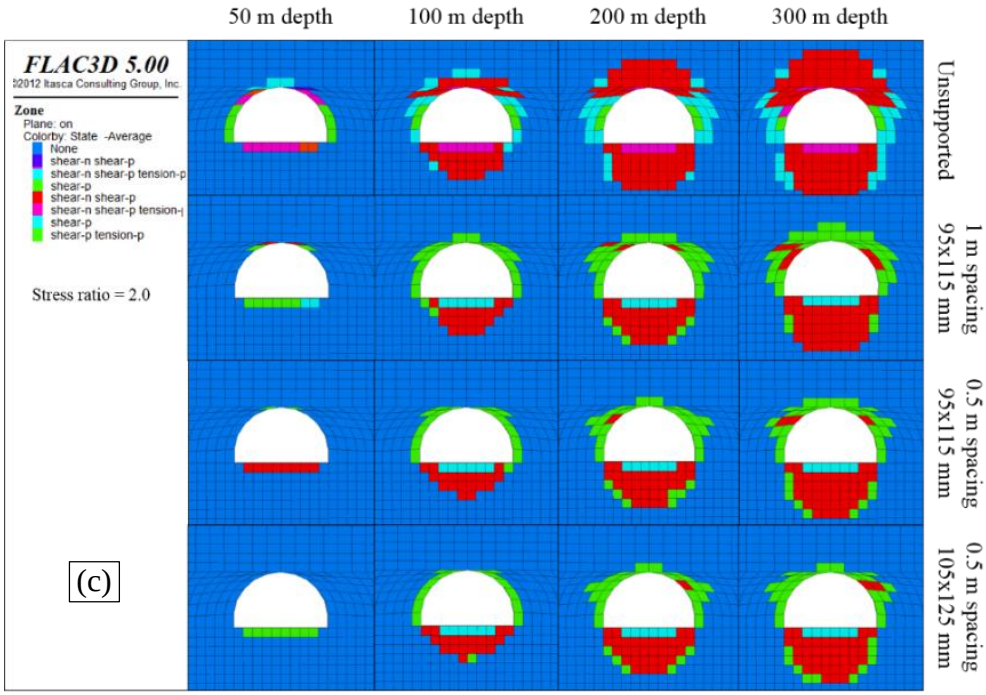

Figure 3. 7. Failure zone of roadway after installation of steel arch with different spaces and sizes (a) k = 1.0 (b) k = 1.5 (c) k = 2.0.

The results of steel arch axial stress in comparison with the maximum yield strength of steel arch SS540 are presented in Figure 3.8. It was obviously seen that a higher stress ratio generated a larger amount of steel arch axial stress. Reduction of the axial stress of steel arch was significantly associated with decreasing the space and increasing the size of the steel arch. From this figure, under k = 1, it suggested that the steel arch of 0.5 m space in both the sizes of 95x115 mm and 105x125 mm was adequate to stabilize the main roadway until 300 m depth. On the other hand, as k increased, the stability control of the roadway at the deep area would be difficult even though the close space and the large size of steel arch were employed. According to the results of the 105x125 mm size steel arch with 0.5 m space, the roadway could be maintained only until 210 m and 165 m depth under k = 1.5 and 2, respectively. It can be said that a higher capacity of the support is needed in order to keep the roadway stable until 300 m depth under k = 1.5 and 2,. For this reason, the use of a stronger steel arch, or the use of the steel arch in combination with other auxiliary supports such as rockbolt or/and shotcrete should be considered. However, it can cause some additional costs to this underground coal mine.

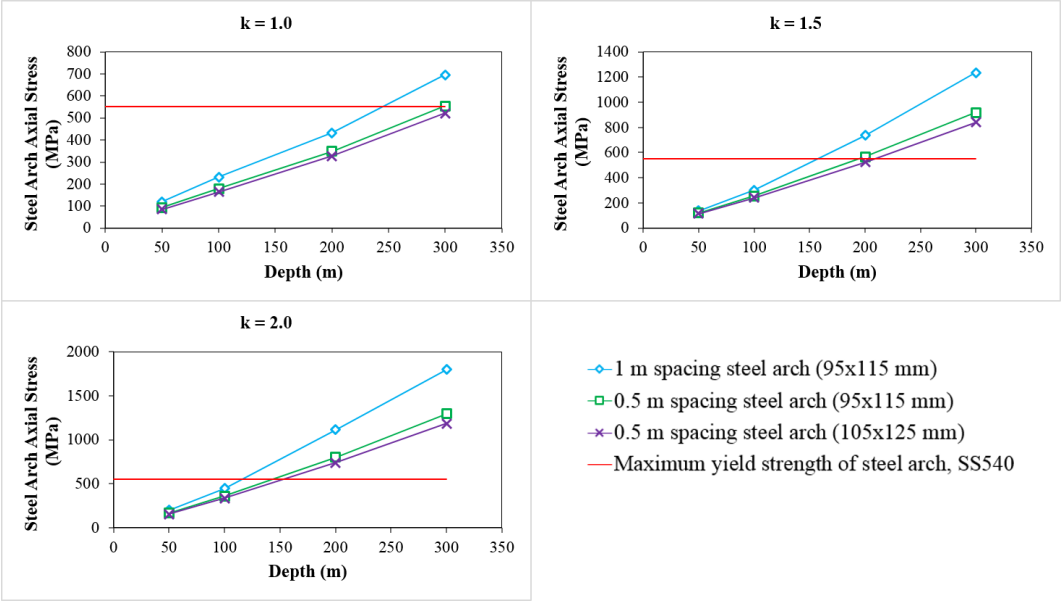

Figure 3.8 Axial stress of steel arch support for roadway under various overburden depths and stress ratios.

3.6. Support Design of Floor of Main Roadway

According to the simulation results presented in the previous sections, although the development of failure zone of the main roadway in roof and sidewalls was controlled effectively by the steel arch support, the large failure and displacement still occurred in the floor due to the floor was left unsupported, especially when the excavation was conducted at a great depth and under high stress ratio. Figures 3.9 and 3.10 represent the failure condition and displacement of the floor at 300 m depth under various stress ratios. This large failure zone and displacement can lead to a severe floor heave unless an adequate support system is provided. Currently, the heaving of the floor of the roadway at GDM coal mine is recognized at the shallow depth, but it is not a serious issue, and easy to be overcome. Based on the simulation results, however, as the large failure and displacement of the floor are likely to occur at the deep area, a serious floor heave of the main roadway is expected. An appropriate design of the floor support is particular important in this situation.

At present, several techniques have been used in order to control the floor, such as digging method, grouting, rockbolt, cablebolt, invert-arch floor, and grooving method. Excavating the heaved floor using a digging machine can be the cheapest

method of control, but it can cause the reduction of coal productivity due to the delay as it needs times to clean the heaved floor. Floor grouting can be the most effective method to control the floor heave. The grouting materials enhance the strength of surrounding rocks by sealing and connecting the fractures within the rock mass. However, it is considered as the most expensive method among the others. Controlling the floor heave using rockbolt or cablebolt, or the combination of these supports has been implemented successfully in an underground mine for many years. Rockbolt or cablebolt is beneficial to strengthen the rock mass, and to restrict the development of rock failure and displacement. The use of these supports becomes popular currently because not only their inexpensiveness, but also they have simple processes of installation. Using an invert-arch floor aims at restricting heaving of the roadway floor. The heave of the roadway floor is strongly restrained by the great stiffness of the arch. The invert-arch floor is normally supported by the concrete (Hudson, Brown, Fairhurst, & Hoek, 2016). The stress distribution in the rock mass surrounding the floor can be improved by adopting the invert-arch floor. It can decrease the high stress concentrations at the corners where the sidewalls meet the invert floor. The invert-arch floor provides the smooth path of stress distribution around the floor, and as a result, the floor heave can be minimized (Hoek, 2006). Grooving method is an alternative floor heave control. It is particular to control the floor heave under high horizontal stress conditions. Compared with other supporting methods such as rockbolt, cablebolt, etc., grooving method has its different mechanism for floor heave control. It changes the stress state of surrounding rocks. Particularly, it makes the floor strata in the stress reduction zone by transferring the maximum stress to the deep rocks, and promotes the stress-relief effect (Jin & Lianguo, 2011; Liu, Ren, Zhang, & Chen, 2017).

In order to prevent the floor heave that may occur due to the large displacement and failure, three techniques of control including the application of cablebolt, invert-arch floor, and grooving method were assessed and discussed in this section. A case of 300 m deep roadway under various stress ratios was simulated numerically.

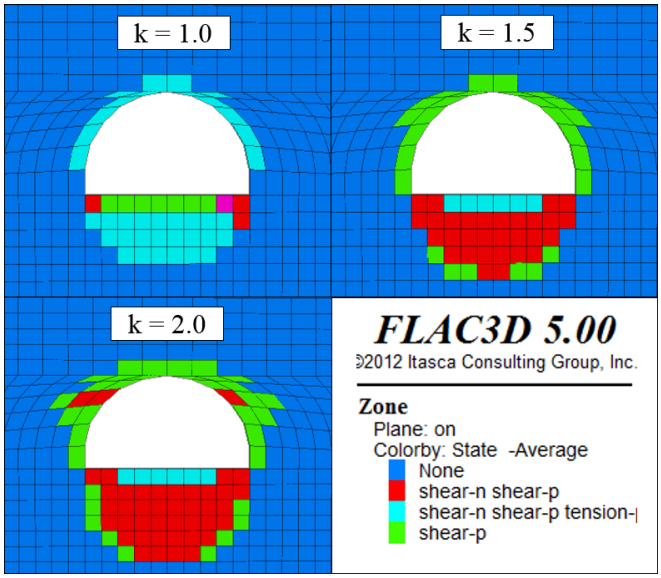

Figure 3.9 Failure zone of unsupported floor of main roadway at 300 m depth.

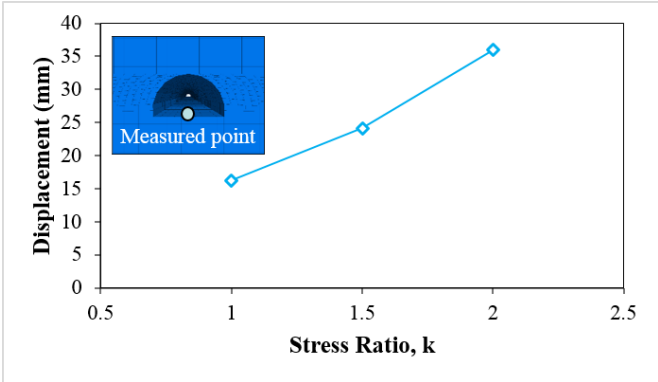

Figure 3.10 Displacement of unsupported floor of main roadway at 300 m depth.

3.6.1. Floor Heave Control by Cablebolt Support

As a rule, to use the cablebolt for controlling the floor heave, the thickness of failure zone indicates the length of cablebolt required, and the minimal length has to be longer than the thickness of the failure zone. According to Figure 3.9, the largest failure zone of 3 m in thickness occurred in a case of k equals to 2. Therefore, the minimal length of cablebolt has to be longer than 3 m. To simulate the effectiveness of cablebolt on the reduction of failure zone and displacement, three cablebolt lengths of 3.5 m, 4 m, and 4.5 m, and two row spaces of 1 m and 0.5 m were investigated. The pattern of support system is presented in Figure 3.11. The support system includes a 0.5 m spaced steel arch of 95x115 mm size in roof and sidewalls,

and six fully grouted cablebolts in the floor. The properties of cablebolt used in the analysis are provided in Table 3.7.

The influence of the row space of cablebolt on the floor stability was firstly analyzed and discussed. Figures 3.12 and 3.13 show the results of failure zone and displacement after the floor was supported by cablebolts with two different row spaces of 1 m and 0.5 m. The length of cablebolt was kept constant at 3.5 m in the case. Compared with the unsupported floor, the floor condition considerably improved as the failure zone and displacement decreased under all stress ratios. This proved that the cablebolt support worked efficiently to control the floor heave problem. The floor which was supported by a closer row spaced cablebolt produced a smaller failure zone and displacement amount. This indicated that a better floor condition could be obtained by reducing the row space of cablebolt. Furthermore, the results also indicated that the floor displacement under high stress ratio decreased significantly. It reduced approximately 60% of the maximum floor displacement when k was 2. This revealed that the floor stability of the roadway in GDM coal mine under high stress ratio could be controlled effectively by the cablebolt support.

Table 3.7 Mechanical properties of cablebolt used in simulation.

Parameter	Value
Diameter (mm)	19
Typical tensile strength (kN)	548
Young's modulus (GPa)	200
Grout compressive strength (MPa)	20
Grout cohesion (MPa)	10
Grout friction angle (˚)	30

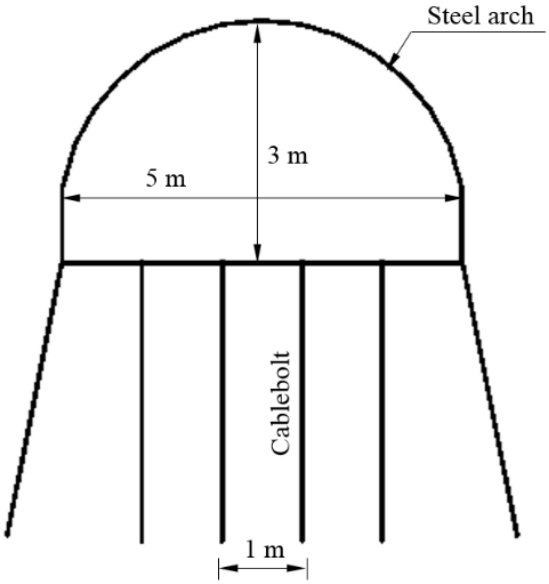

Figure 3.11 Support pattern of main roadway for floor stability analysis using cablebolt.

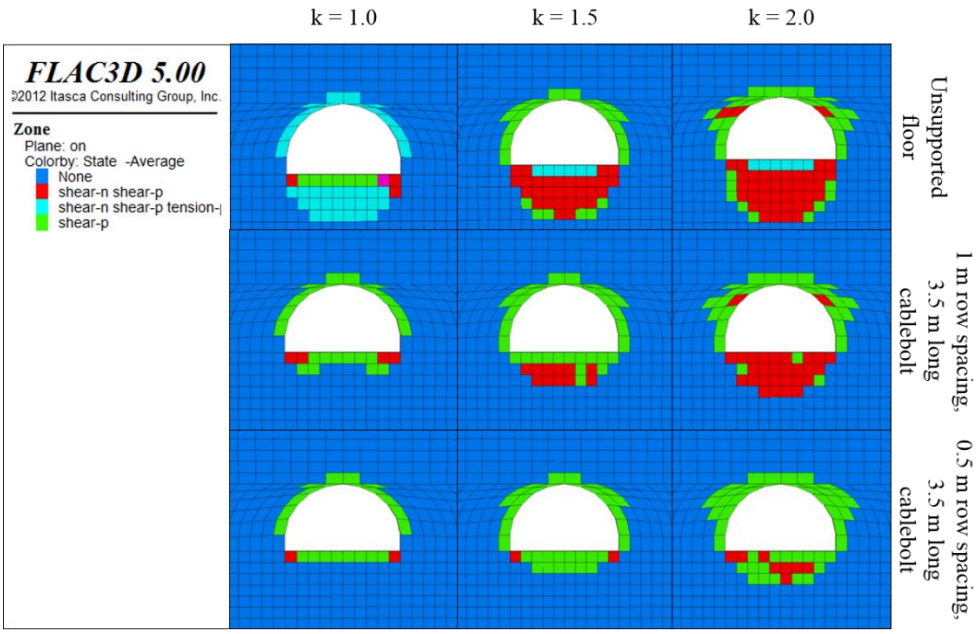

Figure 3.12 Failure zone of supported floor of main roadway at 300 m depth under different row spaces of cablebolt.

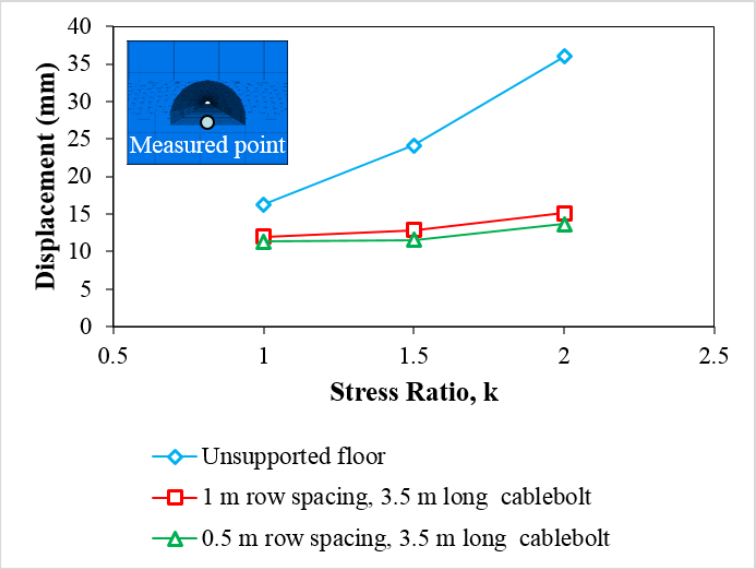

Figure 3.13 Displacement of supported floor of main roadway at 300 m depth under different row spaces of cablebolt.

The effect of the length of cablebolt on the floor stability was secondly studied. Three lengths of 3.5 m, 4 m, and 4.5 m were simulated, and the row space was fixed at 0.5 m throughout the analyses. The results of failure zone and displacement are demonstrated in Figures 3.14 and 3.15, respectively. From the failure zone results, no reduction of the floor failure was observed even though the long cablebolt of 4.5 m was applied. The floor failure under all cases of stress ratios remained the same as the cablebolt length increased. It can be said that increasing the length of cablebolt has no influence on the reduction of floor failure. The cablebolt of 3.5 m length will be sufficient to restrict the failure development of the floor. However, based on the displacement results, the floor displacement reduced when the length of cablebolt increased from 3.5 m to 4 m. After that the displacement remained almost stable although the length increased to 4.5 m. Thus, it can be confirmed that the cablebolt with the length over 4 m will not provide a significant improvement of the floor stability. Over-design of the length will only lead to unnecessary additional costs. An appropriate length must be designed carefully on the basis that an adequate length of cablebolt has to be longer than that the thickness of failure zone, so that they can be anchored in an undamaged floor region.

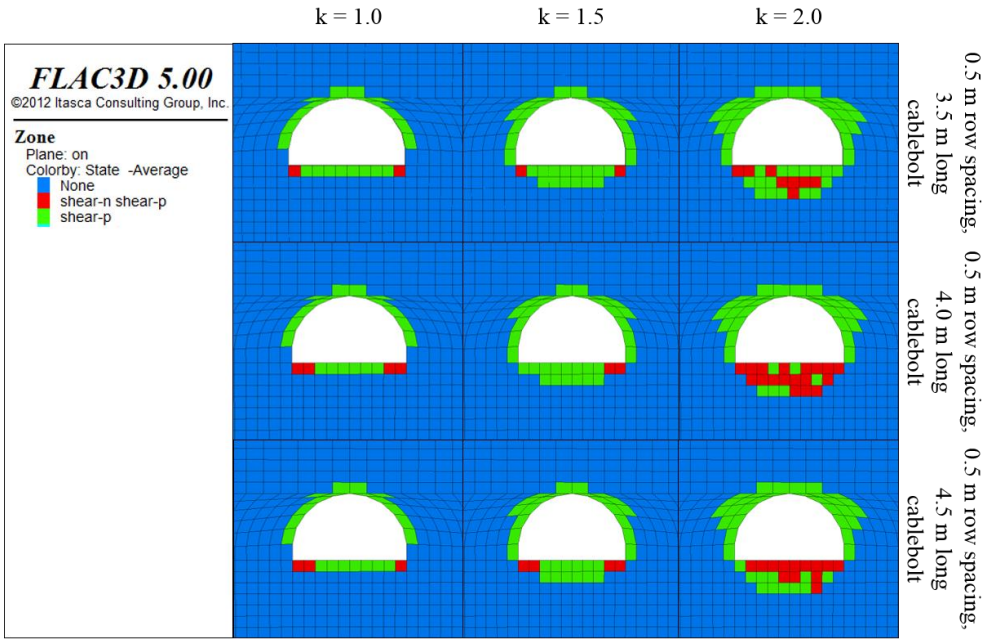

Figure 3.14 Failure zone of supported floor of main roadway at 300 m depth under different lengths of cablebolt.

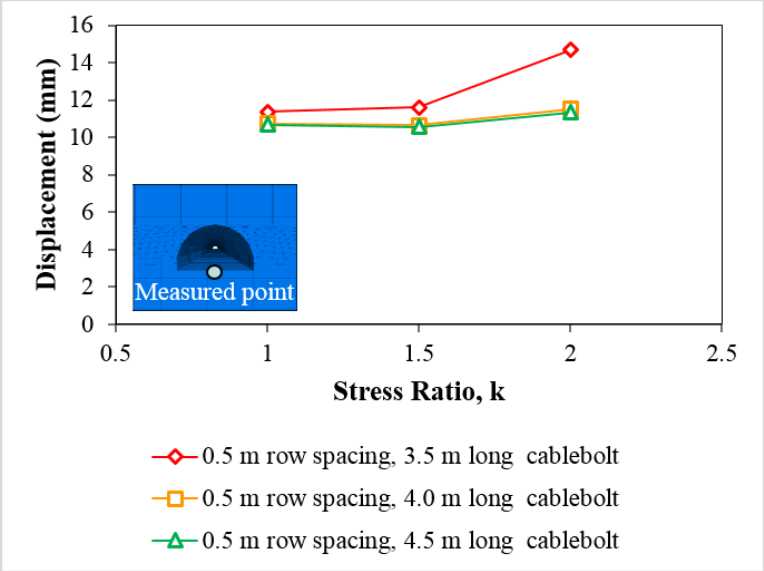

Figure 3.15 Displacement of supported floor of main roadway at 300 m depth under different lengths of cablebolt.

3.6.2. Floor Heave Control by Invert-arch Floor Method

In order to control the floor heave by an invert-arch floor method, the invert-arch was constructed in the floor. After the invert-arch floor was constructed, the

shotcrete of 10 cm in thickness was applied on the floor surface. Figure 3.16 shows the support pattern of the roadway. The roadway was supported by 0.5 m spaced steel arches (95x115 mm) in roof and sidewalls, and the shotcrete in the floor. In order to investigate the effect of the invert-arch depth, three depths of the invert-arch were simulated, such as 0.5 m, 1 m, and 1.5 m.

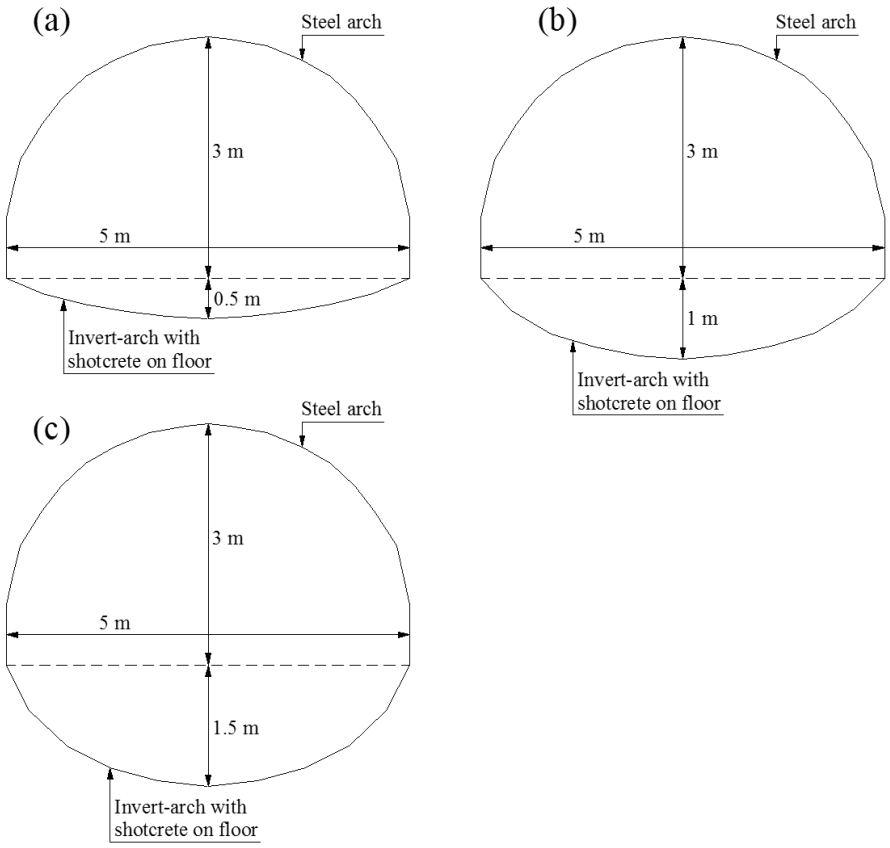

Figure 3.16 Support pattern of main roadway for floor stability analysis using invert-arch floor method (a) 0.5 m deep invert-arch (b) 1 m deep invert-arch (c) 1.5 m invert-arch.

Figures 3.17 and 3.18 illustrate the failure zone and displacement of the floor of the main roadway under different invert-arch depths, respectively. Compared with the unsupported floor without invert-arch, the failure zone and displacement decreased significantly, especially when the main roadway was excavated under high stress ratio. From these figures, it was clearly seen that the flat floor of the main roadway allowed more heaving of the floor. The sharp corners at the junction between the floor and the roadway sidewalls created high stress concentrations. Failure of the

floor generally initiated at these corners. In contrast, failure zone and heaving of the floor were reduced considerably by the presence of the invert-arch in the floor. The invert-arch provided the surrounding rocks with a smooth stress distribution around the floor, and it helped to reduce the stress concentrations at the corners. At the same time, the shotcrete on the floor increased the strength of the floor surface, and it also helped to resist to the stresses imposed on the floor. As a result, the smaller failure zone and displacement generated.

Furthermore, the simulated results revealed that an increase in the invert-arch depth was very effective to minimize the failure zone and displacement of the floor. Existence of a deeper invert-arch in the floor produced a smaller failure zone and displacement. This happened because the invert-arch with a deeper depth created less stress concentrations at the corners, and it promoted a smoother stress distribution around the floor rocks. For example under k = 2, compared with the floor with no invert-arch, 0.5 m deep invert-arch, and 1 m deep invert-arch, the displacement of the floor with 1.5 m deep invert-arch decreased considerably from 36 mm, 19.28 mm, and 11.59 mm to 8.38 mm, respectively. Based on the simulated results discussed above, it can be said that the invert-arch floor method is very effective to control the floor heave problem. A better floor stability condition can be achieved by constructing a deeper invert-arch in the floor. However, even though the method works effectively for controlling the floor heave, since the main roadway with the invert-arch floor will not give a wide flat floor, it decreases the working space, and may limit the size and shape of the equipment used during the construction and production of the mine.

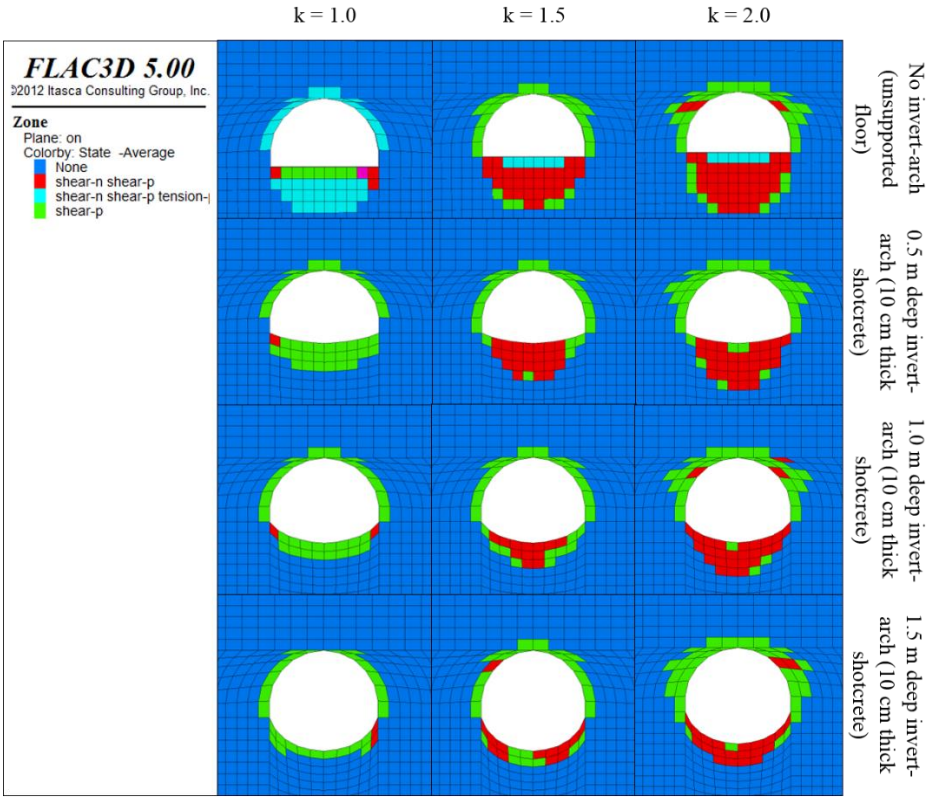

Figure 3.17 Failure zone of supported floor of main roadway at 300 m depth under different depths of invert-arch.

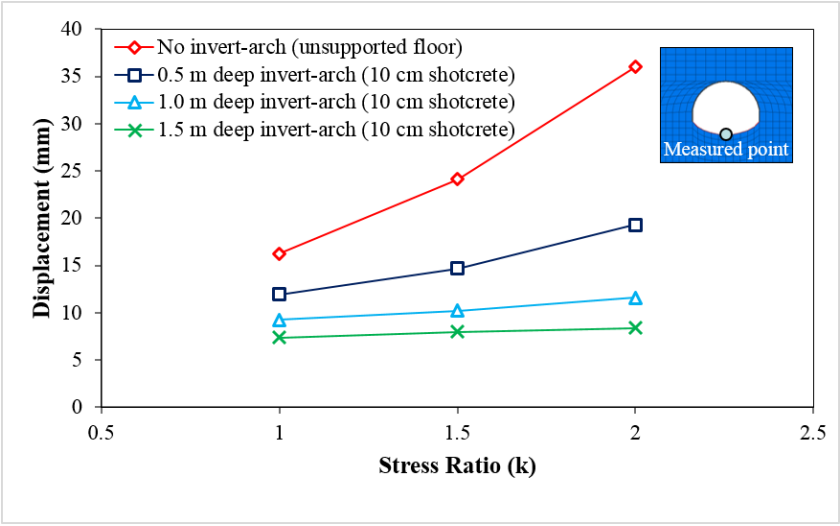

Figure 3.18 Displacement of supported floor of main roadway at 300 m depth under different depths of invert-arch.

3.6.3. Floor Heave Control by Grooving Method

In order to study the floor heave control by grooving method, a 1 m wide crevice was excavated in the middle of the floor. Four crevice depths of 0.5 m, 1 m, 1.5 m, and 2 m were simulated in order to investigate the effect of the crevice depth. The roadway was supported by 0.5 m spaced steel arches (95x115 mm) in roof and sidewalls throughout the simulations (see Figure 3.19).

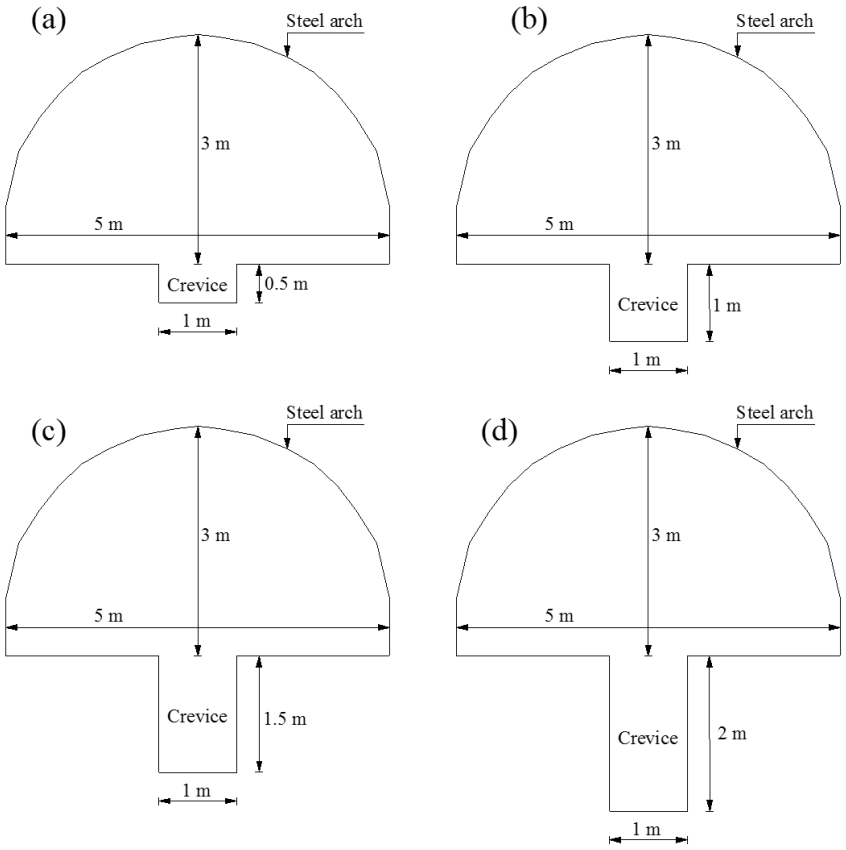

Figure 3.19 Support pattern of main roadway for floor stability analysis using grooving method (a) 0.5 m deep crevice (b) 1 m deep crevice (c) 1.5 m deep crevice (d) 2 m deep crevice.

Figure 3.20 demonstrates the horizontal stress distribution below the floor corners of the roadway under various crevice depths. The horizontal stress in the range of 5 m below the floor corners was monitored. The results show that the presence of the crevice promoted the stress-relief effect. The relief of floor stress is significantly favorable to control the floor heave. The horizontal stress close to the floor corners

dropped gradually with existing the crevice. Without the crevice, the direct floor is in a high stress state. As the crevice depth increased, the effect of stress transfer was noticeable, the stress of the floor was continuously reduced by transferring to the deep rocks. The deepest crevice depth of 2 m showed the best depth of the crevice since it produced the smallest direct floor stress and transferred the peak stress to the deepest rocks. This means that the floor heave can be more effectively controlled by increasing the crevice depth. Compared the results, grooving method worked more effectively to control the floor heave under higher stress ratio. Under higher stress ratio, the peak stress was transferred to a deeper area below the floor corners. This indicates that the grooving method is appropriate to be adopted when the roadway is excavated in the area where the horizontal stress is larger than the vertical stress.

Figure 3.21 illustrates the displacement vectors of the main roadway. It can be seen that the grooving method provided surrounding rocks with a deformation space. It modified the direction of floor movement. The floor moved toward the crevice room which moderated the extrusion deformation of the floor, resulted in reduction of the floor heave. The roadway with a deeper crevice generated a smaller floor heave as the floor moved more horizontally toward the crevice space. In addition, the displacement vector results support the results of horizontal stress distribution. Grooving method controlled the floor heave more effectively under higher stress ratio. More horizontal movement of the floor was observed when the roadway was excavated under a higher stress ratio. However, although this method is effective to control the floor heave problem, since the crevice is excavated in the middle of the floor, it may cause the accident during the transportion of miners, equipment, and coal. The risk of the accident can be reduced by constructing the crevice at the floor corners, or backfilling the crevice with the appropriate materials that can restrict the closing trend and making full use of the effects achieved by grooving.

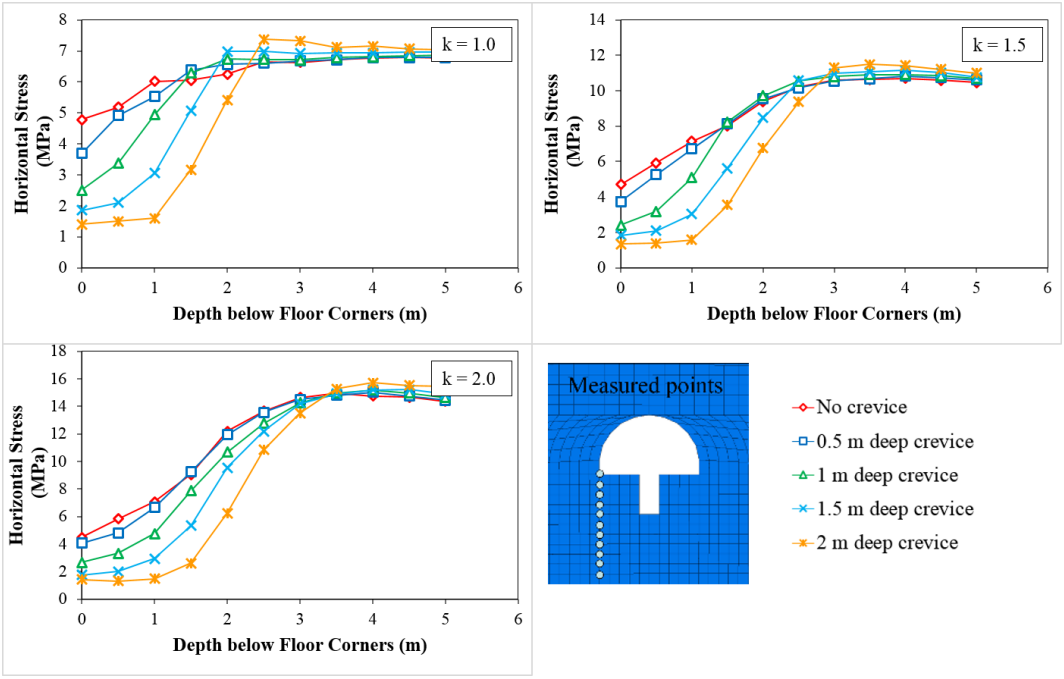

Figure 3.20 Relationship between crevice depth and horizontal stress below floor corners of main roadway at 300 m depth.

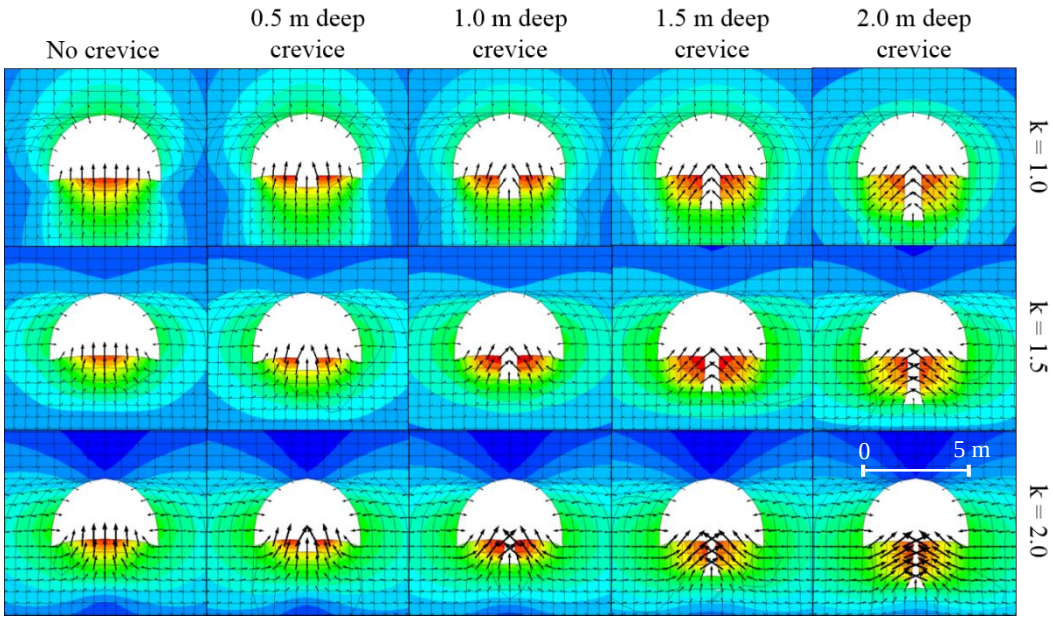

Figure 3.21 Displacement vectors of main roadway with existence of crevice in floor at 300 m depth.

Although the three methods of cablebolt support, invert-arch floor, and grooving methods are effective to control the floor heave problem, controlling the floor heave

by cablebolt support can be considered as the most appropriate technique in GDM underground coal mine. The cablebolt is simple to be installed, and it remains the floor flat and wide in an original shape. Unlike the invert-arch floor and grooving methods, the floor has to be excavated in order to form the invert-arch and crevice in the floor. These methods change the floor shape and decrease the working space of the floor. The grooving method also tends to decrease the safe working conditions since the crevice is constructed in the middle of the floor. In addition, the shotcrete which is applied on the floor surface for the invert-arch method needs times for achieving the desired strength. Additionally, the installation price in 1 m length of the shotcrete (2,368 USD) is much higher than that the cablebolt (540 USD) (Karian, 2016). This makes the floor heave control by the invert-arch floor method is more expensive than the cablebolt support.

3.7. Conclusions

The stability of the main roadway under various overburden depths and stress ratios with different support systems is studied by means of numerical simulations using finite difference code software, FLAC3D. Based on the results, it is found that the overburden depth and stress ratio significantly influence the roadway stability. The thickness of the failure zone increases with increasing the overburden depth and stress ratio. The roadway which is excavated at a deeper depth and under a greater stress ratio, experiences a larger failure zone, and needs a higher capacity of the support. The use of friction rockbolt, steel arch, and shotcrete as the support system for roof and sidewalls is investigated. The steel arch is considered as the most appropriate support to be used as the main support system for the roof and sidewalls comparing with the others. It meets the qualifications of stability control, fast installation process, and economy. The steel arch significantly improves the stability condition of the roof and sidewalls, and the failure zone decreases considerably after the steel arch is applied. In this chapter, the use of friction rockbolt and shotcrete as an auxiliary support is also investigated. Compared with the roadway supported by steel arch only, the failure zone decreases apparently.

As the steel arch is the most appropriate support to be used as the main support system for roof and sidewalls, to optimize the use of steel arch, the effect of space

and size of the steel arch on the main roadway stability is investigated. It is found that the steel arch with closer space and larger size gives a better stability condition. Based on the results of steel arch axial stress, under k = 1, it suggests that the steel arch SS540 of 0.5 m space in both the sizes of 95x115 mm and 105x125 mm is adequate to stabilize the roadway until 300 m depth. On the other hand, as k increases, the stability control of the main roadway in roof and sidewalls at the deep area will be difficult even though the close space and the large size of steel arch are employed. According to the results of the 105x125 mm size steel arch with 0.5 m space, the roof and sidewalls of the main roadway can be maintained only until 210 m and 165 m depth under k = 1.5 and 2, respectively. For this reason, the use of a stronger steel arch, or together with rockbolt or shotcrete is recommended when the roadway is excavated under a high stress ratio and at a great depth.

Although the roof and sidewalls of the main roadway are well controlled by steel arch support, the large floor failure and displacement still occur, especially when the roadway is excavated at a great depth and under a high stress ratio. The floor heave problem can be expected if no appropriate control measure is provided. The use of cablebolt is firstly investigated for stability control of the floor. It works effectively to restrain the failure zone and displacement, especially under high stress ratio. About 60% of the maximum floor displacement is reduced under k = 2. Row space of cablebolt has a significant influence on the floor stability. A closer row space provides a smaller floor failure and displacement. Furthermore, the floor is also supported with different lengths of cablebolt. Increasing the length from 3.5 m to 4 m and 4.5 m does not reduce the thickness of failure zone. This reveals that a cablebolt of 3.5 m length will be sufficient to restrain the development of floor failure. However, the decrement of floor displacement is observed when the length of cablebolt increases.

The invert-arch floor method is secondly investigated for floor heave control. The method is very effective to reduce the heaving of the floor, especially under a high stress ratio. The floor failure and displacement significantly decrease with presence of the invert-arch in the floor. The invert-arch reduces the stress concentrations at the corners where the sidewalls meet the floor, and it provides the surrounding rocks with a smooth stress distribution around the floor. At the same time, the shotcrete

applied on the floor increases the floor strength, and resists to the stresses imposed on the floor. Consequently, the failure zone and displacement decrease. In addition, by increasing the depth of the invert-arch, more failure zone and displacement can be reduced. A deeper invert-arch creates less stress concentrations at the floor corners, and provides a smoother stress distribution around the floor rocks. As a result, a smaller failure zone and displacement occur in the floor.

Controlling the floor heave by grooving method is lastly investigated. The method promotes the stress-relief effect of the floor, which helps to minimize the floor heave amount. Increase in crevice depth induces the relief of floor stress by transferring the peak stress to the deep rocks, so that the floor heave can be more effectively controlled. Grooving method provides the surrounding rocks with a deformation space. It modifies the movement direction of the floor. The floor moves toward the crevice space, and the floor heave can be minimized. Increasing the crevice depth enlarges the deformation space, as a result, the floor heave can be more effectively minimized. The simulated results indicate that the use of grooving method is more appropriate when the roadway is excavated under higher stress ratio. Under higher stress ratio, the peak stress is transferred to a deeper area, and more horizontal movement of the floor is observed.

Although the heaving of the floor can be controlled effectively by the cablebolt, invert-arch floor, and grooving methods, controlling the floor heave by cablebolt support can be the most appropriate technique in GDM coal mine comparing with other methods in terms of installation process, providing a flat and safe working condition of floor, and economy.

References

Hoek, E., & Brown, E. T. (1980). Underground excavations in rock. London, UK.

Hoek, E., & Wood, D. F. (1987). Support in underground hard rock mines. Underground Support Systems, 35, pp. 1-6.

Hoek, E., Kaiser, P. K., & Bawden, W. F. (1993). Support of underground excavations in hard rock. West Broadway Professional Centre, Vancouver, British Columbia.

Hoek, E. (2006). Practice rock engineering. North Vancouver, B. C., Canada V7R 4X1.

Hudson, J., Brown, E. T., Fairhurst, C., & Hoek, E. (2016). Comprehensive rock engineering volume 4: Excavation, support and monitoring. Imperial College of Science, Tecnology & Medicine, London, UK: Pergamon Press.

Itasca Consulting Group, Inc. (2009). FLAC3D Fast Lagrangian Analysis of Continua in 3 Dimensions: User's Guide, Mill Place, Minneapolis, 55401 USA.

Jin, S., & Lianguo, W. (2011). Numerical simulation of grooving method for floor heave control in soft rock roadway. International Journal of Mining Science and Technology (China), 21, 49-56.

Karian, T. (2016). Stability Control Measures for Crown Pillar in Cut and Fill Underground Gold Mine under Protected Forest Area, Indonesia (PhD dissertation). Kyushu University, Fukuoka, Japan.

Liu, C., Ren, J., Zhang, K., & Chen, S. (2017). Numerical study on surrounding rock deformation controlled by pressure relief groove in deep roadway. International Symposium on Resource Exploration and Environmental Science, 64, 1-9.

CHAPTER 4

EFFECT OF LONGWALL MINING ON STABILITY OF MAIN AND GATE ROADWAYS

4.1. Background

In Chapter 3, the simulated results reveal that the stability of main roadway prior to longwall mining in GDM coal mine can be effectively controlled by the steel arch in roof and sidewalls, while the floor can be controlled by cablebolt support, invert-arch floor, and/or grooving method. The results confirm the possibility of the longwall mining development in this underground coal mine. The next issue that should be taken into an account is that the stability of the main and gate roadways affected by the longwall mining.

In longwall mining, after the main roadways reach the targeted coal seam, the coal seam is blocked into panels by developing the gate roadways along the panel sides. The gate roadways are then connected, forming the chain pillar. Another pillar is also formed in order to separate the main roadway from the excavation area. This pillar is called as a barrier pillar (see Figure 4.1).

During the mining of a longwall panel, the rock strata above the mined-out area are allowed to collapse and cave into the goaf. Cave-in of the roof strata above the mined-out area induces the stress redistributions of the surrounding rocks. The stresses which previously existed in the rocks are redistributed to the face and rib sides of the panel as illustrated in Figure 4.2 (Hoek & Brown, 1982; Hudson, 1993; Bardy & Brown, 2004). These stress redistributions have a pronounced impact on the stability of main and gate roadways. An adequate width of barrier/chain pillar and longwall panel is needed in order to prevent the failure of the main/gate roadway due to the panel extraction. Undersized barrier/chain pillar width and oversized panel width may lead to a severe instability of the main/gate roadway. In contrast, oversized barrier/chain pillar width and undersized panel width can result in the reduction of coal productivity.

Therefore, this chapter attempts to study the effect of longwall mining on the stability of main and gate roadways by means of numerical simulations using FLAC3D software. The influence of panel extraction is analyzed and discussed, and the appropriate widths of barrier pillar, chain pillar, and longwall panel are investigated and proposed in this chapter.

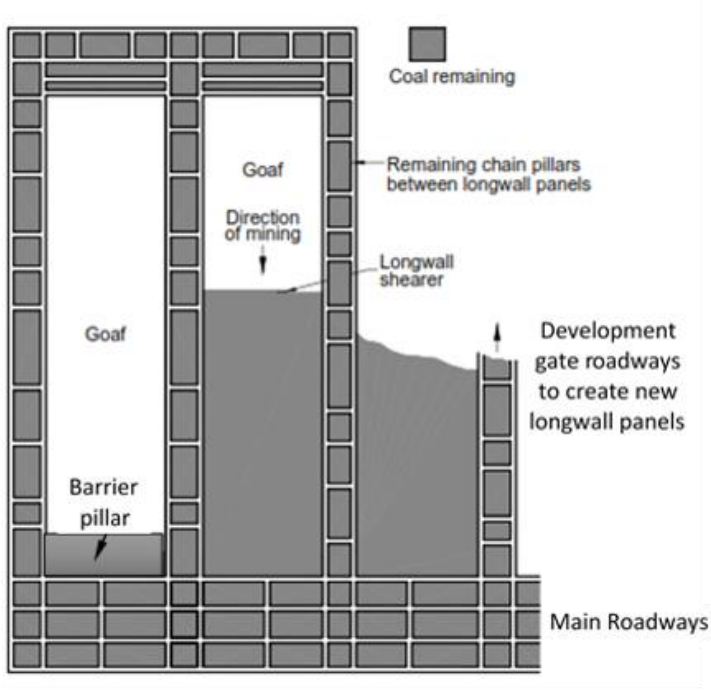

Figure 4.1 Typical panel layout of a longwall coal mine (MSEC, 2007).

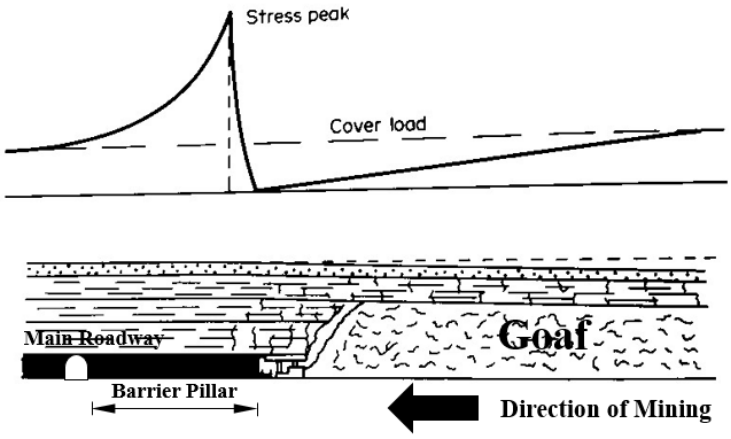

Figure 4.2 Vertical stress redistribution ahead longwall panel face (modified after Hudson, 1993).

4.2. Effect of Longwall Mining on Stability of Main Roadway

4.2.1. Description of Numerical Model

To study the effect of longwall mining on the main roadway stability, and to investigate the appropriate width of barrier pillar and longwall panel, several numerical models at various depths of 50 m, 100 m, 150 m, and 200 m were created using the finite difference code FLAC3D software. The width and length of the model is 230 m and 235 m, respectively, while the height is varied depending on the depth of longwall mining. Figure 4.3 demonstrates an example of numerical model of longwall mining at 200 m depth. The bottom of the model was fixed in the vertical direction, the sides were fixed in the horizontal direction, and the surface was free in all directions. In GDM coal mine, based on the field observation and measurement data of main roadway, the deformation of the main roadway is more likely to occur in the roof than those in the sidewalls and floor. This evidence indicates that the horizontal stress can be the same or less than the vertical stress. In simulations, therefore, the stress ratio of 1 (k = 1) was considered. The elasto-plastic Mohr-Coulomb was used as a constitutive model in the analyses. Three-dimensional analysis under symmetric condition was considered, and only half side from the center of the model was analyzed. The main roadway was excavated in the coal seam, and it was designed as a semi-circular shape of 5 m width, 3 m height, and 230 m length. The main roadway was supported by the steel arch SS540 (95x115 mm) with different spaces of 1 m and 0.5 m. The mechanical properties of rock mass and coal seam used in the simulations are presented in Table 4.1.

The influence of barrier pillar width on the stability of main roadway at various depths was firstly studied, and the appropriate width of barrier pillar was designed and proposed based on the results. Several widths of barrier pillar ranging from 20 m to 60 m were investigated. As a longwall panel width of 130 m is an initial design of GDM coal mine, hence the fixed panel width of 130 m was considered in this case. In addition, the influence of panel width on main roadway stability was also investigated. The simulations were carried out at 50 m, 100 m, 150 m, and 200 m depth. Three panel widths of 70 m, 100 m, and 130 m were simulated numerically. Based on the simulated results, appropriate width of barrier pillar for each panel

width and mining depth was suggested in order to maintain the stability of the main roadway with the aim of maximizing the coal recovery. In order to observe the effect of longwall mining, the failure zone and steel arch axial stress were monitored in the main roadway as illustrated in Figure 4.3. The results of these parameters were measured after every step of longwall panel extraction.

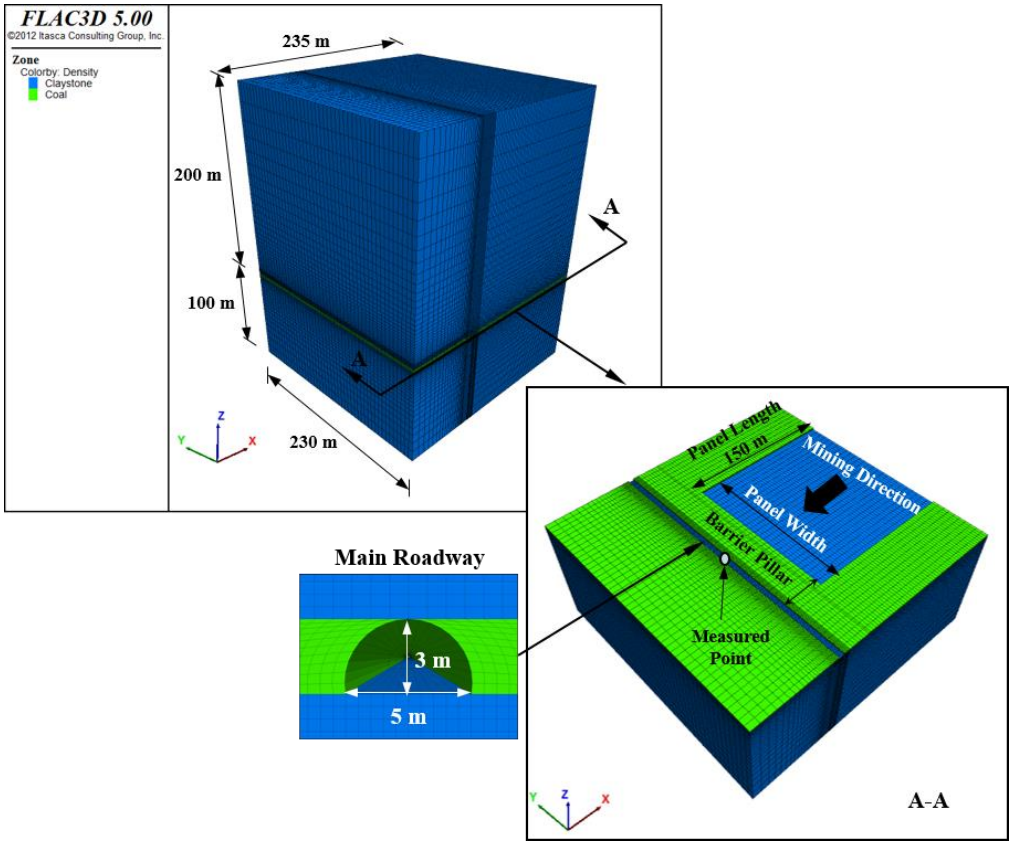

Figure 4.3 Numerical model of longwall mining for main roadway stability analysis at 200 m depth.

Table 4.1 Mechanical properties of materials used in simulations.

Parameter	Rock mass	Coal seam
Uniaxial compressive strength (MPa)	10.49	8.16
Density (kg/m^3)	2,140	1,380
Young's modulus (MPa)	2,325	1,296
Poisson's ratio	0.27	0.32
Friction angle (˚)	37.5	45.7
Cohesion (MPa)	0.56	2.63

4.2.2. Modeling of Goaf

After extraction of the coal seam, the immediate roof strata above the mined-out area bend and cave into the stope void behind the excavation face, known as a caved area or goaf. The goaf is mainly made of broken rock pieces, hence it was modeled as aggregate of fractured rocks (Yasitli & Unver, 2005). In order to simulate the goaf in longwall mining, both the coal seam and immediate caved roof are excavated, and then the caved area is filled with a very soft material (Cheng, Wang, Xie, & Wei, 2010). Since the measurement of deformations in the goaf is difficult due to the inaccessibility, there is still no standard method for modeling the goaf. In this research, the approach proposed by Yavuz (2004) was employed, and the following equation was used for estimating the height of caved roof.

$$H_c = 100h/(c_1h+c_2) \quad (4.1)$$

Where H_c (m) is the height of caved roof, h (m) is the seam height, and c_1 and c_2 are coefficients depending on the strata lithology.

To estimate the height of caved roof using an above-mentioned method, the height of extracted coal seam and the uniaxial compressive strength of the roof rocks must be known. The uniaxial compressive strength (UCS) of the roof rocks is used for selecting the values of c_1 and c_2. The values of c_1 and c_2 for different lithologies are presented in Table 4.2. The method is developed in China from various sets of data for longwall mining environments with different lithological and geometric characteristics, and it widely used to estimate the height of caved roof used in longwall mining simulation for US and Australian coal mines where the rocks are medium to strong. However, since the method is still applicable for the weak rocks (UCS < 20 MPa), hence this method was employed for estimating the height of caved roof used in longwall mining simulation for GDM coal mine. By considering the conditions of GDM coal measure rocks, the height of caved roof was calculated as 5.93 m. In simulation, a longwall panel was extracted step by step. After the excavation face moved forward, the caved area behind the coal face was filled with the very soft goaf material. The excavation steps were repeated until the longwall panel was entirely extracted. An example of goaf installation in the longwall mining

simulation is illustrated in Figure 4.4. The properties of the goaf used in the analyses are given in Table 4.3.

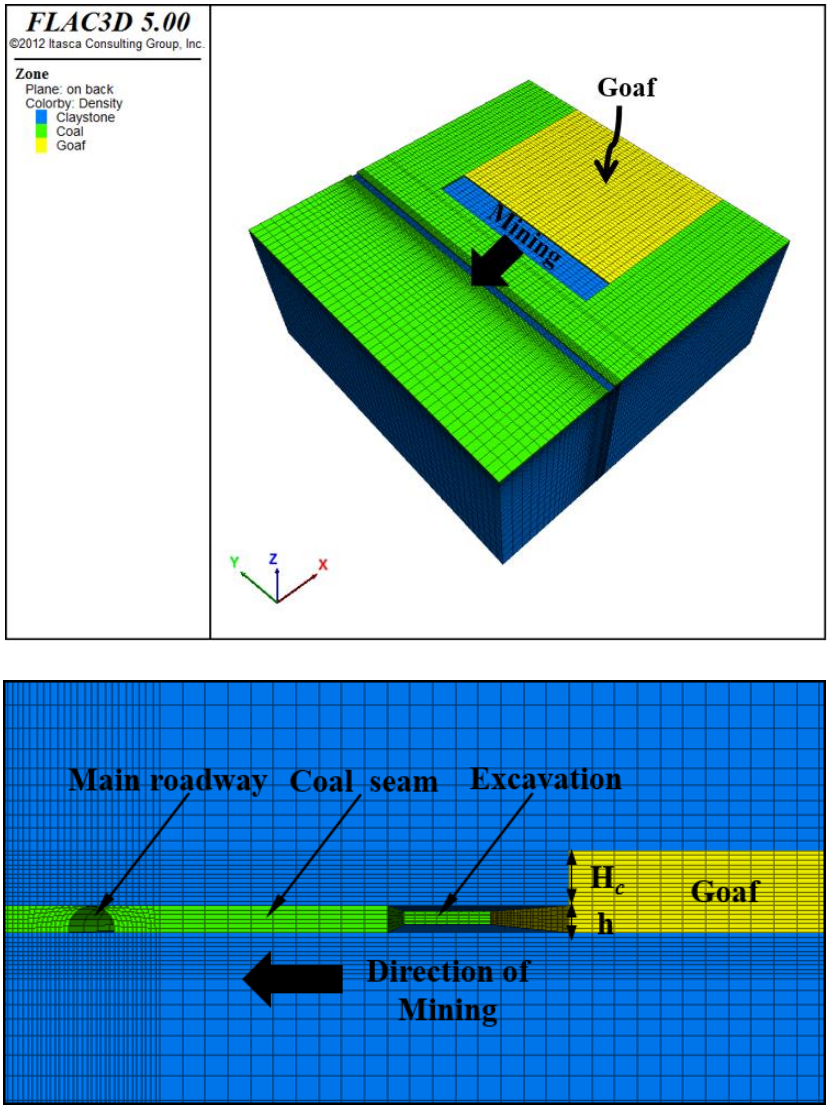

Figure 4.4 Installation of goaf in longwall mining simulation.

Table 4.2 Coefficients for different strata lithologies (Peng & Chiang, 1984; Bai, Kendorski, & Van, 1995).

Lithology	Uniaxial compressive strength (MPa)	c_1	c_2
Strong and hard	> 40	2.1	16
Medium strong	20-40	4.7	19
Soft and weak	<20	6.2	32

Table 4.3 Mechanical properties of goaf used in simulations (Thin, Pine, & Trueman, 1993; Xie, Chen, & Wang, 1999; Yasitli & Unver, 2005).

Parameter	Goaf
Uniaxial compressive strength (MPa)	-
Density (kg/m^3)	1,700
Young's modulus (MPa)	15
Poisson's ratio	0.25
Friction angle (˚)	25
Cohesion (MPa)	1.0x10^{-3}

4.2.3. Influence of Barrier Pillar Width on Main Roadway Stability and Its Design for Fixed Panel Width as 130 m

The effect of longwall mining on the stability of the main roadway was firstly investigated by leaving different barrier pillar widths during the panel extraction. The panel width was fixed at 130 m, and four mining depths of 50 m, 100 m, 150 m, and 200 m were considered in the simulations. The simulated results were used as a guideline for designing the appropriate barrier pillar width. Figure 4.5 shows an example of the strata deformation above the mined-out panel at 50 m depth. The figure illustrates how the panel extraction influences the stability of the main roadway. It is clear that the stability of the main roadway during the panel extraction will greatly depend on the width of barrier pillar and longwall panel. Therefore, an appropriate design of barrier pillar and longwall panel widths is very important to minimize the effect of the longwall mining on the main roadway stability.

Figure 4.6 illustrates the failure zone of the main roadway affected by longwall mining under different barrier pillar widths and mining depths. The main roadway was supported by 1 m and 0.5 m spaced steel arches (SS540, 95x115 mm). The column in the figure indicates the width of barrier pillar, while the row indicates the depth of longwall mining. It was noticed from the results that the additional failure zone progressively increased as the barrier pillar width decreased. This was because when the excavation face moved closer to the main roadway, or when the barrier

pillar width became narrower, the main roadway experienced higher impacts of longwall mining, and more additional failure zones developed. A significant increment of failure zone was observed when a narrow barrier pillar width was left at all mining depths. Based on the failure zone results, it can be said that the width of barrier pillar significantly influences the stability of the main roadway. Instability of the main roadway can be expected unless an adequate width of barrier pillar is provided.

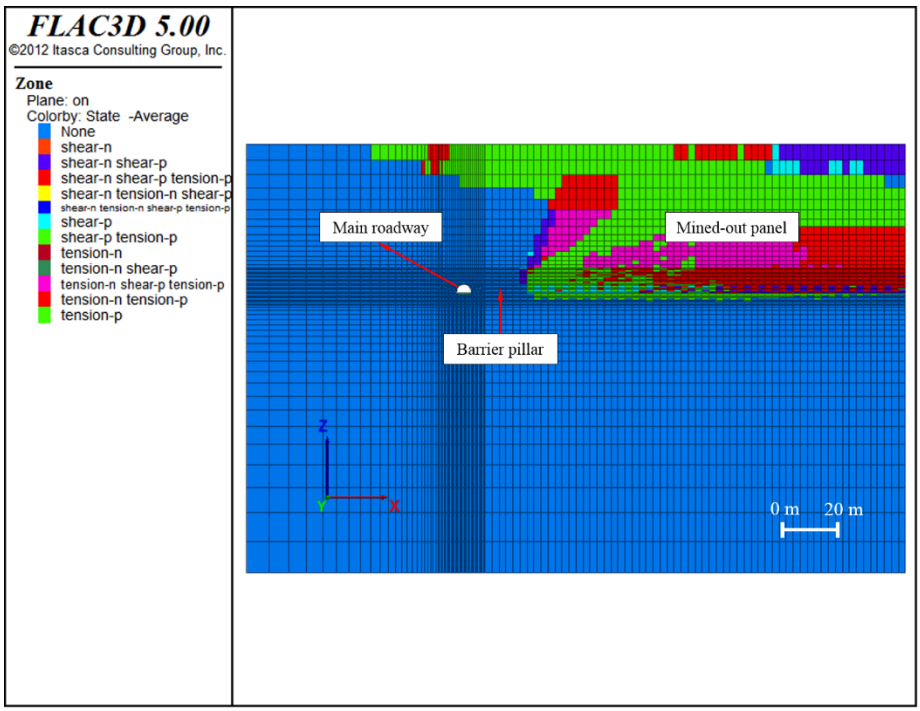

Figure 4.5 Illustration of strata deformation above mined-out panel and visualization of how panel extraction influences stability of main roadway.

Figure 4.7 illustrates the results of steel arch axial stress. The results confirm that the width of barrier pillar has a significant impact on the stability of main roadway. An increase in steel arch axial stress was associated with a decrease in barrier pillar width. The steel arch axial stress increased gradually after the longwall mining started, and a significant change of steel arch axial stress occurred when a narrow barrier pillar width was left. It revealed that a narrower barrier pillar produced greater steel arch axial stress, and this can deliver a worse stability condition to the main roadway. Therefore, careful design of barrier pillar width is particular necessary in order to keep the main roadway stable during the longwall panel

extraction. An appropriate width of barrier pillar was designed based on the results of steel arch axial stress in comparison with the maximum yield strength of steel arch SS540. According to the results, when the roadway was supported by the 1 m spaced steel arch, a barrier pillar width of 20 m, 20 m, 32 m, and over 60 m was sufficient to control the stability of main roadway at 50 m, 100 m, 150 m, and 200 m depth, respectively. On the contrary, a barrier pillar width of 20 m was adequate to maintain the main roadway at 50 m, 100 m, and 150 m depth, while a barrier pillar width of 34 m was needed at 200 m depth, when the roadway was supported by the 0.5 m spaced steel arch.

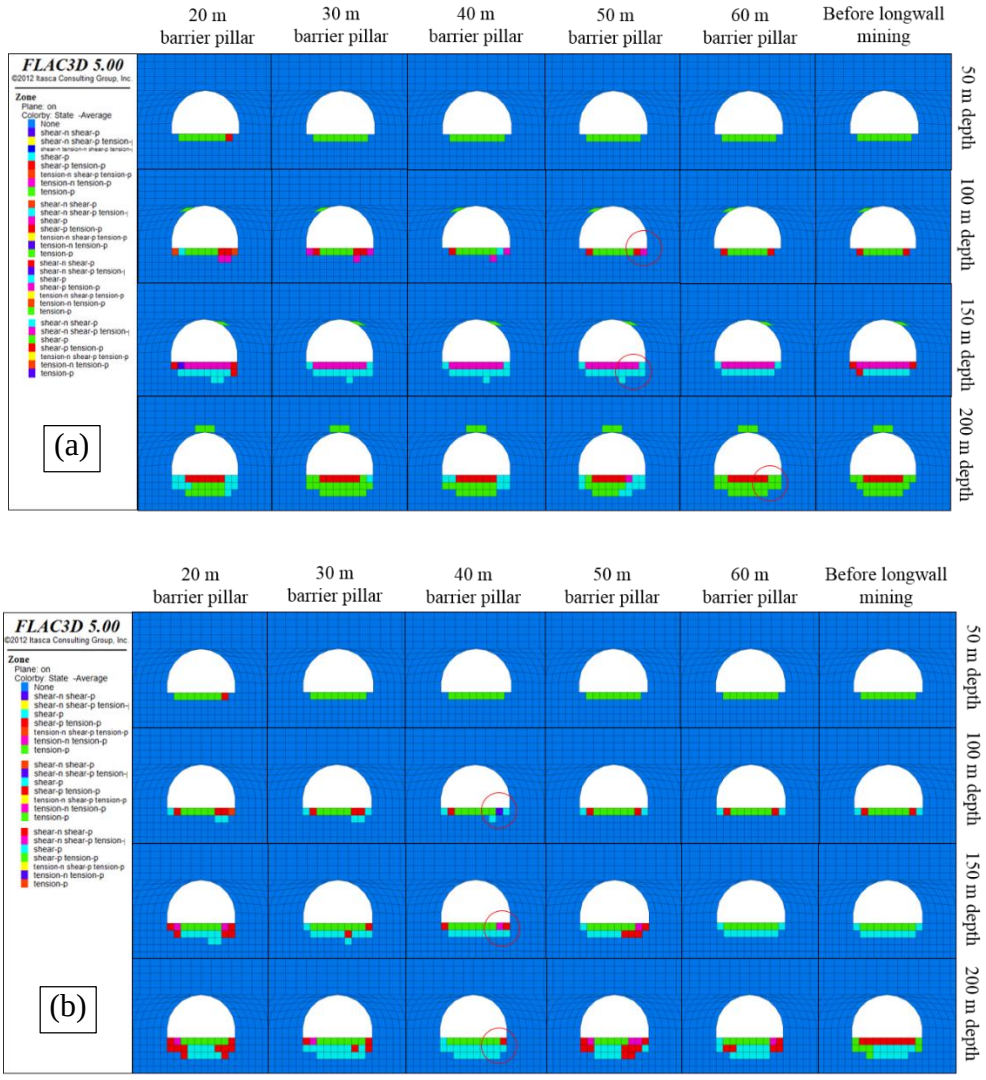

Figure 4.6 Failure zone of main roadway under different barrier pillar widths at various depths for fixed panel width as 130 m (a) roadway supported by 1 m spaced steel arch (b) roadway supported by 0.5 m spaced steel arch.

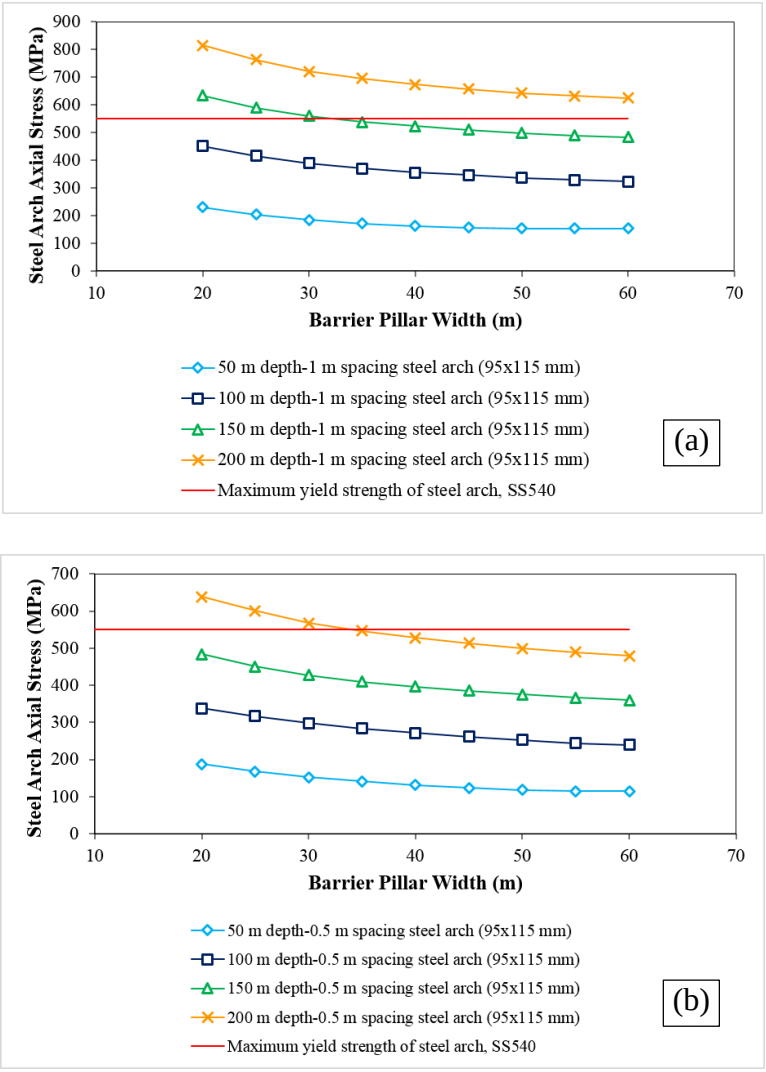

Figure 4. 7. Axial stress of steel arch support for main roadway under different barrier pillar widths at various depths for fixed panel width as 130 m (a) roadway supported by 1 m spaced steel arch (b) roadway supported by 0.5 m spaced steel arch.

From Figure 4.7, the relationships between the barrier pillar width, mining depth, and steel arch axial stress (use for representing the maximum yield strength of the steel arch) in form of equations were made. The equation form that fits the most to the graph and has the highest value of correlation coefficient (R^2) was selected. These equations can be used only for longwall mining of a 130 m panel width.

$$BP = (SS/(10.61H+99.44))^{-1/0.31} \quad ; R^2 = 0.89 \qquad (4.2)$$

$$BP = (SS/(8.39H+63.43))^{-1/0.32} \quad ; R^2 = 0.93 \qquad (4.3)$$

Where *BP* (m) is the barrier pillar width, *SS* (MPa) is the steel arch axial stress, and *H* (m) is the mining depth.

Note: Equation 4.2 is used when the main roadway is supported by the steel arches of 1 m space, whereas the Equation 4.3 is used when the main roadway is supported by 0.5 m spaced steel arches. The dimension of steel arch is 95x115 mm.

4.2.4. Influence of Panel Width on Main Roadway Stability and Barrier Pillar Width Design

The effect of longwall mining on the main roadway stability under various panel widths was investigated in this section. Three panel widths of 70 m, 100 m, and 130 m were simulated numerically. Similar to the previous section, four mining depths of 50 m, 100 m, 150 m, and 200 m, and the barrier pillar width ranging from 20 m to 60 m, were considered in the simulations. Figure 4.8 illustrates the failure zone around the main roadway affected by coal panel extraction under various panel and barrier pillar widths, and mining depths. The figure only shows the results of the main roadway supported by 0.5 m spaced steel arches. The row of the figure indicates the panel width, while the column indicates the width of barrier pillar. Based on the results, it was obviously seen that the effect of longwall mining on the main roadway stability was minimized effectively by reducing the panel width. The additional failure zone of the main roadway developed earlier at a larger barrier pillar width when a wider panel was mined. On the other hand, it developed later at a smaller barrier pillar width when a narrower panel was extracted. For example, at 200 m depth, the additional failure was noticed at 40 m and 20 m pillar width when a 130 m and 100 m panel width was mined, respectively, while no additional failure zone was observed when a 70 m panel width was extracted. This confirms that a smaller barrier pillar width can be designed if a narrower panel width is adopted.

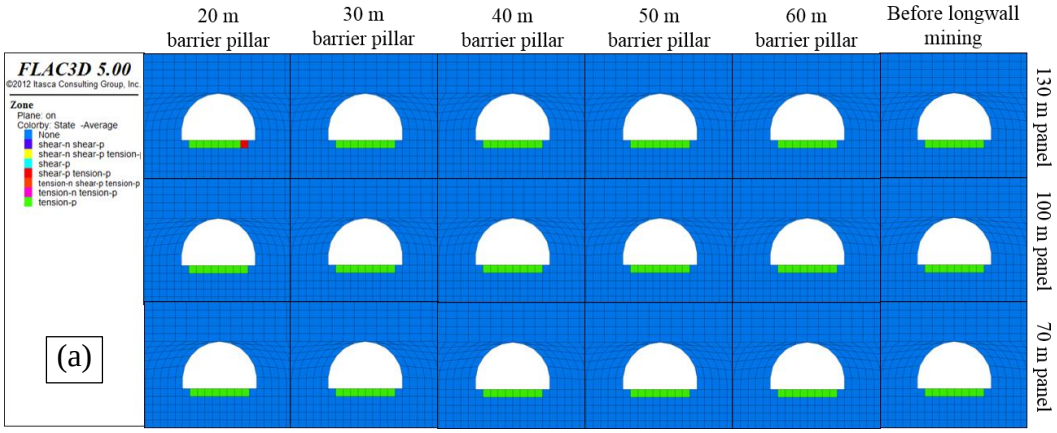
20 m barrier pillar
30 m barrier pillar
40 m barrier pillar
50 m barrier pillar
60 m barrier pillar
Before longwall mining
130 m panel
100 m panel
70 m panel
FLAC3D 5.00
(a)

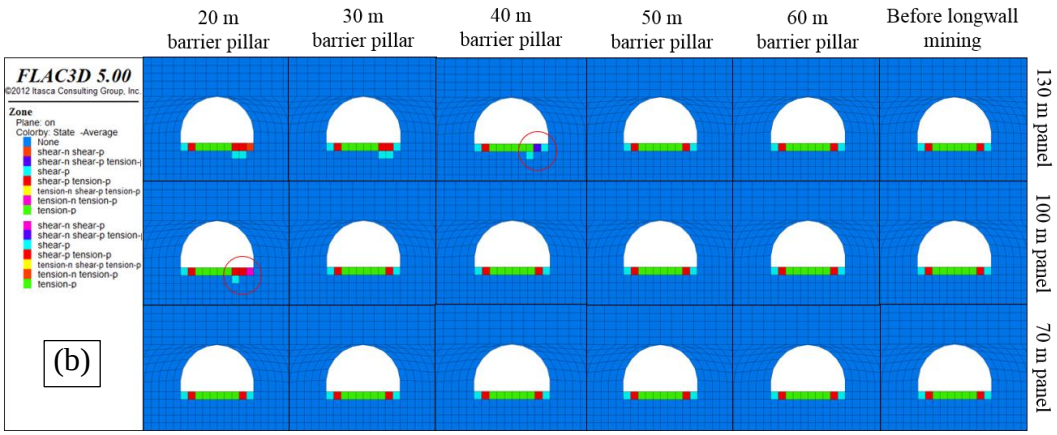
20 m barrier pillar
30 m barrier pillar
40 m barrier pillar
50 m barrier pillar
60 m barrier pillar
Before longwall mining
130 m panel
100 m panel
70 m panel
FLAC3D 5.00
(b)

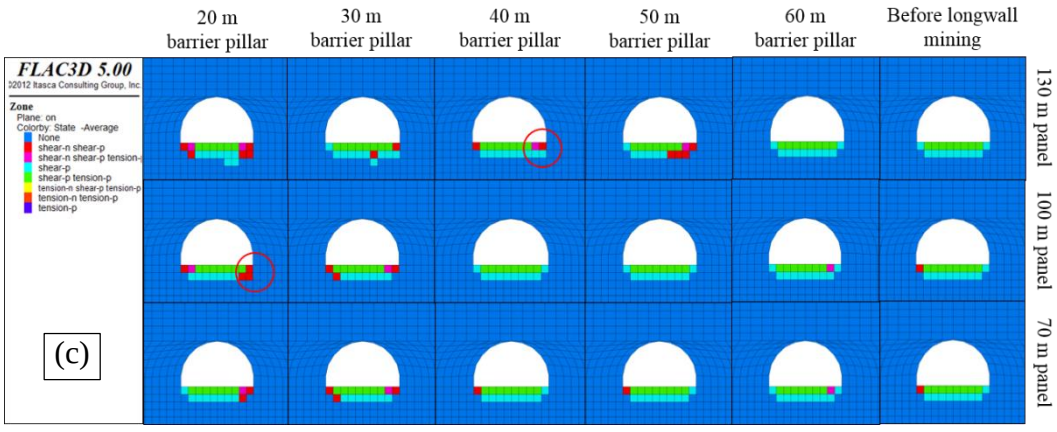
20 m barrier pillar
30 m barrier pillar
40 m barrier pillar
50 m barrier pillar
60 m barrier pillar
Before longwall mining
130 m panel
100 m panel
70 m panel
FLAC3D 5.00
(c)

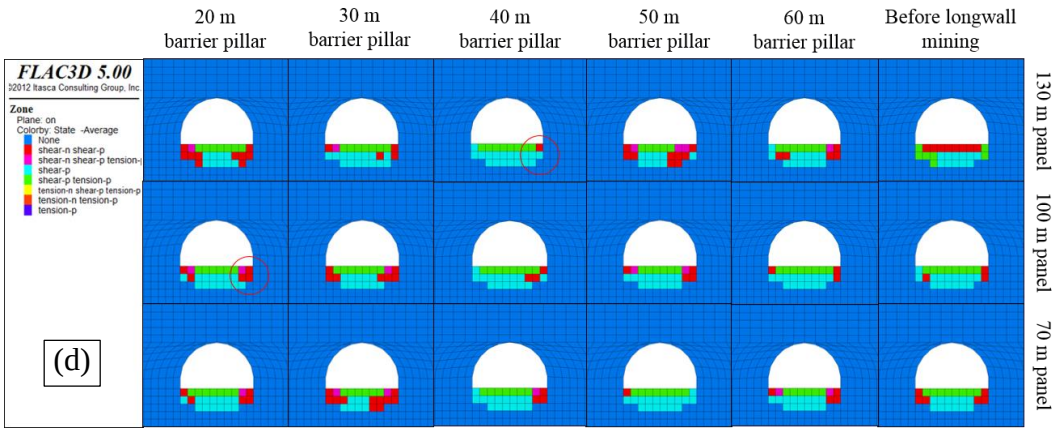

Figure 4.8 Failure zone of main roadway affected by longwall mining under various panel widths (a) at 50 m depth (b) at 100 m depth (c) at 150 m depth (d) at 200 m depth.

The results of steel arch axial stress obtained from longwall mining of three different panel widths are presented in Figure 4.9. The steel arch axial stress results support the results of failure zone. It revealed that the stability of the main roadway was improved by decreasing the panel width. A decrease in panel width considerably influenced the decrement of the steel arch axial stress. A less amount of steel arch axial stress was observed when a narrower panel width was mined. Compared the results of steel arch axial stress with the maximum yield strength of the steel arch SS540, the widths of the barrier pillar for different panel widths at various depths are suggested and summarized in Table 4.4. It can be seen from the table that a smaller barrier pillar width can be designed if a narrower panel width is adopted. When the main roadway was supported by 1 m spaced steel arches, the use of a barrier pillar width of 20 m was sufficient for longwall mining of a 70 m, 100 m, and 130 m panel width at 50 m and 100 m depth. At 150 m depth, a barrier pillar width of 20 m was enough for longwall mining of a 70 m panel width, while a wider barrier pillar width of 25 m and 32 m was required for longwall mining of a 100 m and 130 m panel width, respectively. At 200 m depth, the use of barrier pillar width larger than 60 m was recommended for longwall mining of all panel widths. On the contrary, when the main roadway was supported by 0.5 m spaced steel arches, a barrier pillar width of 20 m was adequate for longwall mining of a 70 m, 100 m, and 130 m panel width at 50 m, 100 m, and 150 m depth. At 200 m

depth, a barrier pillar width of 20 m was enough for longwall mining of a 70 m panel width, while a wider barrier pillar width of 23 m and 34 m was needed for longwall mining of a 100 m and 130 m panel width, respectively.

Table 4.4 Barrier pillar widths (m) for different panel widths at various depths.

Support of main roadway (SS540, 95x115 mm)		1.0 m space			0.5 m space		
Panel width (m)		70	100	130	70	100	130
Depth (m)	50	20	20	20	20	20	20
	100	20	20	20	20	20	20
	150	20	25	32	20	20	20
	200	>60	>60	>60	20	23	34

From Figure 4.9, the relationships between the barrier pillar width, panel width, and steel arch axial stress in form of equations were also made and summarized in Table 4.5.

Table 4.5 Equations of relationship between barrier pillar width, panel width, and steel arch axial stress.

Mining depth (m)	Support of main roadway (steel arch SS540, 95x115 mm)	
	0.5 m space	1.0 m space
50	$BP = (SS/(3.76PN+19.21))^{-1/0.29}$ $R^2 = 0.87$	$BP = (SS/(4.51PN+67.77))^{-1/0.28}$ $R^2 = 0.86$
100	$BP = (SS/(5.54PN+162.08))^{-1/0.26}$ $R^2 = 0.88$	$BP = (SS/(7.26PN+218.46))^{-1/0.3}$ $R^2 = 0.89$
150	$BP = (SS/(7.11PN+336.11))^{-1/0.3}$ $R^2 = 0.86$	$BP = (SS/(8.98PN+457.03))^{-1/0.294}$ $R^2 = 0.87$
200	$BP = (SS/(10.25PN+449.23))^{-1/0.32}$ $R^2 = 0.88$	$BP = (SS/(13.07PN+560.87))^{-1/0.27}$ $R^2 = 0.85$

Where *BP* (m) is the barrier pillar width, *SS* (MPa) is the steel arch axial stress, and *PN* (m) is the panel width.

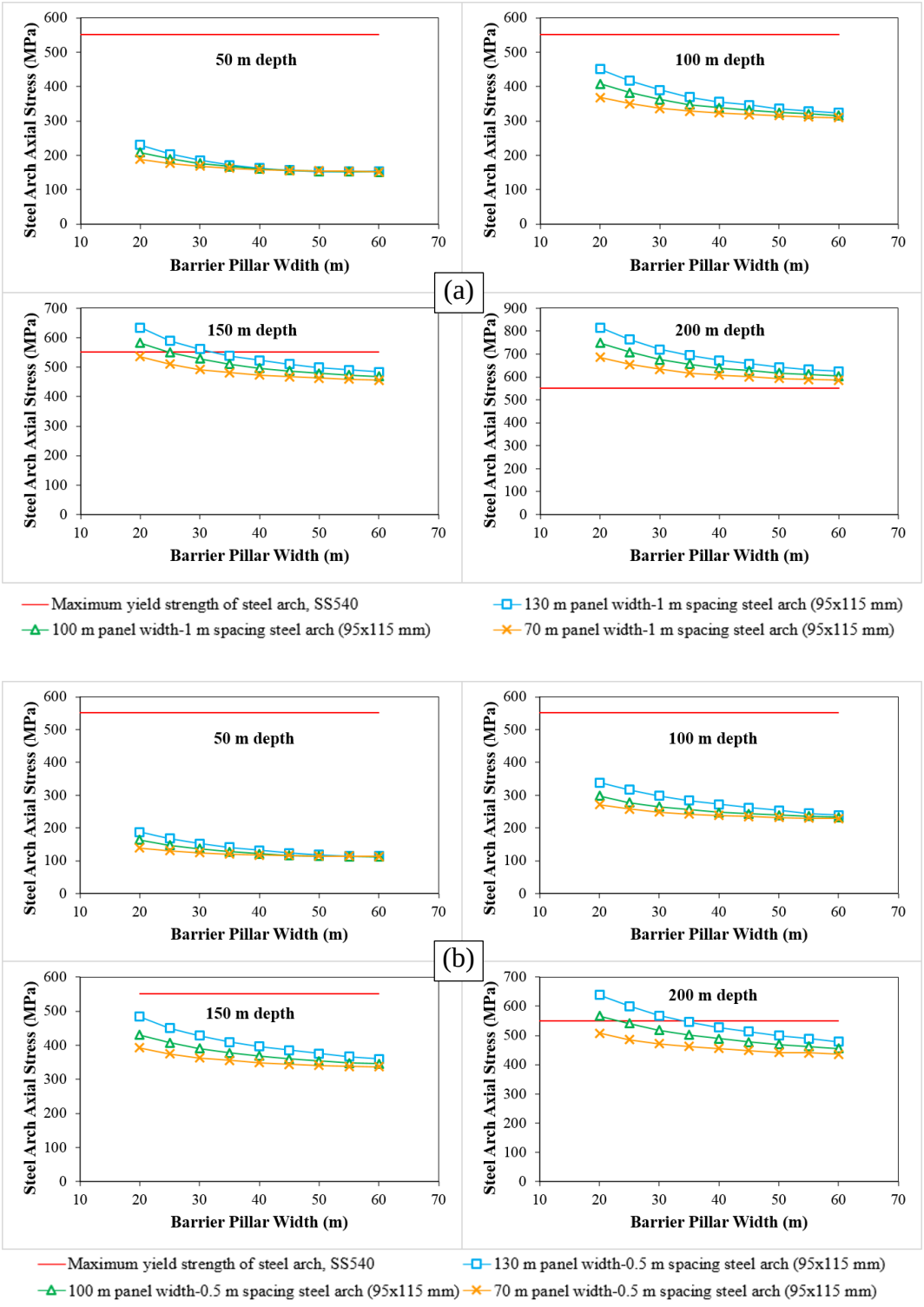

Figure 4.9 Axial stress of steel arch support for main roadway under different panel widths at various depths (a) roadway supported by 1 m spaced steel arch (b) roadway supported by 0.5 m spaced steel arch.

4.3. Effect of Longwall Mining on Stability of Gate Roadway

4.3.1. Description of Numerical Model

The effect of the longwall mining on the stability of the gate roadway was also studied in this chapter. The simulation includes the influence of chain pillar and panel widths. Several numerical models were created at various depths of 50 m, 100 m, 150 m, and 200 m. The model is 200 m in width, 400 m in length, while the height is varied depending on the mining depth. An example of the numerical model created at 200 m depth is illustrated in Figure 4.10. The model was fixed at two sides and bottom, and it was free at the surface. The stress ratio of 1 (k = 1) was considered, and the constitutive model of Mohr-Coulomb was employed. Generally, a single-entry gate roadway is a typical gate roadway system for longwall mining in Indonesia. However, due to the coal measure rocks are very weak, for safety reasons, the two-entry gate roadway system is adopted in GDM coal mine. In simulation, therefore, the two-entry gate roadway system was considered. The gate roadway was excavated inside a 3 m thick coal seam, semi-circular in shape, 5 m in width, and 3 m in height. The steel arch support was applied to maintain the stability of the gate roadway. The properties of rock mass, coal seam, and steel arch used in the simulations are the same with those that applied in the simulations of section 4.2.

As illustrated in Figure 4.10, two gate roadways were developed along the panel sides, forming the chain pillar. However, only the stability of gate roadway along the adjacent panel (to be mined-panel) was studied. The stability of the gate roadway along the mined-out panel was not considered in this study since this gate roadway has already finished its task and will not be used any longer. In simulation, the longwall mining started from the far end of the panel. The coal panel with the length of 300 m was extracted step by step, and the mined void behind the excavation face was filled with the goaf material. The extraction steps were repeated until the coal panel was entirely extracted. The panel extraction was simulated under the symmetric condition, so that only half side from the center of the model was analyzed. In order to observe the effect of longwall mining on the stability of the gate roadway, the results of failure zone and steel arch axial stress

were monitored at the middle of the gate roadway after the coal panel was completely mined out.

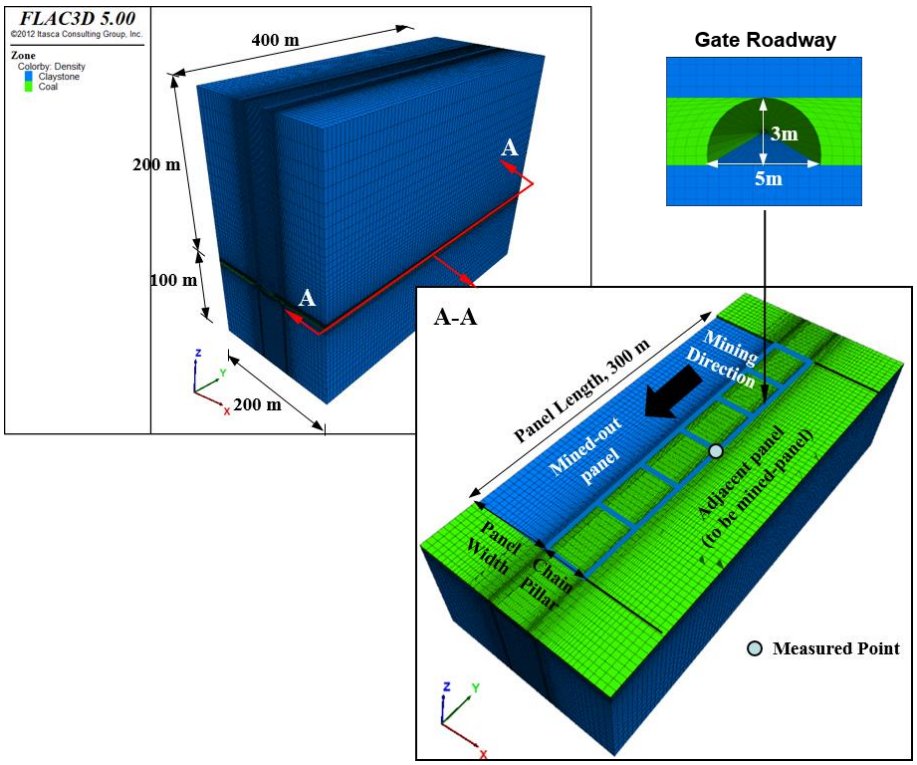

Figure 4.10 Numerical model of longwall mining for gate roadway stability analysis at 200 m depth.

4.3.2. Influence of Chain Pillar Width on Gate Roadway Stability and Its Design for Fixed Panel Width as 130 m

Figure 4.11 shows an example of the strata deformation above the mined-out panel and the visualization of how the panel extraction affects the stability of the gate roadway at 50 m depth. It can be expected from the figure that the stability of the gate roadway will significantly depend on the width of the chain pillar and longwall panel. Hence, having an appropriate width of the chain pillar and longwall panel is very important to minimize the effect of the longwall mining on the gate roadway stability. In this section, the influence of the chain pillar width on the gate roadway stability during the longwall mining was studied and discussed. In simulation, four chain pillar widths of 30 m, 40 m, 50 m, and 60 m, and four mining depths of 50 m, 100 m, 150 m, and 200 m were considered. The panel width was fixed at 130 m.

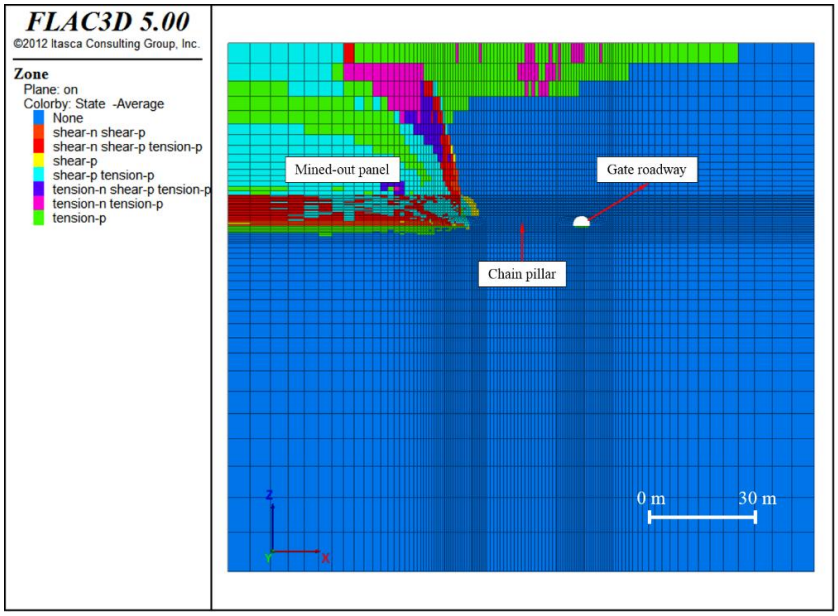

Figure 4.11 Illustration of strata deformation above mined-out panel and visualization of how panel extraction influences stability of gate roadway.

The failure zone of gate roadway after longwall mining under different chain pillar widths and mining depths is presented in Figure 4.12. The chain pillar width is arranged in the column, while the mining depth is arranged in the row of the figure. The results show that the additional failure zone increased with decreasing the chain pillar width. This could be due to that when a narrower chain pillar width was used during the longwall mining, the gate roadway experienced larger induced stresses caused by the coal panel extraction, resulting in a larger additional failure zone developed. Thus, it can be said that the chain pillar width has a significant influence on the stability of the gate roadway. A longwall mining with a wider chain pillar gives a better stability condition to the gate roadway.

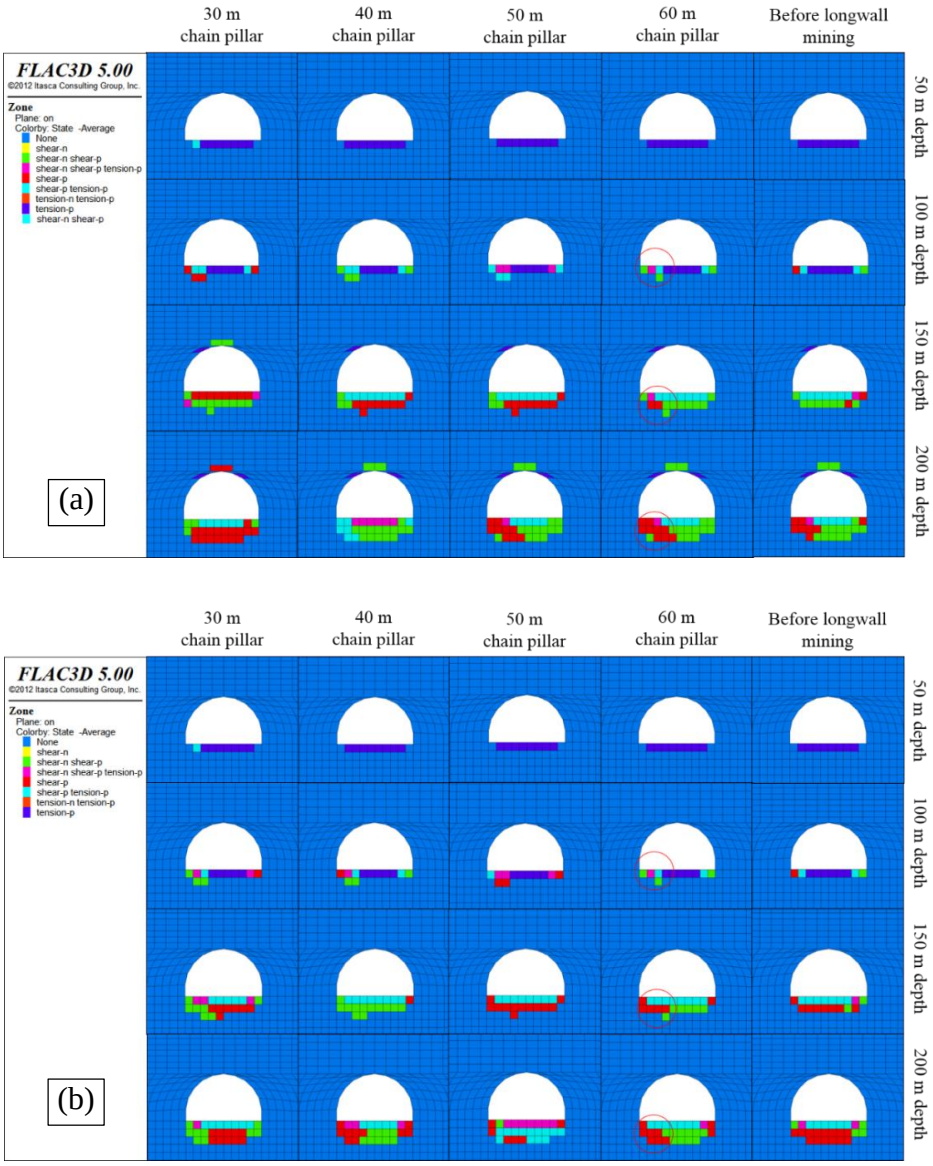

Figure 4.12 Failure zone of gate roadway under different chain pillar widths at various depths for fixed panel width as 130 m (a) roadway supported by 1 m spaced steel arch (b) roadway supported by 0.5 m spaced steel arch.

Figure 4.13 illustrates steel arch axial stress results of the steel arch support installed in the gate roadway. The same thing happened here as that happened with the failure zone. The steel arch axial stress increased significantly as the chain pillar width decreased. This confirms that a decrease in chain pillar width promoted an increase in longwall mining effect on the gate roadway stability. A proper chain pillar width must be selected in order to ensure the stability control of the gate roadway during the mining of coal panel. The appropriate chain pillar width was recommended

based on the comparison of steel arch axial stress results and the maximum yield strength of the steel arch. According to the comparisons, when the roadway was supported by the 1 m spaced steel arch, a chain pillar width of 30 m was sufficient to ensure the stability of gate roadway at 50 m and 100 m depth, whereas a 50 m chain pillar width was needed at 150 m depth, and a chain pillar width wider than 60 m was required at 200 m depth. In contrast, a chain pillar width of 30 m was adequate to maintain the gate roadway at 50 m, 100 m, and 150 m depth, while a chain pillar width of 50 m was adequate at 200 m depth, when the gate roadway was supported by the 0.5 m spaced steel arch.

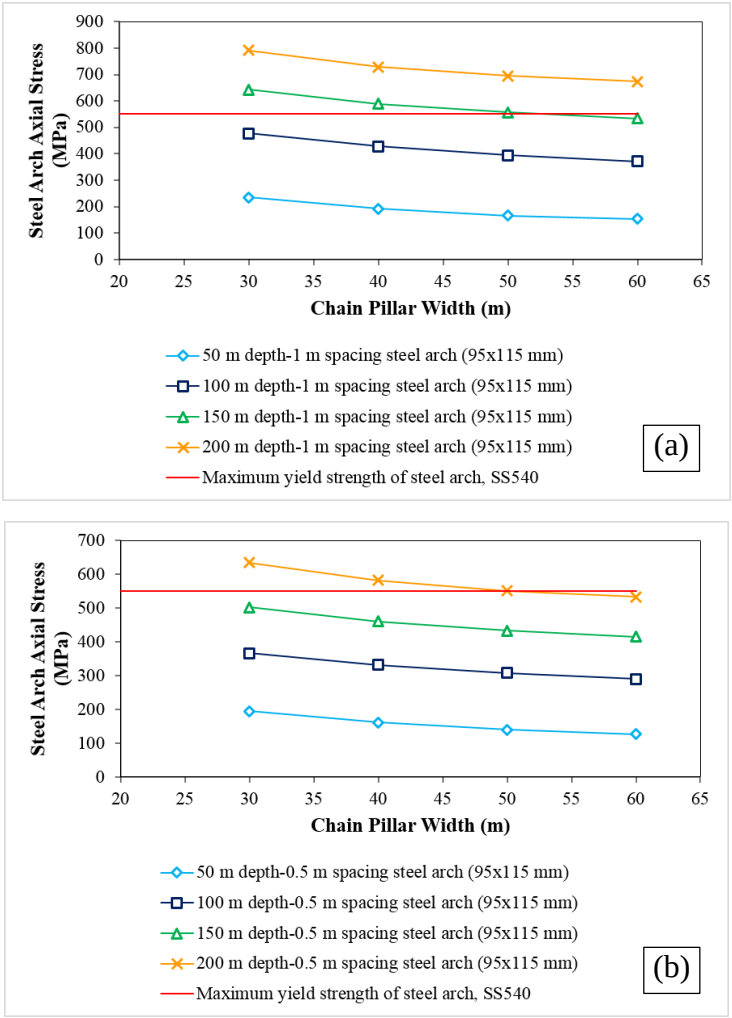

Figure 4.13 Axial stress of steel arch support for gate roadway under different chain pillar widths at various depths for fixed panel width as 130 m (a) roadway supported by 1 m spaced steel arch (b) roadway supported by 0.5 m spaced steel arch.

From Figure 4.13, the relationships between the chain pillar width, mining depth, and steel arch axial stress (use for representing the maximum yield strength of the steel arch) in form of equations were made. The equation form that fits the most to the graph and has the highest value of correlation coefficient (R^2) was selected. The use of these equations is limited to the longwall mining of a 130 m panel width only. The equations are written as below.

$$CP = (3.87H+147.27-SS)/3.42 \quad ; R^2 = 0.96 \quad (4.4)$$

$$CP = (3.11H+112.37-SS)/3.33 \quad ; R^2 = 0.96 \quad (4.5)$$

Where *CP* (m) is the chain pillar width, *SS* (MPa) is the steel arch axial stress, and *H* (m) is the mining depth.

Note: Equation 4.4 is used when the gate roadway is supported by the steel arches of 1 m space, whereas the Equation 4.5 is used when the gate roadway is supported by 0.5 m spaced steel arches. The dimension of steel arch is 95x115 mm.

4.3.3. Influence of Panel Width on Gate Roadway Stability and Chain Pillar Width Design

The effect of longwall mining on the gate roadway stability under various panel widths of 70 m, 100 m, and 130 m was studied numerically in this section. Four mining depths of 50 m, 100 m, 150 m, and 200 m, and four chain pillar widths of 30 m, 40 m, 50 m, and 60 m, were considered in the simulations. Figure 4.14 demonstrates the comparison of failure zones occurred in the gate roadway after three panel widths were extracted. The figure only shows failure zone results of the gate roadway supported by 0.5 m spaced steel arches. The row of the figure indicates the panel width, while the column indicates the width of chain pillar. The results show that a decrease in effect of longwall mining on the stability of the gate roadway was considerably associated with a decrease in panel width. The additional failure zone developed earlier at a larger chain pillar width when a wider panel width was mined. In contrast, it developed later at a smaller chain pillar when a narrower panel width was extracted. For example, at 200 m depth, the additional failure was noticed at 60 m, 40 m, and 30 m chain pillar width when a 130 m, 100

m, and 70 m panel width was mined, respectively. This confirms that a smaller chain pillar width can be designed if a narrower panel width is adopted.

Figure 4.15 presents the results of steel arch axial stress obtained from longwall mining under different panel widths. The results represent that the effect of longwall mining on the gate roadway stability can be minimized by decreasing the panel width. A narrower panel width gave less effect of longwall mining, while a wider panel width gave more. A decrement of steel arch axial stress was observed when the panel width decreased. Several widths of the chain pillar for different panel widths at various depths were recommended based on the results of steel arch axial stress compared with the maximum yield strength of the steel arch SS540. These chain pillar widths are summarized in Table 4.6. It can be seen from the table that a smaller chain pillar width can be designed if a narrower panel width is adopted. When the gate roadway was supported by 1 m spaced steel arches, a chain pillar width of 30 m was enough at 50 m and 100 m depth for longwall mining of all panel widths of 70 m, 100 m, and 130 m. At 150 m, a chain pillar width of 37 m, 45 m, and 50 m was sufficient for longwall mining of a 70 m, 100 m, and 130 m panel width, respectively. Besides, the use of chain pillar width wider than 60 m was suggested at 200 m depth for longwall mining of all panel widths. In contrast, when the gate roadway was supported by 0.5 m spaced steel arches, a chain pillar width of 30 m was adequate until 150 m for longwall mining of all panel widths. However, the use of a wider chain pillar width of 32 m, 40 m, and 50 m was recommended at 200 m depth for longwall mining of a 70 m, 100 m, and 130 m panel width, respectively.

Table 4.6 Chain pillar widths (m) for different panel widths at various depths.

Support of gate roadway (SS540, 95x115 mm)		1.0 m space			0.5 m space		
Panel width (m)		70	100	130	70	100	130
Depth (m)	50	30	30	30	30	30	30
	100	30	30	30	30	30	30
	150	37	45	50	30	30	30
	200	>60	>60	>60	32	40	50

From Figure 4.15, the relationships between the chain pillar width, panel width, and steel arch axial stress in form of equations were also made and summarized in Table 4.7.

Table 4.7 Equations of relationship between chain pillar width, panel width, and steel arch axial stress.

Mining depth (m)	Support of gate roadway (steel arch SS540, 95x115 mm)	
	0.5 m space	1.0 m space
50	$CP = (0.88PN+145.51-SS)/2.23$ $R^2 = 0.96$	$CP = (1.11PN+167.39-SS)/2.5$ $R^2 = 0.93$
100	$CP = (1.4PN+258.42-SS)/2.52$ $R^2 = 0.97$	$CP = (1.59PN+374-SS)/3.55$ $R^2 = 0.97$
150	$CP = (1.63PN+373.61-SS)/2.47$ $R^2 = 0.96$	$CP = (1.29PN+575.5-SS)/3.19$ $R^2 = 0.95$
200	$CP = (1.64PN+514.34-SS)/2.98$ $R^2 = 0.95$	$CP = (1.17PN+747.37-SS)/3.61$ $R^2 = 0.94$

Where *CP* (m) is the chain pillar width, *SS* (MPa) is the steel arch axial stress, and *PN* (m) is the panel width.

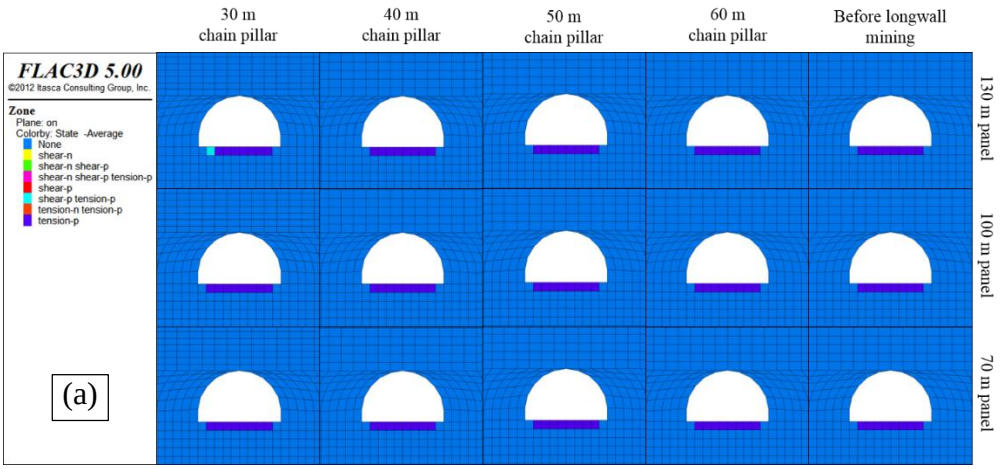

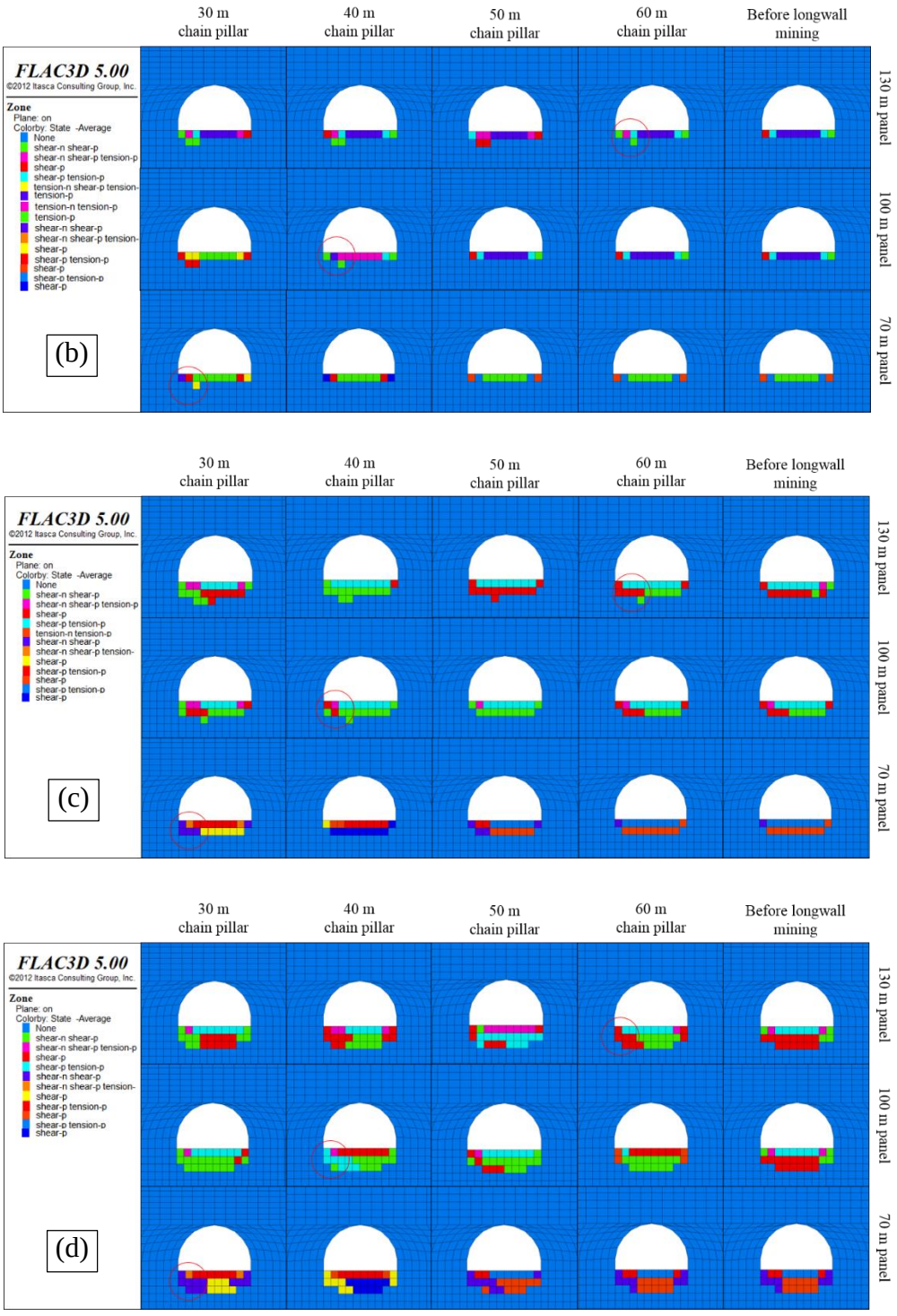

Figure 4.14 Failure zone of gate roadway affected by longwall mining under various panel widths (a) at 50 m depth (b) at 100 m depth (c) at 150 m depth (d) at 200 m depth.

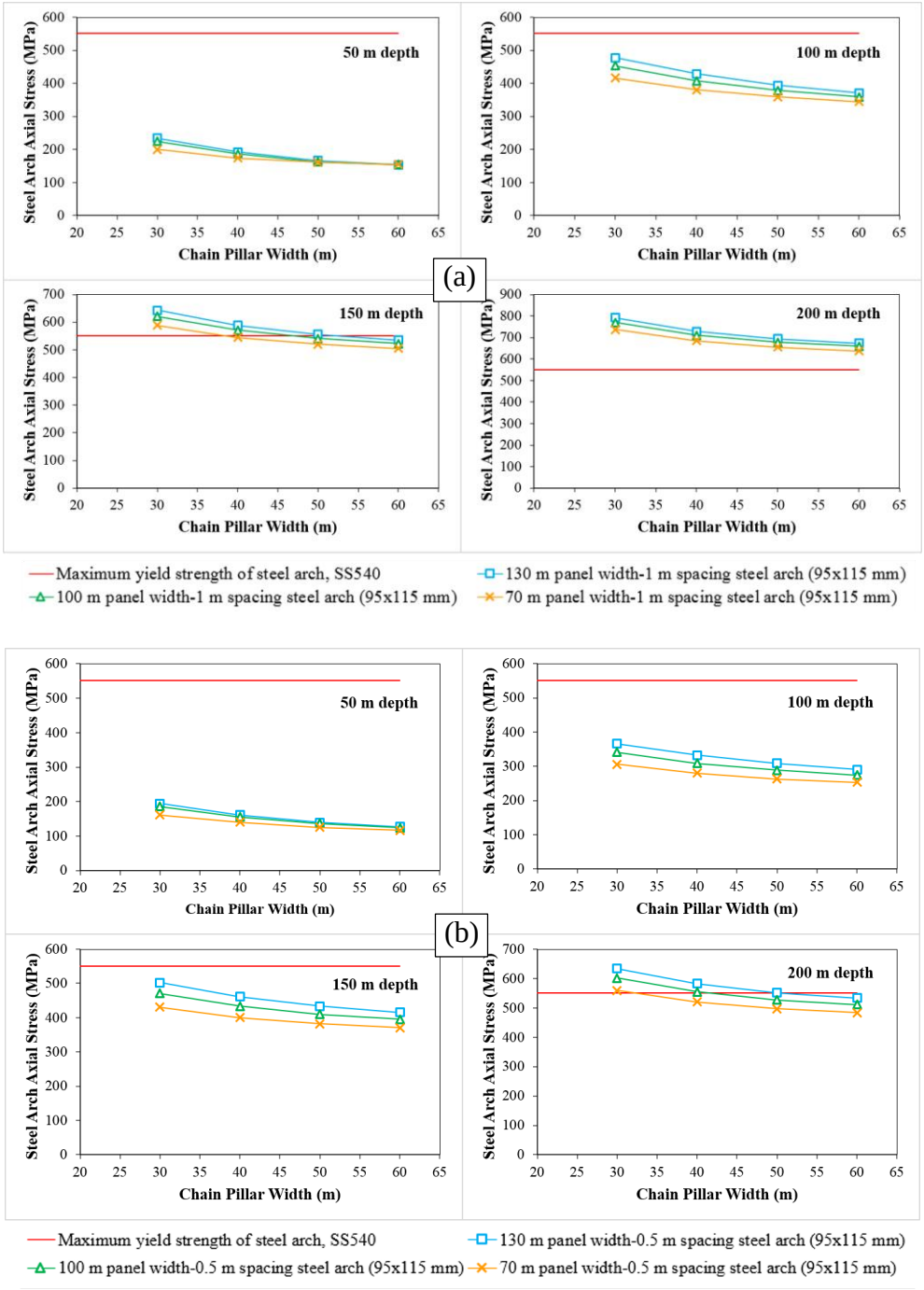

Figure 4.15 Axial stress of steel arch support for gate roadway under different panel widths at various depths (a) roadway supported by 1 m spaced steel arch (b) roadway supported by 0.5 m spaced steel arch.

4.4. Conclusions

In this chapter, the effect of longwall mining on the stability of the main/gate roadway under various barrier/chain pillar and panel widths at different mining depths are studied numerically using a three-dimensional finite difference code software, FLAC3D. The simulated results indicate that the effect of longwall mining on the main/gate roadway stability depends mainly on the barrier/chain pillar and panel widths and the mining depth. The greatest effect occurs when the wide panel width and the narrow barrier/chain pillar width are applied, whereas the smallest effect happens when the narrow panel width and the wide barrier/chain pillar width are adopted. The stability of the main/gate roadway can be improved by increasing the barrier/chain pillar width or decreasing the width of the panel. Mining a wide coal panel, a large barrier/chain pillar width is needed. A small barrier/chain pillar width can be designed if a narrow longwall panel width is adopted.

Based on the results of steel arch axial stress in comparison with the maximum yield strength of the steel arch SS540, an appropriate barrier pillar width is suggested in order to maintain the main roadway during the longwall mining. When the main roadway is supported by 1 m spaced steel arches, the use of a barrier pillar width of 20 m is sufficient for longwall mining of a 70 m, 100 m, and 130 m panel width at 50 m and 100 m depth. At 150 m depth, a barrier pillar width of 20 m is enough for longwall mining of a 70 m panel width, while a wider barrier pillar width of 25 m and 32 m is required for longwall mining of a 100 m and 130 m panel width, respectively. At 200 m depth, the use of barrier pillar width wider than 60 m is recommended for longwall mining of all panel widths. On the contrary, when the main roadway is supported by 0.5 m spaced steel arches, a barrier pillar width of 20 m is adequate for longwall mining of a 70 m, 100 m, and 130 m panel width at 50 m, 100 m, and 150 m depth. At 200 m depth, a barrier pillar width of 20 m is enough for longwall mining of a 70 m panel width, while a wider barrier pillar width of 23 m and 34 m is needed for longwall mining of a 100 m and 130 m panel width, respectively.

In addition, to maintain the gate roadway during the longwall mining, an appropriate width of chain pillar is also recommended in this chapter. When the gate roadway is supported by 1 m spaced steel arches, a chain pillar width of 30 m can be used at 50 m and 100 m depth for longwall mining of all panel widths of 70 m, 100 m, and 130 m. At 150 m, a chain pillar width of 37 m, 45 m, and 50 m is sufficient for longwall mining of a 70 m, 100 m, and 130 m panel width, respectively. Besides, the use of chain pillar width wider than 60 m is suggested at 200 m depth for longwall mining of all panel widths. In contrast, when the gate roadway is supported by 0.5 m spaced steel arches, a chain pillar width of 30 m can be used until 150 m for longwall mining of all panel widths. However, the use of a wider chain pillar width of 32 m, 40 m, and 50 m is recommended at 200 m depth for longwall mining of a 70 m, 100 m, and 130 m panel width, respectively.

References

Bai, M., Kendorski, F., & Van, R. D. (2004). Chinese and North American high-extraction underground coal mining strata behaviour and water protection experience and guidelines. Proceedings of the 14th International Conference on Ground Control in Mining, Morgantown.

Brady, B. H. G., & Brown, E. T. (2004). Rock mechanics for underground mining (3rd Ed.). Dordrecht.

Cheng, Y. M., Wang, J. A., Xie, G. X., & Wei, W. B. (2010). Three-dimentional analysis of coal barrier pillars in tailgate area adjacent to the filly mechanized top coal caving mining face. International Journal of Rock Mechanics and Mining Sciences, 47, 1372-1383.

Hoek, E., & Brown, E. T. (1982). Underground excavations in rock. Institution of Mining and Mettalurgy.

Hudson, J. A. (1993). Comprehensive Rock Engineering. Pergamon Press.

Itasca Consulting Group, Inc. (2009). FLAC3D Fast Lagrangian Analysis of Continua in 3 Dimensions: User's Guide, Mill Place, Minneapolis, 55401 USA.

MSEC (Mine Subsidence Engineering Consultants). (2007). Introduction to longwall mining and subsidence. PO Box 3047 Willoughby North NSW 2068, Australia.

Peng, S. S., & Chiang, H. S. (1984). Longwall mining. John Wiley & Sons.

Thin, I. G. T., Pine, R. J., & Trueman, R. (1993). Numerical modelling as an aid to the determination of the stress distribution in the goaf due to longwall coal mining. International Journal of Rock Mechanics and Mining Sciences and Geomechanics Abstracts, 30(7), 1403-1409.

Xie, H., Chen, Z., & Wang, J. (1999). Three-dimensional numerical analysis of deformation and failure during top coal caving. International Journal of Rock Mechanics and Mining Sciences, 36(5), 651-658.

Yavuz, H. (2004). An estimation method for cover pressure re-establishment distance and pressure distribution in the goaf of longwall coal mines. International Journal of Rock Mechanics and Mining Sciences, 41, 193-205.

Yasitli, N. E., & Unver, B. (2005). 3D numerical modeling of longwall mining with top-coal caving. International Journal of Rock Mechanics and Mining Sciences, 42(2), 219-235.

CHAPTER 5

SURFACE SUBSIDENCE INDUCED BY LONGWALL MINING

5.1. Background

In the previous chapter, the effect of longwall mining on the stability of main and gate roadways was analyzed and discussed. To maintain the stability of main and gate roadways during the coal panel extraction, several widths of barrier and chain pillar were suggested for different panel widths under various depths. In the situation of GDM coal mine, as some houses and rice fields exist at the surface above the mining area, not only the effect of longwall mining on the roadway stability needs to be taken into consideration, but also the surface subsidence induced by longwall mining operation.

Although longwall mining method provides high productivity and safe working conditions in underground mining, because of a large extent of coal is removed from the seam, many underground mines have been experienced with the geotechnical problems due to surface subsidence. Peng and Chiang (1984) demonstrated the mechanisms of roof strata movement above a longwall mining (see Figure 5.1). The roof strata behind the excavation face are collapsed to fill the stope void when a longwall panel of sufficient width and length is mined, resulting in subsiding of the immediate roof strata toward the surface. Whittaker and Reddish (1989) illustrated the basic subsidence profile resulting from longwall mining of a single panel (see Figure 5.2). Two parameters are used to define the magnitude, shape, and limitation of the subsidence at the surface, such as maximum surface subsidence (S_{max}) and angle of draw (AoD).

Because of a large extent of coal will be removed from the seam, and due to the coal measure rocks are weak, a large subsidence at the surface can be expected when a longwall mining is applied in GDM underground coal mine. Undeniably, a study of surface subsidence is needed in order to avoid the adverse impacts of subsidence at the surface. The knowledge will improve a design of longwall mining. The objective of this chapter is to study the surface subsidence induced by longwall

mining. The characteristics of surface subsidence induced by single-panel and multi-panel longwall mining are studied by means of numerical simulation method using a three-dimensional finite difference code software, FLAC3D. The countermeasures for subsidence control and mitigation are also discussed in this chapter. The angle of draw (AoD) and maximum surface subsidence (S_{max}) are used to describe the characteristics of subsidence at the surface.

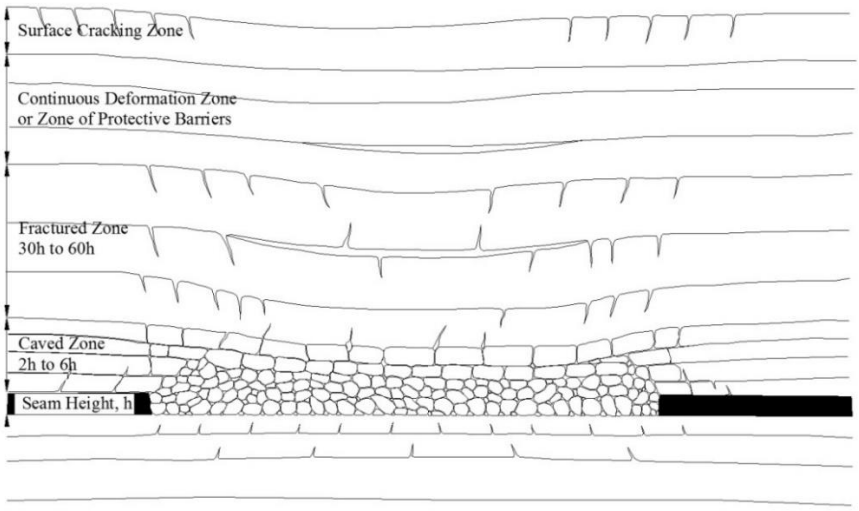

Figure 5.1 Strata movement resulting from longwall mining (Peng, & Chiang, 1984).

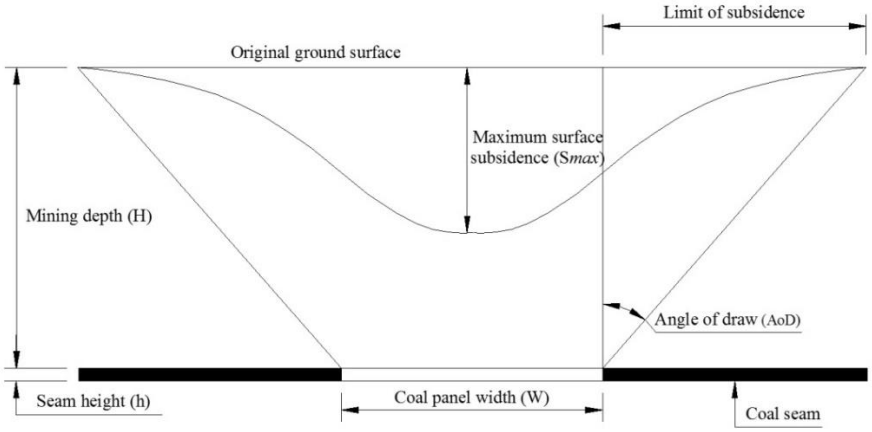

Figure 5.2 Basic subsidence profile above single longwall mining (Whittaker & Reddish, 1989).

5.2. Applicability of Numerical Simulation Method for Prediction of Surface Subsidence under Weak Geological Conditions

Because the GDM underground coal mine is still in the process of developing the main roadways, the measurement data of surface subsidence at this mine site is unavailable currently. The subsidence results presented in this chapter are only simulated results obtained from the numerical simulations. To verify the simulated results with the field measurement data for this coal mine is impossible at present. There exists a doubt whether the numerical simulation method is applicable for subsidence prediction in this study or not. Therefore, in order to confirm this doubt, the applicability of numerical simulation method using FLAC3D was confirmed in the case of Fajar Bumi Sakti (FBS) coal mine. The characteristics of surface subsidence obtained from the field measurement, empirical method, and numerical simulation were compared and discussed. FBS underground coal mine is located in East Kalimantan, Indonesia, only 15 km far from GDM coal mine (see Figure 5.3). The FBS coal mine is situated in the Balikpapan coal-bearing formation the same as that the GDM coal mine. The stratigraphy of FBS coal mine is shown in Figure 5.4. The overburden rocks at this mine site consist of mudstone and siltstone. The UCSs of the rocks are 3 MPa for siltstone and 1-4 MPa for mudstone (Sasaoka et al., 2015b). The UCS results indicate that the rocks in this coal mine are very weak (Bieniawski, 1974; Hoek & Brown, 1997). Figure 5.5 illustrates the monitoring points of the subsidence at the surface with a longwall panel layout. The monitoring points were located along the center line of the mined-out panel. The depth of the longwall mining is 50 m. The thickness of extracted seam is 1.9 m, and the width and length of the mined-out panel is 83 m and 140 m, respectively.

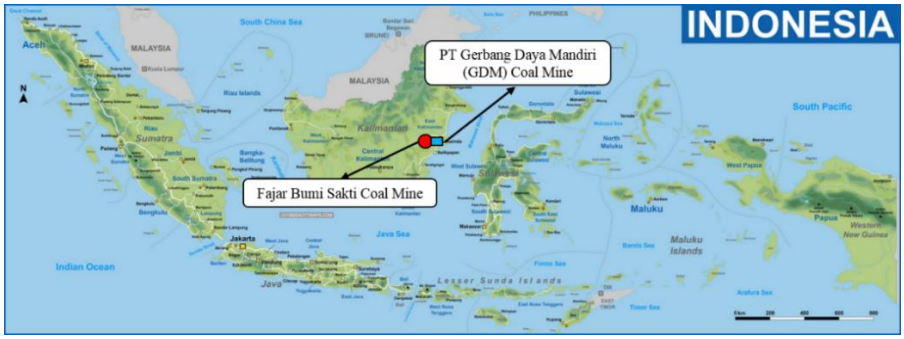

Figure 5.3 Location of GDM and FBS coal mines.

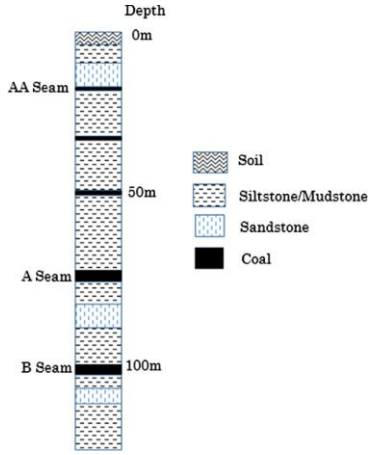

Figure 5.4 Stratigraphic column of FBS coal mine (Sasaoka et al., 2015b).

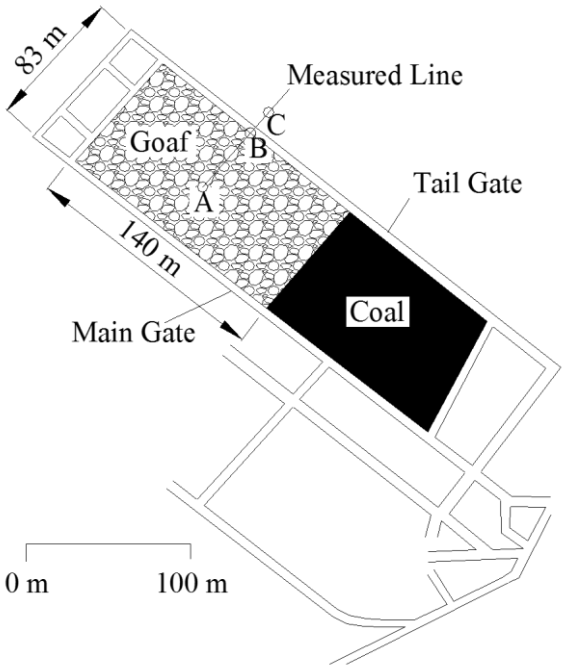

Figure 5.5 Layout of subsidence monitoring points (Sasaoka et al., 2015b).

Figure 5.6 shows the final subsidence profile along the measured line. The subsidence data at each point were measured for eight months from the date the longwall mining started. The maximum surface subsidence of 1.4 m, 0.12 m, and 0.05 m was obtained at point A, B, and C, respectively.

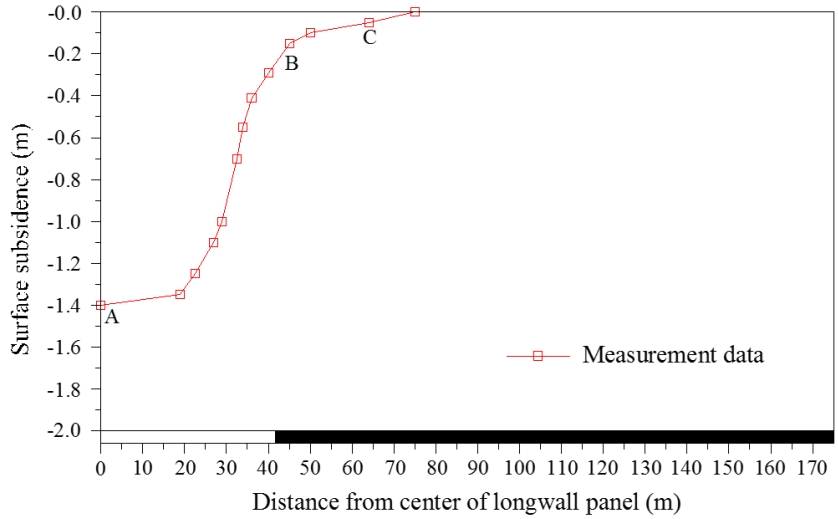

Figure 5.6 Final subsidence profile along measured line (Sasaoka et al., 2015b).

The surface subsidence data measured at FBS coal mine was compared with the results obtained from the empirical method and numerical simulation in order to confirm the most applicable method for prediction of surface subsidence under weak geological condition. The empirical methods are easy to use and the calculations can be performed by hand or simple scientific calculators. A number of empirical methods have been developed and used in the major coal producing countries. However, the National Coal Board (NCB) method is the most comprehensive and popular empirical method in the field of mining subsidence. It was developed from subsidence observations at numerous mine sites in UK and US. The application procedure to use the NCB method in predicting the final surface subsidence is outlined in the following sections. Figure 5.7 shows the chart for determining the apparent subsidence factor (*a'*) using the panel width (*W*) and overburden depth (*H*). In the case of FBS coal mine, for a longwall panel width of 83 m (272 ft) at a depth of 50 m (164 ft), the apparent subsidence factor (*a'*) was read as about 0.65. The maximum subsidence (S_{max}) was then determined as 0.69 m using an equation expresses as below (Luo, 1989).

$$S_{max} = 1.2a'hH(1/LW)^{0.5} \quad (5.1)$$

Where *h* is the thickness of extracted coal seam (m), and *L* is the length of longwall panel (m).

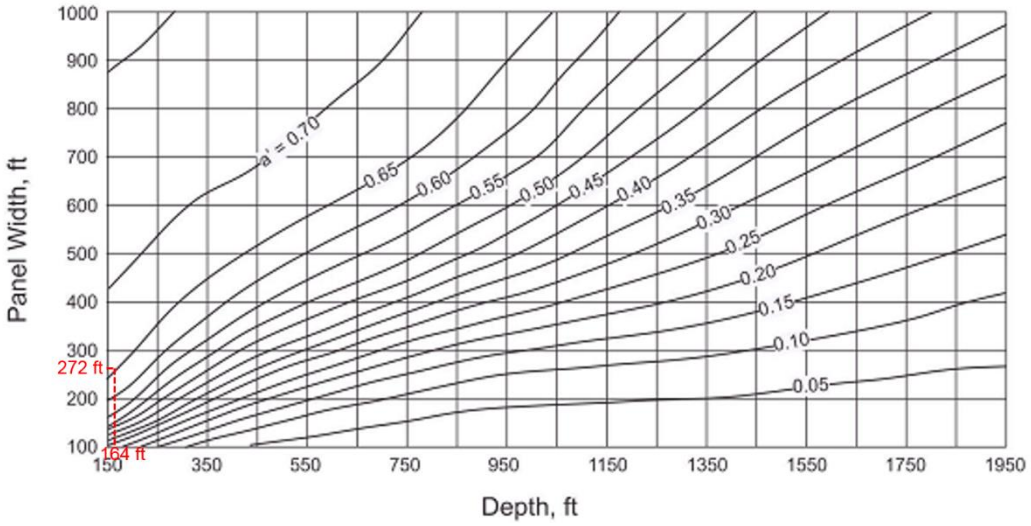

Figure 5.7 NCB chart for determining apparent subsidence factor (Luo, 1989).

Figure 5.8 provides means to determine the subsidence distribution along a transvers cross-section at the center of mined-out panel. The contour lines in this figure show the final surface subsidence distribution in fractions of the maximum subsidence (S_{max}). The position of the panel edge (ribline) and the edge of subsidence trough (limit of subsidence) are also marked. In order to calculate the subsidence distribution at each distance from the mined-out panel center at FBS coal mine, a horizontal line was drawn from the vertical axis at the value of 1.66 of the panel width to depth ratio (W/H). Points can be selected on this horizontal line for reading the locations where the different fractions to S_{max} are given. Table 5.1 summarizes the surface subsidence at each distance from the panel center. The predicted surface subsidence were then plotted into the graph in order to show the subsidence profile. Figure 5.9 shows the comparison of surface subsidence profiles based on field measurement data and empirical calculation results. It can be seen from this figure that the surface subsidence predicted using the empirical method is very much different from the ones that measured at the mine site. A large maximum surface subsidence (S_{max}) of 1.4 m was obtained from the measurement data, while a small maximum surface subsidence of 0.69 m was obtained from the empirical calculation results. From this difference, it can be said that the empirical method using NCB technique is not appropriate for prediction of surface subsidence induced by longwall mining under weak geological conditions at FBS coal mine.

The NCB method can be used appropriately to predict the surface subsidence in UK and US, but it cannot be applied directly to predict the surface subsidence at FBS coal mine. The main reason can be because of that the strengths of coal measure rocks of this underground coal mine are much lower than that the coal mines in UK and US. The limitation of using the empirical method is that the subsidence for the mine sites that have different geological and mining conditions cannot be predicted. In short, another appropriate technique should be applied for predicting the surface subsidence caused by longwall mining under weak geological conditions. Recently, the numerical simulation methods using advanced computer software are widely used as alternative techniques to empirical methods. The numerical simulation methods can be used in any mining environments at least if the reliable input data such as mechanical properties of rocks and in-situ stresses are available. Therefore, the numerical simulation method using FLAC3D software was used to predict the surface subsidence at FBS coal mine. The results obtained from the numerical simulation were then compared with the measurement data and the empirical calculation results.

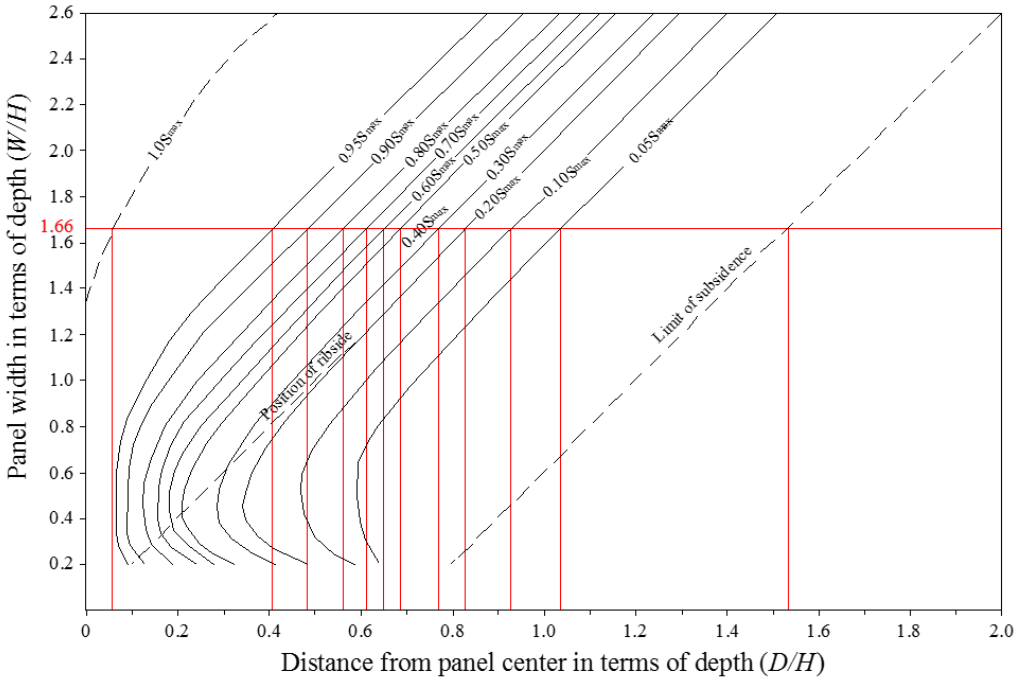

Figure 5.8 Chart for determining subsidence distribution at each distance from panel center (NCB, 1975).

Table 5.1 Surface subsidence distribution at each distance from panel center in case of FBS coal mine.

Fraction to S_{max}	S_{max} (m)	Distance from panel center in terms of depth (D/H)	Depth, H (m)	Distance from center of panel, D (m)	Subsidence at unique distance (m)
1.00	0.69	0.07	50	3.50	0.69
0.95		0.41		20.50	0.66
0.90		0.44		22.00	0.62
0.80		0.56		28.00	0.55
0.70		0.61		30.50	0.48
0.60		0.65		32.50	0.41
0.50		0.69		34.50	0.35
0.40		0.77		38.50	0.28
0.30		0.77		38.50	0.21
0.20		0.83		41.50	0.14
0.10		0.93		46.50	0.07
0.05		1.03		51.50	0.03
0.00		1.53		76.50	0.00

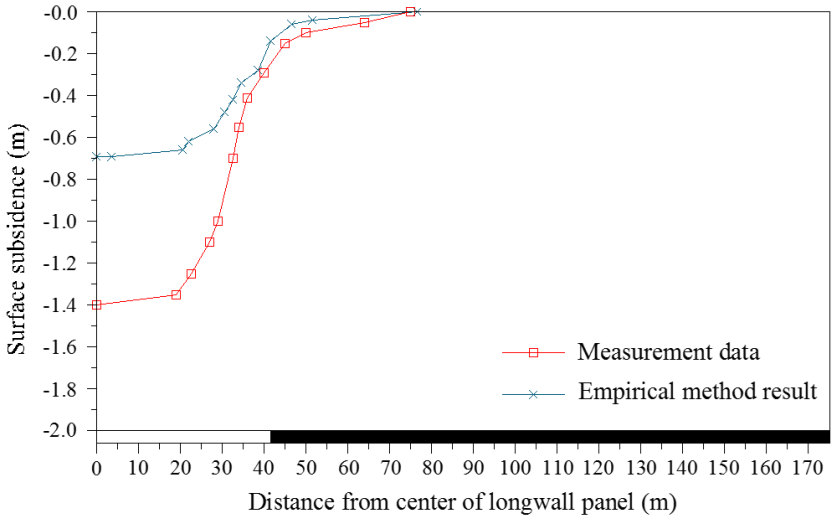

Figure 5.9 Comparison of subsidence profiles obtained from measurement data and empirical calculation results of FBS coal mine.

To predict the surface subsidence at FBS coal mine by means of numerical simulation method, the finite difference code software, FLAC3D was used as a tool for numerical simulation. The numerical model was constructed conforming the real extraction conditions. The width, length, and thickness of the longwall panel was 83 m, 140 m, and 1.9 m, respectively. The overburden depth was modelled as 50 m. Figure 5.10 describes the geometries of numerical model. The numerical model was fixed at two sides in horizontal direction and at the bottom in vertical direction, and it was set free at the surface in all directions. The stress ratio of 1 was simulated, and the constitutive model of Mohr-Coulomb was employed. The average properties of rock mass and coal were used in the simulation, and they are given in Table 5.2.

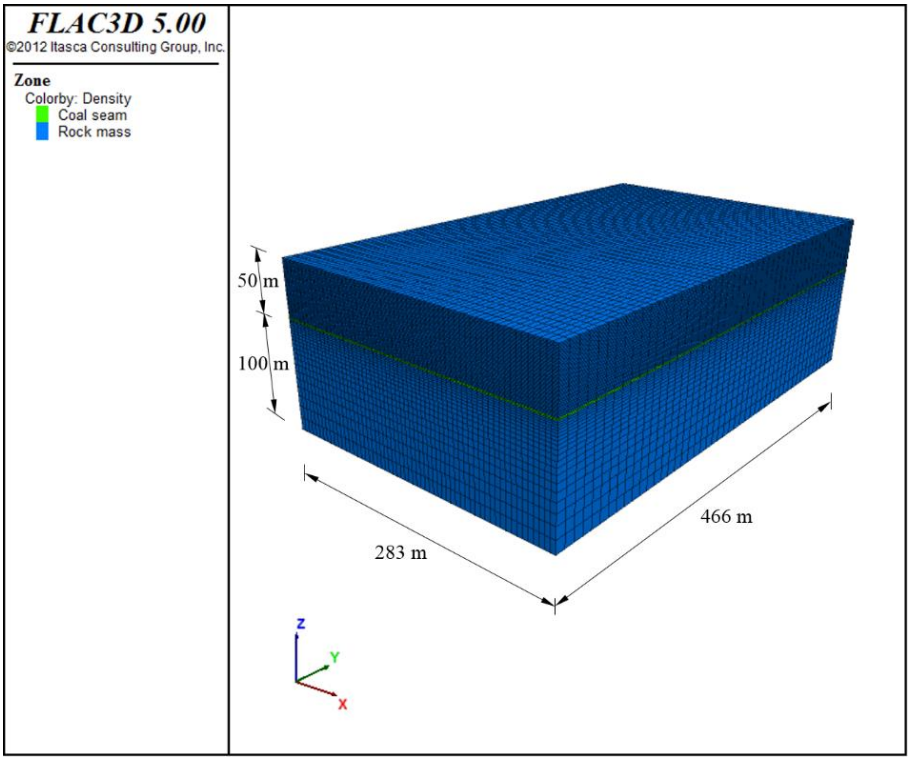

Figure 5.10 Numerical model of subsidence simulation at FBS coal mine.

Table 5.2 Mechanical properties of rock mass and coal seam used in simulation.

Parameter	Rock mass	Coal seam
Uniaxial compressive strength (MPa)	2.75	8.16
Density (kg/m^3)	2,170	1,380
Young's modulus (MPa)	1,583	1,296
Poisson's ratio	0.26	0.32
Friction angle (˚)	28.5	45.7
Cohesion (MPa)	0.14	2.63

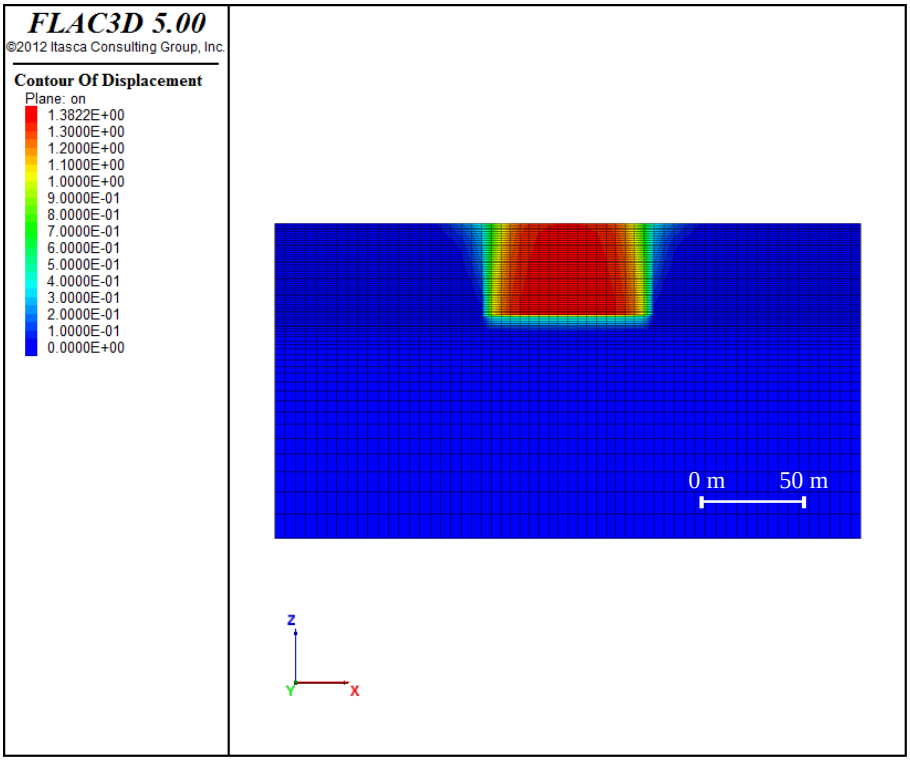

Figure 5.11 Simulation results of subsidence contours above mined-out panel at FBS coal mine.

Figure 5.11 illustrates the simulation results of subsidence contours occurred above the mined-out panel at FBS coal mine. The subsidence contours from this figure were plotted into the graph in order to create the surface subsidence profile. The surface subsidence profile created based on the simulation results were then compared with the ones that generated from the field measurement data and

empirical calculation results as summarized in Figure 5.12. From this figure, it can be obviously seen that the maximum surface subsidence (S_{max}) obtained from the numerical simulation is much closer to the S_{max} measured at the mine site than that the S_{max} calculated from the empirical method. The S_{max} of 1.35 m was obtained from the numerical simulation results, while the S_{max} of 1.4 m was obtained from the field measurement data. Moreover, the simulation results also indicate that using the average properties of rocks and coal has no big influence on the S_{max} value. According to the comparison of S_{max} values, it can be undoubtedly said that the numerical simulation method using FLAC3D is applicable for prediction of surface subsidence induced by longwall mining under weak geological conditions at FBS coal mine, and the average properties of rocks and coal can be adopted in the simulation. In short, it can be said that the characteristics of surface subsidence caused by longwall mining at GDM coal mine can be well simulated by means of numerical simulation method using FLAC3D software.

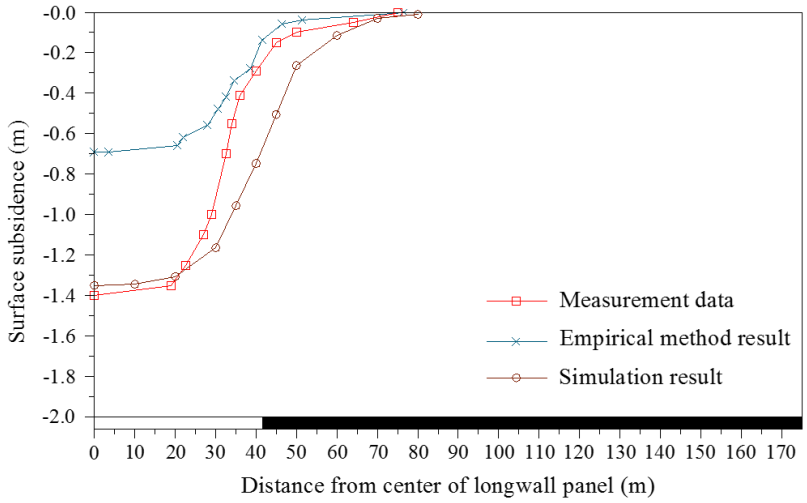

Figure 5.12 Surface subsidence profiles resulted from longwall mining at FBS coal mine by field measurement data and empirical calculation and simulation results.

5.3. Description of Numerical Model

It has been confirmed from the previous section that the numerical simulation method using a three-dimensional finite difference code, FLAC3D software is applicable for studying the surface subsidence induced by longwall mining under

weak geological conditions. Therefore, the characteristics of surface subsidence at GDM coal mine were studied numerically using the FLAC3D software in this chapter. In this section, the surface subsidence induced by longwall mining at GDM coal mine was studied and discussed. Several models were constructed in FLAC3D for numerical simulations. An example of a 200 m mining depth model is illustrated in Figure 5.13. The model is 1,330 m in width, 2,000 m in length, and with the height of 350 m. The bottom of the model was fixed in the vertical direction, the sides were fixed in the horizontal direction, and the surface was set free in all directions. The vertical stress component was modeled as a function of overburden thickness or mining depth ($P_v = \gamma H$, γ is unit weight of overburden, and H is overburden thickness) (Hoek & Brown, 1980; Hoek, Kaiser, & Bawden, 1993; Hoek, 2006), while the horizontal stress component was assumed to be equal to the vertical stress. The elasto-plastic Mohr-Coulomb was used as a constitutive model throughout the analyses. The properties of rock and coal seam, and the properties of goaf (Thin, Pine, & Trueman, 1993; Xie, Chen, & Wang, 1999; Yasiti & Unver, 2005) are summarized in Table 5.3.

Table 5.3 Properties of materials used in simulations.

Parameter	Rock mass	Coal seam	Goaf
Uniaxial compressive strength (MPa)	10.49	8.16	-
Density (kg/m^3)	2,140	1,380	1,700
Young's modulus (MPa)	2,325	1,296	15
Poisson's ratio	0.27	0.32	0.25
Friction angle (˚)	37.5	45.7	25.0
Cohesion (MPa)	0.56	2.63	1.0×10^{-3}

Firstly, the characteristics of surface subsidence in cases of single-panel and multi-panel longwall mining under various depths were studied. The mining depth was changed ranging from 50 m to 200 m. Only one panel was considered in single-panel mining simulation (see Figure 5.14 a), while three panels were considered in

multi-panel mining simulation (see Figure 5.14 b). A longwall panel was 130 m in width, 1,000 m in length, and 3 m in thickness. The panels were separated by a 30 m wide chain pillar in the case of multi-panel mining. Secondly, the countermeasures for subsidence control were investigated, including the effect of the width of chain pillar and longwall panel, and the application of backfilling material. To investigate the effect of the pillar width on the surface subsidence, four chain pillar widths of 30 m, 40 m, 50 m, and 60 m were simulated (see Figure 5.15 a). The model consisted of three longwall panels. The panel width was 130 m, and the mining depth was 50 m, 100 m, 150 m, and 200 m. Moreover, to investigate the effect of the panel width on the surface subsidence, three panel widths of 70 m, 100 m, and 130 m were also considered in the simulations (see Figure 5.15 b). The model included three longwall panels. The chain pillar between the panels was 30 m in width, and the mining depth was 50 m, 100 m, 150 m, and 200 m. In addition, the application of cohesive backfill was also investigated for surface subsidence control. Three longwall panels were included in the model. The panel width of 130 m, the chain pillar width of 30 m, and the mining depths of 50 m, 100 m, 150 m, and 200 m, were considered in the simulations (see Figure 5.15 c).

In longwall mining, the magnitude of surface subsidence is normally less than the thickness of extracted coal seam due to some voids have been left within the goaf. Many factors affect the extent of surface subsidence such as rock mass strength, panel and pillar widths, and mining depth. In this chapter, the AoD and S_{max} were used to describe the characteristics of surface subsidence. S_{max} is defined as the maximum extent of settlement at the surface, which occurs above mined-out panels. AoD is defined as an angle between the vertical line above an extraction edge and the inclined line joining the extraction edge with the edge of the subsidence trough (see Figure 5.2). AoD is commonly used as a subsidence engineering term to determine the limit of subsidence trough at the surface. The surface subsidence of less than 2 cm is generally accepted as a value that have no effect on any man-made structures and surface environments. However, it should be noted that in some environments, up to 5 cm or more of surface subsidence is accepted due to seasonal moisture changes. This value is normally adopted as the cut-off point for determination of the AoD (Mine Subsidence Engineering Consultants [MSEC],

2007; Independent Expert Scientific Committee [IESC], 2015). In this research, as some rice fields exist above the mining area at GDM coal mine, therefore, the surface subsidence of 5 cm was used as a cut-off point to calculate the AoD value. The results presented in the following sections were taken from the model centre and expressed in the cross-section.

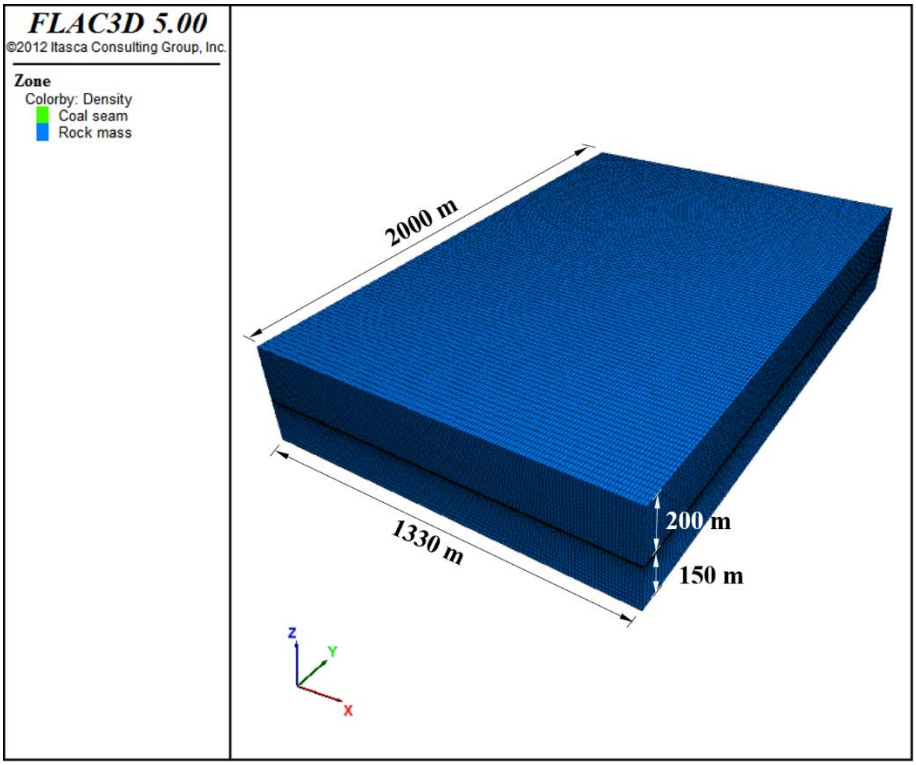

Figure 5.13 Model geometries of subsidence simulation at 200 m mining depth.

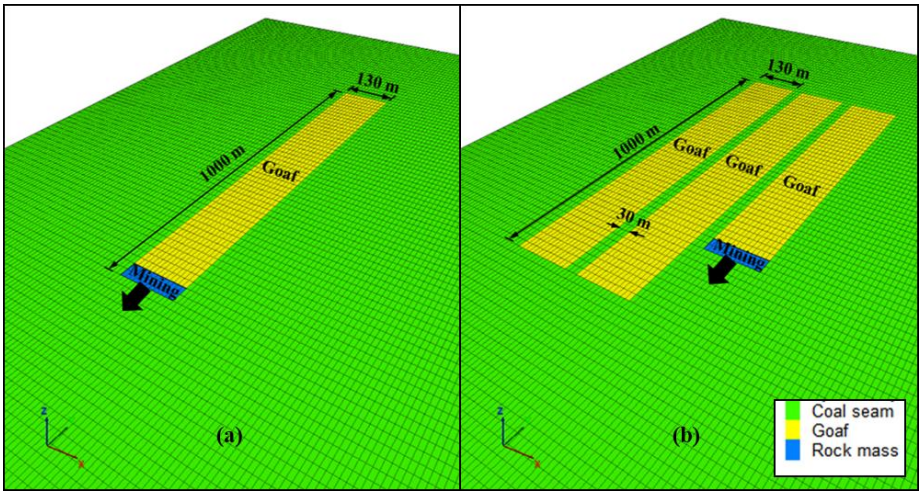

Figure 5.14 Surface subsidence models for (a) single-panel mining (b) multi-panel mining.

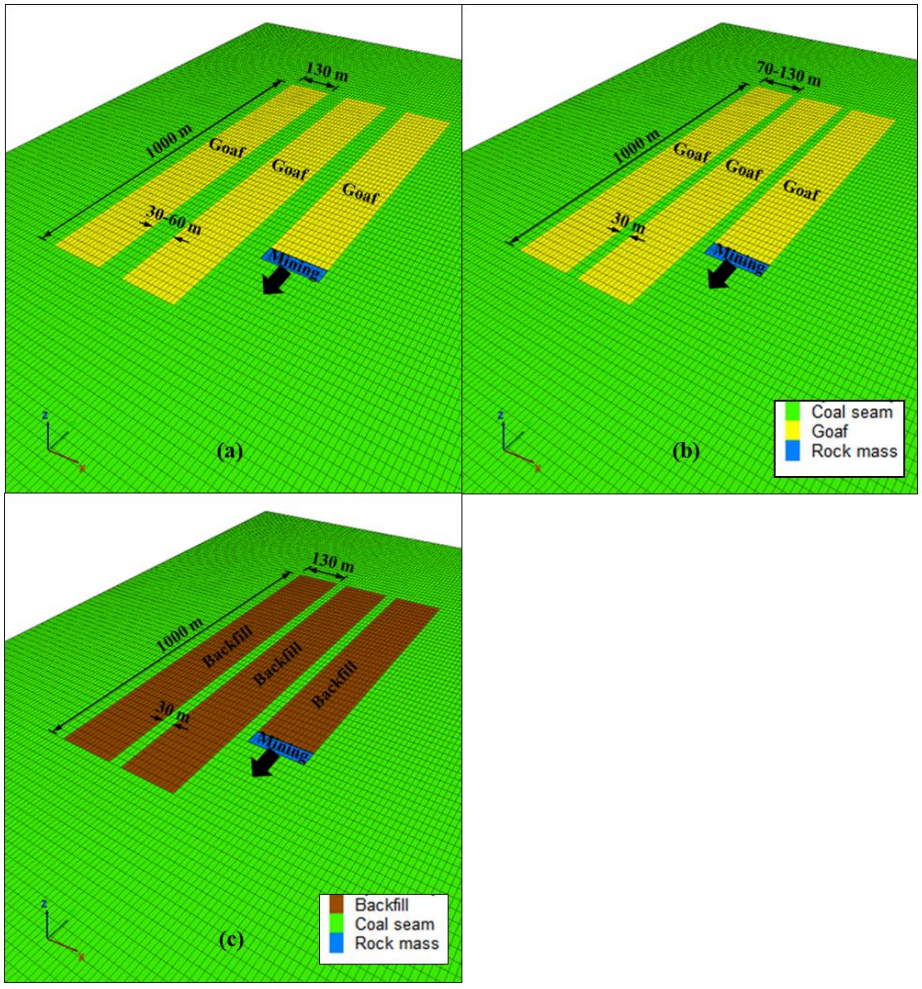

Figure 5.15 Surface subsidence models for (a) effect of chain pillar width (b) effect of panel width (c) application of backfilling material.

5.4. Characteristics of Surface Subsidence induced by Single-panel Longwall Mining

Figure 5.16 shows the subsidence contours and the AoD values resulted from single-panel mining at various depths. A single panel of 130 m in width was simulated, and the mining depths of 50 m, 100 m, 150m, and 200 m, were modelled. Under all mining depths, the largest subsidence occurred directly above the mined-out panel, and its magnitude gradually reduced toward the surface. Based on the simulation results, it was found that the degree of AoD was significantly associated with the mining depth. The AoD increased with increasing the depth of mining. This means that when the longwall mining is developed at the deeper site, the wider subsidence area at the surface will be generated. The AoD occurred at 50 m, 100 m,

150 m, and 200 m mining depth, was 10˚, 26˚, 46˚, and 53˚, respectively.

The data of subsidence contours were plotted into the graph in order to see subsidence profiles (see Figures 5.16 b and 5.16 c). From the subsidence profiles, the S_{max} at each depth was then determined. The largest S_{max} was observed at 50 m depth, while its magnitude gradually decreased as the depth increased. This was due to a decrease in the panel width to mining depth ratio (W/H), resulted in an increase in bridging ability of overburden strata over the mined-out panel. The highest W/H happened at 50 m depth. In this case, the overburden strata were less able to bridge across the mined-out area, as a result, a larger S_{max} occurred. In contrast, as the mining depth increased, the W/H decreased, the overburden rocks were more able to bridge over the mined-out area by arching between the solid coal supports on each side of the panel, as a result, the magnitude of S_{max} reduced. The S_{max} was 1.37 m, 1.31 m, 1.29 m, and 1.03 m under the mining depths of 50 m, 100 m, 150 m, and 200 m, respectively. Based on the results of S_{max}, it indicates that a narrow panel width should be applied at the shallow depth in order to prevent the large subsidence occurring at the surface. Interestingly, it was observed that the values of S_{max} occurred at 50 m, 100 m, and 150 m depth were not dramatically different, while they were significantly different from that the S_{max} occurred at 200 m depth. This phenomena can be explained by the occurrence of the failure zone above the mined-out panel. At all mining depths, the failure zone was developed and extended to the surface after the panel was mined (see Figure 5.17). However, although the failure zone above mined-out panel at 200 m depth was connected to the surface, the separation degree of overburden strata near the surface at this depth was considerably smaller than those occurred at 50 m, 100 m, and 150 m depth, while no significant difference of separation degree of the overburden strata near the surface was observed between the depths of 50 m, 100 m, and 150 m (see also Figure 5.16 a for comparison). As a result, a smaller S_{max} occurred at 200 m depth, and larger S_{max} occurred at 50 m, 100 m, and 150 m depth.

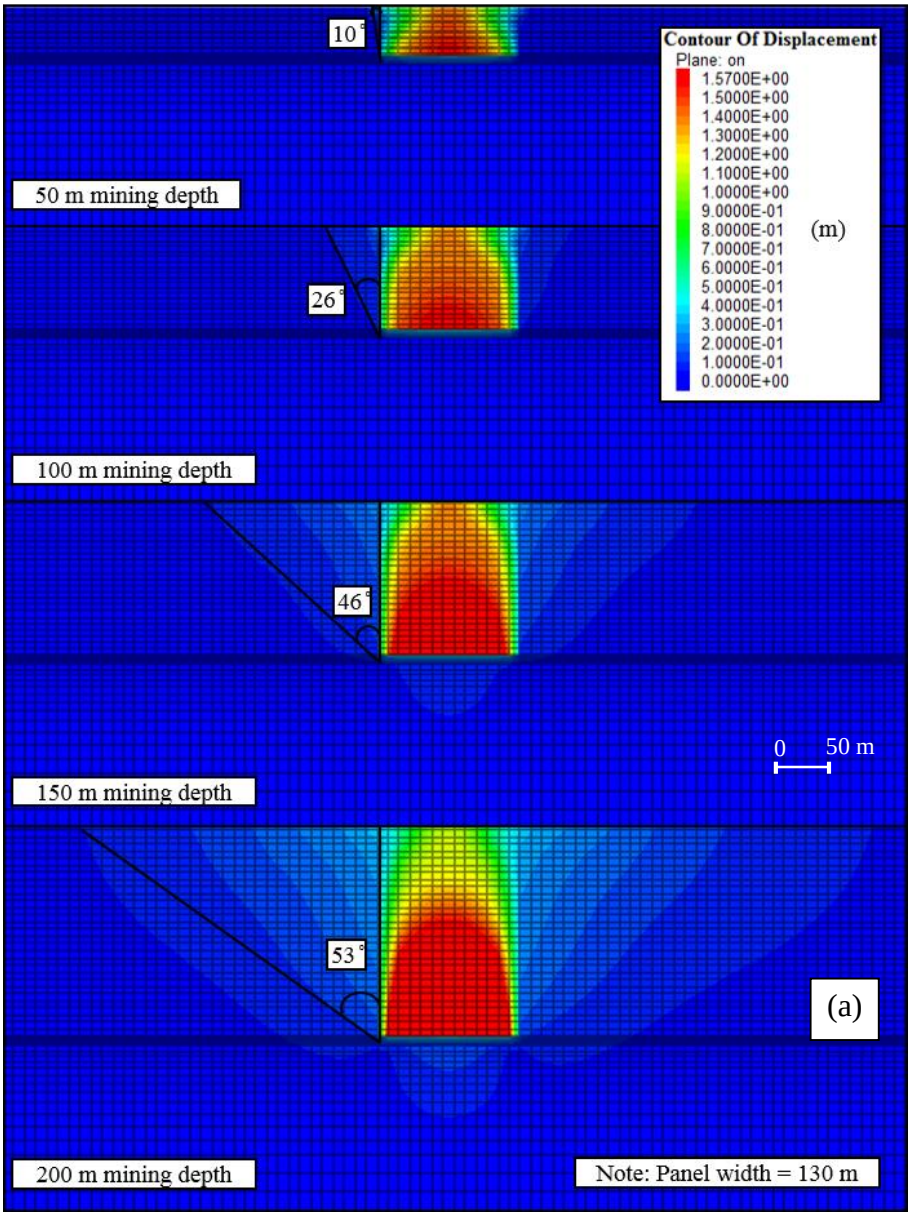
Contour Of Displacement
Plane: on
1.5700E+00
1.5000E+00
1.4000E+00
1.3000E+00
1.2000E+00
1.1000E+00
1.0000E+00
9.0000E-01
8.0000E-01
7.0000E-01
6.0000E-01
5.0000E-01
4.0000E-01
3.0000E-01
2.0000E-01
1.0000E-01
0.0000E+00
(m)
10°
50 m mining depth
26°
100 m mining depth
46°
0 50 m
150 m mining depth
53°
(a)
200 m mining depth
Note: Panel width = 130 m

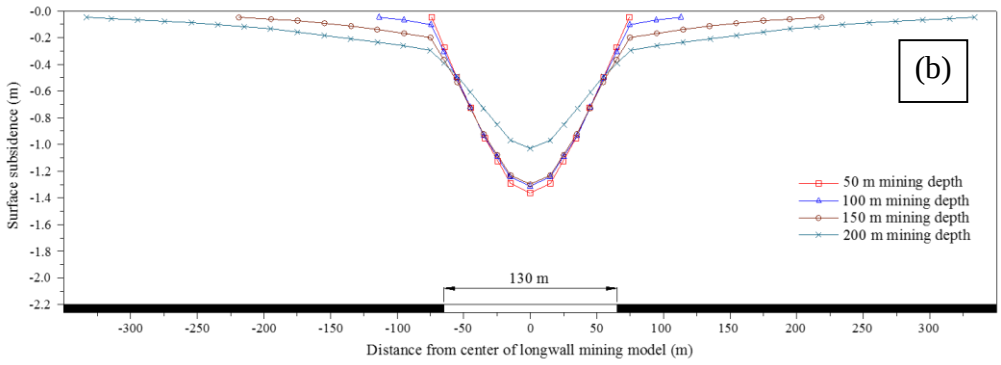
(b)
Surface subsidence (m)
-0.0
-0.2
-0.4
-0.6
-0.8
-1.0
-1.2
-1.4
-1.6
-1.8
-2.0
-2.2
50 m mining depth
100 m mining depth
150 m mining depth
200 m mining depth
130 m
-300
-250
-200
-150
-100
-50
0
50
100
150
200
250
300
Distance from center of longwall mining model (m)

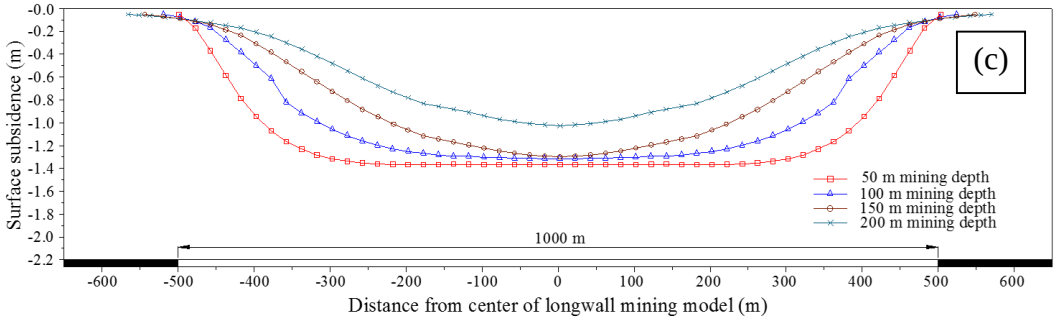

Figure 5.16 Simulation results of surface subsidence induced by single-panel longwall mining at various mining depths (a) contour of subsidence and angle of draw (b) & (c) cross-section and longitudinal-section profiles of surface subsidence.

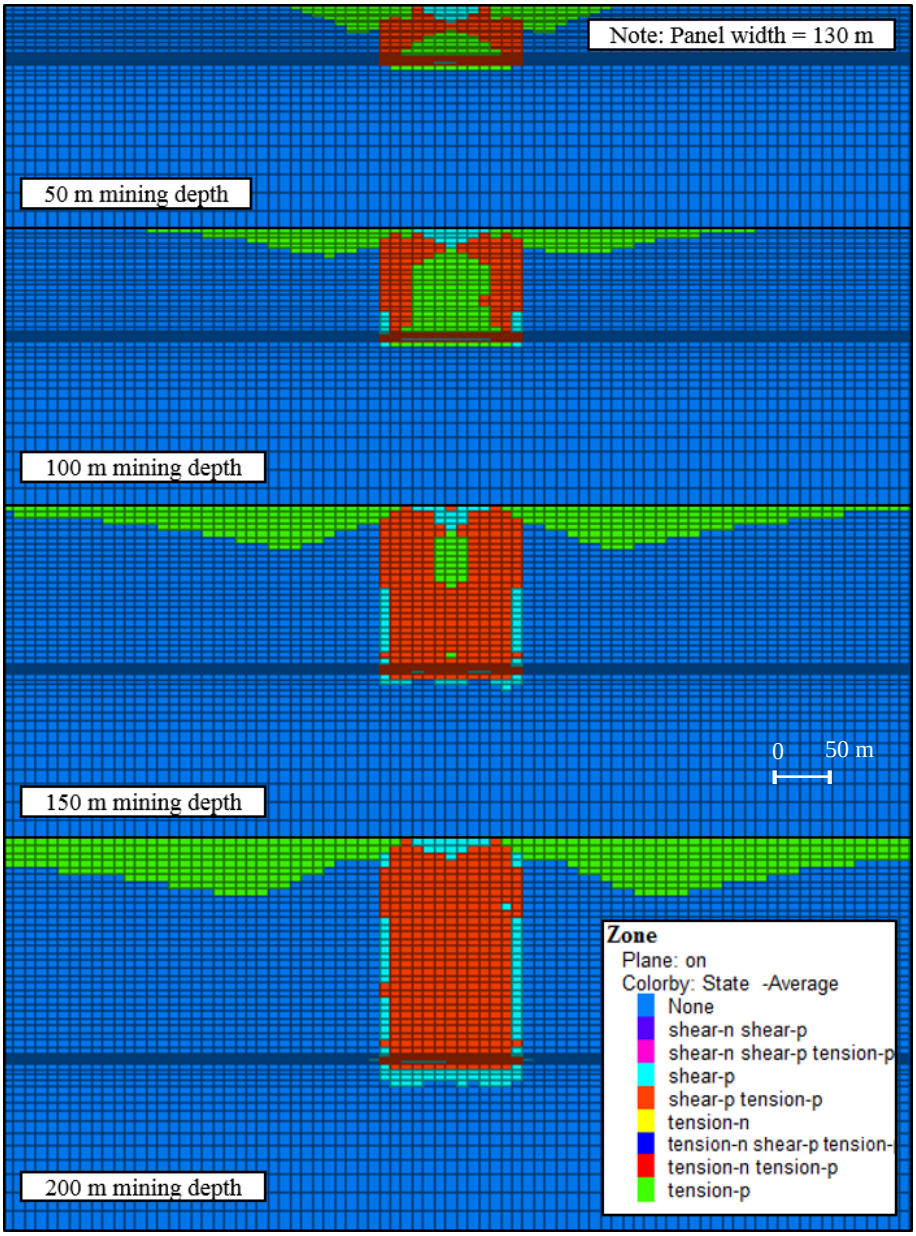

Figure 5.17 Failure zone of overburden strata induced by single-panel longwall mining under various depths.

5.5. Characteristics of Surface Subsidence induced by Multi-panel Longwall Mining

In order to study the characteristics of surface subsidence induced by multi-panel mining, three longwall panels were simulated at four mining depths such as 50 m, 100 m, 150 m, and 200 m. The panel width of 130 m, and the chain pillar width of 30 m, were considered in the simulations. Figure 5.18 illustrates the subsidence

contours, AoD values, and subsidence profiles. The results indicated that the AoD and S_{max} tended to increase as the depth increased when several panels were mined in a series. As the second and third panels were mined, additional subsidence developed over the panel centre, and the AoD extended further from the edge of extraction area. Compared with the single-panel mining, the AoD increased from 26˚, 46˚, and 53˚ to 29˚, 50˚, and 55˚, while the S_{max} increased from 1.31 m, 1.29 m, and 1.03 m to 1.38 m, 1.68 m, and 1.90 m under the mining depths of 100 m, 150 m, and 200 m, respectively. The AoD and S_{max} under 50 m depth remained unchanged after the subsequent panels were mined. The AoD and S_{max} remained as 10˚and 1.37 m, respectively.

Based on the S_{max} results, it was observed that the S_{max} at 50 m depth remained unchanged, while it remained almost stable at 100 m depth even though after the second and third panels were mined. Differ from the S_{max} at 150 m and 200 m depth, the S_{max} increased significantly after mining the second and third panels. The reason of this phenomena can be explained by the ratio of pillar width to mining depth (P/H). At 50 m and 100 m depth, the P/H was higher than that of 150 m and 200 m depth. In this case, the pillars provided an adequate amount of support to the rock strata above them. Hence, the development of additional S_{max} was restricted, and a wavy subsidence profile was produced. On the other hand, the P/H decreased as the mining depth increased. Under this situation, the bearing capacity of the pillar was reduced, thus the pillars were less able to support the roof strata. As a result, the S_{max} increased, and a deeper and smoother subsidence profile was produced.

Additionally, the failure zone results also support the explanation of the phenomena discussed above (see Figure 5.19). It can be observed from the figure that the chain pillars between the longwall panels at 50 m and 100 m depth have not failed. The pillars remained intact after all panels were mined. Under this situation, the pillars provided an adequate support to the roof strata above them, consequently, the development of additional S_{max} was restricted. Therefore, it can be said that the pillar width of 30 m will be enough at 50 m and 100 m depth. In order to minimize the magnitude of surface subsidence at these depths, it is unnecessary to increase the width of chain pillar, but a decrease in panel width will be more effective. On the contrary, it was observed from the results that the failure of chain pillars

occurred at 150 m and 200 m after the second and third panels were mined. Under this situation, the pillars provided less support to the roof strata, as a result, some additional values of S_{max} occurred. From this reason, it indicates that the use of pillar width wider than 30 m should be considered in order to minimize the surface subsidence at 150 m and 200 m depth. Moreover, it can be expected that the magnitude of subsidence at these depths can be decreased more when a wider chain pillar width is used with a narrower panel width.

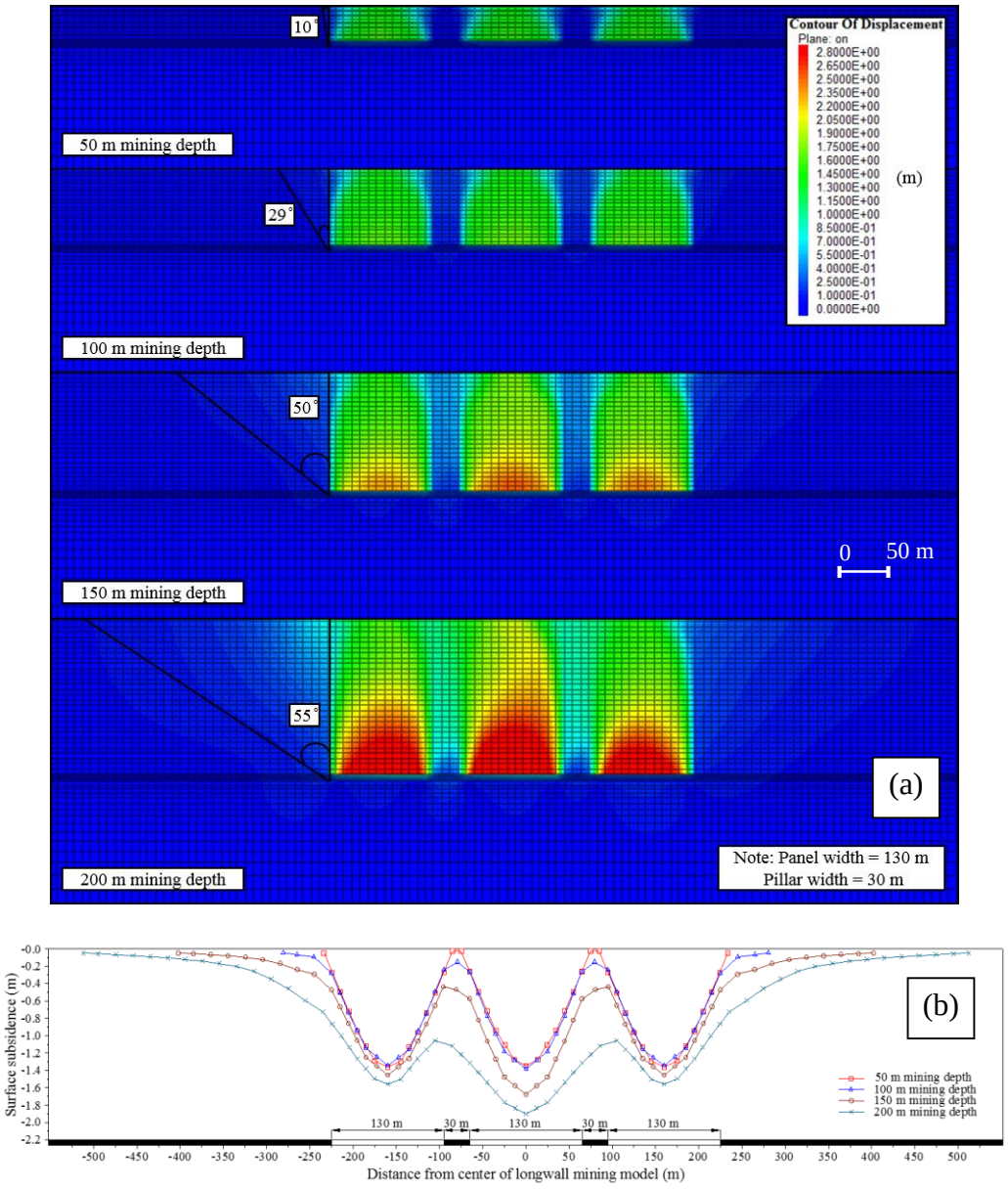

Figure 5.18 Simulation results of surface subsidence induced by multi-panel longwall mining at various mining depths (a) contour of subsidence and angle of draw (b) profile of surface subsidence.

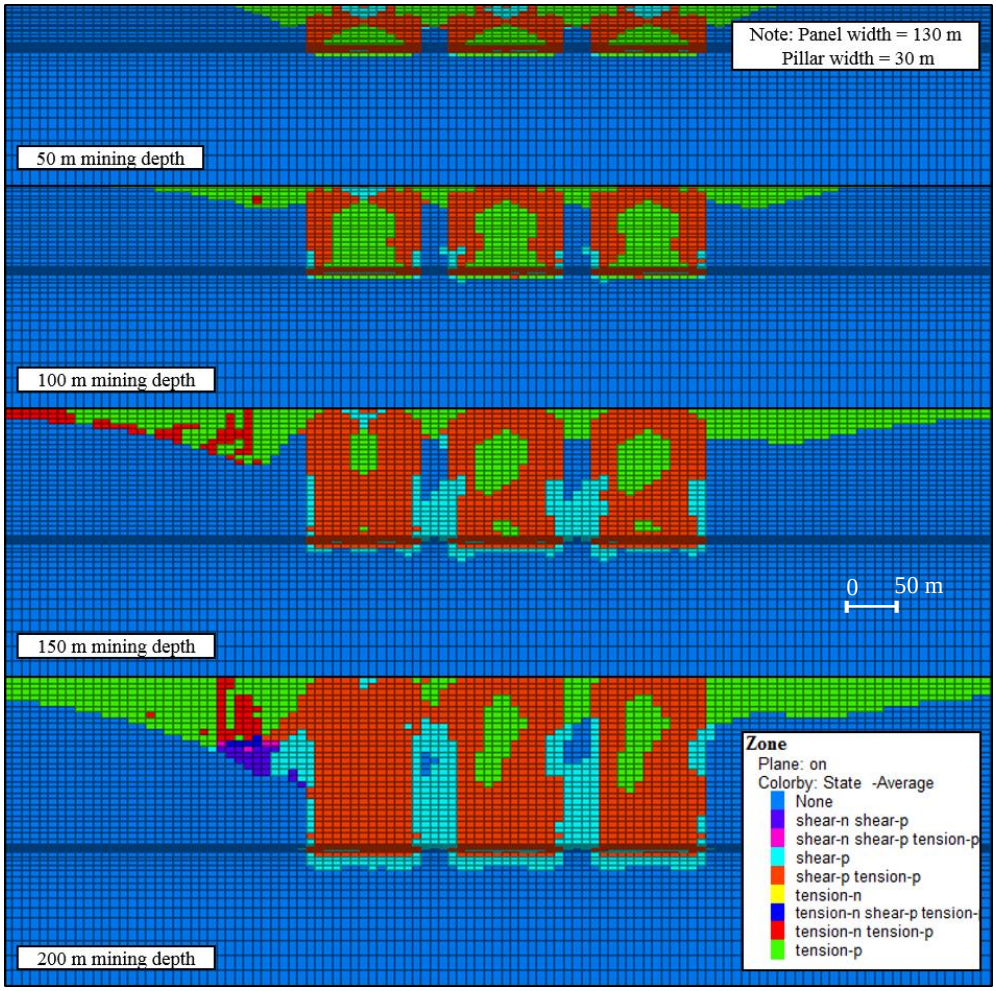

Figure 5.19 Failure zone of overburden strata induced by multi-panel longwall mining under various depths.

5.6. Countermeasures for Controlling Surface Subsidence

According to the simulation results of surface subsidence presented in the previous sections, it is found that the occurrence of large subsidence at the surface is expected when the longwall mining is applied at GDM coal mine. In order to prevent the adverse impacts that may occur at the surface due to the large subsidence, some countermeasures for subsidence control must be anticipated. In this research, three countermeasure techniques for controlling the surface subsidence were investigated, including the effect of the width of chain pillar and longwall panel, and the application of backfilling technique. The characteristics of surface subsidence under different pillar and panel widths, and after the application of backfilling technique, were given in the following sections.

5.6.1. Effect of Chain Pillar Width on Surface Subsidence

Minimizing the magnitude of surface subsidence induced by longwall mining by increasing the pillar width was investigated in this section. The simulations were made for four chain pillar widths such as 30 m, 40 m, 50 m, and 60 m. Three longwall panels of 130 m in width and four mining depths of 50 m, 100 m, 150 m, and 200 m, were considered. The results of subsidence contour, subsidence profile, and failure zone of overburden strata obtained from longwall mining under different pillar widths are illustrated in Figures 5.20-5.23. Based on the simulation results, it was observed that the AoD and S_{max} tended to decrease as the chain pillar width increased, particularly at the deep areas. This was due to an increase in the chain pillar width to mining depth ratio (P/H). A wider pillar provided a higher support capacity to the roof strata, resulted in a smaller AoD and S_{max}.

Table 5.4 summarizes the values of AoD and S_{max} resulted from longwall mining under various pillar widths and mining depths. According to the subsidence profile and the S_{max} values given in this table, it can be noticeably seen that with increasing the pillar width at 50 m depth, the S_{max} remained unchanged as 1.37 m, while the S_{max} at 100 m depth remained almost stable (The difference is only about 1-2 cm). It was because the narrow pillar width of 30 m could maintain in a very stable condition during the panel extractions, and no failure of the pillars was observed (see Figures 5.20 c and 5.21 c). This indicates that the pillar width of 30 m will be sufficient to restrict the development of additional S_{max} at 50 m and 100 m depth. The large subsidence occurred at these depths not because the narrow pillar width was used, but due to the wide panel width was applied, coupled with the existence of the thin overburden thickness. Thus, decreasing the panel width will be more effective to minimize the surface subsidence at 50 m and 100 m depth.

On the other hand, at 150 m depth, a decrease in S_{max} was observed apparently when the pillar width increased from 30 m to 40 m (S_{max} decreased from 1.68 m to 1.59 m). This was due to the failure of the chain pillar was reduced (see Figure 5.22 c), and the pillar could provide higher support to the roof strata in this case. As a consequence, the S_{max} decreased. Additionally, when the pillar width continued increasing from 40 m to 50 m and 60 m, no failure of the pillar was recognized, and the S_{max} became almost stable (The difference is only about 3-4 cm). From this, it

can be said that the pillar width of 40 m will be adequate for the longwall mining at 150 m depth. Again, to minimize more magnitude of the surface subsidence at this depth, the use of narrower panel width must be considered.

On the contrary, increasing the pillar width at 200 m depth is very effective to control the surface subsidence. The S_{max} considerably decreased as the pillar width increased. The S_{max} decreased from 1.90 m to 1.70 m, 1.53 m, and 1.44 m when the pillar width was decreased from 30 m to 40 m, 50 m, and 60 m, respectively. This was because the failure zone of the pillar significantly reduced (see Figure 5.23 c). From these results, it can be suggested that a wider chain pillar should be applied at 200 m depth. Furthermore, a smaller magnitude of surface subsidence can be achieved at this depth, when a wide chain pillar is used together with a narrow longwall panel.

Table 5.4 Comparison of AoD and S_{max} values under different chain pillar widths and mining depths.

Mining depth (m)	30 m pillar width		40 m pillar width		50 m pillar width		60 m pillar width	
	AoD (˚)	S_{max} (m)	AoD (˚)	S_{max} (m)	AoD (˚)	S_{max} (m)	AoD (˚)	S_{max} (m)
50	10	1.37	10	1.37	10	1.37	10	1.37
100	29	1.38	28	1.36	28	1.35	27	1.34
150	50	1.68	50	1.59	49	1.56	49	1.52
200	55	1.90	55	1.70	55	1.53	54	1.44

However, although the magnitude of S_{max} can be controlled by increasing the pillar width, the recovery ratio of the coal can be reduced. Recovery ratio is the percent of minable coal recovered from the seam. In this section, the recovery ratio was calculated only for the coal block of 450 m in width, 1000 m in length, and 3 m in thickness. The width of two chain pillars was increased and the minable area of three coal panels was reduced within the block. Figure 5.24 shows the relationship between the recovery ratio of coal and the chain pillar width. From this figure, it was observed that the recovery ratio reduced as the chain pillar width increased, because larger parts of coal have left in place when a wider chain pillar width was used. The recovery ratio reduced from 86.67% to 82.22%, 79.78%, and 73.33%

when the pillar width increased from 30 m to 40 m, 50 m, and 60 m, respectively. This indicates that a smaller quantity of the coal will be recovered when a wider chain pillar width is applied.

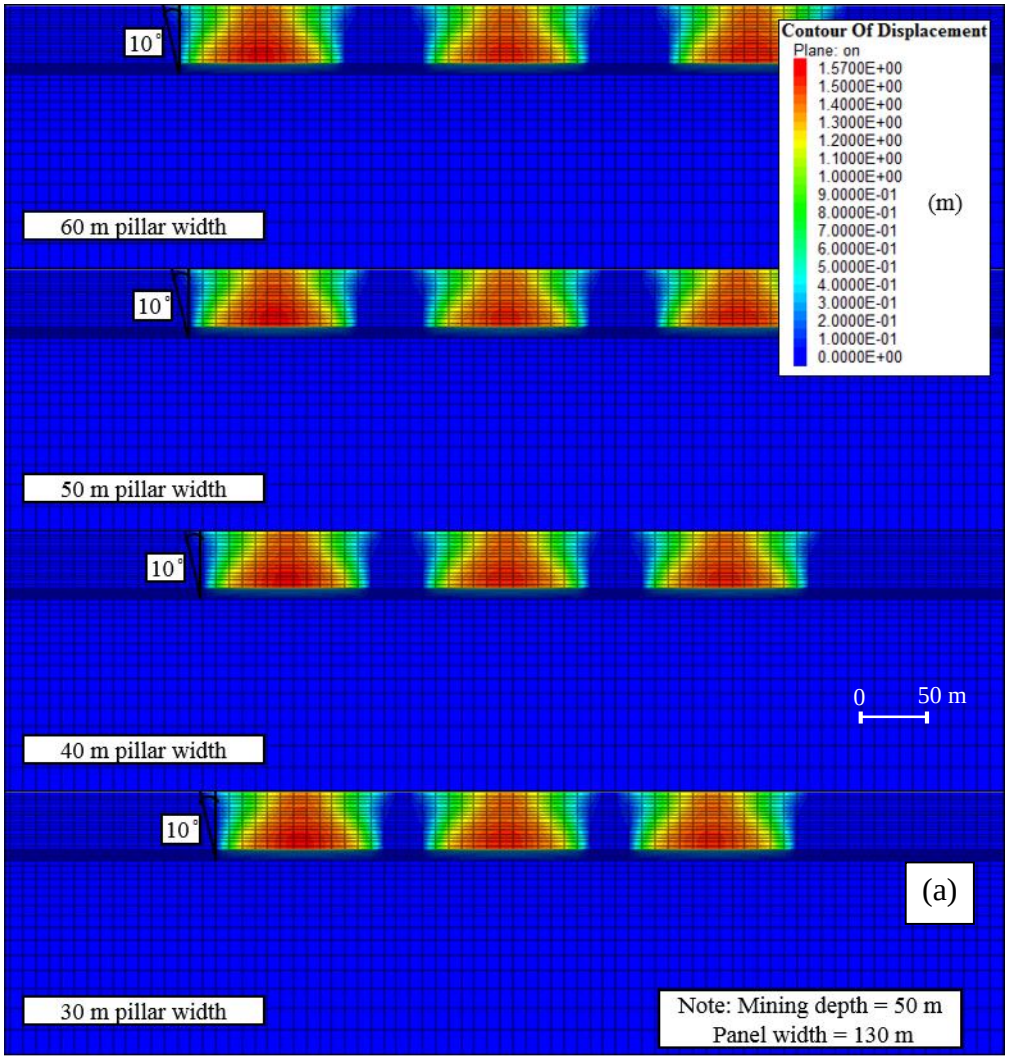

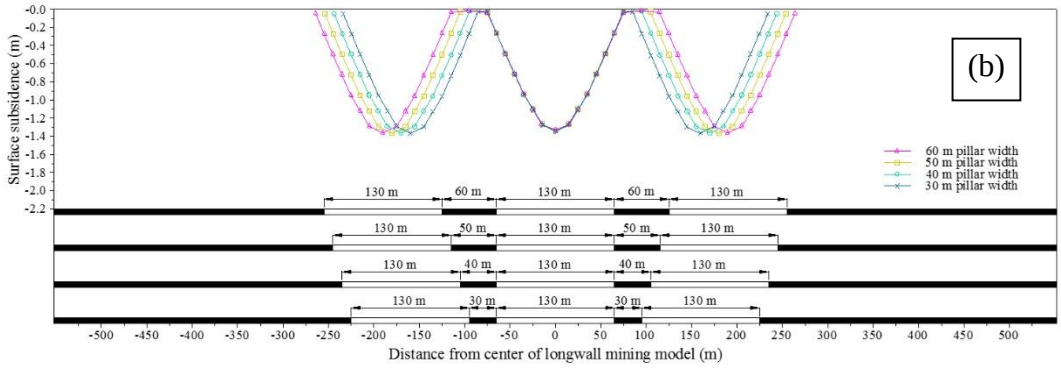

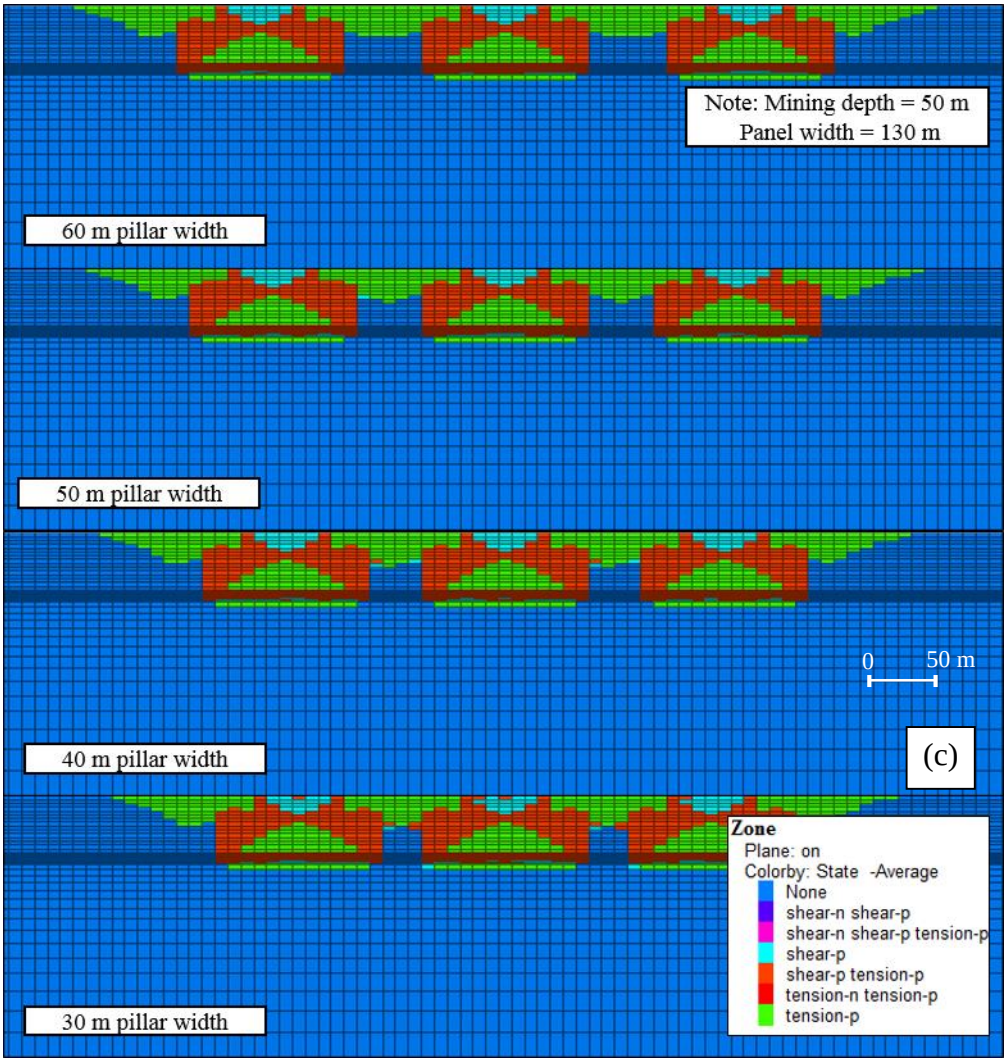

Figure 5.20 Simulation results of surface subsidence resulted from longwall mining under various chain pillar widths at 50 m depth (a) contour of subsidence and angle of draw (b) profile of surface subsidence (c) failure zone of overburden strata.

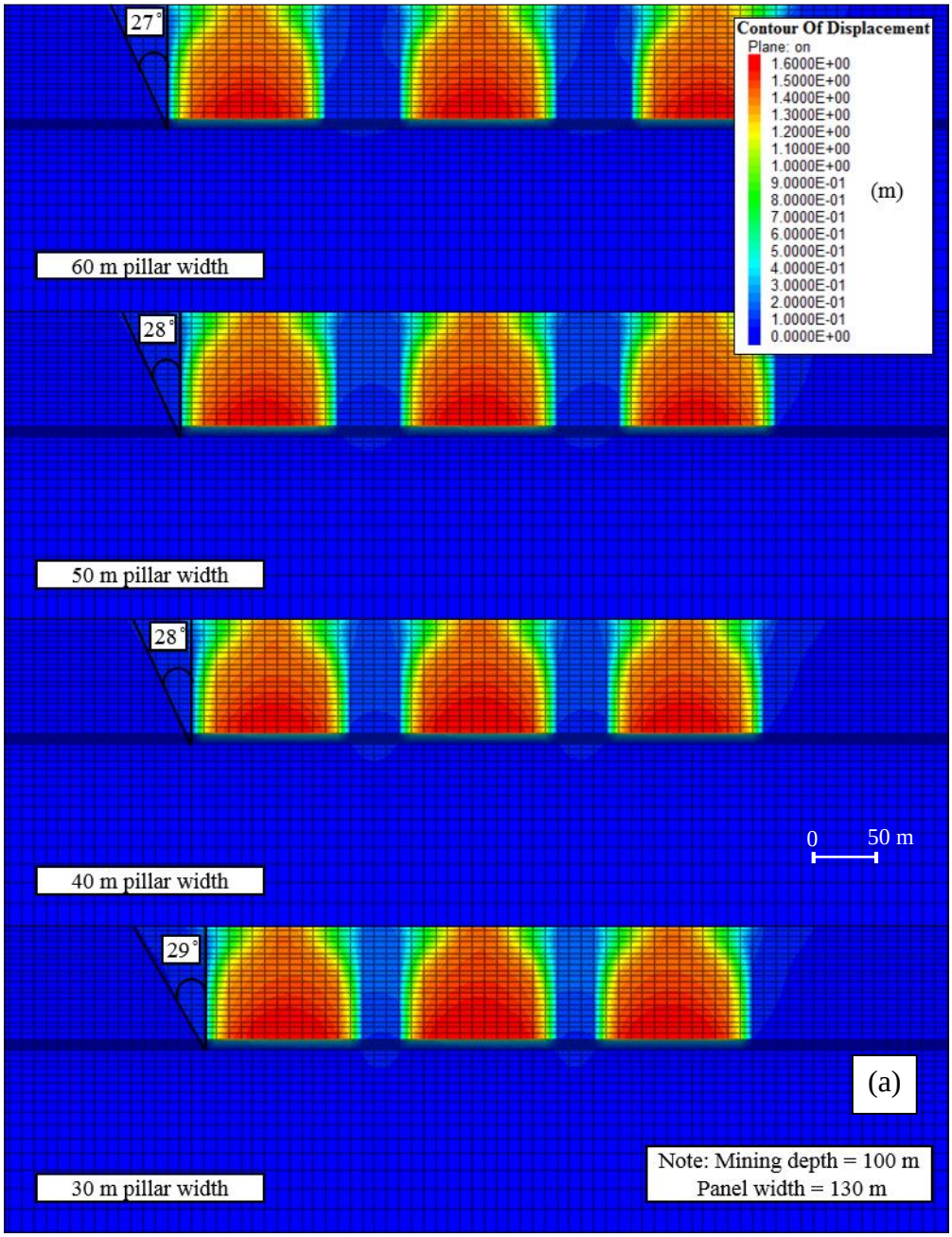
Contour Of Displacement
Plane: on
1.6000E+00
1.5000E+00
1.4000E+00
1.3000E+00
1.2000E+00
1.1000E+00
1.0000E+00
9.0000E-01
8.0000E-01
7.0000E-01
6.0000E-01
5.0000E-01
4.0000E-01
3.0000E-01
2.0000E-01
1.0000E-01
0.0000E+00
(m)
27°
60 m pillar width
28°
50 m pillar width
28°
0
50 m
40 m pillar width
29°
(a)
Note: Mining depth = 100 m
Panel width = 130 m
30 m pillar width

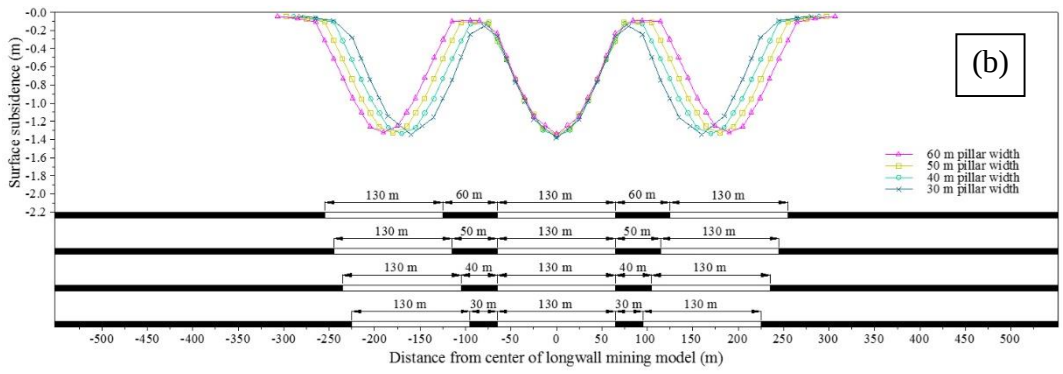
Surface subsidence (m)
-0.0
-0.2
-0.4
-0.6
-0.8
-1.0
-1.2
-1.4
-1.6
-1.8
-2.0
-2.2
(b)
60 m pillar width
50 m pillar width
40 m pillar width
30 m pillar width
130 m
60 m
130 m
60 m
130 m
130 m
50 m
130 m
50 m
130 m
130 m
40 m
130 m
40 m
130 m
130 m
30 m
130 m
30 m
130 m
-500
-450
-400
-350
-300
-250
-200
-150
-100
-50
0
50
100
150
200
250
300
350
400
450
500
Distance from center of longwall mining model (m)

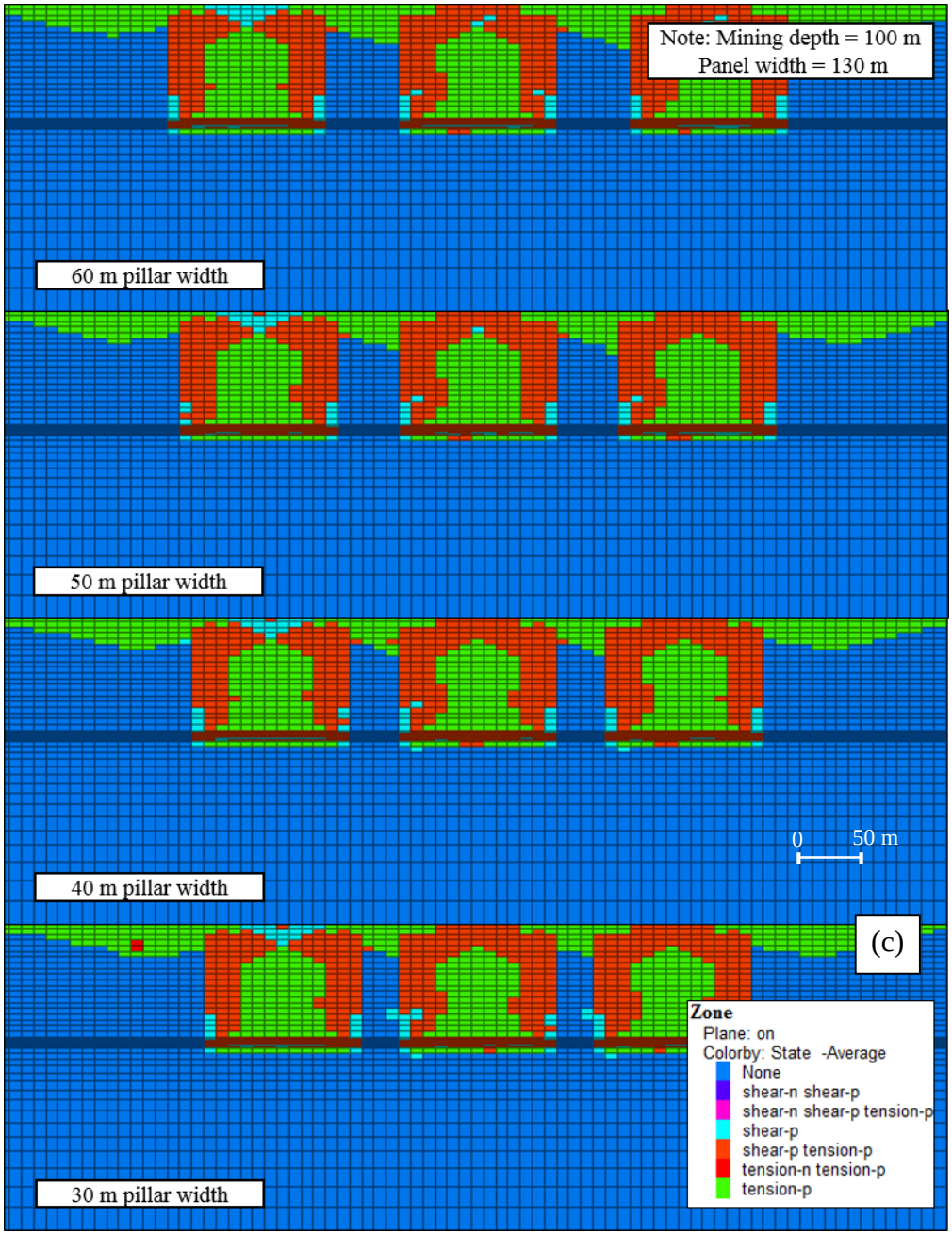

Figure 5.21 Simulation results of surface subsidence resulted from longwall mining under various chain pillar widths at 100 m depth (a) contour of subsidence and angle of draw (b) profile of surface subsidence (c) failure zone of overburden strata.

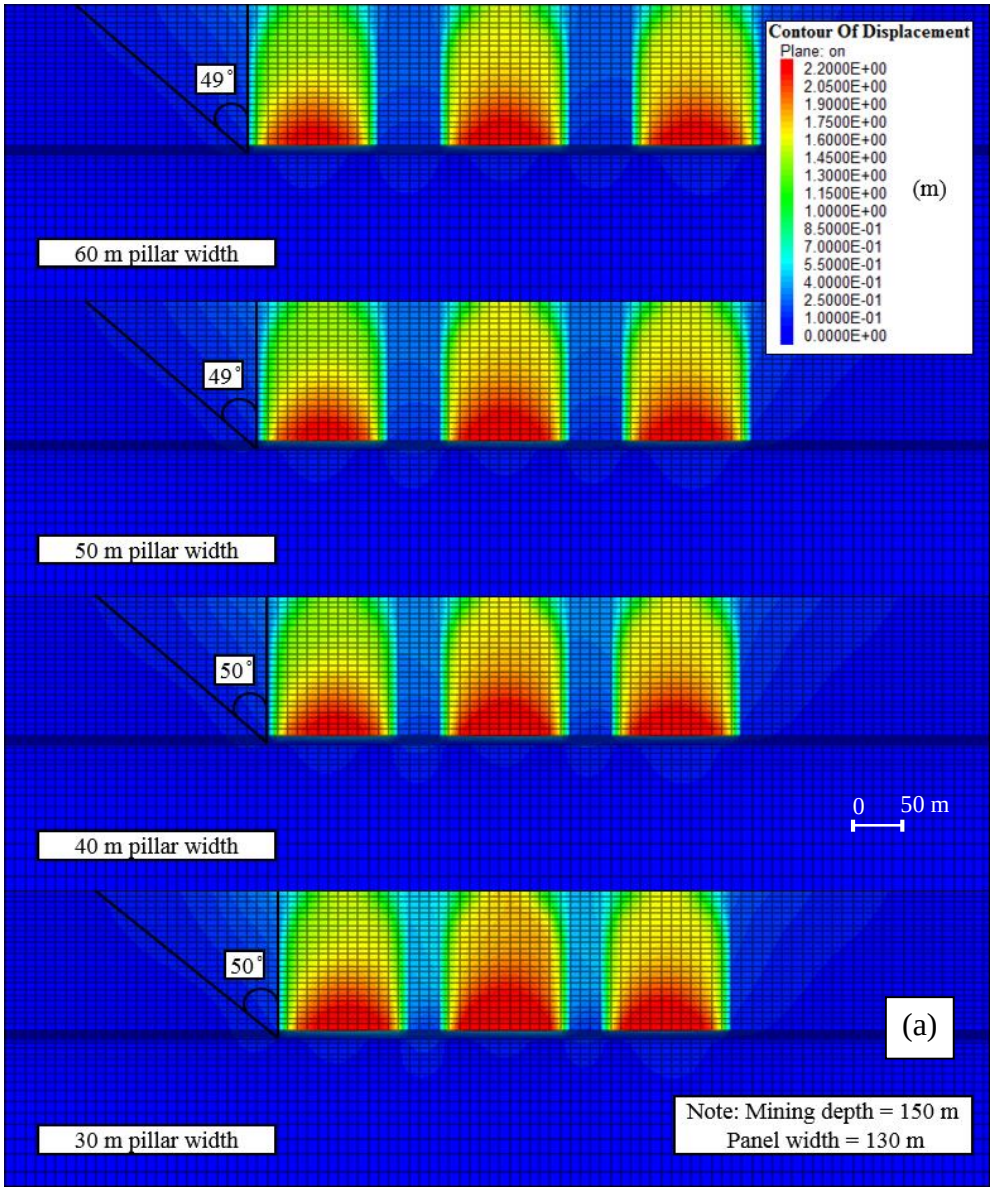
Contour Of Displacement
Plane: on
2.2000E+00
2.0500E+00
1.9000E+00
1.7500E+00
1.6000E+00
1.4500E+00
1.3000E+00
1.1500E+00
1.0000E+00
8.5000E-01
7.0000E-01
5.5000E-01
4.0000E-01
2.5000E-01
1.0000E-01
0.0000E+00
(m)
49°
60 m pillar width
49°
50 m pillar width
50°
0
50 m
40 m pillar width
50°
(a)
Note: Mining depth = 150 m
Panel width = 130 m
30 m pillar width

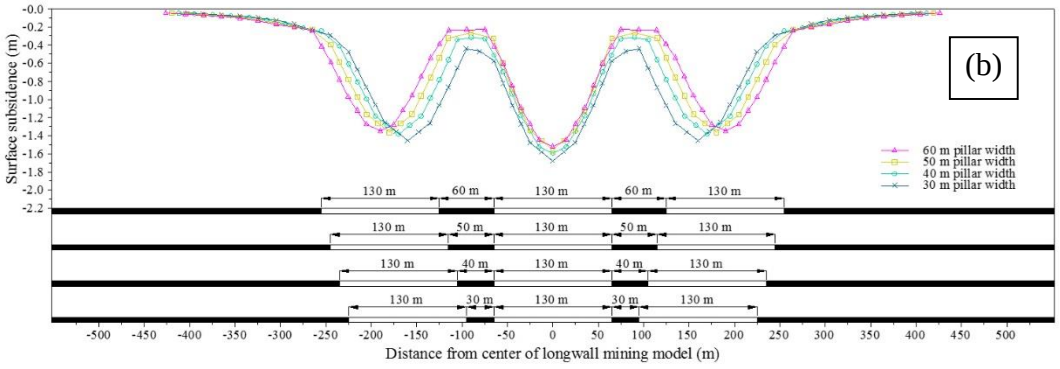
Surface subsidence (m)
-0.0
-0.2
-0.4
-0.6
-0.8
-1.0
-1.2
-1.4
-1.6
-1.8
-2.0
-2.2
(b)
60 m pillar width
50 m pillar width
40 m pillar width
30 m pillar width
130 m
60 m
50 m
40 m
30 m
-500
-450
-400
-350
-300
-250
-200
-150
-100
-50
0
50
100
150
200
250
300
350
400
450
500
Distance from center of longwall mining model (m)

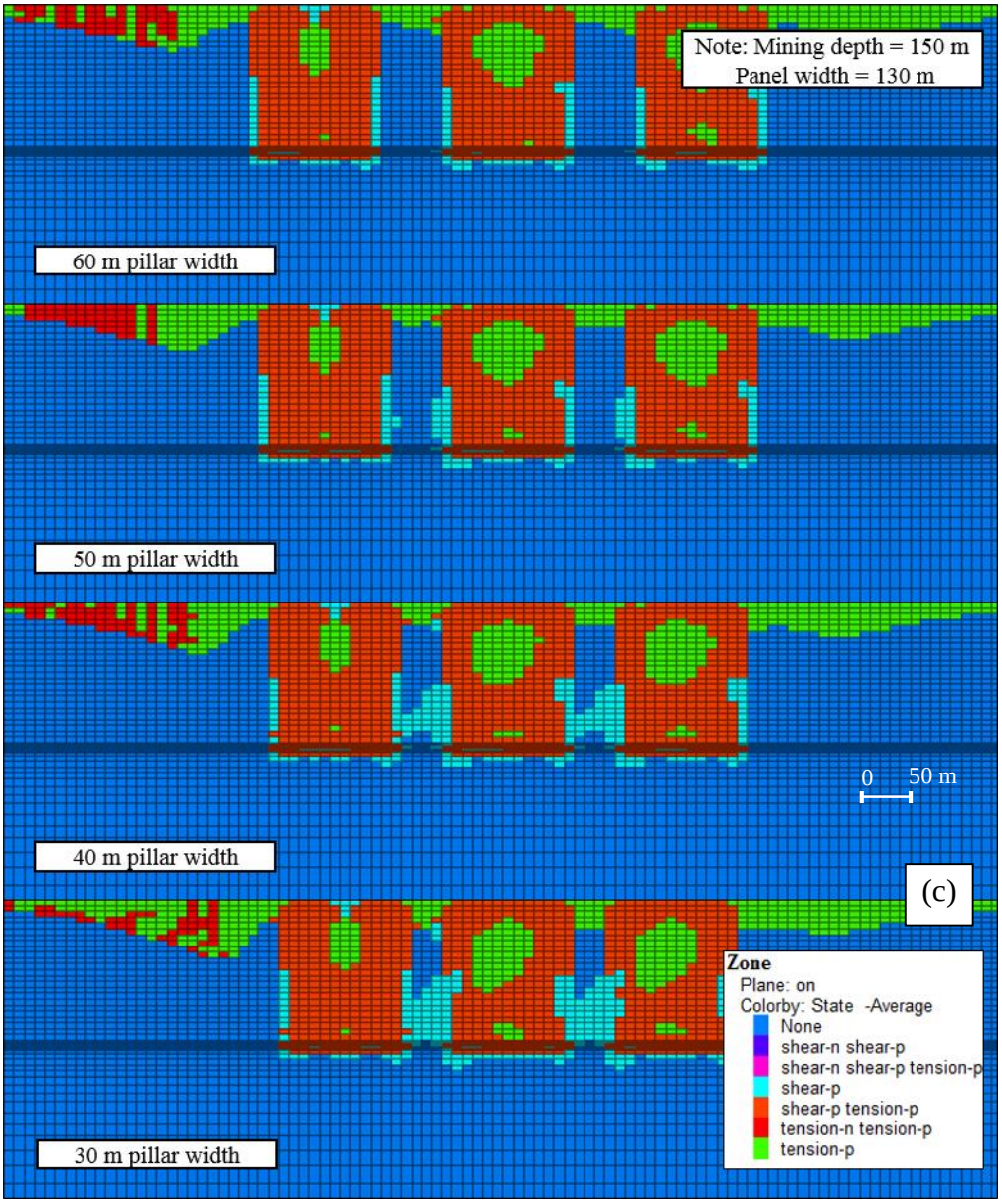

Figure 5.22 Simulation results of surface subsidence resulted from longwall mining under various chain pillar widths at 150 m depth (a) contour of subsidence and angle of draw (b) profile of surface subsidence (c) failure zone of overburden strata.

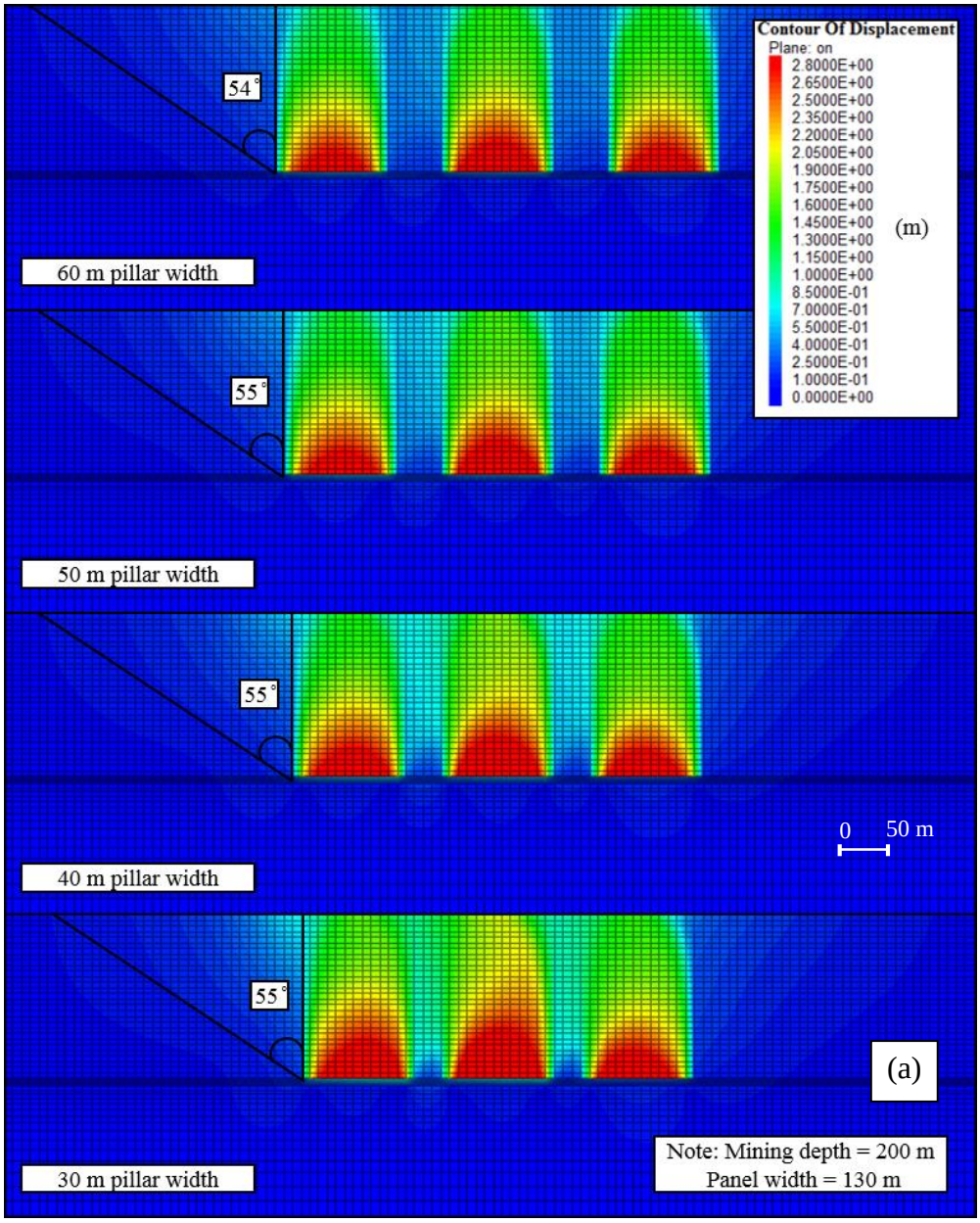
Contour Of Displacement
Plane: on
2.8000E+00
2.6500E+00
2.5000E+00
2.3500E+00
2.2000E+00
2.0500E+00
1.9000E+00
1.7500E+00
1.6000E+00
1.4500E+00
1.3000E+00
1.1500E+00
1.0000E+00
8.5000E-01
7.0000E-01
5.5000E-01
4.0000E-01
2.5000E-01
1.0000E-01
0.0000E+00
(m)
54°
60 m pillar width
55°
50 m pillar width
55°
40 m pillar width
55°
30 m pillar width
0 50 m
(a)
Note: Mining depth = 200 m
Panel width = 130 m

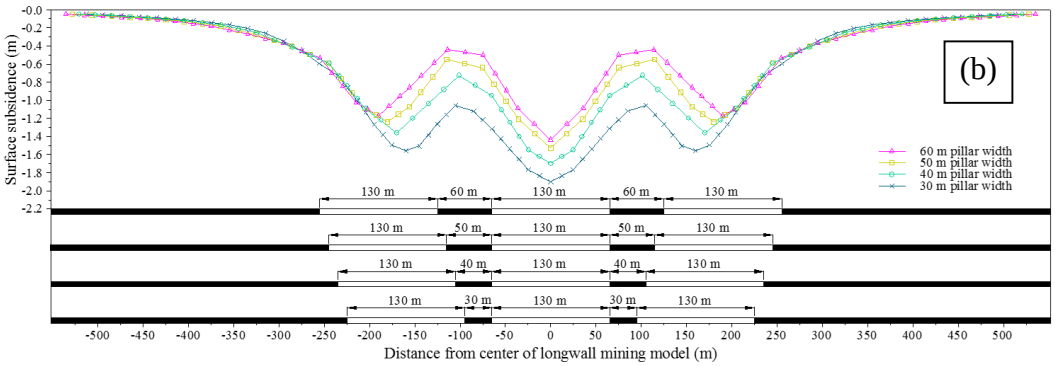
Surface subsidence (m)
-0.0
-0.2
-0.4
-0.6
-0.8
-1.0
-1.2
-1.4
-1.6
-1.8
-2.0
-2.2
(b)
60 m pillar width
50 m pillar width
40 m pillar width
30 m pillar width
130 m
60 m
50 m
40 m
30 m
-500 -450 -400 -350 -300 -250 -200 -150 -100 -50 0 50 100 150 200 250 300 350 400 450 500
Distance from center of longwall mining model (m)

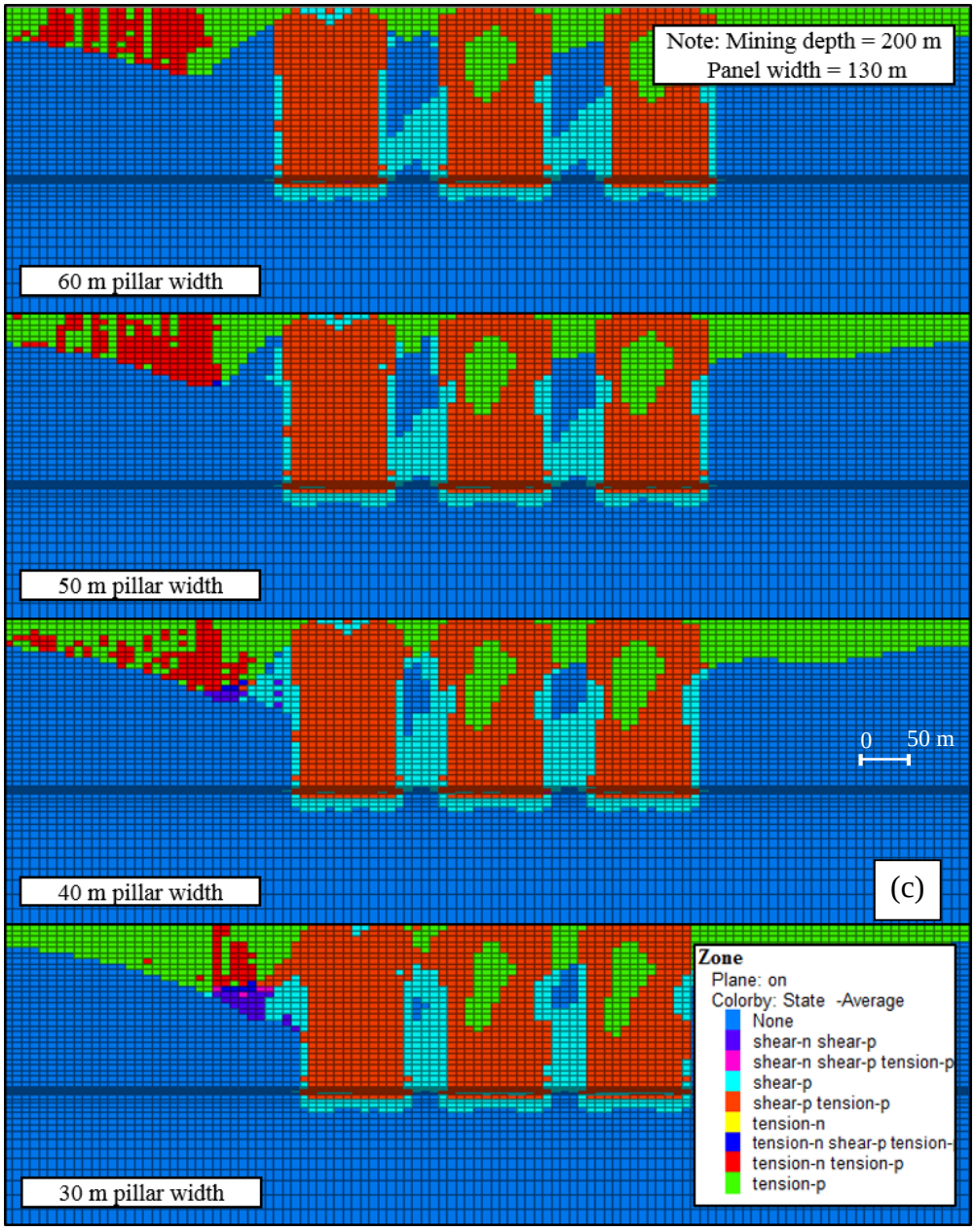

Figure 5.23 Simulation results of surface subsidence resulted from longwall mining under various chain pillar widths at 200 m depth (a) contour of subsidence and angle of draw (b) profile of surface subsidence (c) failure zone of overburden strata.

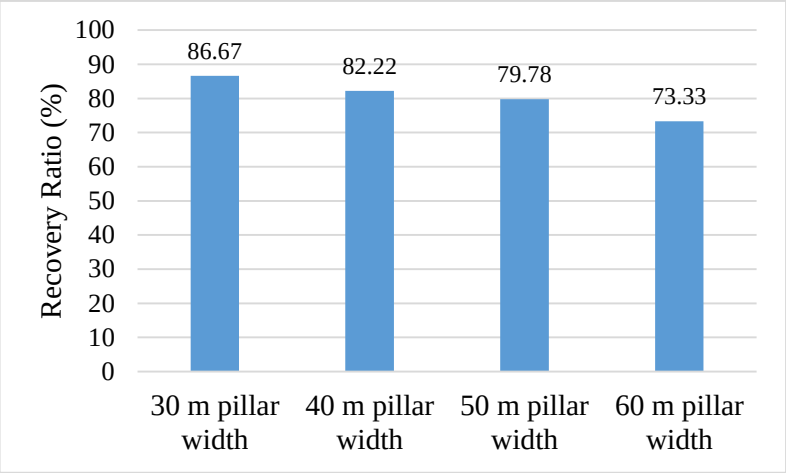

Figure 5.24 Relationship between recovery ratio of coal and chain pillar width.

5.6.2. Effect of Panel Width on Surface Subsidence

Minimizing the magnitude of surface subsidence by decreasing the panel width was investigated numerically in this section. The numerical model included three panels, and various panel widths such as 70 m, 100 m, and 130 m were studied. The chain pillar width of 30 m and the mining depths of 50 m, 100 m, 150 m, and 200 m were considered in the simulations. Figures 5.25-5.28 illustrate the results of subsidence contour, subsidence profile, and failure zone of overburden strata obtained from longwall mining of three different panel widths. From the results, it was found at all mining depths that very large AoD and S_{max} were recognized when the panel width of 130 m was applied. This indicates that the narrower panel width should be applied in order to minimize the magnitude of surface subsidence. Differently, the AoD and S_{max} significantly decreased when the panel widths of 100 m and 70 m were applied. This was due to a decrease in panel width to mining depth ratio (W/H). Based on the failure zone results, it can be seen that once the panel width reduced, the extraction area in the underground also reduced. Under this situation, the failure zone developed smaller above the mined-out panel, and this made the overburden strata were more able to bridge across the mined-out area. At the same time, as the chain pillars remained stable after the panel extraction (except at 200 m depth when a 100 m wide longwall panel was used), they also helped to support the roof strata appropriately. As a result, the AoD and S_{max} reduced, and a flat and shallow subsidence profile generated. Therefore, it can be said that

decreasing the panel width is very effective to decrease the magnitude of surface subsidence in longwall mining.

At 200 m depth, as mentioned above that the failure of the chain pillar was observed when the panel width of 100 m was mined (see Figure 5.28 c). In this case, although the pillar completely failed, the magnitude of surface subsidence was still small. It was due to the overburden itself could still bridge across the mined-out panel sufficiently. In addition, the failure of the chain pillar under this situation has no influence on the stability of the gate roadway, since the gate roadway along the mined-out panel has already finished its task and will not be used any longer. This indicates that when a narrow panel width of 100 m or 70 m is applied, a small chain pillar width of 30 m can be adopted at all mining depths. However, it is still expected that the magnitude of surface subsidence can be more minimized when a narrow panel width is used together with a wide pillar width, especially at 200 m depth.

Table 5.5 compares the AoD and S_{max} obtained from the longwall mining under three different panel widths and mining depths. From this table, for example under 200 m depth, the AoD considerably reduced from 55˚to 50˚and 34˚, while the S_{max} significantly decreased from 1.90 m to 0.38 m and 0.14 m when compared the results of the 130 m panel width with the 100 m and 70 m panel width, respectively.

Table 5.5 Comparison of AoD and S_{max} values under different panel widths and mining depths.

Mining depth (m)	70 m panel width		100 m panel width		130 m panel width	
	AoD (˚)	S_{max} (m)	AoD (˚)	S_{max} (m)	AoD (˚)	S_{max} (m)
50	-	0.06	10	0.22	10	1.37
100	8	0.09	27	0.24	29	1.38
150	25	0.12	43	0.29	50	1.68
200	34	0.14	50	0.38	55	1.90

According to the results, it is agreed that the magnitude of the surface subsidence can be minimized effectively by decreasing the panel width. However, by

decreasing the panel width, the recovery ratio of the coal will be reduced due to the coal extracting area decreases. In this section, the recovery ratio was calculated only for the coal block of 450 m in width, 1000 m in length, and 3 m in thickness. By decreasing the panel width, three chain pillars were left in case of 100 m panel width and four chain pillars were left in case of 70 m panel width within the calculated block, consequently, the minable area of coal was reduced. Figure 5.29 shows the relationship between the recovery ratio and the panel width. It was clearly seen from this figure that the recovery ratio of the coal reduced as the panel width decreased. The reason for this was that the coal lost at the chain pillars as more number of chain pillars were left when a narrower panel width was applied. The recovery ratio significantly reduced from 86.67% to 80% and 73.33% when the panel width decreased from 130 m to 100 m and 70 m, respectively. This indicates that a smaller quantity of the coal will be recovered when a narrower panel width is used. For this reason, in order to increase the coal recovery and also minimize the magnitude of surface subsidence, an alternative subsidence controlling method using the cohesive backfill was studied and discussed in the next section.

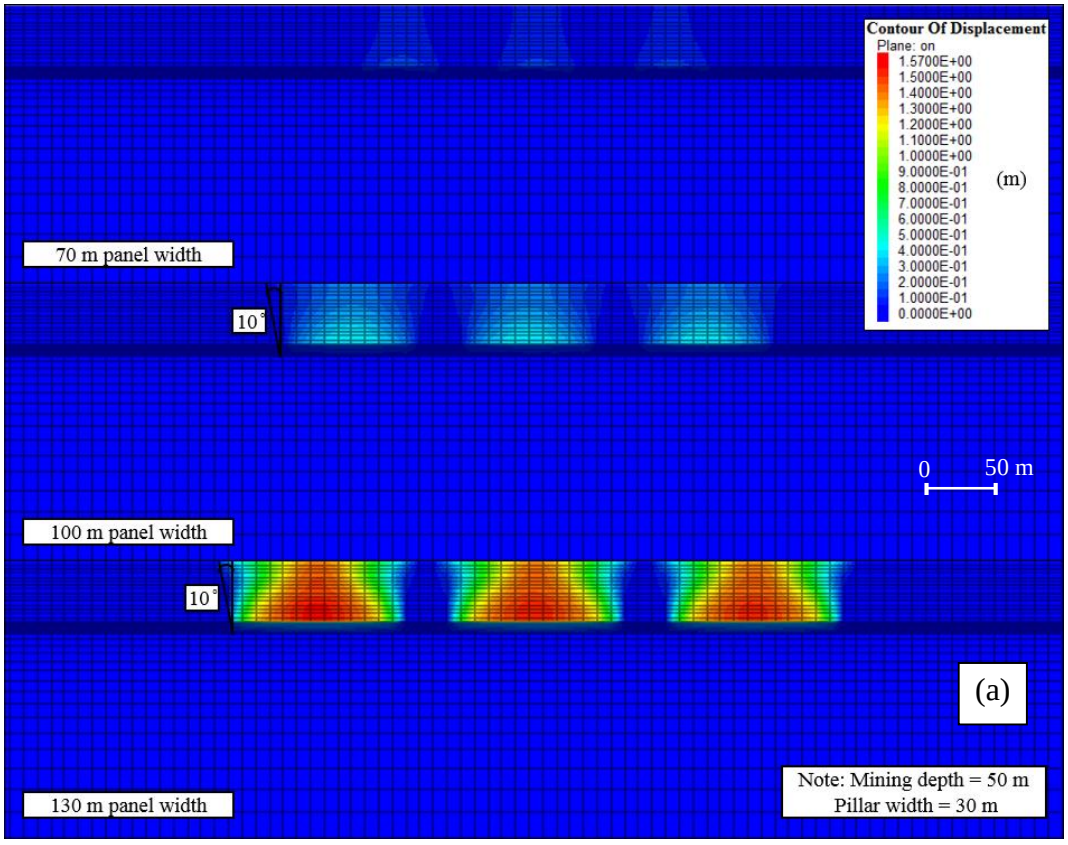

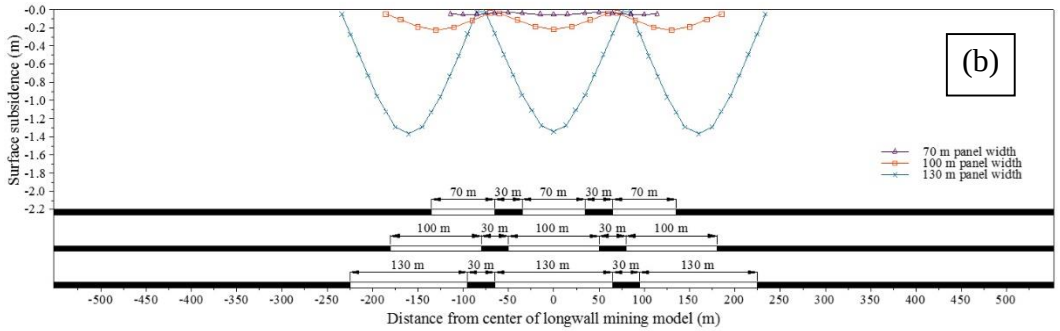

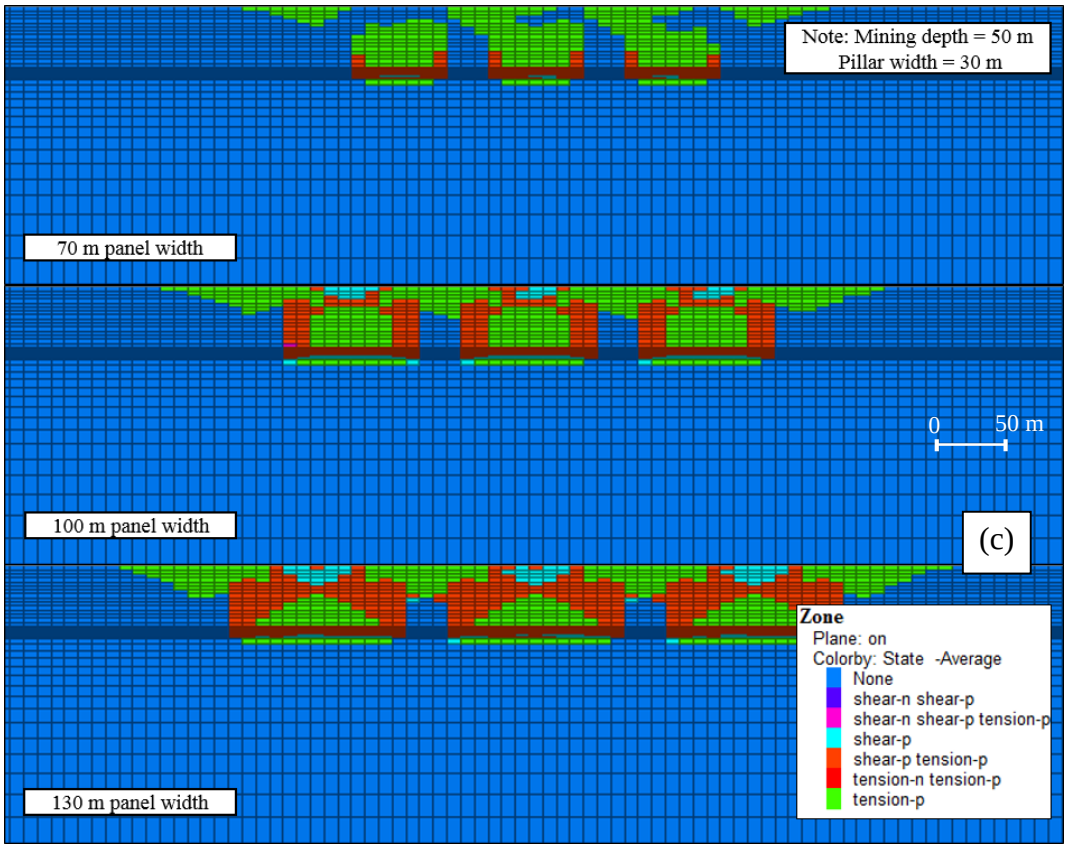

Figure 5.25 Simulation results of surface subsidence resulted from longwall mining under various panel widths at 50 m depth (a) contour of subsidence and angle of draw (b) profile of surface subsidence (c) failure zone of overburden.

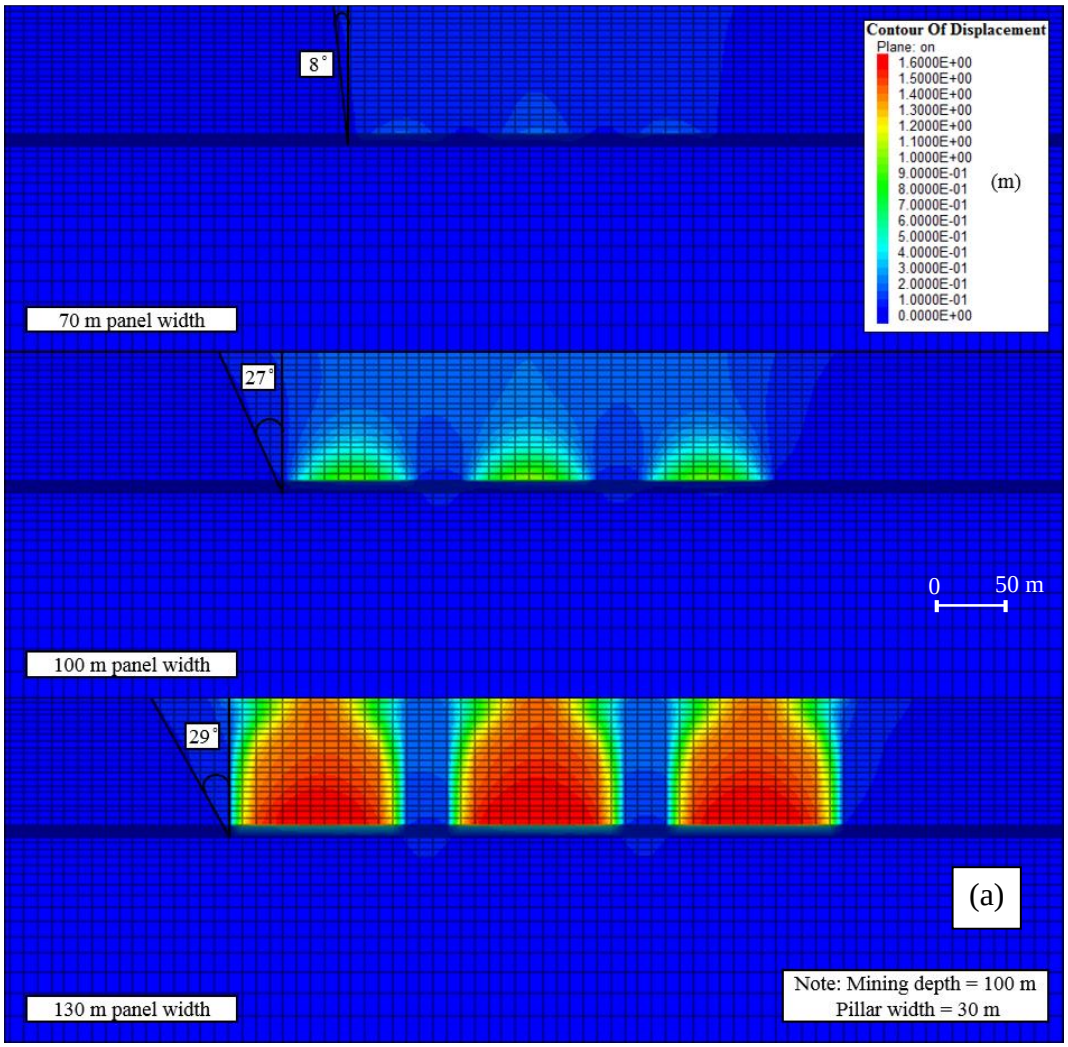
Contour Of Displacement
Plane: on
1.6000E+00
1.5000E+00
1.4000E+00
1.3000E+00
1.2000E+00
1.1000E+00
1.0000E+00
9.0000E-01
8.0000E-01
7.0000E-01
6.0000E-01
5.0000E-01
4.0000E-01
3.0000E-01
2.0000E-01
1.0000E-01
0.0000E+00
(m)
8°
70 m panel width
27°
0
50 m
100 m panel width
29°
(a)
Note: Mining depth = 100 m
Pillar width = 30 m
130 m panel width

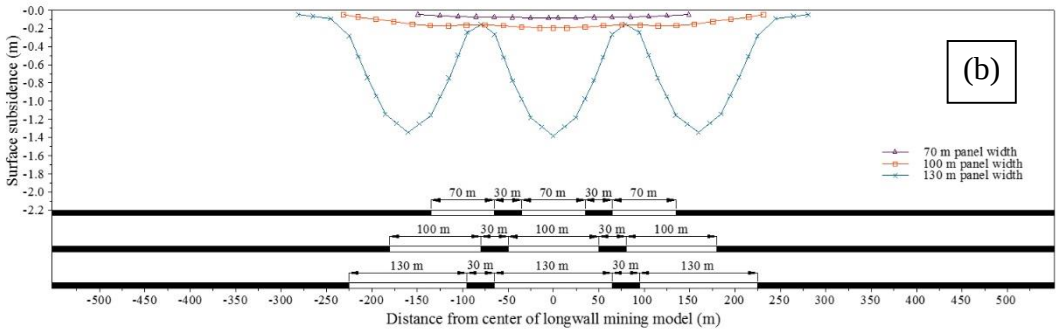
Surface subsidence (m)
-0.0
-0.2
-0.4
-0.6
-0.8
-1.0
-1.2
-1.4
-1.6
-1.8
-2.0
-2.2
(b)
70 m panel width
100 m panel width
130 m panel width
70 m
30 m
100 m
130 m
-500
-450
-400
-350
-300
-250
-200
-150
-100
-50
0
50
100
150
200
250
300
350
400
450
500
Distance from center of longwall mining model (m)

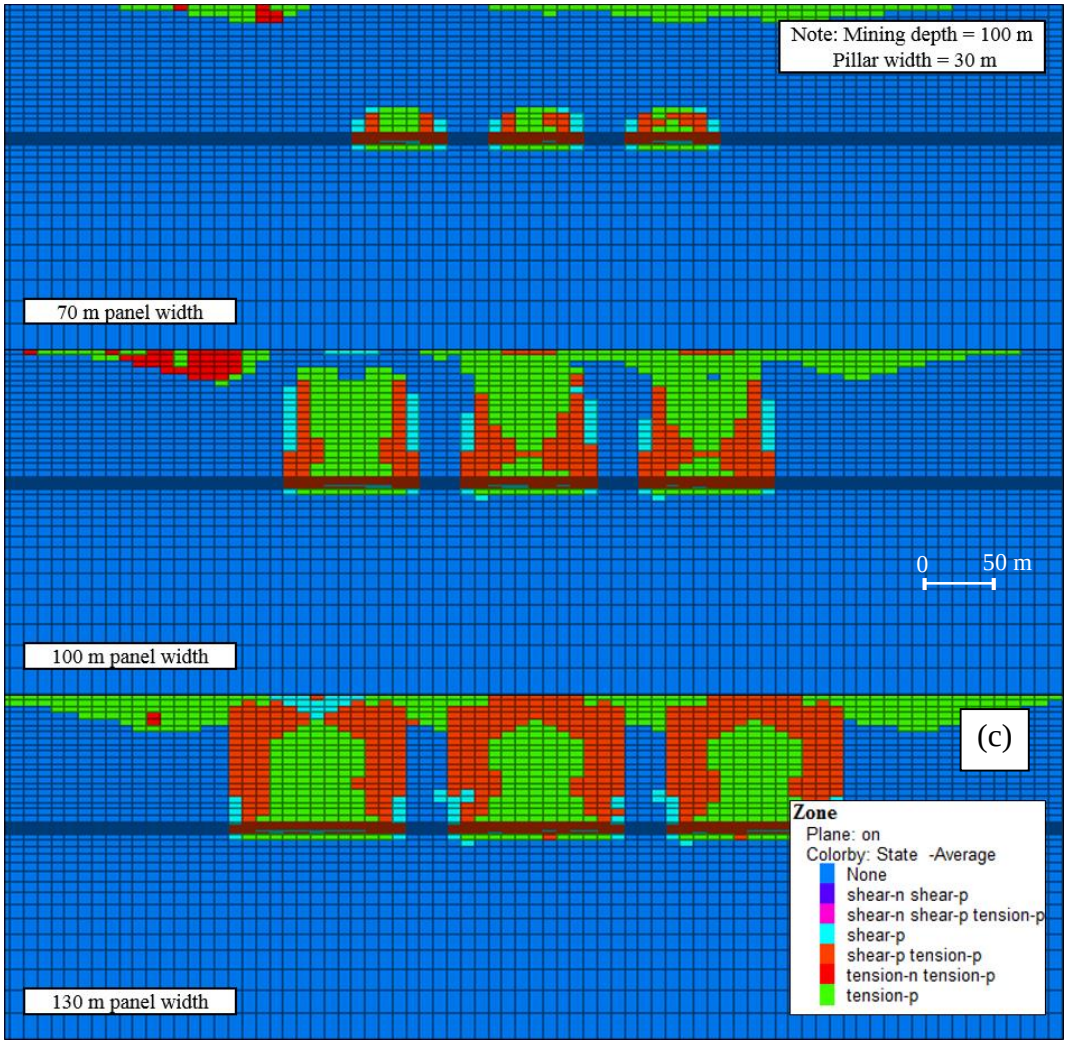

Figure 5.26 Simulation results of surface subsidence resulted from longwall mining under various panel widths at 100 m depth (a) contour of subsidence and angle of draw (b) profile of surface subsidence (c) failure zone of overburden.

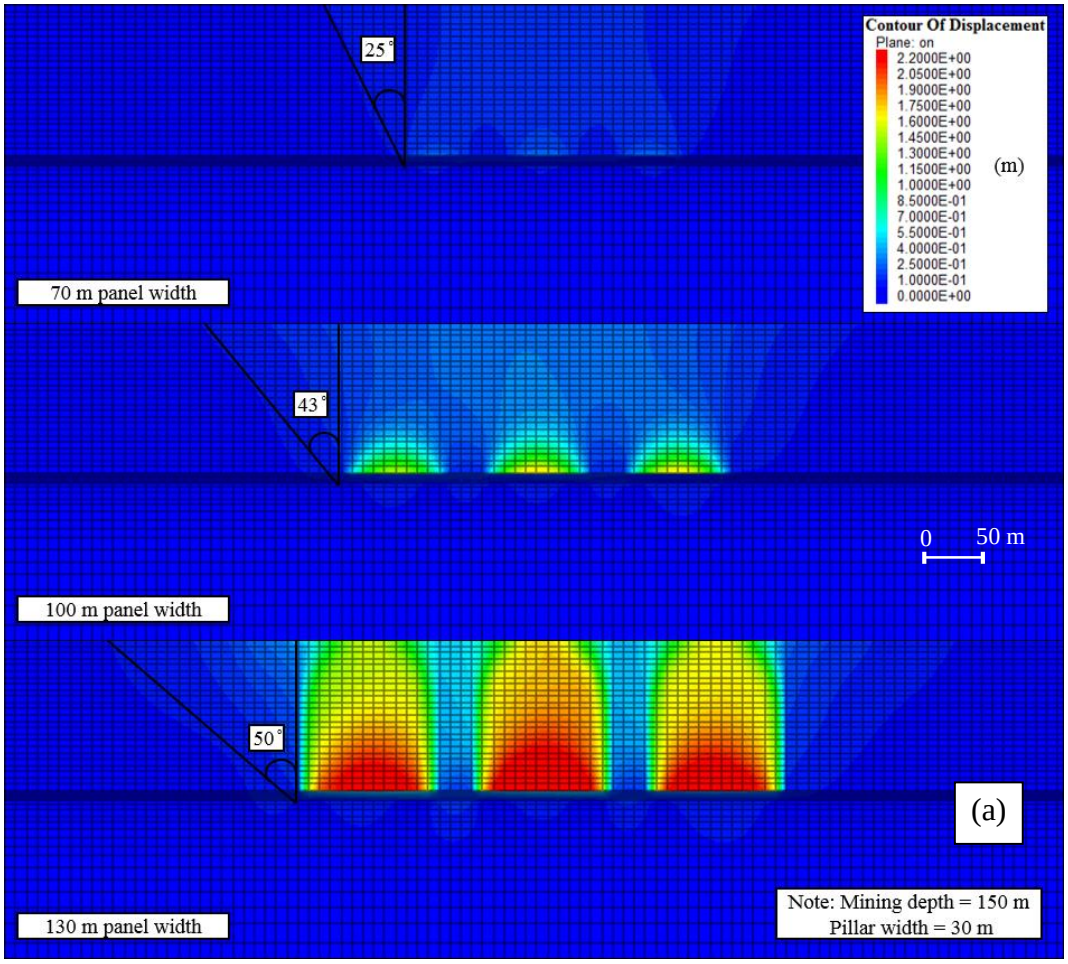
Contour Of Displacement
Plane: on
2.2000E+00
2.0500E+00
1.9000E+00
1.7500E+00
1.6000E+00
1.4500E+00
1.3000E+00
1.1500E+00
1.0000E+00
8.5000E-01
7.0000E-01
5.5000E-01
4.0000E-01
2.5000E-01
1.0000E-01
0.0000E+00
(m)
25°
70 m panel width
43°
0
50 m
100 m panel width
50°
(a)
Note: Mining depth = 150 m
Pillar width = 30 m
130 m panel width

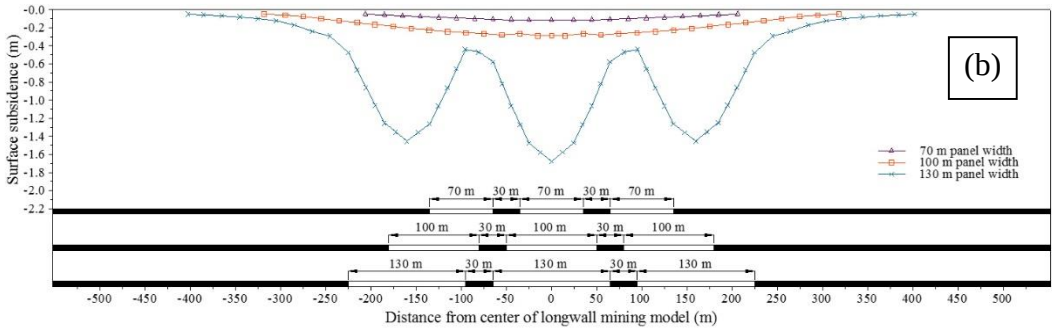
Surface subsidence (m)
-0.0
-0.2
-0.4
-0.6
-0.8
-1.0
-1.2
-1.4
-1.6
-1.8
-2.0
-2.2
(b)
70 m panel width
100 m panel width
130 m panel width
70 m
30 m
70 m
30 m
70 m
100 m
30 m
100 m
30 m
100 m
130 m
30 m
130 m
30 m
130 m
-500
-450
-400
-350
-300
-250
-200
-150
-100
-50
0
50
100
150
200
250
300
350
400
450
500
Distance from center of longwall mining model (m)

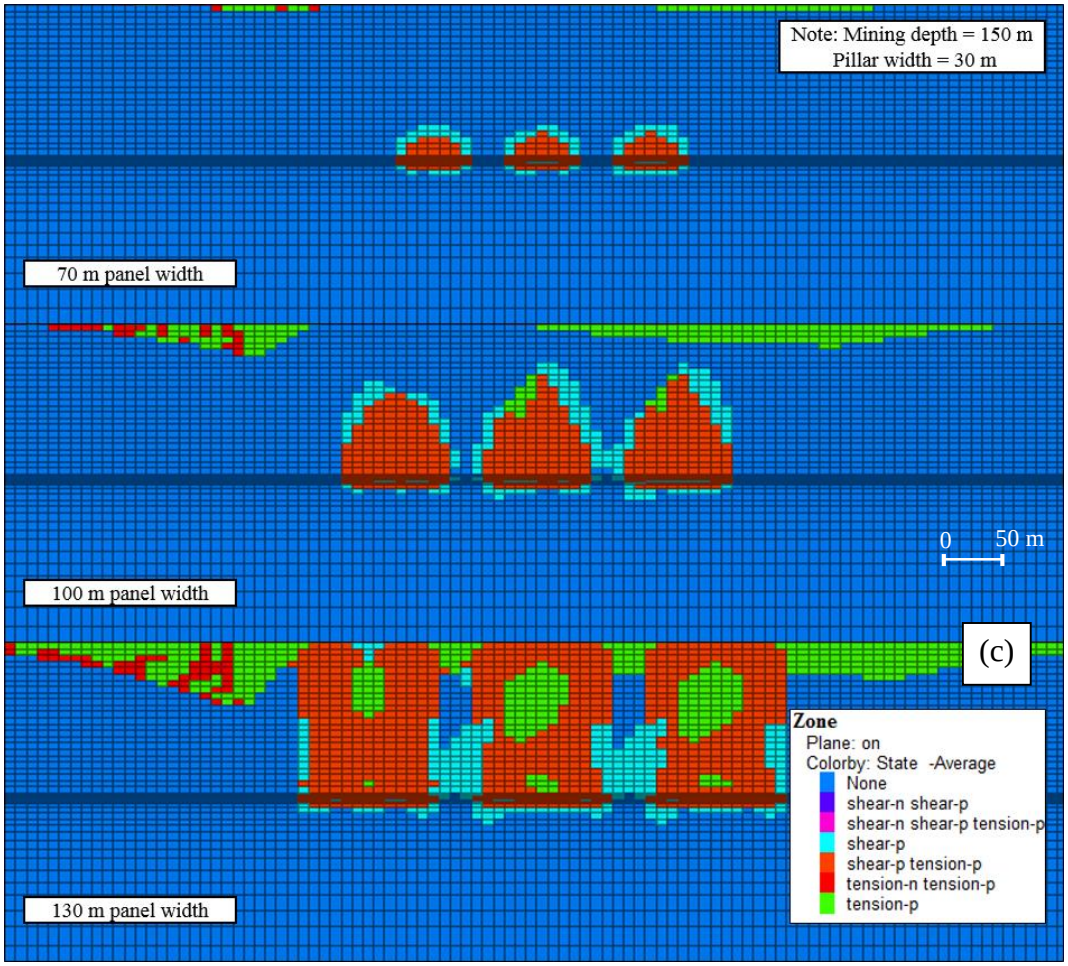

Figure 5.27 Simulation results of surface subsidence resulted from longwall mining under various panel widths at 150 m depth (a) contour of subsidence and angle of draw (b) profile of surface subsidence (c) failure zone of overburden.

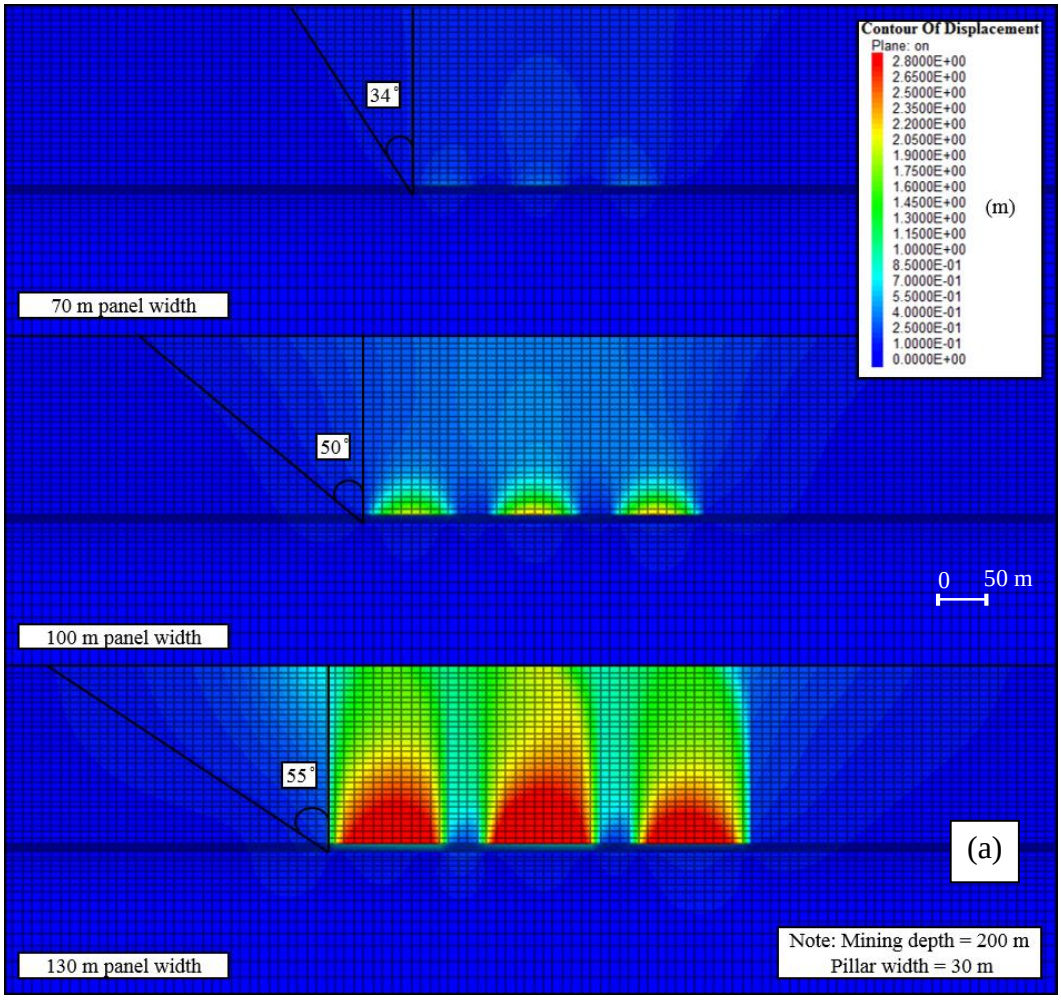
Contour Of Displacement
Plane: on
2.8000E+00
2.6500E+00
2.5000E+00
2.3500E+00
2.2000E+00
2.0500E+00
1.9000E+00
1.7500E+00
1.6000E+00
1.4500E+00
1.3000E+00
1.1500E+00
1.0000E+00
8.5000E-01
7.0000E-01
5.5000E-01
4.0000E-01
2.5000E-01
1.0000E-01
0.0000E+00
(m)
34°
70 m panel width
50°
0 50 m
100 m panel width
55°
(a)
Note: Mining depth = 200 m
Pillar width = 30 m
130 m panel width

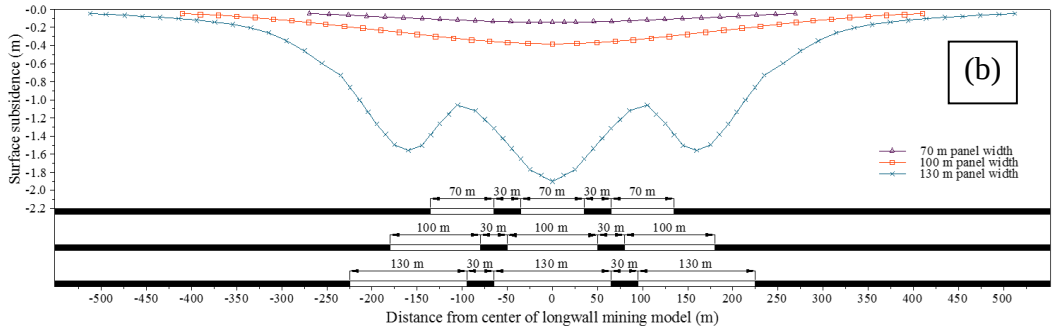
Surface subsidence (m)
-0.0
-0.2
-0.4
-0.6
-0.8
-1.0
-1.2
-1.4
-1.6
-1.8
-2.0
-2.2
(b)
70 m panel width
100 m panel width
130 m panel width
70 m
30 m
70 m
30 m
70 m
100 m
30 m
100 m
30 m
100 m
130 m
30 m
130 m
30 m
130 m
-500 -450 -400 -350 -300 -250 -200 -150 -100 -50 0 50 100 150 200 250 300 350 400 450 500
Distance from center of longwall mining model (m)

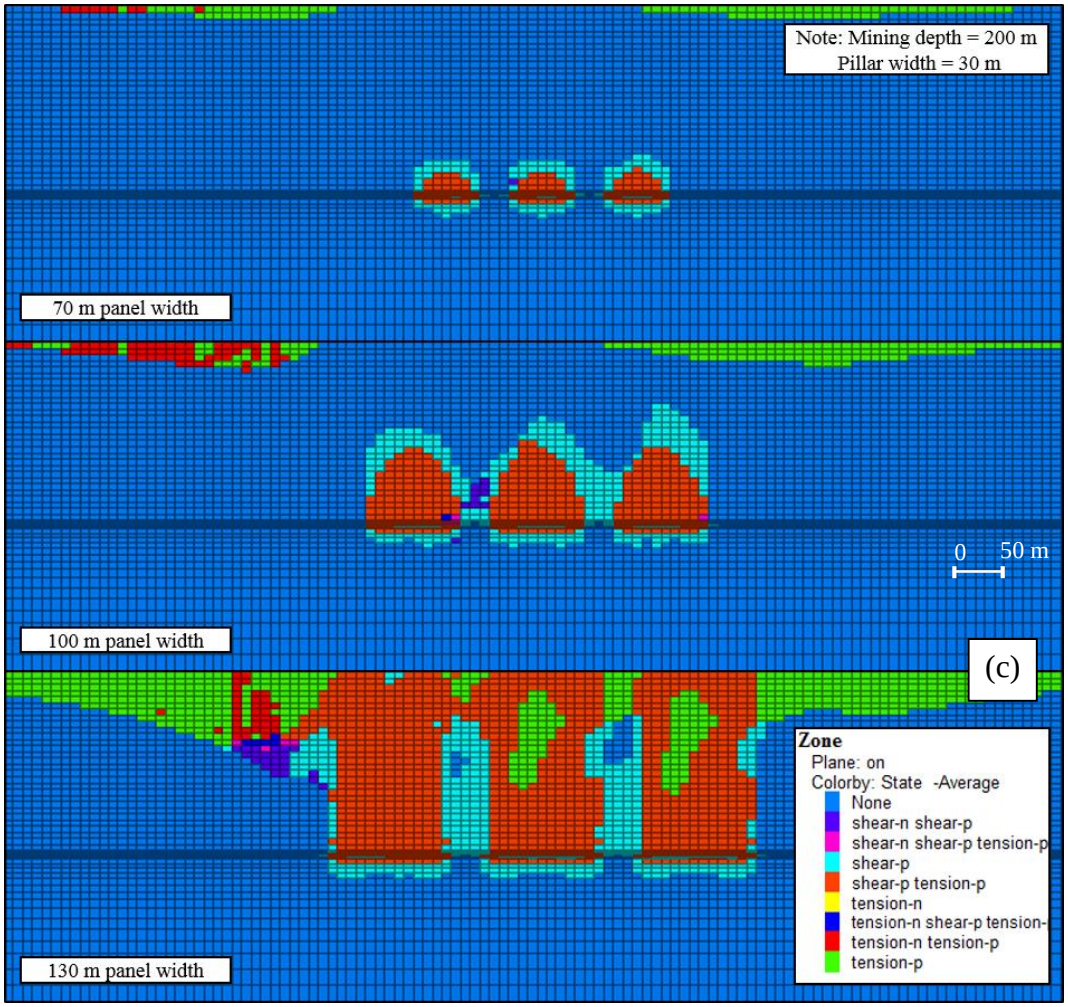

Figure 5.28 Simulation results of surface subsidence resulted from longwall mining under various panel widths at 200 m depth (a) contour of subsidence and angle of draw (b) profile of surface subsidence (c) failure zone of overburden.

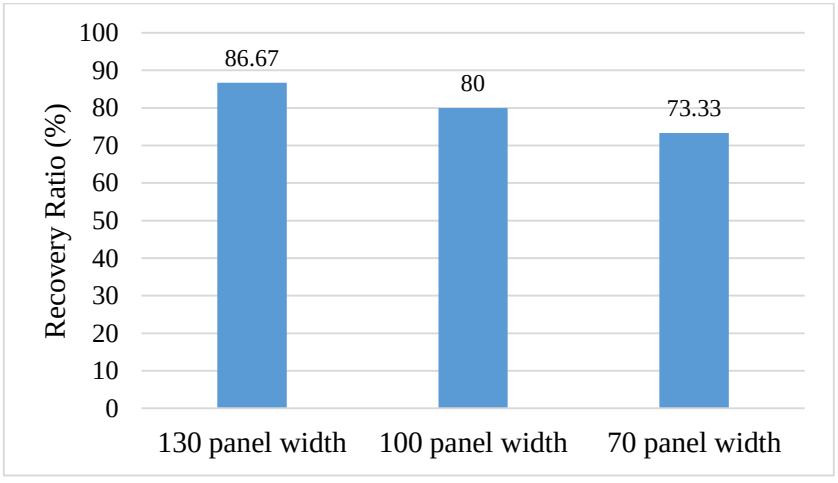

Figure 5.29 Relationship between recovery ratio of coal and panel width.

5.6.3. Effect of Backfilling Material on Surface Subsidence

Backfilling of mine void is one of the controlling methods that are being used to minimize the surface subsidence induced by longwall mining. Backfill is the term for material that is used to fill voids created by mining activity. The use of backfilling material is to prevent the ground movement and fracturing of overburden strata. It improves the ground conditions of the mine, resulting in the enhancement of economic operations and safety. The purpose of the backfill is not to transmit the rock stresses, but to reduce the relaxation of the overburden strata so that the overburden itself will maintain the load carrying capacity. Thus, it is reasonable to say that the surface subsidence can be reduced and the production of the coal mine can be improved by using backfilling technology. The cost of backfilling materials greatly depends on their strengths. The backfilling materials with UCS of 1-2 MPa will cost about 52 USD/m^3, while the ones with UCS of 4-7 MPa will cost about 82 USD/m^3. This price includes materials, transport, and labor costs (Islam, Faruque, Hasan, Hussain, & Ahammod, 2013).

The effect of backfilling material on the surface subsidence was studied in this section. The cohesive backfill was simulated in the simulations. In here, the cohesive backfill represents the materials that have cemented properties, such as fly ash, by-product left over after the mineral processing activities (i.e., milling slag). In this study, the fly ash with a gypsum additive at 4 % by weight was chosen as a cohesive backfill. The properties of cohesive backfill used in analyses are given in Table 5.6 (Choudhary, 2013). In order to investigate the effect of the cohesive backfill strength on the surface subsidence, the cohesive backfill with strength reduction by 20%, 40%, and 60% was also simulated. Considering the conditions of GDM coal measure rocks, the roof strata will soon collapse into the goaf area after the excavation face is moved. Thus, the cohesive backfill must be placed immediately behind the excavation face in order to prevent the collapse of the roof strata. The fly ash and gypsum are mixed with water and transported to the goaf area by pipelines using pumps. As the excavation face advances, the cohesive backfill of fly ash and gypsum is repeatedly fed into the goaf area until the coal panel is entirely mined out (see Figure 5.30). In simulation, therefore, the cohesive

backfill was installed immediately behind the coal face after the excavation face moved forward.

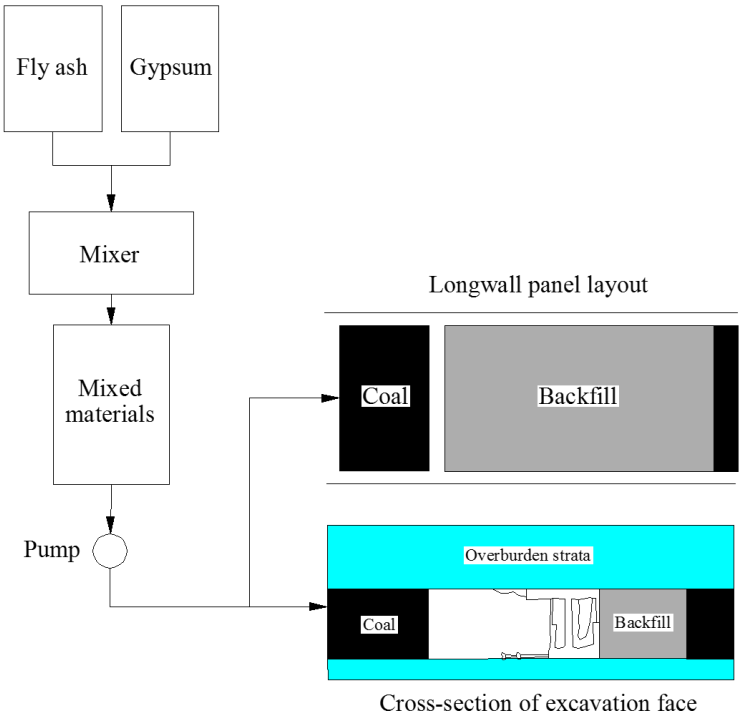

Figure 5.30 Concept of cohesive backfill installation in GDM coal mine.

In simulation, three longwall panels (130 m width), and four mining depths (50 m, 100 m, 150 m, and 200m) were considered. The width of chain pillar was 30 m in this case. The results of subsidence contour, subsidence profile, and failure zone of overburden strata obtained from longwall mining with and without application of cohesive backfill are illustrated in Figures 5.31-5.34. At all mining depths, the simulation results indicate that the cohesive backfill played an important role to minimize the surface subsidence. Compared with longwall mining without cohesive backfill application, the results of subsidence contour and subsidence profile show that the AoD and S_{max} reduced significantly after the cohesive backfill was applied. The AoD reduced from 10˚to 8˚and the S_{max} reduced from 1.37 m to 0.11 m at 50 m depth, while the AoD reduced from 29˚to 26˚and the S_{max} reduced from 1.38 m to 0.19 m at 100 m depth, whereas the AoD reduced from 50˚to 40˚and the S_{max} reduced from 1.68 m to 0.25 m at 150 m depth, and the AoD reduced from 55˚to 46˚and the S_{max} reduced from 1.90 m to 0.31 m at 200 m depth. This happened because the cohesive backfill reduced the failure zone in the overburden strata,

resulted in an improvement of its bridging ability over the mined-out area (see results of failure zone of overburden). At the same time, as the pillars remained stable under this situation, they also helped to support the overburden strata. As a result, the AoD and S_{max} reduced, and a flatter and shallower subsidence profile produced. Noticeably, the use of a 30 m chain pillar width can be adopted at all mining depths when the cohesive backfill is applied. Based on the simulation results, it indicates that a cohesive backfill can be the most appropriate countermeasure for controlling the surface subsidence at GDM underground coal mine. By applying a cohesive backfill, the coal recovery can be increased because a narrow chain pillar width of 30 m can be used appropriately with a wide panel width of 130 m.

Moreover, the AoD and S_{max} tended to increase with decreasing the strength of cohesive backfill. It was because the application of a weaker cohesive backfill strength induced more failure zone in the overburden strata, at the same time the pillars provided less support to the overburden as some pillar failures occurred, especially at 150 m and 200 m depth. Under this situation, the overburden strata were less able to bridge across the mined-out area. Consequently, a larger AoD and S_{max} occurred. Based on this, it indicates that the use of cohesive backfill with stronger strength is more effective to control the surface subsidence.

Table 5.6 Mechanical properties of cohesive backfill used in analyses.

Parameter	Cohesive backfill (96% Fly ash+4% Gypsum)	Cohesive backfill with 20% strength reduction	Cohesive backfill with 40% strength reduction	Cohesive backfill with 60% strength reduction
Uniaxial compressive strength (MPa)	1.0	0.8	0.6	0.4
Density (kg/m^3)	1,450	1,400	1,350	1,300
Young's modulus (MPa)	185.00	148.16	111.12	74.08
Poisson's ratio	0.36	0.36	0.36	0.36
Friction angle (˚)	27.0	21.6	16.2	10.8
Cohesion (MPa)	0.57	0.46	0.34	0.23

Table 5.7 summarizes the AoD and S_{max} obtained from the longwall mining with and without the application of cohesive backfill. At 50 m and 100 m depth, it can be seen from the table that the S_{max} increased slightly when the strength of cohesive backfill was reduced by 20% and 40%, whereas the S_{max} increased dramatically when the cohesive backfill strength was reduced by 60%. Differ from the depths of 150 m and 200 m, a small increment of the S_{max} was observed when the strength of cohesive backfill was reduced by 20%, while a significant increment of the S_{max} could be observed when the cohesive backfill strength was reduced by 40% and 60%. From this phenomena, it indicates that the cohesive backfill with weaker strength can be used at 50 m and 100 m depth, while the use of stronger cohesive backfill strength is recommended at 150 m and 200 m depth.

Table 5.7 Comparison of AoD and S_{max} values obtained from longwall mining with and without application of cohesive backfill under various depths.

Mining depth (m)	No backfill		Cohesive backfill (96% Fly ash+4% Gypsum)		Cohesive backfill with 20% strength reduction		Cohesive backfill with 40% strength reduction		Cohesive backfill with 60% strength reduction	
	AoD (˚)	S_{max} (m)	AoD (˚)	S_{max} (m)	AoD (˚)	S_{max} (m)	AoD (˚)	S_{max} (m)	AoD (˚)	S_{max} (m)
50	10	1.37	8	0.11	9	0.20	9	0.26	9	0.40
100	29	1.38	26	0.19	26	0.26	27	0.30	28	0.46
150	50	1.68	40	0.25	42	0.32	45	0.46	47	0.67
200	55	1.90	46	0.31	49	0.40	52	0.61	53	0.86

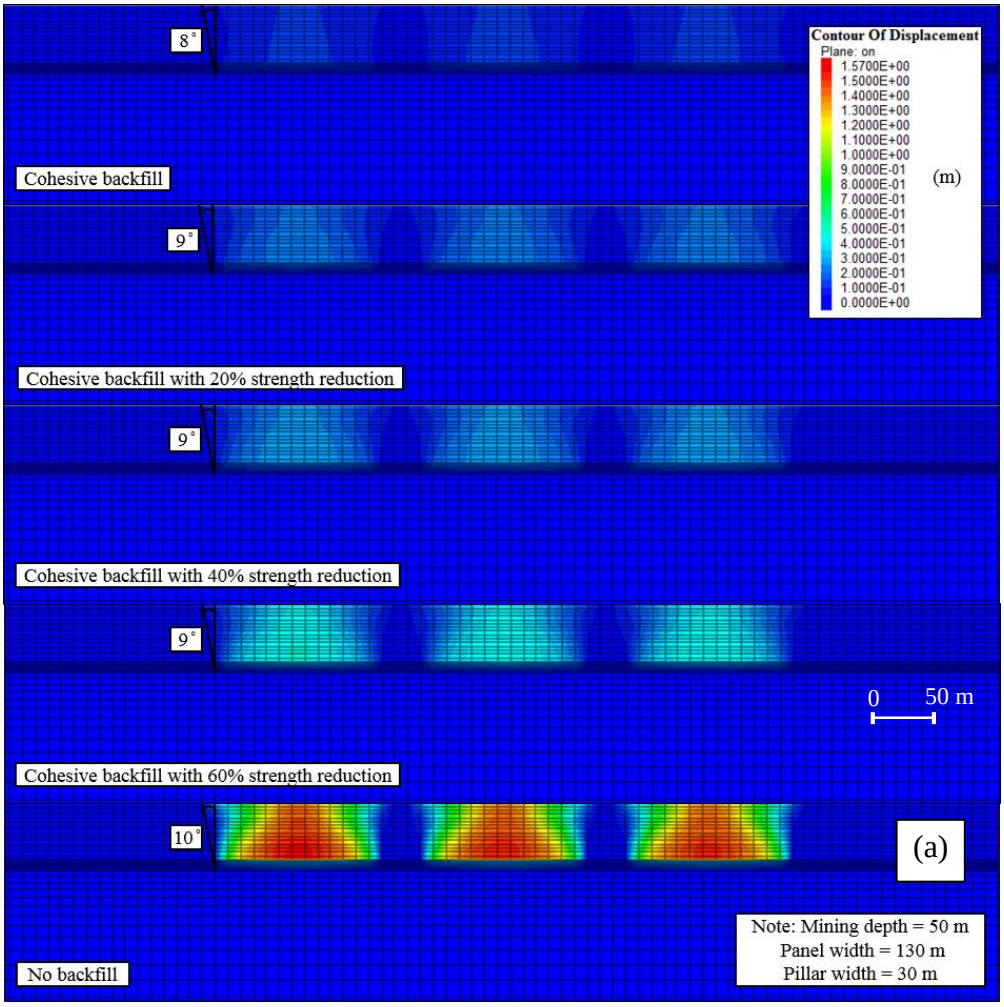
Contour Of Displacement
Plane: on
1.5700E+00
1.5000E+00
1.4000E+00
1.3000E+00
1.2000E+00
1.1000E+00
1.0000E+00
9.0000E-01
8.0000E-01
7.0000E-01
6.0000E-01
5.0000E-01
4.0000E-01
3.0000E-01
2.0000E-01
1.0000E-01
0.0000E+00
(m)
8°
Cohesive backfill
9°
Cohesive backfill with 20% strength reduction
9°
Cohesive backfill with 40% strength reduction
9°
0
50 m
Cohesive backfill with 60% strength reduction
10°
(a)
Note: Mining depth = 50 m
Panel width = 130 m
Pillar width = 30 m
No backfill

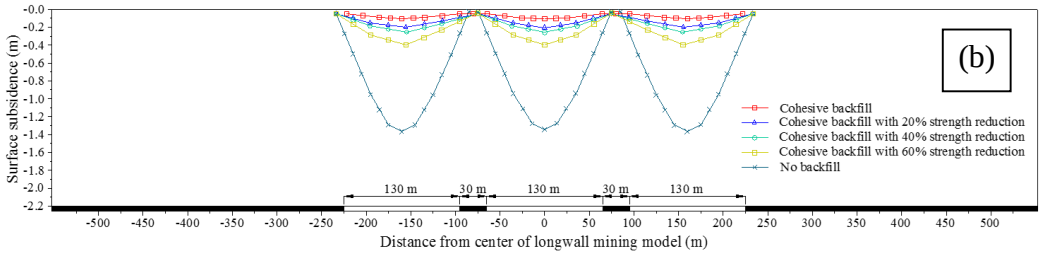
Surface subsidence (m)
-0.0
-0.2
-0.4
-0.6
-0.8
-1.0
-1.2
-1.4
-1.6
-1.8
-2.0
-2.2
130 m
30 m
130 m
30 m
130 m
(b)
Cohesive backfill
Cohesive backfill with 20% strength reduction
Cohesive backfill with 40% strength reduction
Cohesive backfill with 60% strength reduction
No backfill
-500 -450 -400 -350 -300 -250 -200 -150 -100 -50 0 50 100 150 200 250 300 350 400 450 500
Distance from center of longwall mining model (m)

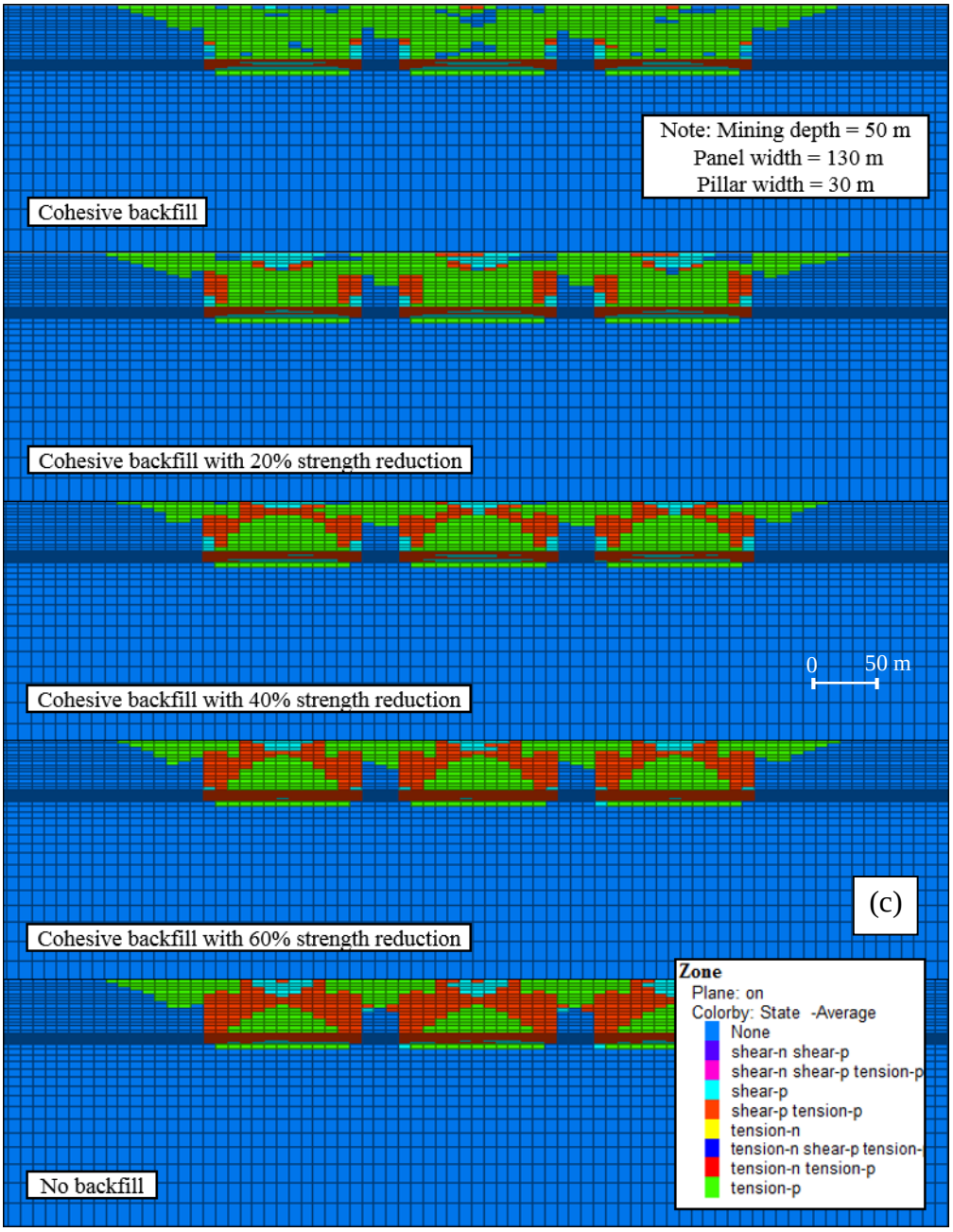

Figure 5.31 Simulation results of surface subsidence resulted from longwall mining with and without application of cohesive backfill at 50 m depth (a) contour of subsidence and angle of draw (b) profile of surface subsidence (c) failure zone of overburden.

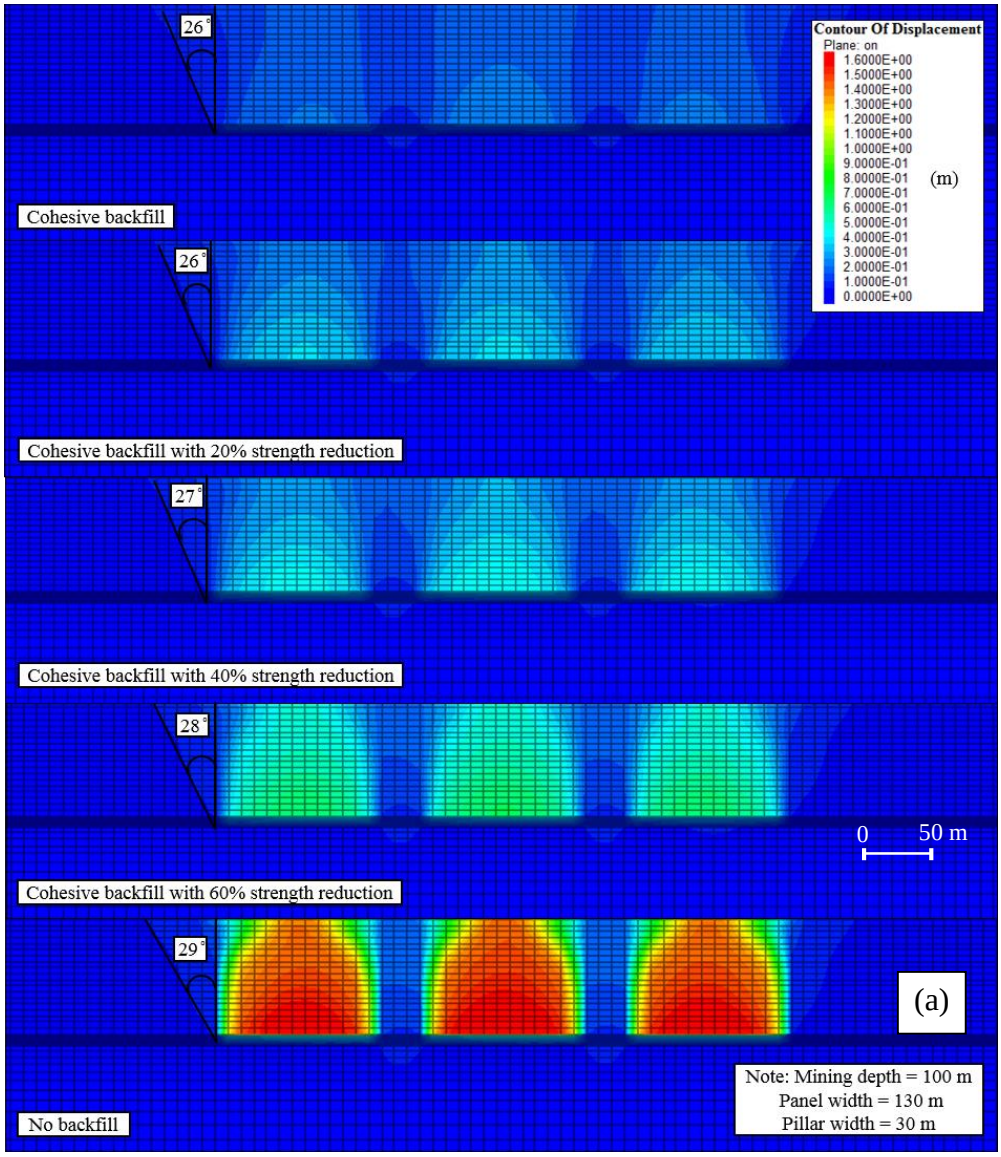
Contour Of Displacement
Plane: on
1.6000E+00
1.5000E+00
1.4000E+00
1.3000E+00
1.2000E+00
1.1000E+00
1.0000E+00
9.0000E-01
8.0000E-01
7.0000E-01
6.0000E-01
5.0000E-01
4.0000E-01
3.0000E-01
2.0000E-01
1.0000E-01
0.0000E+00
(m)
26°
Cohesive backfill
26°
Cohesive backfill with 20% strength reduction
27°
Cohesive backfill with 40% strength reduction
28°
0 50 m
Cohesive backfill with 60% strength reduction
29°
(a)
Note: Mining depth = 100 m
Panel width = 130 m
Pillar width = 30 m
No backfill

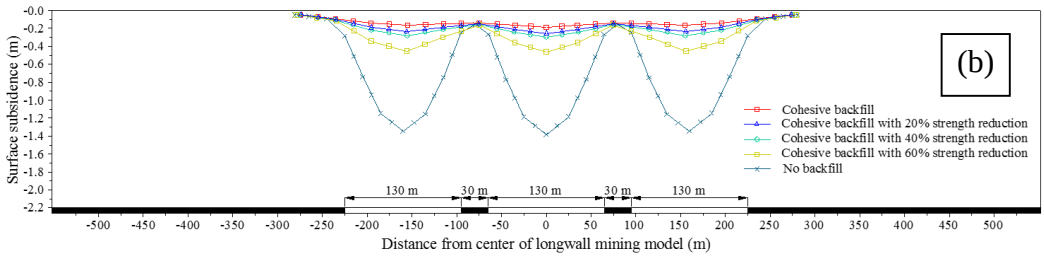
Surface subsidence (m)
-0.0
-0.2
-0.4
-0.6
-0.8
-1.0
-1.2
-1.4
-1.6
-1.8
-2.0
-2.2
(b)
Cohesive backfill
Cohesive backfill with 20% strength reduction
Cohesive backfill with 40% strength reduction
Cohesive backfill with 60% strength reduction
No backfill
130 m
30 m
130 m
30 m
130 m
-500 -450 -400 -350 -300 -250 -200 -150 -100 -50 0 50 100 150 200 250 300 350 400 450 500
Distance from center of longwall mining model (m)

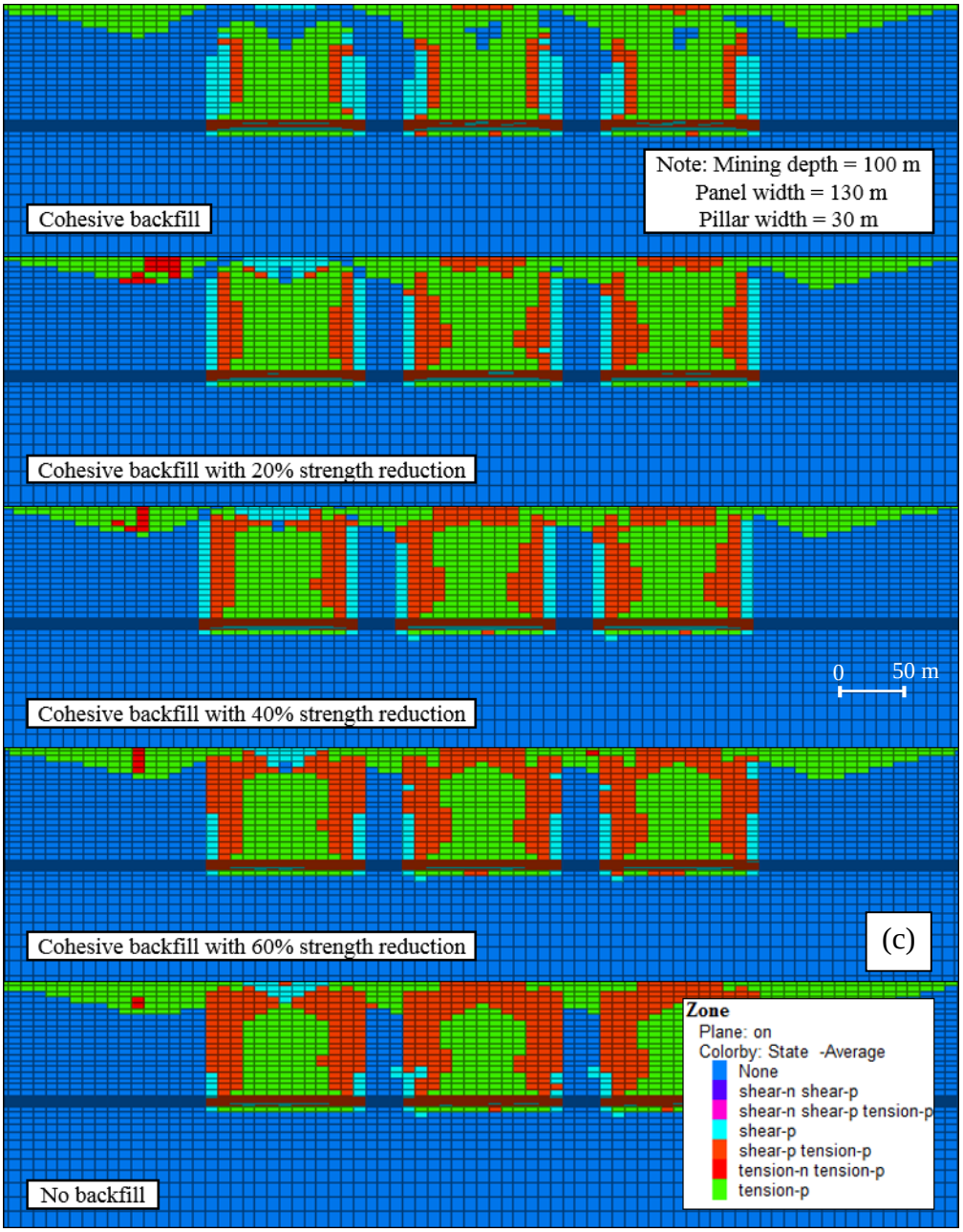

Figure 5.32 Simulation results of surface subsidence resulted from longwall mining with and without application of cohesive backfill at 100 m depth (a) contour of subsidence and angle of draw (b) profile of surface subsidence (c) failure zone of overburden.

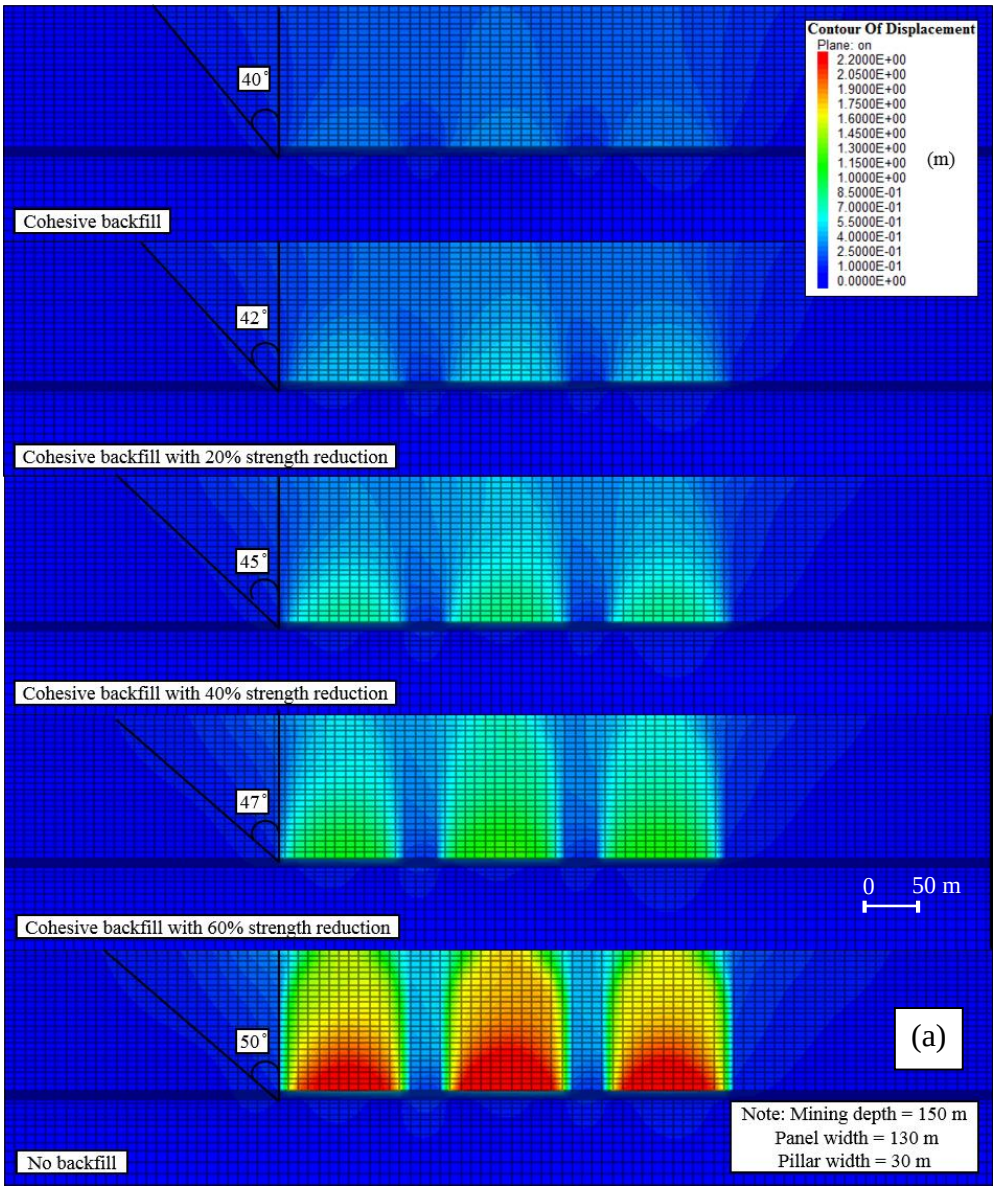
Contour Of Displacement
Plane: on
2.2000E+00
2.0500E+00
1.9000E+00
1.7500E+00
1.6000E+00
1.4500E+00
1.3000E+00
1.1500E+00
1.0000E+00
8.5000E-01
7.0000E-01
5.5000E-01
4.0000E-01
2.5000E-01
1.0000E-01
0.0000E+00
(m)
40°
Cohesive backfill
42°
Cohesive backfill with 20% strength reduction
45°
Cohesive backfill with 40% strength reduction
47°
0 50 m
Cohesive backfill with 60% strength reduction
50°
(a)
Note: Mining depth = 150 m
Panel width = 130 m
Pillar width = 30 m
No backfill

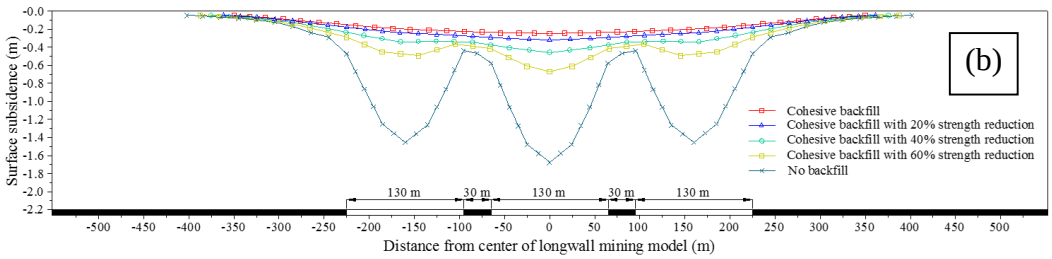
Surface subsidence (m)
-0.0
-0.2
-0.4
-0.6
-0.8
-1.0
-1.2
-1.4
-1.6
-1.8
-2.0
-2.2
(b)
Cohesive backfill
Cohesive backfill with 20% strength reduction
Cohesive backfill with 40% strength reduction
Cohesive backfill with 60% strength reduction
No backfill
130 m
30 m
130 m
30 m
130 m
-500 -450 -400 -350 -300 -250 -200 -150 -100 -50 0 50 100 150 200 250 300 350 400 450 500
Distance from center of longwall mining model (m)

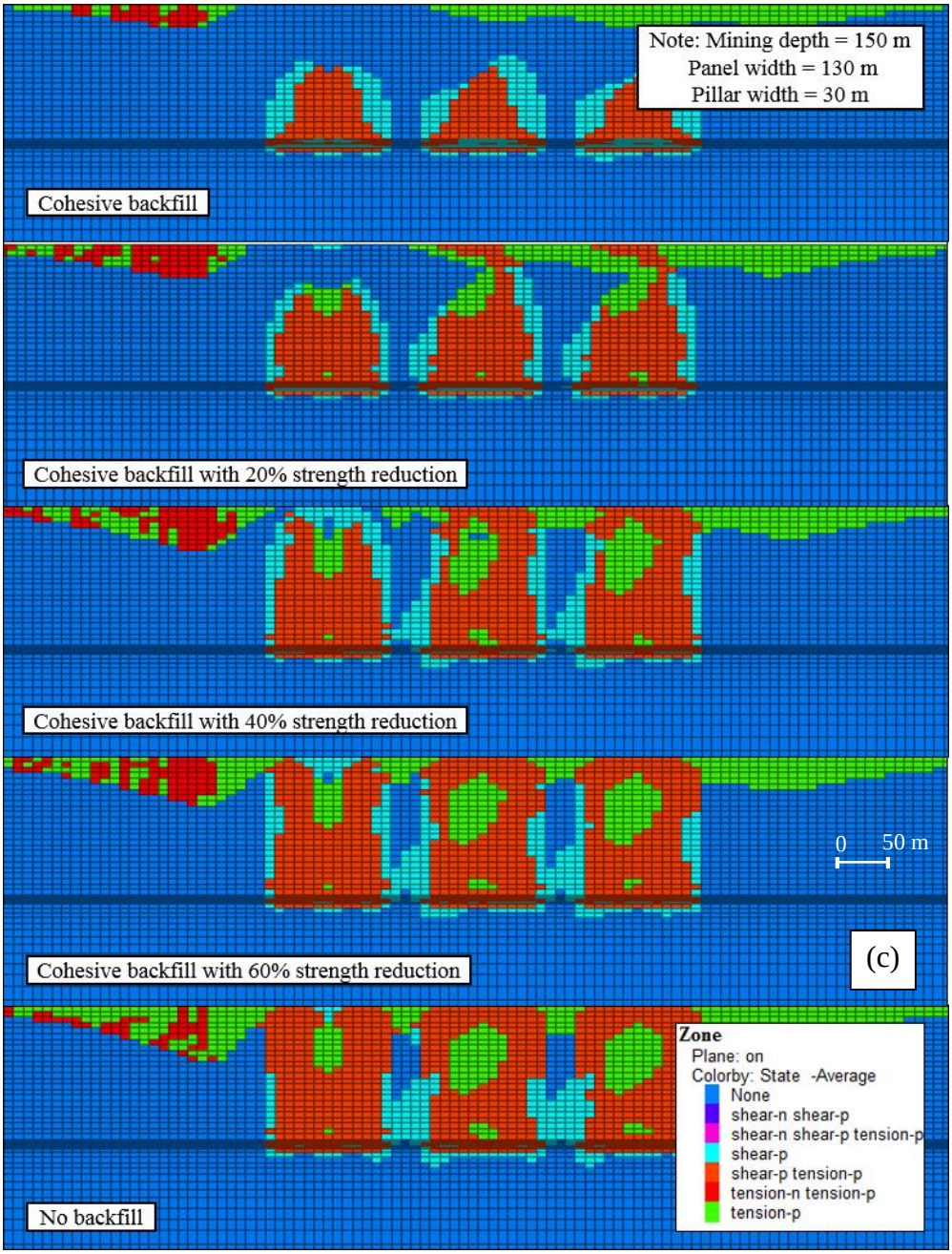

Figure 5.33 Simulation results of surface subsidence resulted from longwall mining with and without application of cohesive backfill at 150 m depth (a) contour of subsidence and angle of draw (b) profile of surface subsidence (c) failure zone of overburden.

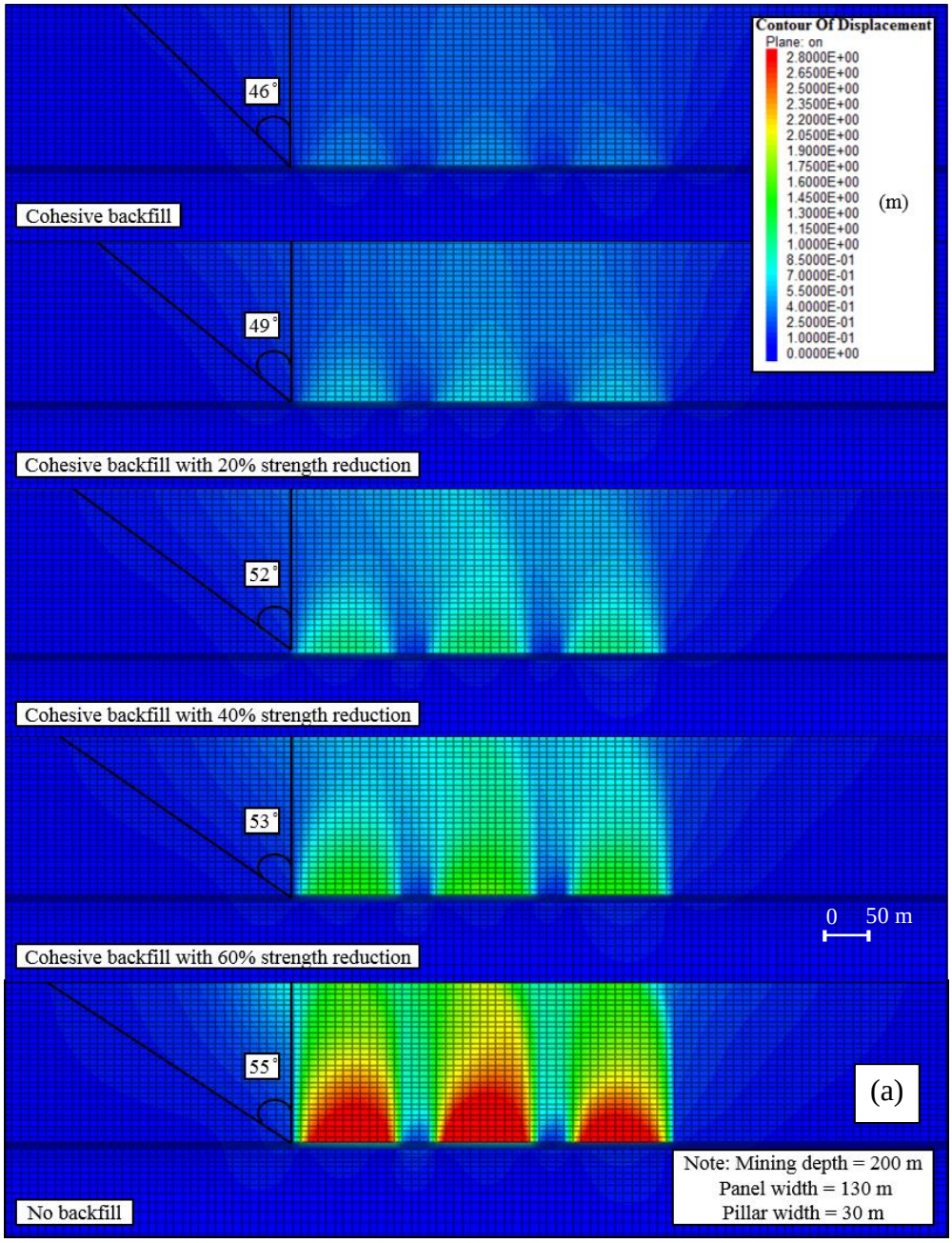
Contour Of Displacement
Plane: on
2.8000E+00
2.6500E+00
2.5000E+00
2.3500E+00
2.2000E+00
2.0500E+00
1.9000E+00
1.7500E+00
1.6000E+00
1.4500E+00
1.3000E+00
1.1500E+00
1.0000E+00
8.5000E-01
7.0000E-01
5.5000E-01
4.0000E-01
2.5000E-01
1.0000E-01
0.0000E+00
(m)
46°
Cohesive backfill
49°
Cohesive backfill with 20% strength reduction
52°
Cohesive backfill with 40% strength reduction
53°
0 50 m
Cohesive backfill with 60% strength reduction
55°
(a)
Note: Mining depth = 200 m
Panel width = 130 m
Pillar width = 30 m
No backfill

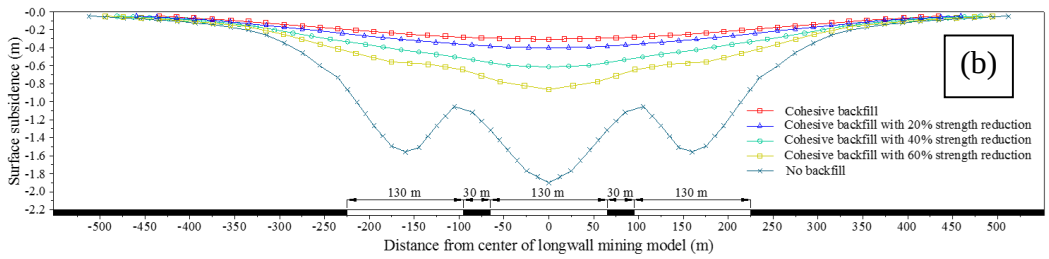
Surface subsidence (m)
-0.0
-0.2
-0.4
-0.6
-0.8
-1.0
-1.2
-1.4
-1.6
-1.8
-2.0
-2.2
(b)
Cohesive backfill
Cohesive backfill with 20% strength reduction
Cohesive backfill with 40% strength reduction
Cohesive backfill with 60% strength reduction
No backfill
130 m
30 m
130 m
30 m
130 m
-500 -450 -400 -350 -300 -250 -200 -150 -100 -50 0 50 100 150 200 250 300 350 400 450 500
Distance from center of longwall mining model (m)

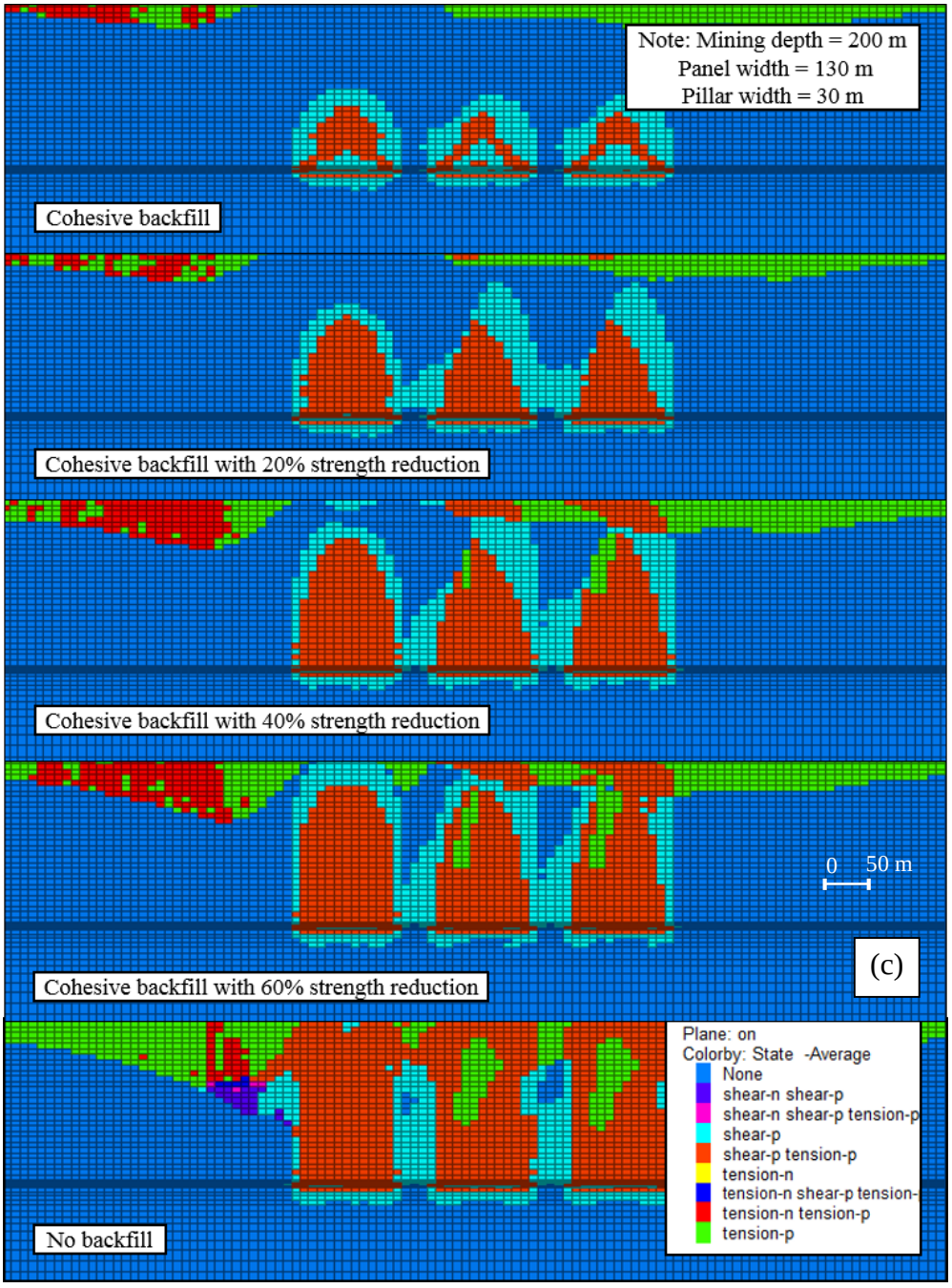

Figure 5.34 Simulation results of surface subsidence resulted from longwall mining with and without application of cohesive backfill at 200 m depth (a) contour of subsidence and angle of draw (b) profile of surface subsidence (c) failure zone of overburden.

5.7. Proposed Graph for Prediction of Surface Subsidence induced by Longwall Mining above Single-panel for GDM Coal Mine

According to the results obtained from a series of numerical simulations, a graph for prediction of maximum surface subsidence induced by single-panel longwall mining in the case of GDM coal mine was proposed in this section (see Figure 5.35). In order to predict the maximum surface subsidence by using this graph, the panel width and mining depth are required. By drawing a horizontal line from the panel width axis and a vertical line from the mining depth axis, an apparent subsidence factor can be estimated at the position of an intersection between the horizontal and vertical lines. The maximum surface subsidence value can be then calculated using an equation expresses as below. Importantly, in order to achieve a more accurate graph for prediction of maximum surface subsidence, the subsidence prediction graph proposed in this section can be modified once the measurement data of surface subsidence at GDM coal mine are obtained.

$$S_{max} = a'h \tag{5.2}$$

Where S_{max} is the maximum surface subsidence (m), a' is the apparent subsidence factor, and h is the thickness of extracted coal seam (m).

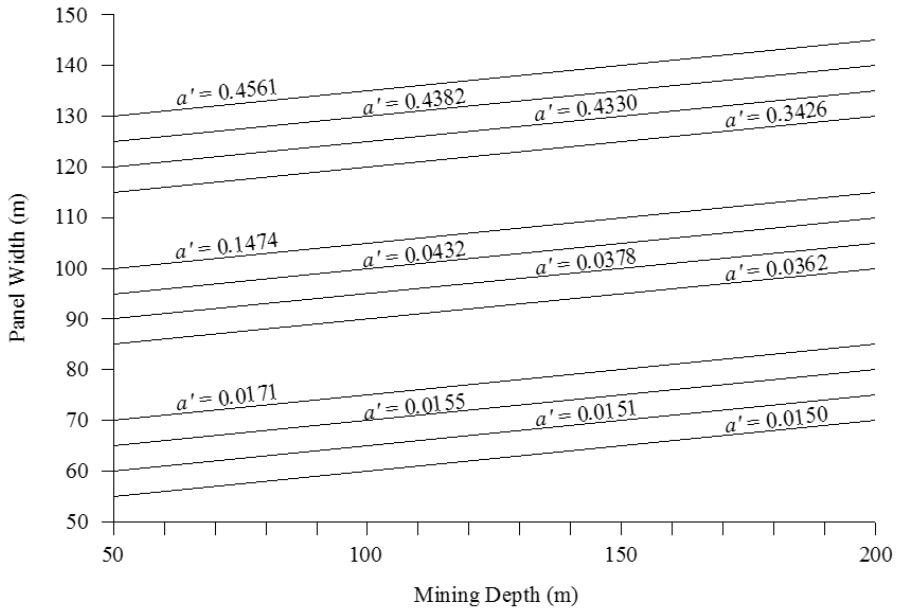

Figure 5.35 Chart for determining apparent subsidence factor (a') for GDM coal mine.

5.8. Rehabilitation of Surface Subsidence after Longwall Mining at GDM Coal Mine

According to the simulation results of surface subsidence presented in the previous sections, it is found that although the magnitude of surface subsidence can be controlled by using a wide pillar width, narrow panel width, and cohesive backfill, some extents of the subsidence are still observed at the surface. At GDM coal mine, as the lands above the underground mining area are used for the rice fields, the leakage of the water can be expected even a small extent of surface subsidence occurs. The leakage of the water can occur due to an increase in permeability of cracked soil and rock strata resulting from subsidence. The water leakage is a serious issue since it will cause an effect on rice productivity.

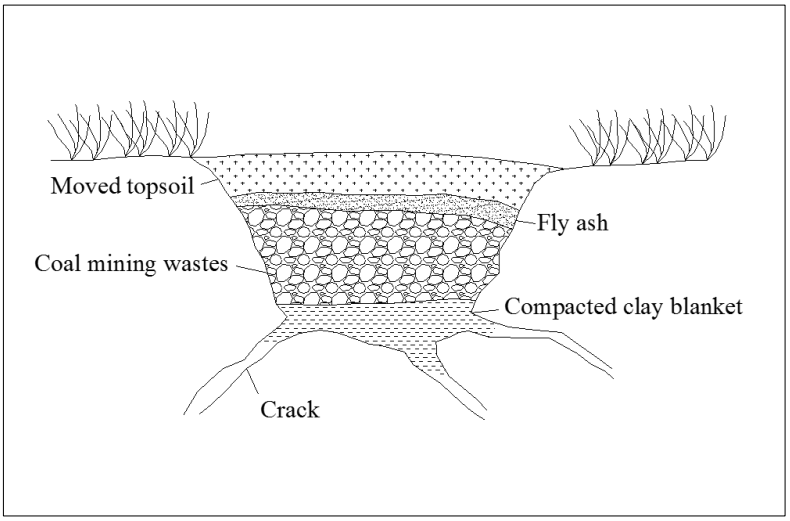

Figure 5.36 Method of subsided land rehabilitation in rice field.

GDM coal mine plans to borrow the lands from the farmers during the lifetime of an underground mining operation. The lands will be returned once the coal has been completely mined out. This means that before returning the lands to the owners, the GDM coal mine has to repair or rehabilitate the subsided land by restoring as close to its original condition as possible, and the leakage of water in the rice field has to be stopped obviously. The subsided land can be rehabilitated, and the leakage of water in the rice field can be stopped by filling method (see Figure 5.36). In order to rehabilitate the subsided area, and to stop the water leakage by filling method, the topsoil of the subsided area is firstly excavated to expose the cracks. The cracks

can be sealed with a compacted clay blanket (Dawkins, 2003). After the cracks are sealed, some filling materials are then filled in the subsided area, following by replacing the moved topsoil as soon as possible in order to minimize the chemical impacts (Lechner, Baumgartl, Matthew, & Glenn, 2016). The coal mining wastes and fly ash are normally used as the filling materials (Hu & Xiao, 2012; Meuser, 2013). However, to use the coal mining wastes as the filling material, the acidity of the waste rocks should be analyzed in order to avoid the long-term acid mine drainage generation.

5.9. Conclusions

This chapter studies the surface subsidence induced by longwall mining mainly based on the numerical simulation method. There exists a doubt whether the numerical simulation method is applicable to study the surface subsidence under weak geological conditions in this study or not. To confirm this doubt, the applicability of numerical simulation method using FLAC3D software for prediction of surface subsidence is verified in the case of Fajar Bumi Sakti (FBS) coal mine. The characteristics of surface subsidence obtained from the field measurement, empirical method, and numerical simulation are compared and discussed. Based on the comparison, it finds that the surface subsidence at FBS coal mine is well predicted by means of numerical simulation method. The surface subsidence obtained from the numerical simulation is much closer to the subsidence measured at the mine site than that the one calculated from the empirical method. Therefore, it can be verified that the numerical simulation method using FLAC3D software is applicable to study the surface subsidence under weak geological conditions in this research.

After the applicability of the numerical simulation method using FLAC3D software has been confirmed, the FLAC3D software is then used for studying the surface subsidence at GDM coal mine. The characteristics of surface subsidence induced by longwall mining are studied, and some countermeasures for controlling the magnitude of surface subsidence are investigated and discussed. Based on the simulation results, following important findings can be concluded.

When a single panel of 130 m in width is mined, the AoD increases as the mining depth increases. It means that when the longwall mining is developed at the deeper depth, the wider subsidence area at the surface will be generated. At the same time, the S_{max} decreases as the mining depth increases. It indicates that a narrower panel width should be applied at the shallow depth in order to prevent the large subsidence occurring at the surface. On the contrary, when several panels of 130 m in width are mined in a series, the AoD and S_{max} tend to increase as the depth increases. According to the S_{max} results, however, it is observed that the S_{max} at 50 m depth remains unchanged, while it remains almost stable at 100 m depth after the second and third panels are mined. It indicates that the chain pillar width of 30 m will be enough at 50 m and 100 m depth. Differ from the S_{max} at 150 m and 200 m depth, the S_{max} increases considerably after mining the second and third panels. It indicates that the use of chain pillar width wider than 30 m should be considered.

To minimize the magnitude of surface subsidence induced by longwall mining of a 130 m wide coal panel, several countermeasures such as adopting a wide pillar width and a narrow panel width, and using a cohesive backfill, are investigated and discussed. Based on the simulation results, it is found that the AoD and S_{max} tend to decrease as the pillar width increases from 30 m to 40 m, 50 m, and 60 m, especially at 150 m and 200 m depth. However, at 50 m depth the S_{max} remains unchanged, while it remains almost stable at 100 m depth. The results indicate that the chain pillar width of 30 m will be sufficient to restrict the development of additional S_{max} at 50 m and 100 m depth. The large subsidence occurs at these depths not because the narrow pillar width is used, but due to the wide panel width is applied, coupling with the existence of the thin overburden thickness. Thus, decreasing the panel width will be more effective to minimize the surface subsidence at 50 m and 100 m depth. Differently, the S_{max} at 150 m and 200 m depth decrease significantly as the chain pillar width increases. It is found from the results that using the chain pillar width of 40 m will be adequate at 150 m depth, while the use of the chain pillar width wider than 40 m is recommended at 200 m depth. Furthermore, decreasing the panel width is very effective to minimize the magnitude of surface subsidence at all mining depths. The AoD and S_{max} decrease significantly when the panel width is decreased from 130 m to 100 m or 70 m. The

simulation results also indicates that when a narrow panel width of 100 m or 70 m is applied, a small chain pillar width of 30 m can be adopted at all mining depths. Although the surface subsidence can be controlled effectively by decreasing the panel width, a decrease in coal recovery ratio can be expected when a narrower panel width is used. In addition, when a cohesive backfill is applied in the mined-out panels, the magnitude of AoD and S_{max} is effectively minimized, and the chain pillar width of 30 m can be adopted at all mining depths. The simulation results also indicate that a cohesive backfill can be the most appropriate countermeasure. By applying a cohesive backfill, the recovery ratio of coal can be increased because a narrow chain pillar width of 30 m can be used appropriately with a wide panel width of 130 m. Noticeably, the AoD and S_{max} tend to increase with decreasing the strength of cohesive backfill. It indicates that the use of cohesive backfill with stronger strength is more effective to control the surface subsidence. Based on the results of S_{max}, when the strength of cohesive backfill is reduced, the S_{max} increases slightly at 50 m and 100 m depth, while it increases significantly at 150 m and 200 m depth. It indicates that the cohesive backfill with weaker strength can be used at 50 m and 100 m depth, while the use of stronger cohesive backfill strength is recommended at 150 m and 200 m depth. Moreover, based on the results of a series of numerical simulations, the prediction graph for the maximum surface subsidence due to the extraction of a single longwall panel in GDM coal mine is proposed.

Although the surface subsidence induced by longwall mining can be controlled by using a wide pillar width, a narrow panel width, and/or cohesive backfill, some extents of surface subsidence are still observed. As the lands above the GDM underground mining area are used for the rice fields, a rehabilitation of the subsided area at the surface has to be implemented. The subsided area can be rehabilitated and the water leakage can be stopped by the filling method. In filling method, the topsoil of the subsided area is firstly excavated to expose the cracks. The cracks can be sealed with a compacted clay blanket. After the cracks are sealed, the coal mining wastes and fly ash are then filled in the subsided area, following by replacing the moved topsoil.

References

Bieniawski, Z. T. (1997). Estimating the strength of rock materials. Journal of the South African Institute of Mining and Metallurgy, 312-320.

Choudhary, S. (2013). Some properties of fly ash for mine backfilling (Bachelor dissertation). National Institute of Technology, Rourkela, India.

Dawkins, A. (2003). Potential management and rehabilitation requirement of environmental effects from longwall subsidence on streams, lakes and groundwater systems. Coal Operators' Conference, 117-124.

Ellenberger, J. L., Chase, F. E., Mark, C., Heasley, K. A., & Marshall, J. K. (2003). Using site case histories of multiple seam coal mining to advance mine design. The National Institute for Occupational Safety and Health, 59-64.

Hoek, E., & Brown, E. T. (1980). Underground excavations in rock. London, UK.

Hoek, E., Kaiser, P. K., & Bawden, W. F. (1993). Support of underground excavations in hard rock. West Broadway Professional Centre, Vancouver, British Columbia.

Hill, R. W. (1994). Multiseam design procedures. Safety in Mines Research Advisory Committee (SIMRAC), Division of Mining Technology.

Hoek, E., & Brown, E. T. (1997). Practical estimates of rock mass strength. International Journal of Rock Mechanics and Mining Sciences, 34(8), 1165-1186.

Hoek, E. (2006). Practice rock engineering. North Vancouver, B. C., Canada V7R 4X1.

Hu, Z., & Xiao, W. (2012). Optimization of cocurrent mining and reclamation plans for single coal seam: A case study in Northern Anhui, China. The 2012 National Meeting of the American Society of Mining and Reclamation, 232-250.

Itasca Consulting Group, Inc. (2009). FLAC3D Fast Lagrangian Analysis of Continua in 3 Dimensions: User's Guide, Mill Place, Minneapolis, 55401 USA.

Islam, D. M. R., Faruque, M. O., Hasan M. A., Hussain, M. A., & Ahammod, S. (2013). Modeling for strength assessment of backfill materials associated with the reduction of surface subsidence at the Barapakuria coal mine area, NW Bangladesh. American Journal of Engineering Research, 2(11), 242-251.

IESC (Independent Expert Scientific Committee). (2015). Monitoring and management of subsidence induced by longwall coal mining activity. GPO Box 787 Canberra ACT 2601, Australia.

Luo, Y. (1989). Intergrated computer model for predicting surface subsidence due to underground coal mining-CISPM (Ph.D. dissertation). West Virginia University, Morgantown.

Lechner, A. M., Baumgartl, T., Matthew, P., & Glenn, V. (2016). The impact of underground longwall mining on primw agricultural land: A review and research agenda. International Journal of Land Degradation and Development, 27(6), 1650-1663.

Mark, C. (2007). Multiple seam longwall mining in the U.S.: Lesson for ground control. The National Institute for Occupational Safety and Health, 1-7.

MSEC (Mine Subsidence Engineering Consultants). (2007). Introduction to longwall mining and subsidence. PO Box 3047 Willoughby North NSW 2068, Australia.

NCB (National Coal Board). (1975). Subsidence engineering's handbook. 2nd ed. London.

Meuser, H. (2013). Soil remediation and rehabilitation: Treatment of contaminated and disturbed land. Osnabruck, Germany.

Peng, S. S., & Chiang, H. S. (1984). Longwall mining. John Wiley & Sons, New York.

Sasaoka, T., Takamoto, H., Shimada, H., Oya, J., Hamanaka, A., & Matsui, K. (2015b). Surface subsidence due to underground mining operation under weak geological in Indonesia. International Journal of Rock Mechanics and Geotechnical Engineering, 7(3), 337-344.

Thin, I. G. T., Pine, R. J., & Trueman, R. (1993). Numerical modelling as an aid to the determination of the stress distribution in the goaf due to longwall coal mining. International Journal of Rock Mechanics and Mining Sciences and Geomechanics Abstracts, 30(7), 1403-1409.

Wang, H., Poulsen, B. A., Shen, B., Xue, S., & Jiang, Y. (2011). The influence of roadway backfill on the coal pillar strength by numerical investigation. Journal of Rock Mechanics and Mining Sciences, 48(3), 443-450.

Whittaker, B. N., & Reddish, D. J. (1989). Subsidence: Occurrence, prediction and control. Amsterdam, The Netherlands.

Xie, H., Chen, Z., & Wang, J. (1999). Three-dimensional numerical analysis of deformation and failure during top coal caving. International Journal of Rock Mechanics and Mining Sciences, 36(5), 651-658.

Yasiti, N. E., & Unver, B. (2005). 3D numerical modeling of longwall mining with top-coal caving. International Journal of Rock Mechanics and Mining Sciences, 42(2), 219-235.

Zipf, R. K. (2014). Failure mechanics of multiple seam mining interactions. Proceeding of the 9th Trienial Conference on Mine Subsidence, 93-106.

Zhou, Y. (1991). Evaluating the impact of multi-seam mining on recoverable coal reserves in an adjacent seam. Virginia Division of Mineral Resources Publication 104, Charlottesvilie, Virginia.

CHAPTER 6

CONCLUSIONS

Indonesia is one of the world's largest coal producers and exporters. The coal production of Indonesia has increased significantly in the past years. Indonesia exports 70%-80% of the total production to China and India, and the remaining is consumed in domestic markets. In Indonesia, the coal production is mainly from the surface mines. Recently, the conditions of surface mines are becoming worse each year because the stripping ratio has increased due to the increase of the mining depth. The resource of high quality coal located in accessible areas have decreased due to the rapid expansion of coal production. Moreover, the development of a new surface mine is constrained due to its environmental impacts and protection law. Therefore, in order to meet the increased demands of the coal, underground coal mines have to be developed in Indonesia. According to the experiences of underground coal mining in Indonesia, due to the coal measure rocks are very weak and the design guidelines of underground mining under weak geological conditions have not been developed so far, the ground control issues have occurred frequently. As a result, some underground coal mines have been abandoned. From these backgrounds, the purpose of this research is to develop the appropriate design guidelines of underground mining system under weak geological conditions. The PT Gerbang Daya Mandiri (GDM) underground coal mine in Indonesia, where the rocks are weak and the coal is planned to be mined by longwall mining method, is chosen as a representative mine site. The finite difference code software FLAC3D is used as a tool for the numerical simulations in order to accomplish the purpose of this research. Based on the results of the study discussed in previous chapters, main conclusions of this research are as follows:

Chapter 2: Site Conditions of GDM Underground Coal Mine and Its Current Situation of Main Roadway

The conditions of GDM underground coal mine are described in this chapter. The GDM coal mine is a new underground coal mine and still in the process of developing the main roadways. Based on the laboratory test results, the rocks of

this underground coal mine are classified into very weak and low strength rock mass. Furthermore, this chapter also discusses the current situation of the main roadway stability at the shallow depth. According to the field measurement data, it is found that the conditions of claystone and roof have an obvious impact on the stability of the main roadway. The large roof displacement of the main roadway occurs when the main roadway is excavated in the deteriorated claystone, whereas the small roof displacement occurs when the main roadway excavation is made in the undeteriorated claystone and when the coal layer is present in the roof.

In order to clarify the ground behavior of the main roadway based on the field measurement data, the numerical simulation method using FLAC3D software is used as a tool for clarification. The simulation results are then compared with the measurement data for verification. From the comparisons, it can be found that they are in good agreement, the simulation results support the field measurement data. Under undeteriorated conditions of claystone, the small failure zone and displacement of the main roadway occur. The current support system using the steel arch SS400 is effective to control the main roadway stability. As the claystone has deteriorated due to groundwater, the failure zone and displacement expand considerably, and the main roadway stability decreases significantly. The use of current support system (steel arch SS400) is difficult to control the stability of the main roadway. Under this situation, a stronger steel arch SS540 is recommended to apply. Furthermore, presence of coal layer during the excavation considerably improves the stability of the main roadway. Compared with the main roadway excavated in claystone only, the displacement decreases significantly. In addition, by leaving a thicker coal layer in the roof, a better stability condition of the main roadway can be achieved.

Chapter 3: Stability Analysis and Support Design of Main Roadway

Although the main roadway is stable in the current situation at GDM coal mine, it is only excavated at the shallow depth. To reach the targeted coal seams, it needs to be extended to the deeper areas. In GDM coal mine, as the main roadway has to be excavated at the deep depth and the coal measure rocks are weak, some ground control problems of roof fall, sidewall collapses, and floor heave can be expected.

Therefore, the appropriate design of support system is of particular necessary for this underground coal mine.

The stability of the main roadway at GDM coal mine under various depths and stress ratios is studied by means of numerical simulations. According to the results, the stability of the main roadway decreases with increasing the depth and stress ratio. Ground control problems such as roof fall, sidewall collapse, and floor heave can be expected unless an appropriate support system is provided. Three support systems such as friction rockbolt, steel arch (SS540), and shotcrete are introduced to stabilize the roof and sidewalls of the main roadway. However, the steel arch is considered as the most appropriate support system comparing with other systems. The steel arch meets the qualifications of stability control, fast installation process, and economy. Moreover, the steel arch with closer space and larger size of cross section provides a better stability condition to the roof and sidewalls of the main roadway. Although the stability of roof and sidewalls of the main roadway can be controlled by steel arch support, the floor heave problem is expected due to large failure zone and displacement still occur in the floor. Therefore, three techniques using cablebolt, invert-arch floor, and grooving method are proposed to control the floor heave. Heaving of the floor is controlled effectively after the cablebolt, invert-arch floor, and grooving methods are employed. However, controlling the floor heave by cablebolt support can be the most appropriate technique in GDM coal mine comparing with other methods in terms of installation process, providing a flat and safe working condition of floor, and economy. In addition, the cablebolt with closer row space and longer length works more effectively to control the floor heave problem.

Chapter 4: Effect of Longwall Mining on Stability of Main and Gate Roadway

In GDM coal mine, after the appropriate support systems of the roadway have been studied and confirmed, the next issue that should be taken into an account is that the stability of the main and gate roadways affected by the longwall mining. In longwall mining, an adequate width of barrier/chain pillar and coal panel is needed in order to prevent the failure of the main/gate roadway due to the panel extraction. This chapter studies the effect of longwall mining on the stability of main and gate

roadways at GDM coal mine. According to the results of simulations, the longwall mining significantly affects the main and gate roadway stabilities. The stability of main/gate roadway decreases with decreasing the barrier/chain pillar width, especially when a wide panel width of 130 m is applied. Some ground control issues can be expected unless an appropriate width of barrier/chain pillar is provided. In the case of main and gate roadways are supported by 0.5 m spaced steel arches (SS540), a 20 m barrier pillar width and a 30 m chain pillar width can be used sufficiently at 50 m, 100 m, and 150 m depth, while a wider barrier pillar width of 34 m and a wider chain pillar width of 50 m should be applied at 200 m depth in order to keep the main and gate roadways stable during the longwall mining, respectively. The simulation results also reveal that the effect of longwall mining on the stability of main and gate roadways can be minimized effectively by decreasing the width of panel. By applying a narrower panel width, not only the main/gate roadway stability can be improved, but also a smaller barrier/chain pillar width can be adopted. At 200 m depth, the stability of main roadway can be controlled effectively by a smaller barrier pillar width of 20 m and 23 m, while the stability of gate roadway can be maintained efficiently by a smaller chain pillar width of 32 m and 40 m, when a narrower panel width of 70 m and 100 m is applied, respectively.

Chapter 5: Surface Subsidence induced by Longwall Mining

As some houses and rice fields exist at the surface above GDM underground coal mine, not only the effect of longwall mining on the roadway stability needs to be taken into consideration, but also the surface subsidence induced by longwall mining. Because of a large extent of coal will be removed from the seam, and due to the coal measure rocks are weak, a large subsidence at the surface can be expected when a longwall mining is applied in GDM underground coal mine. Undeniably, a study of surface subsidence is needed in order to avoid the adverse impacts of subsidence at the surface. The characteristics of surface subsidence induced by single-panel and multi-panel longwall mining are studied, and some countermeasures for controlling the subsidence are investigated by means of numerical simulations. Based on the simulation results, a large surface subsidence

occurs at all depths (50 m, 100 m, 150 m, and 200 m) when a wide panel width of 130 m is used. When a single panel is mined, a larger surface subsidence occurs at the shallow depth, hence a narrower panel width should be applied at the shallow area. After several panels are mined in a series, the surface subsidence increases with increasing the depth. It indicates that a wider chain pillar width is needed at the deeper depth. In order to control the surface subsidence, three countermeasures of using a wider chain pillar width, a narrower panel width, and a cohesive backfill are investigated. As a wide panel width of 130 m is applied, a large surface subsidence still occurs at all depths even though the chain pillar width is increased from 30 m to 40 m, 50 m, and 60 m. It suggests that a longwall mining with narrower panel width or cohesive backfill should be adopted for reduction of the surface subsidence. The surface subsidence decreases significantly with decreasing the panel width. A small chain pillar width of 30 m can be used sufficiently at all depths when a 100 m or 70 m panel width is applied. Although the surface subsidence can be controlled effectively by decreasing the panel width, a decrease in coal recovery ratio can be expected when a narrower panel width is used. On the other hand, the surface subsidence can also be controlled effectively by using a cohesive backfill. A small surface subsidence occurs after a cohesive backfill is applied. The simulation results also indicate that a cohesive backfill can be the most appropriate countermeasure. By applying a cohesive backfill, the recovery ratio of coal can be increased because a narrow chain pillar width of 30 m can be used appropriately with a wide panel width of 130 m. Moreover, based on the results of a series of numerical simulations, the prediction graph for the maximum surface subsidence due to the extraction of a single longwall panel in GDM coal mine is proposed.